CARBON TRANSFER IN THE WESTERN SOUTH CHINA SEA – BIOGEOCHEMICAL PERSPECTIVES ON ORGANIC CARBON POOLS IN SURFACE SEDIMENTS, FROM SOURCE TO BURIAL

By:

Lena Süreyya Narman

to obtain the degree:

Doctor of Philosophy

Heriot Watt University, the Lyell Centre

School of Energy, Geoscience, Infrastructure and Society

Submitted:

June 2020

Abstract

Organic carbon (OC) entrainment, transmission and transformation along the terrestrial-marine continuum is fueled by terrestrial sources, modified by progressive *in-situ* mixing, production, and decomposition of marine OC.

Bulk (OC, Nitrogen), molecular (Fatty acid methyl esters, FAME) and isotopic ($\delta^{13}C_{org}$, $\Delta^{14}C$) geochemical data are used in combination with mineral surface area and advanced computational models (Bayesian statistics, inversion models) to identify OC sources and their geochemical composition in estuarine and marine surface sediments of the South China Sea (SCS). A novel inversion modelling approach is presented that estimates OC pools (incl. petrogenic and dead carbon) validated against end-members. Dominance of marine OM is confirmed for coastal environments, implying efficient net loss of terrestrial OM, as it crosses the land-sea interface. The $\Delta^{14}C$ values range from modern to ~-970‰, with oldest OC focussed to the Red River outflow and remote regions of the Sunda Shelf palaeoriver systems, modern marine surface sediments are dominant in oceanic and shelf areas, which contrasts results from other studies from different river-marine shelf-open ocean systems available in the literature (e.g. the northern part of the SCS). Also reported, for the first time, anthropogenic synthetic organic compounds demonstrating the impact of potential pollution on the modern marine environment.

Acknowledgements

I thank my supervisor Prof. Dr. Thomas Wagner and Dr. Martin G. Wiesner who initially set in motion my PhD project. Thank you Martin for the numerous discussions and the many coffees that we had. I also thank my international collaboration partners for their cooperation. Special thanks go to Prof. Dr. Timothy I. Eglington and the ETH Zurich, where I spent a few months working and making friends. I also thank my co-supervisor-team at the Lyell Centre, Dr. Ryan Pereira, and Dr. Clayton Magill. In particular, I thank Dr. Clayton Magill for the countless and fruitful discussions, for the enormous input, especially at the molecular level discussion over the past three years.

I thank Sara Trojahn and Melanie Mertesdorf for their support on very long evenings and nights in the lab and at the desks. Thank you Sara for the emotional support, constant discussions, and suggestions. It was a pleasure and an honour to have laughed and cried with you. I will miss our living room and our time together. You are and have been a real friend to me. Wherever it will take us and whatever time brings, this journey will connect us and you will ever be my friend.

Thank you Melissa Schwab who welcomed me very warmly at the ETH and helped me, especially on my first visit. Without you, it would have been a lot more of a challenging time.

Special thanks go to the team of the University of Hamburg, for the measurements carried out for me. I also thank all the other technicians who have supported me in my work, in particular Dr. Negar Haghipour for the numerous ^{14}C measurements, which are an essential part of my work. Thanks to the entire Lyell Centre team for the community and its support.

I thank my partner Dr. Andre N. Paul for his tremendous support and his love as well as my mum and dad. I could not have come this far without your endless love and support, you always believe in me. I thank my friends, especially my best friends, for their love and support.

Thank you to all of you.

Research Thesis Submission

Name*:*	Lena Süreyya Narman		
School:	School of Energy, Geoscience, Infrastructure and Society		
Version: *(i.e. First, Resubmission, Final)*	final	Degree Sought:	Doctor of Philosophy

Declaration

In accordance with the appropriate regulations I hereby submit my thesis and I declare that:

1. The thesis embodies the results of my own work and has been composed by myself
2. Where appropriate, I have made acknowledgement of the work of others
3. The thesis is the correct version for submission and is the same version as any electronic versions submitted*.
4. My thesis for the award referred to, deposited in the Heriot-Watt University Library, should be made available for loan or photocopying and be available via the Institutional Repository, subject to such conditions as the Librarian may require
5. I understand that as a student of the University I am required to abide by the Regulations of the University and to conform to its discipline.
6. I confirm that the thesis has been verified against plagiarism via an approved plagiarism detection application e.g. Turnitin.

ONLY for submissions including published works

7. Where the thesis contains published outputs under Regulation 6 (9.1.2) or Regulation 43 (9) these are accompanied by a critical review which accurately describes my contribution to the research and, for multi-author outputs, a signed declaration indicating the contribution of each author (complete)
8. Inclusion of published outputs under Regulation 6 (9.1.2) or Regulation 43 (9) shall not constitute plagiarism.

* *Please note that it is the responsibility of the candidate to ensure that the correct version of the thesis is submitted.*

Signature of Candidate*:*		Date:	08.06.2020

Submission

Submitted By *(name in capitals):*	LENA SÜREYYA NARMAN
Signature of Individual Submitting:	
Date Submitted:	17.06.2020

For Completion in the Student Service Centre (SSC)

Limited Access	Requested	Yes		No		Approved	Yes		No	
E-thesis Submitted (**mandatory for final theses)**										
Received in the SSC by *(name in capitals):*						Date:				

Contents

Table of figures

Table of tables

Table of Equations

Appendix

1 Introduction

1.1 General introduction

Continental shelf systems mark a critical transition zone between terrestrial freshwater environments (e.g. river deltas, estuaries) and deep and open marine environment. These systems exhibit complex transport and storage mechanisms for carbon, minerals, nutrients, and their reactivity and interaction with the environment. Costal and inner shelf sediments store complex combinations of terrigenous (vegetation, soils and fossil reworked) and marine OM, each with different reactivity and fate when transported through the environment and buried in the sediments. These variables are crucial when modelling global carbon cycles [2] and monitoring hazardous materials exported from e.g. agriculture or industry operations. Previous studies suggest that OM from marine bio-production is characterised by simpler chemical structures relative to terrestrial OM, which implies faster decomposition of marine OM [3]. Therefore to more accurately describe and model global climate change, it is essential to obtain accurate and quantitative information on the concentration, origin, reactivity/degree of preservation, age and transport pathways of organic carbon and associated components (OM) on shelf systems.

Along with riverine runoff and aeolian dust, potentially hazardous compounds, such as pesticides and/or herbicides, can be introduced into coastal and shelf environments. Once in the marine environment they are spatially dispersed along with the fine (clay) mineral fraction (e.g. “mud”, [4]) by shallow ocean current systems to further degrade parts of complex deposition-resuspension loops. The dispersal and storage of these compounds of environmental concern as part of the total continental mineral load is not well understood but likely important for marine ecosystems, as they can be toxic and become part of the food chain, feeding back into fish ecosystems and finally important food sources for society. According to the Food and Agriculture Organization of the United Nations and the World Health Organization, global food production is expected to increase by more than 70 % by 2050 (relative to 2007) [5], which in turn implies an increasing use of herbicides, at the global scale. This may cause massive and unforeseeable challenges, affecting the environment and ecosystems, from local, to regional and possibly global scales.

This PhD project targets the westernmost part of the South China Sea (SCS) as part of the international research collaboration program "**S**ources, **T**ransport Pathways, **Re**sidenc**e** **T**imes and **S**inks of Organic Matter in the South China Sea" (STREETS). STREETS combines the expertise and capacities of Heriot-Watt University Edinburgh, University of Hamburg, Eidgenoessische Technische Hochschule Zurich (ETH), Tongji University Shanghai (TONGJI), and the Second Institute of Oceanography, Hangzhou (SOI). All partners of STREETS have actively contributed to this project, by sharing sample material, data, and expertise.

Decades of earlier research in the SCS, led by the Hamburg and Chinese research groups of STREETS, have culminated in a large database that enables to monitor and understand the fundamental controls on OM transport and burial in the region, including oceanography, (clay) mineralogy, micropalaeontology, and inorganic and organic geochemistry. This PhD study takes full advantage of this data and sample base, to investigate OM transfer across three interconnected shelf systems from Vietnam to Indonesia and its exchange with the deep SCS basin. The shelf systems under investigation include (A) the Gulf of Tonkin in the north, (B) the narrow shelf along the east coast of Vietnam, and (C) major parts of the Sunda Shelf connecting with Indonesia/Borneo-Sumatra (Fig. 1). This geographically diverse region covers a total length of about 2300 km (N-S), with numerous small and large rivers draining the shelf and highly variable climatic and oceanographic conditions, in combination controlling the export, movement and final burial of sediment and OM on the shelf and the adjacent deep marine basins. To enable this project, the STREETS network provided 320 river and marine surface sediment samples for detailed organic geochemical and sedimentological analyses.

The Mekong River drainage system in southern Vietnam is controlled mainly by the East Asian monsoon and its evolution since the last glacial period. Observations from modern shelf carbon processes and budgets, however, suggest that factors such as the lateral advection of OM, time scales of particle transport, carbon production rates and deposition efficiency strongly impact on the abundance and fate of OM in shelf/slope surface sediments [6–9].

High resolution studies on the temporal relationships of different OM pools in the marine environment have only recently become available, pioneered by the ^{14}C dating of OM in bulk sediments and grain-size fractions (e.g. Bao et al. [7, 10]). The spatial heterogeneity

in ^{14}C age of OM ($\Delta^{14}C$ age) reported for surface sediments of the East China Sea [10], emphasises the relevance of redistribution of organic carbon (OC) from different sources and age pools. The identification and quantification of petrogenic and inert carbon sources is important for $\Delta^{14}C$ dating, enabling the correction of the $\Delta^{14}C$ age for modern carbon sources. A recent study by Blattmann et al. [11] addresses this challenge in the northern SCS (Taiwan), just outside of the study area of this project, illustrating the contribution of terrestrial surface of lithology to $\Delta^{14}C$ systematics. The occurrence of pre-aged organic carbon (OC) in continental margin surface sediments is a commonly observed phenomenon, yet the nature, sources, and causes of this aged OC remains largely undetermined for many continental shelf settings [10]. This study focusses its investigations on the causes of $\Delta^{14}C$ variability and interactions of fresh and degraded organic carbon within the southern SCS. For this purpose, the OM in terms of concentration, origin, species, maturity, diagenesis, and isotopic carbon signature ($\delta^{13}C$ and $\Delta^{14}C$) along the western part of the continental margin of the SCS has been investigated.

Carbon isotopes help identifying and quantifying carbon cycle processes, such as the transfer of terrestrial carbon to the ocean and its burial [10]. This has led to an improved understanding of natural processes and anthropogenic impact [12–14]. For example, Bao et al. [10] show a distinct heterogeneity of $\Delta^{14}C$ ages in bulk OM surface sediments in the East China Sea, emphasising the complex interplay of OM sources, hydrodynamic processes and sediment transport on the OC found in the modern shelf. Further studies focussing on carbon cycle processes are essential for deepening and expanding these recent observations in $\Delta^{14}C$ isotope systematics, as evident by recent studies of [12–14] (in China, Siberian Arctic and the Arctic). Furthermore, redistribution processes of lithogenic particles in shallow and deep water have been shown to be important in the SCS [15, 16]. Riverine input is known to play a dominate role for the composition of the sediments in the SCS, at least for coastal and inner shelf systems. Suspended solids and surface sediments capture the composition of shelf-slope sedimentary OM, with radiocarbon ($\Delta^{14}C$) ages typically older than modern signatures [17, 18]. This observation suggests a time lag between the initial production and the final storage of OM, favouring mobilisation, export and burial of stratigraphically older strata and deeper soil layers [12, 19, 20] in the marine environment. In order to identify and quantify this re-worked and potentially older OM, end-member mixing models have been developed using $\delta^{13}C$, $\Delta^{14}C$, and molecular biomarker [21].

The molecular biomarker approach provides a powerful tool to identify the origins of OM and can help to identify the associated biogeochemical processes, thus helping to reconstruct the environmental changes previously occurring in the OM origins [22–25]. Organic biomarkers (such as fatty acids) can provide abundant information about the original sedimentary source material composition, change in geochemical and biochemical processes, climatic changes [26–28].

A molecular marker here is defined as "a molecule whose carbon skeleton can be unambiguously linked to that of a known biological precursor compound" [29] or as "a complex organic compound having little to no changes in its chemical structure from the precursor molecules once existed in living organisms" [30–32]. To qualify as a molecular marker, i) source specificity and ii) conservative behaviour [29] must be ensured. Under ideal conditions, molecular markers should present a direct and unique link with the given sources, and they should be refractory over the time scales of the processes of interest [25]. Concerning criterion i) and ii) in natural environments, organic molecules are likely to be under the influence of various processes, including physical (particle transport and phase transfer), chemical, and microbial processes, which affect the spatial distribution and the fate and even induce chemical changes in their structures which can lead to misinterpretation.

In this study, the focus lays on source-specific fatty acids (FA) coupled together with radiocarbon measurements ($\Delta^{14}C$) of bulk OM to resolve possible transport and burial mechanisms. Furthermore, the potential entrainment of compounds of environmental concern in the shelf and deep sea sediments is traced.

The presented study contains four science Chapters (Chapters 3 to 6), with each Chapter summarised in brief below.

Chapter 3: Assessment of transport and accumulation of organic matter in the western SCS – implications from estuary and marine surface sediments

A new dataset covering fundamental variables including TOC, $\delta^{13}C_{org}$ and C_{org}/N_{total} is presented from a comprehensive set of surface samples. The focus of the analysis lies on the identification of source variability, homogenisation of terrestrial OM during deposition, and the identification of OM storage sites. Additionally, fatty acid methyl esters (FAME) are analysed and used as a sensitive geochemical proxy in the interpretation of OC modification during transport from land to sea and to attempt to correlate FAME abundances and composition to region-specific changes in e.g.

vegetation. The observation from FAME is then compared with interpretations based on $\delta^{13}C_{org}$ and C_{org}/N_{total} data. The key finding of this assessment is that marine OM dominates in surface sediments across the SCS, including coastal and estuary/riverine settings. The relative contribution of different OM sources is based on multiple geochemical variables ($\delta^{13}C_{org}$, C_{org}/N_{total}, FAME distribution, and the occurance of short-chain to mid-chain FA). Meaningful interpretation of FAME biomarker data requires simultaneous evaluation, achieved graphically using multi-variable histogram plots (spider diagram), which is previously undocumented. The FAME data require smoothing through sample normalisation, for which two potential reservoirs are defined here. Emphasis is placed on the need for specialised and localised reservoirs, which are linked to local geographic and geologic features.

Chapter 4: Controls on regional mixing and degradation of organic matter in the South China Sea – implications of mineral surface area, $\Delta^{14}C$, $\delta^{13}C_{org}$ and TOC

The geographic extent of the SCS requires the identification of pertinent data that can be used to constrain (sub) regional details of the carbon cycle within the SCS. These will include the evaluation of mineral surface area, radiocarbon $\Delta^{14}C$, stable $\delta^{13}C_{org}$ and TOC data. Variations in the $\Delta^{14}C$ values are expected, which can be caused by e.g. different transport timescales and variable size fractions of petrogenic carbon, which is predominantly perceived to be mobilised from terrestrial sources, with highly variable isotopic composition. The radiocarbon $\Delta^{14}C$ values of most marine sediments of the SCS are positive, consistent with relatively recent/modern carbon supply and burial. This observation points to a very fast and probably also very efficient net loss of terrestrial OM at the terrestrial-marine interface, compared to other shelf regions. The TOC data imply low carbon concentration on the shelf areas, while at the same time dominated by marine OM. This conflicts with the general relationship between sources to sink processes, questioning the global validity of computational models to predict or reconstruct carbon budgets and cycles on global and regional scales.

Chapter 5: Model estimates of OC pools in the SCS – comparing simulation and calculation-based approaches

To investigate potential bias in numerical models, several different solutions are compared and evaluated to identify the most accurate approach. To increase the accuracy and likelihood of the model, several numerical solutions are combined. The output of these models is compared with the geological setting and used to extract potential carbon

source regions composition ($\Delta^{14}C$ and $\delta^{13}C_{org}$). Such information concerning source compositions is currently unavailable for the study area. Chapter 5 features a Bayesian statistical approach, which, in combination with an iterative framework, leads to novel insights of diverse OC pools, some of which cannot be not directly measured (e.g. petrogenic carbon). The iterative approach validates different OC end-members and gradually refines the model outcome. Using this novel approach OC pools can be validated and missing OC pools (e.g. petrogenic or dead carbon) identified. The new approach emphasises the importance of individually picked end-members for different environments as opposed to the common approach to apply generallised end-members. The used model allows identifying the general distribution of OM, segmented into different fractions of carbon pools and the trend of an accumulated type of OM can be confirmed. The iteration first identifies components, while the Bayesian statistics provides a mathematical estimate, creating a robust and reliable overview of carbon pools and their approximate size fractions.

Chapter 6: Distribution patterns and transport mechanisms of synthetic halocarbons in the SCS – an 'unconventional biomarker' approach to trace ocean contamination

The presence and distribution of persistent organic pollutions caused by anthropogenic activity are documented using the selected compounds tris(2-chloroethyl)phosphate, tris(2-chloroisopropyl)phosphate and triallate to build a foundation for future work concerning marine pollution. The distribution and abundance of these compounds is compared with observations made for organic matter (Chapter 1- General Introduction and 2 – Material and Methods) to investigate similarities in transport pathways and mechanisms. The presence of these compounds requires immediate action, such as quantification and study of toxicologic impact on marine life, to prevent accumulation over critical thresholds, which also need to be identified.

To provide a broader interpretational framework, detailed information is provided in the general introduction (Chapter 1 - General Introduction), the Methods chapter (Chapter 2 - Material and Methods), and a summary conclusion and future work perspective (Chapter 7).

1.2 Study Area

1.2.1 Geographical setting

South Asia covers an area of approximately 5.2 x 10^6 km^2 and is characterised by high biological diversity and climatic variations. The mean annual temperature varies from 2 °C - 50 °C and covers the tropical, subtropical, temperate, and alpine zones (Southeast Asia, 2009 in [33].

The SCS covers an area of approximately 3.5 x 10^6 km^2, with an average water depth of about 1.140 m [34] and a maximum water depth in some places of 5500 m [35], making it the largest marginal sea of the Pacific Ocean (e.g. Chu et al. and Chen et al. [36, 37]). The shelf sea along the study area is highly diverse, with the Gulf of Tonkin in the north having a maximal water depth of 120 m and an average water depth of about 45 m [38]. Further south and west, the Gulf of Thailand has a water depth of not more than 100 m and an average water depth of 50 m [35]. Including the Gulf of Thailand and southern part of the Vietnam Shelf, the Sunda Shelf embraces a large area of about 1.8 × 10^6 km^2 [39] with a spatially diverse but maximum water depth of about 120 m [40] (Fig. 1).

The SCS is bordered by China in the North, Taiwan, and the Philippines in the East, Brunei, Singapore, and the Malayan Peninsula in the South and Vietnam in the West (Fig. 1). The SCS covers over 250 small islands and atolls, most of which are uninhabitable since they are permanently below the ocean surface or submerged by tide.

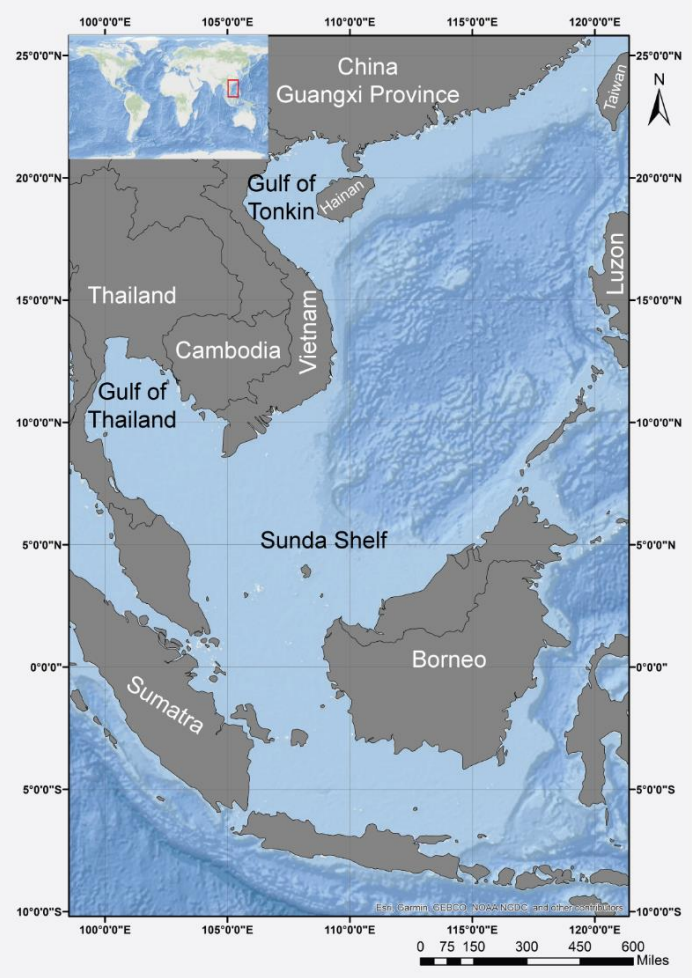

Figure 1) Geographic overview of the study area, located in South-East-Asia. The Sunda Shelf, Gulf of Tonkin, and Gulf of Thailand are pre-defined geographic landmarks. Bathymetric data indicates shallow areas (light blue) and deeper areas (darker blue)

The study area covers the westernmost part of the SCS, which is segmented into the Gulf of Tonkin, Vietnamese Shelf, Vietnamese Coast, Sunda Shelf, and Slope/Deep Sea (Fig. 2). The working area includes estuaries from major and small rivers from Vietnam, Hainan (China), Thailand, Malaysia and Indonesia, to capture the link between continent and ocean. The Vietnamese coastline offers a unique opportunity to study a variety of different shelf systems in a relatively small-scaled region. The region includes very narrow shelves (western-central coast of Vietnam) to wide ranged (Gulf of Tonkin) and very wide range systems (Sunda Shelf). On the western-central Vietnamese Shelf, the transport distance from land to deep sea is short. The Gulf of Tonkin is a semi-closed system with large river in-flow from the Red River, providing significant input of continental OM. The Sunda Shelf in the south is characterised by long transportation distances from land to the deep sea. Major rivers flow into the western part of the SCS, e.g. the Red River, Mekong River, Rajang River and Chao Phraya (Fig. 2). The Gulf of Tonkin is connected to the deep sea through a narrow mouth (Fig. 1 and 2), while the

regions Vietnamese Shelf, Vietnamese Coast and Sunda Shelf exhibit direct, unobstructed pathways to the deep sea. Furthermore, the Gulf of Tonkin is a Cenozoic rift basin [41] with the occurrence of neritic relict sediments, which primarily consist of terrigenous material. These neritic relict sediments might act as preferential storage/ source for pre-aged carbon, which is relevant to $\Delta^{14}C$ dating and related interpretations, making this region a prime area for geochronological studies of mixing between multiple sources. The continental margin east of central Vietnam is very narrow and acts as a direct link between land and the deep sea. These distinct geographical differences have implications when comparing $\Delta^{14}C$ data, as mixing of pre-aged sediments and fresh material is expected to be less likely or less efficient along the Vietnamese Shelf. Additionally, recent measurements and simulations [16] discuss the influence of the Qiongzhou Strait between Hainan and the Chinese mainland, which flows westwards year-round, forcing a cyclonic circulation in the Gulf of Tonkin throughout the year (6). This cyclonic setting limits the number of external sources of OM in the gulf.

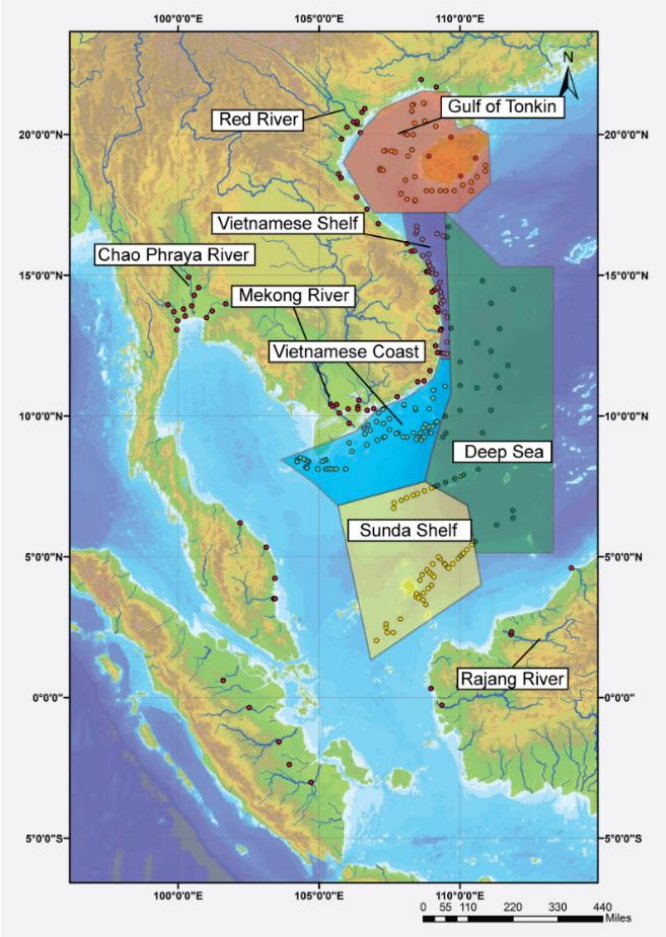

Figure 2) Geographic overview of sample locations, such as rivers (red dots), marine surface sediments up to 200 m depth (yellow dots) and marine surface sediments with depth greater than 200 m (blue dots). Samples are grouped into geographic regions named: Gulf of Tonkin (red); Vietnamese Shelf (purple); Vietnamese Coast (blue), Sunda Shelf (yellow) and Deep Sea (green).

1.2.2 Geological setting

The SCS is tectonically located at the intersection of the Eurasian, Pacific, and Indo-Australian plates. It formed between ~ 32 Ma to ~ 16 Ma on the Cenozoic continental margin [42]. Since then, it has undergone almost a complete Wilson cycle, from continental breakup to seafloor spreading and subduction of the seabed [16]. South China has been tectonically stable (cratonic) since the Mesozoic [16].

In the western part of SCS, in the province of Guangxi, Palaeozoic-Mesozoic carbonate rocks (mainly Permian-Triassic limestone) dominate. The Indochina Peninsula to the west of the SCS, with the adjacent eastern Tibetan Plateau, consists mainly of Palaeozoic-Mesozoic sedimentary rocks with a low proportion of plutonites and volcanics [43]. Along the fault zone of the Red River and in the coastal mountains of the eastern peninsula small amounts of magmatic and Precambrian metamorphic rocks are found [44]. The Red River fault zone is still tectonically active with an average slip rate of at least 5 mm/yr. since the Pliocene [45–47]. Mesozoic sedimentary rocks (mainly sandstone and mudstone) dominate lowlands of the southern Indochina peninsula. Larger Neogene basalt bodies (Fig. 3) intrude them.

In the south, the Malay Peninsula consists mainly of Palaeozoic-Mesozoic granite and granodiorite as well as Palaeozoic sedimentary rocks [48], comparable to the lithology of the eastern part of southern China. As part of the Sunda Lands, the Malay Peninsula has been tectonically stable since the Mesozoic [49] (Fig. 3).

On Sumatra, the main surface rocks exposed are Quaternary interstitial and basic volcanic rocks in the mountains and sedimentary rocks in the northwest [48].

By contrast, Borneo is predominantly comprised of sedimentary units, some of which are described as deep marine sediments. Igneous intrusive and extrusive rocks are rarely exposed at the surface [50] (Fig. 3).

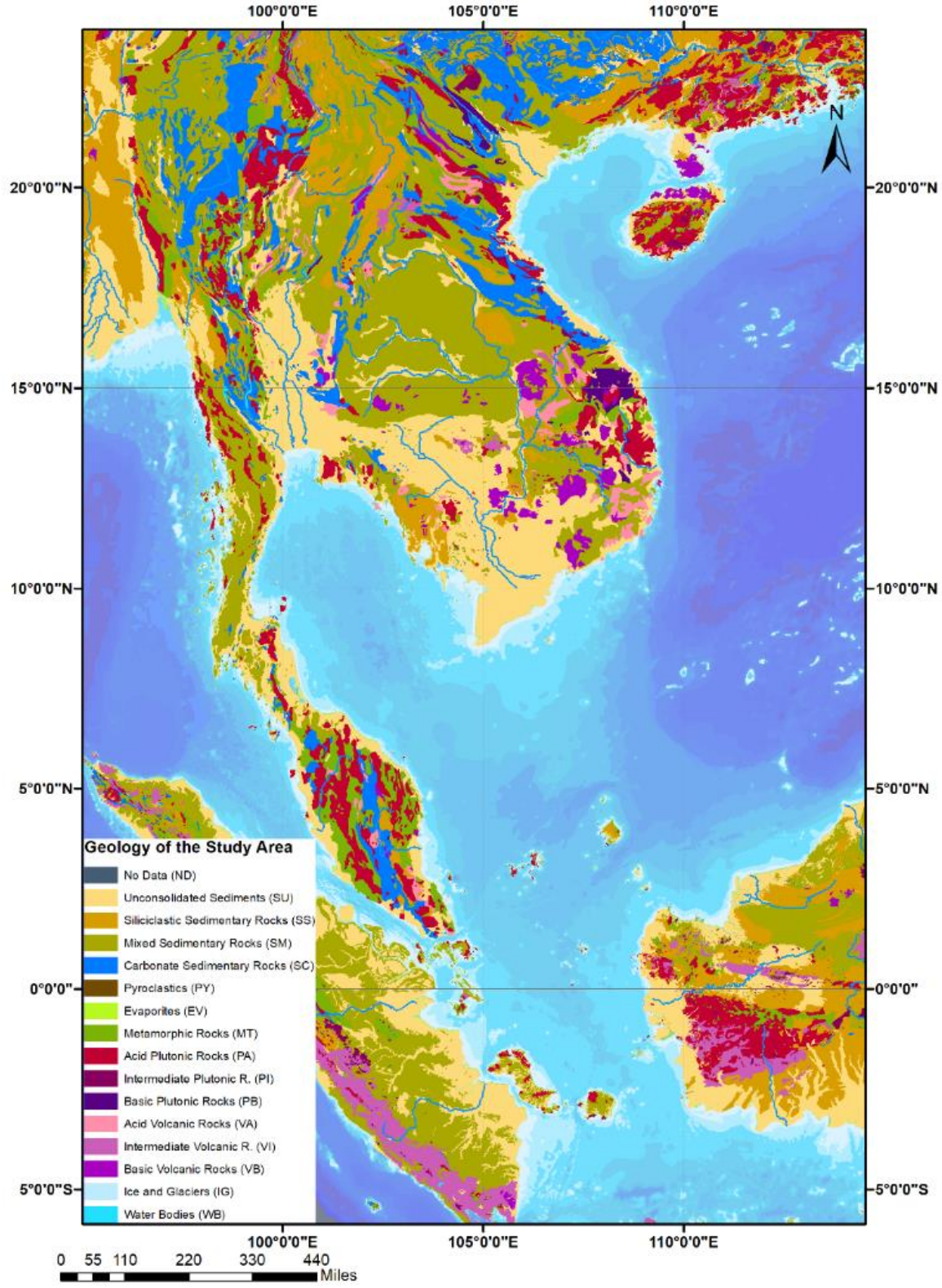

Figure 3) Lithological map of the terrestrial land masses adjacent to the study area, data from Hartmann and Moosdorf [44]. Important features are the presence of carbonate sedimentary rocks (blue), felsic igneous rocks (red) and basic igneous rocks (purple), which can have distinct $\delta^{13}C$ isotopic composition

1.2.3 Climate conditions

The SCS has a tropical to subtropical climate characterised by the bi-annual occurrence of monsoons. For the SCS, the East Asian monsoon system is most important [51].

The monsoon system results from complex interplay of physical parameters (solar radiation, heat capacity, etc.), which forces a horizontally oriented energy gradient [52]. Seasonality in mean air surface temperatures creates variation in the observed monsoonal patterns [52]. The duration of the monsoon period in winter is approximately six months, while the summer monsoon is shorter and of lower intensity [53]. The most notable feature relevant for this study is the chance in mean surface wind stress, which reaches its maximum of 0.3 N/m^2 during December (winter-monsoon), while the summer monsoon has values of 0.1 N/m^2. This has direct effects on the surface currents of the study area. For a detailed explanation on how the monsoon systems form, a detailed summary can be found in e.g. Paeth et al. [52] (Fig.4).

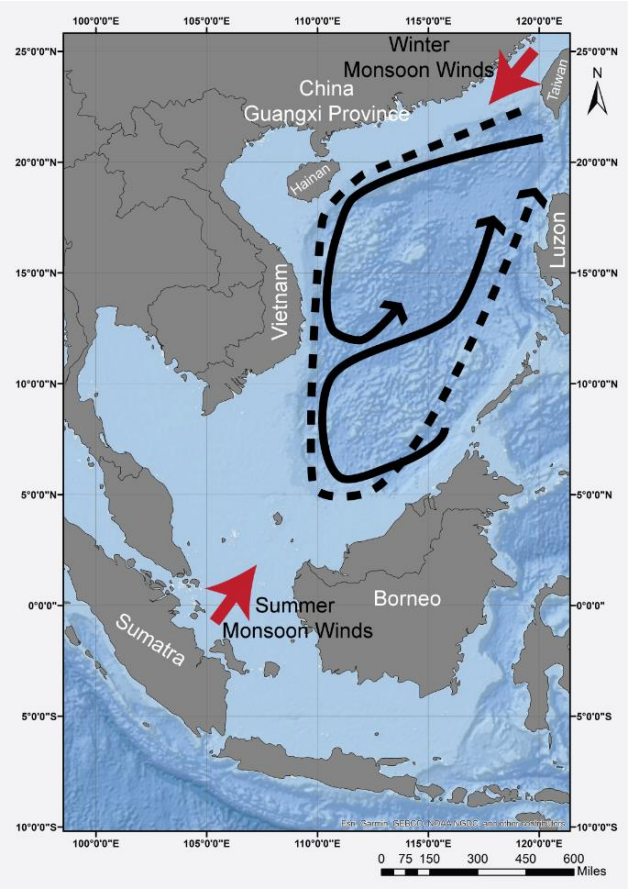

Figure 4) Simplified overview of oceanographic features, dotted line: ocean current circulation during winter, black solid lines: ocean current circulation during summer. The red arrows indicate the direction of monsoon winds as labelled in figure, based on Wang et al. [54] and Liu et al. [55]

The main wind axis during the winter monsoon stretches in the SCS from the southern tip of Taiwan to the southwest to Borneo [56]. Between the summer and winter monsoons, there are inter-monsoon phases over a period of one to two months. In these situations, the prevailing wind direction turns, the phase has relatively low precipitation. Wind strengths up to 4 m/s are achieved. During the summer monsoon, temperatures are between 28 °C - 30 °C throughout the SCS, and fall by 4 °C - 7 °C during the winter monsoon [56]. The main monsoon seasons are between mid-May to mid-September [53] and between December and February.

Every couple of years El Niño Southern Oscillation (ENSO) affects the study region causing a marked increase in the sea surface temperature (up to 3 °C e.g. Narman [57] data from https://www.cpc.ncep.noaa.gov/products/precip/CWlink/MJO/enso.shtml), while the wind intensity is reduced, and the surface circulation comes to an almost completely halt. This situation effectively overheats surface waters across the study region, which leads to a collapse of the primary bio-production and thus a lower flux of marine OM to the sea floor, effectively slowing the carbon pump. La Niña events have the opposite effects on wind and temperature, relative to El Niño, and typically follow the occurrence of El Niño. Under La Niña conditions, surface circulation and surface water perturbation are increased due to higher wind speeds, reducing surface water temperatures but enhancing primary production. The dynamics of monsoons and ENSO are intimately linked [58], with ENSO events having a direct impact on regular monsoon conditions.

1.2.4 Vegetation zones and Types of plants present in the study area

Southeast Asia is divided into two different main climatic zones, which strongly influence the type of vegetation. These regions are the Indochina Peninsula (includes Thailand, Vietnam, Cambodia, Laos and Myanmar) and the Insular Southeast Asia. The study area has a humid subtropical climate with a dry winter season; much of the area receives a high amount of annual rainfall [33]. Most of the Indochina Peninsula is covered by tropical forests, which includes both rainforests with rainfall during the entire year and monsoon forests which experience dry episodes [33]. Prior to the description of vegetation zones, a general classification of plant types is provided, as these are intertwined with the vegetation zones. This is followed by a country and region specific characterisation. Some regions adjacent to the study area are reported for completeness, since the data have been used to formulate first hypotheses of this thesis. However, continuous work has rendered some of these regions redundant in this study, as no

immediate link could be established. Still they contribute to the solidification of the scientific framework and are made available to the reader.

Since the vegetation cover has immediate impact on the OM composition transported from land to ocean interface mainly by river systems, regions and countries are described individually. This anticipated complexity in regional OM source composition is supported by $\delta^{13}C_{org}$ isotopic data and C_{org}/N_{total} data presented and discussed in Chapter 3.

The different types of metabolism of different plants (C_3, C_4, Crassulacean acid metabolism (CAM)) result in indistinct geo-chemical signatures. These signatures are highly useful for the interpretation of OM sources in SCS surface sediments. Below these main types of vegetation are briefly introduced along with their diagnostic properties .

C_3 and C_4 type plants have different optimum conditions for growth. C_4 plants generally prefer high temperatures and low pCO_2 ecosystems [59]. C_3 plants, C_4 plants and CAM plants (which are not a focus of this study) have three different metabolic pathways for carbon fixation in photosynthesis, with C_3 being the most common one. The C_3 carbon fixation converts CO_2 and ribulose bisphosphate into two molecules of 3-phosphoglycerate. This reaction is the first step of the Calvin-Benson cycle. The Calvin-Benson Cycle converts CO_2 and other compounds into glucose, with three phases of light independent reactions: carbon fixation, reduction reactions, and ribulose 1.5-bisphosphate (RuBP) regeneration. These processes only occur when light is available. The key enzyme for carbon fixation is Ribulose-1,5-bisphosphate carboxylase/ oxygenase (RuBisCO), which mediates carboxylation of C_5 sugar during carbon assimilation. Different from that, C_4 plants are using the Hatch-Stack pathway for the fixation of carbon in addition to the Calvin-Benson Cycle. C_4 plants internally concentrate CO_2 before carbon fixation, giving C_4 plants a competitive advantage over C_3 plants when the ratio of atmospheric CO_2 to O_2 is low. C_4 plants have a similar advantage when growth temperatures are high and the oxygenation functionality of the Rubisco enzyme can out-compete the carboxylation functionality in the absence of a CO_2-concentrating mechanism. The ability to increase internal CO_2 concentrations also allows C_4 plants to decrease their stomatal conductance, thereby increasing their water use efficiency. This provides C_4 plants with an advantage over C_3 plants under hot, high irradiance water-stressed conditions. Both C_3 and C_4 plants are using CO_2 out of the atmosphere but they discriminate differently against $\delta^{13}C$ [60], which is reflected in the

metabolism of the plant and in the growth environment [61]. The primary cause of photosynthetic carbon isotope fractionation is driven by differences in molecular diffusion of CO_2 through stomatal pores on leaves and followed by differences in carboxylation rates by the RuBisCo enzyme in C_3 plants [62]. The presence of carbonic anhydrase in C_4 plants causes an equilibrium or near equilibrium state, which reduces carbon isotopic fractionation relative to C_3 plants [60]. The important controls on vascular plant $\delta^{13}C$ values are the isotopic composition of the atmosphere and environmental and physiological variables [63, 64]. The stable carbon isotopic range of C_3 plants (-21 ‰ to -32 ‰) is strongly depleted relative to C_4 plants (-9 ‰ to -17 ‰) [65]. The $\delta^{13}C$ values for C_4 plants are much less dependent on environmental variables, than C_3 plants [66]. Examples for C_3 plants are grasses, crops etc., while examples for C_4 plants are sweetcorn, sugarcane, millet etc..

In Chapter 3, the bulk sediment $\delta^{13}C$ isotopic composition is used to identify the most likely source reservoir, using the compositional difference expected between C_3 and C_4 plants. The bulk sediment $\delta^{13}C$ values range from -20.3 ‰ to -29.5 ‰, which overlaps with the range ascribed to C_3 plants. In Chapter 3, this observation will also be compared with vegetation cover information and other geochemical data, to corroborate the interpretation of the $\delta^{13}C$ isotope data.

1.2.4.1 Guangxi province - China

Guangxi is a Chinese province, located directly on the Vietnamese border in the east (Fig.4). The coastal zones of Guangxi are in the southwest of mainland China and the northern region of the Gulf of Tonkin. The Province is influenced by southern subtropical monsoon climate. Guangxi's coastline is covered by mangroves, and, according to the results of a comprehensive inventory in 2007 [67], the total area of mangroves in Guangxi is 9,197.4 ha [67]. Humid rain forest covers Guangxi, like Hainan and tropical karst rain forest [68]. The presence of mangroves is important when attempting to interpret the $\delta^{13}C$ isotopic composition of riverine and marine sediments. Mangrove root systems act as filters for debris and POC [69], and thus variations in the $\delta^{13}C$ isotopic composition could reflect variations in the terrestrial input controlled by physical factors.

1.2.4.2 Hainan

The climate of Hainan is strongly controlled by the monsoon. Hainan itself is characterised by a mountainous landscape in its centre. The mountains reach an altitude of ~1900 m above sea level. Tropical deciduous forests and grass forests at altitudes

between > 500 m and 1000 m usually characterise the vegetation. The vegetation is otherwise dominated by evergreen, deciduous dwarf forests, and farmland (e.g. rice, corn, and sugar cane) in the lowlands. Along the sandy beaches and mangroves, there are coconut palms. Muddy sediments can be found in the coastal areas [70]. These features are combined with the newly established geochemical data that reflect local influence on those signatures.

1.2.4.3 Vietnam

Vietnam divides into two different climate zones; predominated subtropical climate in the north, while the south is tropical. In the southern part and the Mekong River delta in particular, 78 % of the agricultural area was used for rice production in 2000 [71]. The rice fields are located in irrigated land and in the rainforest, lowlands, and highlands. Rice is grown throughout Vietnam, also in the Red River delta in the north, where 74 % of agricultural land is used for rice cultivation, which equivalents to 573,900 ha [72]. This information is important to evaluate potential C_3 plant biomarker signals (e.g. rice), as these may provide insight into the source and distribution of OM transported from the continent to marine environment. In the Mekong River delta, mangrove forests are abundant. They cover the entire Ngoc Hien district and part of the Nam Can district of Ca Mau province [73] in the south of Vietnam. Mangrove vegetation is also found in the north of Vietnam along the Red River Delta coastline [74].

1.2.4.4 Thailand

Tropical deciduous forest is one of the natural assets in Thailand [75]. It consists of mixed deciduous trees, dry dipterocarp, and savanna forest. The deciduous forests occupy 53 % of the land in the north and 11 % in the west and northeast. In Thailand, mangroves occupy the tidal zone of the western and eastern coasts [76]. These mangrove forests continue to fade through deforestation, albeit their area is used for shrimp aquaculture. While only a few samples from Thailand have been available for this study, the estuaries and OM input potentially influence the NW part of the Sunda Shelf.

1.2.4.5 Malaysia

Malaysia is mainly covered with rainforest; a special focus should be laid on the region Sabah. Sabah is located on the island of Borneo and Malaysia's second largest state. It is possible, but very rare to find pristine tropical rainforest with a very diverse flora and fauna. They distinguish from other main tropical rainforests because of the dominance

of one family of trees (Dipterocarpaceae, commonly known as dipterocarps) [77]. The localised occurrences of species can potentially be used to explore novel tracers, such as FAME. This requires OM samples from leaves, branches, and stems, to permit comparison with bulk sediment compositions. Another potentially diagnostic plant is *Durio graveolens* [78], which is a source of the FAME *n*-$C_{15:0}$, but occurs throughout the southern SCS.

Forests are distributed along the coast as well as on some offshore islands (Sabah Forestry Department 1989). In drier areas between mangroves, nipa palms and wet swamp forest rest transitional forest.

1.2.4.6 Sumatra

Rainforest and mangroves mainly cover Sumatra, as part of Indonesia. Both habitats are threatened by deforestation. From 1985 to 2010, Sumatra lost nearly 7 million hectares of rainforest and much of its rich biodiversity [79]. The reasons for this massive deforestation and forest degradation are due to the large-scale conversion to wood or oil palm plantations, including illegal logging and forest fires [80].

Mangrove forests are located on the east coast of northern Sumatra. They are severely threatened by anthropogenic interventions such as aquaculture, oil palm plantations and urban development [81–83]. The mangrove forests decreased by more than 61 % between 1990 and 2015 [84].

1.2.5 Fluvial Discharge

Rivers are of critical importance for transport of terrigenous material from land to the ocean. The terrigenous material composition influences the geochemical processes close to the coast, including degradation processes. Nearly every large river on earth is modified by human interactions and these modifications have wide reaching impacts on the global water cycle and ecosystems [85–88]. In Chapter 5, numerical models used to estimate marine and terrestrial proportions seemingly respond to changes in terrestrial lithologies. This however requires evidence that sufficient water masses, which carry the geochemical composition of these source regions, are transported. Therefore, available literature data is presented here. Most river systems in the study area are well constrained, except for Borneo and Sumatra, for which only estimates exist. It was therefore decided in this study not to include flows and signatures of OC from Borneo and Sumatra.

Almost half of the total sediment discharge in the SCS is derived from the island of Borneo and Sumatra and is estimated as 957 Mt/yr. [89]. Continental rivers in the source regions of the SCS supplied ~2.5 x 10^9 t/yr. (Gigatonnes per year) of suspended sediment in the past [90]; this flux is now less than 1 x 10^9 t/yr. as of 2007 [91], accounting for more than 10 % of the global sediment discharge [90]. The consequences of these fundamental changes in river sediment runoff are not foreseeable. The SCS is the world's largest sink of fluvial sediments in semi-enclosed and enclosed systems [16]. Nearly 80 % of the total SCS surface sediments are transported by rivers [92]. The role of dam construction is considered to be of strongest influence on sediment discharge estimates, requiring careful re-evaluation of sediment discharge rates [91, 93].

Across the wider study region, annual sediment discharge has decreased to less than 1 Gt over the past decade (as of 2007) as a result of human activities [91]. During the last 2000 years the sediment discharge has been a source of land formation, especially in delta regions [91]. Jointly, all major rivers in the wider study region (Yellow River, Yangtze River, Pearl River, Red River, Mekong River, Chao Phraya, and Irrawaddy River) deposited more than 40 km^2 of new land annually, sustaining delta plains along the Southeast and East Asian coasts. At present, new land formation has reached a standstill, with some delta areas starting to shrink [91].

Some of the main rivers that feed into the SCS are described in the following section. These include the Red River, the Mekong River, the Chao Phraya, and the Rajang, but also some small rivers like the Nanliu River in China or the Song Ba in central Vietnam (Fig. 5).

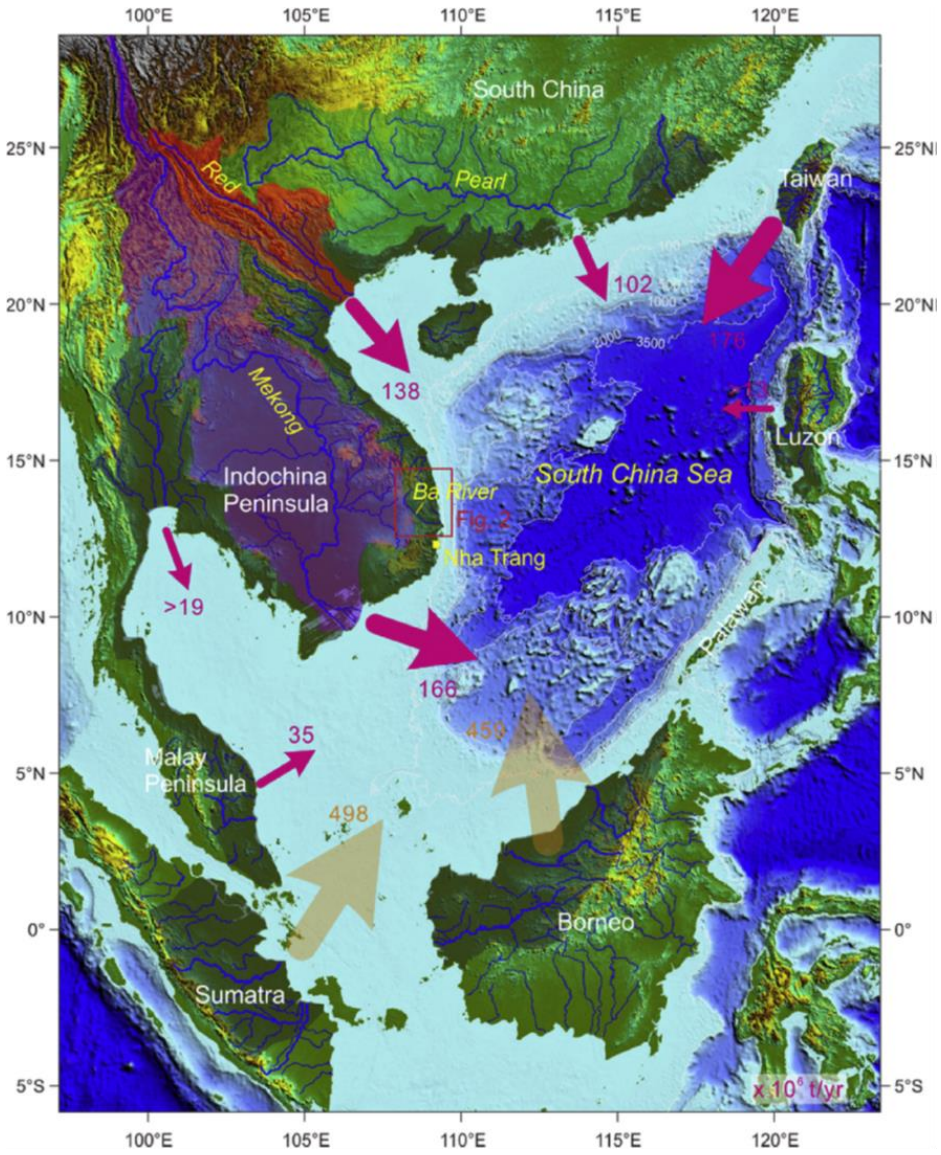

Figure 5) Sediment discharge has been estimated as taken from the study of Liu et al. [16]. The Mekong River and Red River are the largest contributors in the study area. Borneo, despite its high discharge rate, is relatively distal to the samples taken. The red arrows and numbers indicate observed fluvial sediment discharge (in million metric tons). The orange arrows and numbers are modal sediment discharge data for Sumatra and Borneo

1.2.5.1 Red River

The Red River is the second largest River of Vietnam; it has a total length of about 1.150 km [94], with the spring located in the Yunnan Province in China, at an elevation of ca. 2000 m [95]. The Red River is a heavily branched river system, widening the effective area it drains. The triangulate delta mouth (14 x 10^3km^2) and its coastal frontier are located in Vietnam with a total length of about 150 km. The Red River has two tributaries, the Da River in the north and the Lo River in the south [96]. Typical for the Red River is its characteristic red colour, caused by its sediment load rich in red laterite soil (mountainous upper reaches in Yunnan, China [97]). The Tectonic setting in East Asia causes a narrow, fault-controlled valley, which embeds the Red River. The valley

is located within the middle reaches [98]. After passing ca. 225 km of terrestrial area, the river flows into its triangular delta, surrounded by limestone cliffs at the northern and southern limits of the delta [97]. The Red River drains a total of ca. 160 x 10^3 km^2 of terrestrial matter [99]. The subtropical monsoon climate contributes to the erosion of the plane, especially during boreal summer. However, the sediment discharge of the main distribution has recently decreased from 20 – 25 Mt/yr. to ~10 Mt/yr., significantly effecting the delta. The principal reason for this massive decrease in sediment discharge is damming [100]. The sediment discharge from the Red River enters the Gulf of Tonkin and is finally deposit in the SCS [101]. The Red River estuary is influenced by tide, with a tidal range of ca. 4 m [102].

1.2.5.2 Song Ba

The Song Ba (Ba River) with a length of 390 km is the longest river of central Vietnam [103]. It has a drainage area of 14 x 10^3 km^2, and supplies 1 x10^6 t/yr. suspended sediment into the SCS [99]. The Ba River has its source in the Kon Tum Province, the river drains the basin in the highlands of Vietnam, which are at an average elevation of about 800 m [103].

1.2.5.3 Mekong River

The Mekong River is the largest river of Vietnam and the twelfth longest river of the world. The river runs also through the Tibetan Plateau, Yunnan Province in China, Myanmar, Laos, Thailand, and Cambodia. It has a total length of about 4800 km and an estimated drainage area of around 795000 km^2 (Lu and Siew 2006). The Mekong River springs in the highlands of eastern Tibet (Himalaya) at a mean altitude of about 5 km [104, 105] above sea level. The river is divided into two sections, the upper (which accounts for ca. 24 % of the total drainage area) and the lower Mekong River basin (with a drainage area of ca. 76 %) [105] and terminates in a triangular shaped delta. The climate of the upper Mekong River basin is very different compared to the lower part of the Mekong River. The upper Mekong River basin is located on the Tibetan plateau, which has a very cold climate. The lower basin part is influenced by tropical climate and by monsoon seasons [104]. The Mekong River had an annual sediment discharge of ca. 160 x 10^6t/yr. in the 90s [90]. Newer publications indicate sediment load discharge of about 110 x 10^6t/yr. [99] a net discharge decrease. The reason for decreasing sediment discharge is damming, with a negative impact on the ecosystem for the Mekong River region [104, 105].

The main part of the delta region is only <2 m above sea level, approximately 1 mi. ha are affected by tidal flooding and 1.7 mi. ha by salt water intrusion [71]. The river-mouth area is mesotidal with irregular semidiurnal tides. The mean tidal range is 2.5 m ± 0.1 m and the maximum tidal range is 3.2 m to 3.8 m [106].

1.2.5.4 Chao Phraya

The Chao Phraya located in Thailand is divided geographically into upper and lower basins. The upper basin is mountainous, with 40 % forest cover and 41 % cultivated land [107]. The lower basin has a total drainage area of 160 x 10^3 km^2 [99], other authors suggest a slightly lager discharge area of about 162 x 10^3 km^2 [108–110]. The river length in the lower basin is 1,200 km [99]. The Chao Phraya River, located in an urbanised region of central Thailand, passes through 11 regions along its 372 km path, including the largest cities in the country, Bangkok (current capital) and Ayutthaya (former capital). The basin covers roughly 31 % of the country's land surface and it is the largest river basin in Thailand. The total sediment discharge decreased from 30 x 10 km^2/yr. to 3 x 10 km^2/yr. [99] due to dam construction. Here the mean tidal range is ca. 1.2 m, and the maximum tidal range is ca. 2.5 m.

1.2.5.5 Rajang River

The Rajang River is located in East Malaysia (Sarawak) and with a total length of 560 km it is the longest river of the country [111, 112]. The size of the Rajang River drainage basin is about 50,000 km^2. The coastal plain is crossed by four large rivers, which have drainage basins of an average of 3,000 km^2 each. At the coast, spring tides range from 2.9 m to 5.8 m [113]. Peatlands with a thickness of 1 m – 20 m cover the delta area by 50 % to 80 %. The flow rates of the Rajang River vary considerably, between <100 m^3/s to about 3,600 m^3/s and transports suspended sediment loads between 0 mg/l to almost 2,300 mg/l. The addition of these fine-grained sediments increases the area of the delta by approximately 1.0 km^2/yr. [114].

1.2.5.6 Nanliu River

The Nanliu River is located in the Guangxi province in China and it is the largest River of southwest China [115]. It enters into the northeastern Gulf of Tonkin. The Nanliu River has a total length of ca. 280 km [115]. The total area of the catchment basin is ca. 9,700 km^2, which covers of cities of Qinzhou in its middle and Beihai in its lower reaches [116]. Topographically, the basin is high in elevation in the north and becomes

progressively lower towards the southwest. Downstream an alluvial plain developed (Hepu County), with fertile land [116]. The river has an annual discharge of $1.7 \times 10^9 m^3 – 8.0 \times 10^{10} m^3$ and an annual average suspended sediment flux of about 1.2×10^6 t [117]. The Nanliu is influenced by tides; mostly diurnal macro tides of up to 4.5 m induce long desiccation times of on average 18 h daily [118].

1.2.5.7 Other Rivers

In addition, there are many smaller rivers adding the SCS from the e.g. Vietnamese coast, without detailed records of sediment transport etc.. Their sediment discharge should not be neglected, but at present are not accurately quantifiable. However, it is estimated that they only contribute a few million tons to the sediment load, which is entering the SCS [16]. In general, most of the world's rivers are largely ungauged [119].

1.2.6 Seasonal surface ocean current dynamics

In the SCS, continental runoff and sea surface temperatures (SST) fluctuate in response to seasonal climate cycles and monsoonal intensity. In boreal summer, SST range between 27.5 °C and 29.5 °C [120], alternating with 20 °C and 24 °C during boreal [121]. Previous studies have demonstrated that the surface waters are partially mixed with water from the Pacific Ocean via the Kuroshio Current, which enters the SCS through the Luzon strait (e.g. Lie et al.; Chern et al.; Chen et al. and Lüdmann et al. [16, 122–124]). The Kuroshio Current mixes with the SCS waters up to a depth of ca. 300 m [125]. The majority of samples investigated in this study are affected only by surface and intermediate current dynamics, which are introduced below.

The upper layer circulation directly responds to the seasonal changes of monsoon wind stress curl, with additional influence from the Kuroshio Current in its northern part tangential to the study area [126]. During boreal winter, a basin-wide cyclonic gyre (the NW Luzon Cyclonic Gyre) develops in the northern SCS (Fig.4). This gyre is comprised of two units, one directly northwest of Luzon (called NW Luzon Cyclonic Eddy) and the other located at about 17 °N and 116 °E [127]. The northeast SCS warm current is a flow separated from the SCS Branch of the Kuroshio Current. The coastal current along the northern shelf (called the Guangdong Coastal Current) flows southwestward during the winter monsoon, controlled by its winds. In summer, the NW Luzon Cyclonic Gyre still exists in the northern SCS but weakens and shifts eastward, while the NW Luzon Cyclonic Eddy remains in position, almost stationary [127]. The mesoscale anti-cyclonic SCS branch of the Kuroshio/SCS warm current eddies shifts southeast ward and the

reversed Guangdong Coastal Current merges with the SCS warm current, to become the prevailing north easterly surface current forced by the summer monsoon winds [16] (Fig. 4). Controlled by the NW Luzon Cyclonic Gyre, the coastal current west of Luzon (called the NW-Luzon Coastal Current) flows to the north, unaffected by monsoon winds. The intrusion of the Kuroshio Current can occur any time of the year but is a transient phenomenon, present less than 30 % of the year [128]. The westward movement of mesoscale eddies originating from the Kuroshio Current intrusion is important for the transport of mass, heat, salt, and sediment in the northern SCS [129]. Driven mainly by monsoon winds, the southern SCS is dominated by the SCS Southern cyclonic gyre in winter, which extends onto the northern Sunda Shelf [127]. At the northern edge of SCS southern anti-cyclonic gyre is a very strong offshore-directed jet called the SE Vietnam Offshore Current, which is located at a latitude of about 11°N [16]. The central SCS circulation is governed largely by the interaction between the northern and southern SCS current systems although it is not yet well understood (e.g. Liu et al. [16]).

Circulation in the Gulf of Tonkin was traditionally considered to follow seasonal monsoon atmospheric patterns with north-easterly winter winds forcing a gulf-wide cyclonic gyre, and south-westerly summer winds driving an anti-cyclonic circulation [121, 130]. Recent measurements and simulations, however, identified that the Qiongzhou Strait (Fig. 4) plays a key role in the establishment of a cyclonic gyre in summer [38], effectively resulting in cyclonic circulation in all seasons for the Gulf of Tonkin [131–133]. In the Gulf of Thailand, surface currents are driven mainly by seasonal monsoon winds and are anti-cyclonic in summer (March – August) and cyclonic in winter (September–November), with weak currents throughout the area during January to February [134].

Satellite images and dynamic computations reveal a cross-basin wind-induced summer surface jet flowing northeastwards from central Vietnam. The jet speed declines to 0.20 m/s at 50 m water depth [53] and extends from 110 ^{o}E, 10 ^{o}N to 120 ^{o}E, 18 ^{o}N. This is proximal to the boundary between the southern and northern parts of the SCS [126, 135] and close to the axis of maximum monsoonal winds [136, 137]. The water temperature in the areas where upwelling occurs is typically ~ 24 °C - 25 °C, 3°C - 5 °C lower than surrounding water [138].

The currents in the western SCS form a complex system that has not yet been fully described [16, 139]. The current lack of a detailed and accurate current map covering the

entire SCS complicates the use of localised current models, since they may well be associated with large uncertainties. Instead, a regional model for marine currents in the SCS seems the more robust approach. Su et al. [1], incorporated global parameters to derive a current model for the entire SCS, based on MPIOM (Fig.6a and b).

MPIOM is a free-surface ocean general circulation model formulated on a z-coordinate system in the vertical and an Arakawa-C Grid [140]. Marsland et al. [141] gives details of the model equations, bulk formulae and physical parameterisations. Arbitrary placement of the model's poles on an orthogonal curvilinear grid offers advantages over conventional grids. It allows for the construction of regionally high-resolution models that maintain a global domain and thus avoid the problems associated with open boundaries [141, 142]. Further details about the used model can be found in Su et al. [1].

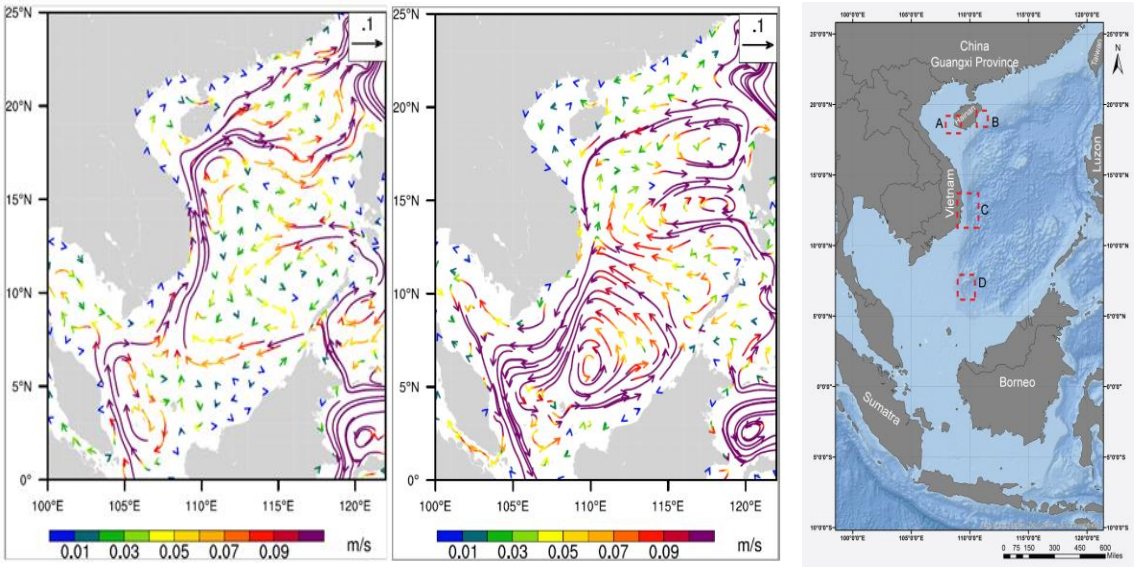

Figure 6) Average surface currents during summer (a (left)) and winter (b (middle)), based on MPIOM model by Su et al. [1] and upwelling areas (c (right)). During winter, the southern and eastern part is characterised by well-defined cyclonic structures. During summer, only loosely defined large-scale patterns are visible

1.2.7 Primary production

The central deep part of the SCS is largely oligotrophic [55], contrasted by the biologically highly productive shelf regions, driven by local fluvial discharge events [51, 143] and seasonal upwelling in certain regions (Fig. 6c).

During the summer monsoon, high biological productivity is augmented by southwest winds and the associated mixing of the upper water column, as well the nutrient supply from the numerous rivers draining the coastline [51, 143]. Marine OM production, especially in the Gulf of Tonkin near Hainan and along the continental margin east of

Vietnam, is strongly influenced by continental upwelling [144]. Similar to cold eddies, these upwelling cells serve as rapid and efficient transport pathways for carbon and nutrients, as documented by high quantities of Chlorophyll-α (Chl-α) during boreal summer [145]. Across the study shelf area, nutrient and Chl-α-concentrations are seasonally influenced by hydrographic patterns, with high variability in winter compared to the summer [145, 146]. Tropical storms during the monsoon seasons contribute to deep mixing of the water column, transporting nutrients to surface waters enhancing primary production [147].

The monsoonal impact on the current dynamics are physically restricted by thermohaline properties, limiting the impact to a maximum of ca. 350 m water depth [148]. This implies that intermediate and deep waters in the SCS are unaffected by direct monsoonal influence. Instead, they are influenced by fluctuations in the inflow from the Western Pacific through the Luzon Strait [149, 150].

1.2.8 Southern SCS shelves as regions of prime carbon production and OM burial – a geological perspective

Although not a direct study object of this project, the geological dimension of the study area is summarised as a dynamic region of major carbon production and burial linked to Late Quaternary glacial-interglacial sea level fluctuations. With sea level lowering well above 100 m during the last glacial maximum [151, 152], a pattern that re-occurred in earlier glacial stages, large parts of the SCS shelf (in particular the Sunda Shelf, which covers 1.85 million km^2 [153]) developed into terrestrial lowland areas, supporting lush tropical vegetation and massive carbon stocks [154]. These lush lowland forests on glacial Sunda Land would have been flushed during terminations and finally drowned during interglacial, turning major terrestrial carbon sinks into carbon source to the atmosphere. This glacial-interglacial perspective is well studied for the Sunda Shelf region, where large palaeo-drainage systems testify to the existence of such lowland terrestrial environments. These changes in sea level are important when interpreting present day marine surface sediment samples, as these sediments might have been above sea level in the past, thus potentially representing a mixed terrestrial and marine milieu. The Sunda Shelf has been identified as a palaeo-plain during the last glacial maximum (ca. 14 ka), while the extent of the SCS was drastically reduced during this time period [155]. During the Pliocene and Pleistocene, this low-gradient coastal plain was tectonically stable, while the modern Malayan Peninsula and the Borneo and Sumatra

Islands constituted highlands. From these highlands, several river systems originated, which drained the coastal lowland during the last glacial maximum and early stage of late-glacial flooding [156]. Detailed palaeo-maps are provided in figure 7. Of importance for the present study is the largest palaeoriver from this area, the Molengraaff River (e.g. Wong et al. [157] Fig. 7 and 8), which flowed in north-eastern direction in proximity to one of our sample transects from the Sunda Shelf into the deep basin.

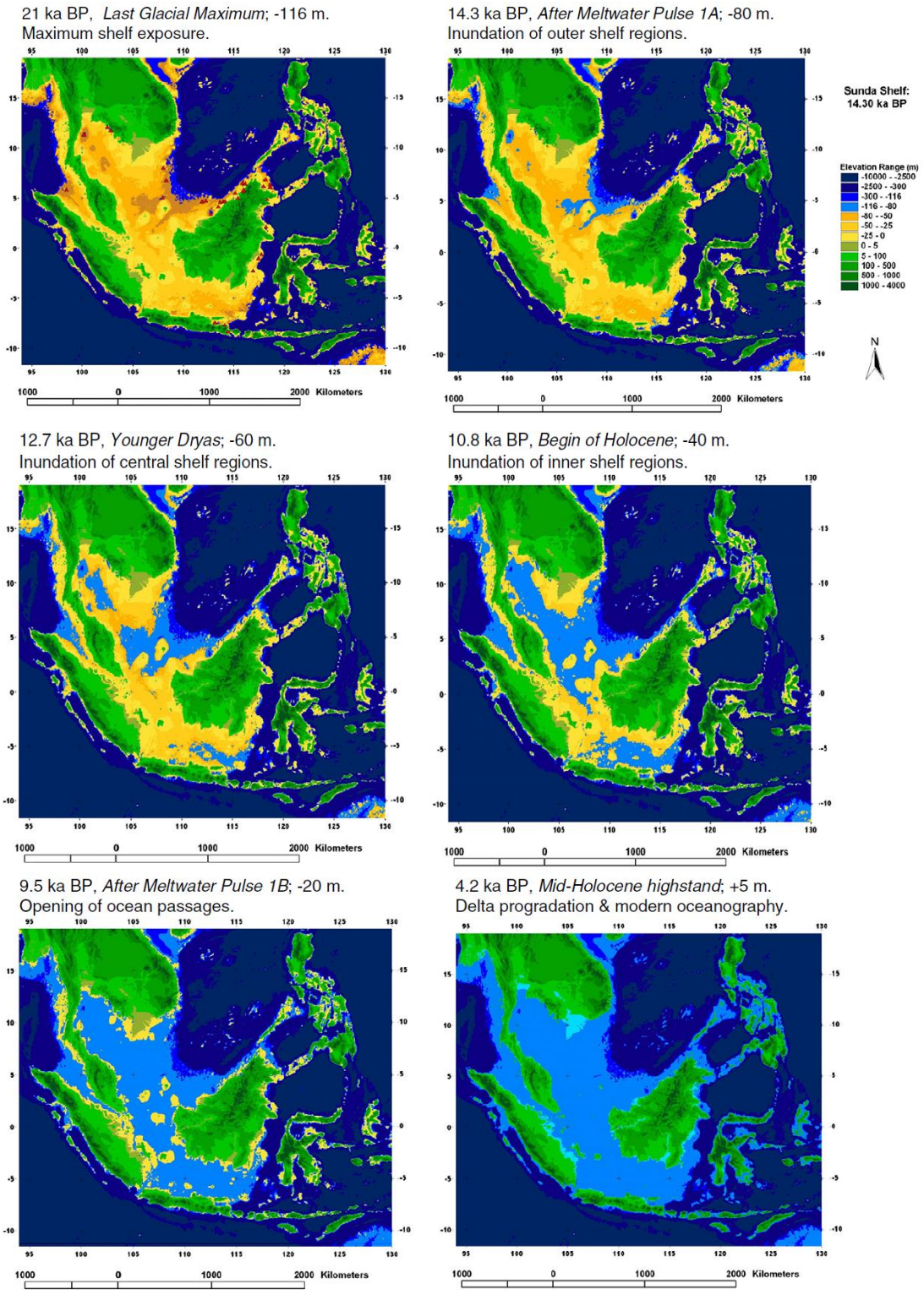

Figure 7) Palaeo-reconstruction of the study area by Hanebuth et al. [152]. The reconstruction is based on present-day bathymetric depth contours taken from the National Geophysical Data Centre (see Hanebuth et al. [152])

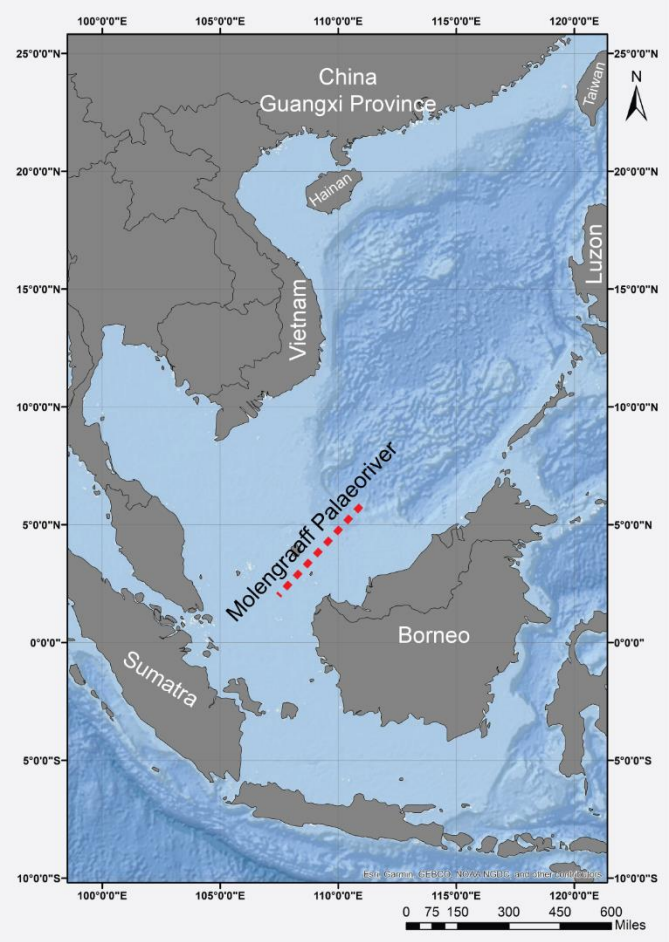

Figure 8) Approximate Molengraaff Palaeoriver location in the present day South China Sea, relevant for the interpretation of data discussed in this study.

1.2.9 Agriculture and synthetic herbicides

This project also takes the opportunity to include persistent organic pollutants (POPs) of environmental concern into its work strategy, namely the thiocarbamate triallate and isomers tris(2-chloroethyl)phosphate and tris(2-chloroisopropyl)phosphate (TCPP 1 and TCPP 2). This aspect directly links with urgent questions about sustainable use of land and oceans and contributes to an up-to-date inventory of organic pollutants in the shallow and deep marine environment. Because of the geographical and historical context of the study region, especially Vietnam, the focus lays on evidence for preservation of synthetic herbicides on the estuarine and marine surface sediments.

At the beginning of the 20th century, scientists in Europe and the US were developing herbicides to increase agricultural productivity by killing unwanted plants [158]. Nowadays, excessive use of herbicide in urban areas and crop farmlands globally leads to concerns about contamination and health in soils, groundwater, lakes, rivers, rainwater, estuaries and the atmosphere [159]. The environmental impacts and toxicity of herbicides

on the flora and fauna are (intentionally) radical, yet the longer-term environmental fate of these synthetic compounds is not well studied and certainly not well mapped/monitored. According to the Food and Agriculture Organization of the United Nations and the World Health Organization, global agriculture production is expected to increase by over 70 % by 2050 (relative to 2007) [5], which will inevitably result in a marked increase in the use of herbicides, globally. This situation is likely to cause massive but unforeseeable challenges that will affect the environment and ecosystems from local to global scale.

Coastal and shelf systems, including the coastal outflow of terrestrial freshwater systems, mark critical transition zones where terrestrially derived OM and mineral load might be associated with export and dispersal of herbicides in the marine environment. Inner-shelf regions off the Mekong River delta and the Vietnamese Shelf are strongly impacted by alternating coastal-parallel currents, where materials form continental export and marine production is re-mobilised and transported away towards areas with reduced current strength further out in the ocean. The abundance and distribution of herbicides are expected to follow the pathways for terrestrial OM, which is known to be controlled by a variety of factors that strongly vary at the local scale (e.g. hydrodynamics, oceanography, seasonality, tectonic regime, OM provenance, and degree of degradation). The robust nature of herbicides [160, 161], however, significantly enhances the preservation potential of these compounds, compared to natural terrestrial and marine OM. The presence of compounds which have existed for less than 100 years in marine surface sediments of the SCS, far off river mouths and the coastline, has not been reported before. But if encountered, provide insights into the settling and fixation of OM in marine settings, while also impacting the evaluation and interpretation of Δ^{14}C age information.

2 Material and Methods

The marine surface sediments for this study were sampled during several trips over two decades. These are SO-115 (1996), SO-140 (1996), SO-187-3 (2006), and SO-220 (2012) for more details see Cruise reports (available: https://www.pangaea.de/expeditions/cr.php/Sonne_1969). The deep sea surface samples were taken by the SIO with the R/V Xiangyanghong-10 (FS Towards-the-Red-Sun 10) in 2015; samples around Hainan were also obtained by SIO using the R/V Zhongguoyuzheng (FS Chinese-Fishery-Service) in 2005. The here used samples are taken by box core samplers, where the surface sediments (1 cm) are extracted. The original box-cores are stored at the University of Kiel (Germany).

The University of Tongji and the University of Hamburg took river sediment samples in Vietnam in 2005, in Malaysia from 2006 to 2009, and in China in 2012 (including Hainan). Sample campaigns from the University of river sample campaigns are described in Liu et al. [16, 43, 48]. The collaboration partners from Germany and China provided the samples investigated in this project and the data are summarised in Appendix.

2.1 Carbon/Nitrogen and Organic Carbon analysis

The most common derived information from C_{org}/N_{total} and TOC data serve to differentiate planktonic / algae OM from terrigenous material. In the aquatic environment, the ratio of organic carbon (OC) to total nitrogen is a variable to distinguish land and sea sources. Land plants generally have a higher C_{org}/N_{total} ratio than aquatic algae. This is related to the fact that land plants have a cellulosic and ligninous support skeleton, which are lacking in marine plants, shifting the ratio of C_{org}/N_{total} towards higher values.

Carbon and nitrogen are the most common elements in OM, besides oxygen and hydrogen. Carbon is a major constituent of lignin, carbohydrates, lipids, waxes, cutins, proteins, and nucleic acids (among others in DNA with the bases adenine, thymine, guanine, and cytosine). Nitrogen, instead, is a main constituent in nucleic acids, proteins, amino acids, purines, biogenic amines, polyamines, creatines, porphyrins and amino sugars [162, 163]. Higher plants have a much lower protein content than animals (C_{org}/N_{total} ratio: 3). Lower plants (primary production - C_{org}/N_{total} ratio: 6), which represent the majority of organic production e.g. algae etc. in the sea, have a nearly equal

C_{org}/N_{total} ratio to zooplankton (secondary production - C_{org}/N_{total} ratio: 5.4 - 5.9) due to the high protein content [164].

OC and nitrogen are representative of the proportion of organic substances in sediments [165], but only small amounts are present in most sediments [29]. Principal sources of OC in marine sediments are primary production (phytoplankton: e.g. diatoms, dinoflagellates, coccolithophores, cyanobacteria and silicoflagellates) and secondary production (zooplankton: e.g. crayfish, foraminifera, radiolarian and medusa) in the euphotic zone. The photosynthetic production of aquatic primary producers is the dominant supplier of OM. Chlorophyll pigments are used to convert dissolved inorganic carbon (DIC) and nutrients into OM while consuming energy (light). Phytoplankton provides a source of food for secondary producers. The faeces of these secondary producers and the remnants of the primary phytoplankton contribute to the aquatic OM budget. A third factor is the admixture of terrigenous OM from higher plants and soils through riverine and aeolian transport [166].

The enrichment with inorganic material in e.g. clastic sediments or carbonates can affect the concentration of total carbon (C_{total}), as well as the particle size fraction of a sediment [167].

In clay minerals, primarily in illite, inorganic nitrogen is predominantly fixed in the form of ammonium [168]. Clay minerals are negative charged and may contain positive charged particles. The bonding strength between the clay mineral and the particle depends on the position of the bond [169]. The strongest bond (as non-exchangeable NH_4 +) occurs at the intermediate layers of clay minerals on aluminium silicates [164, 170].

In the analysis of sediments, it is complicated to distinguish between organic and inorganic nitrogen. Therefore, the total nitrogen content is used. Phytoplankton and zooplankton are particularly enriched in proteins (containing nitrogen) that make up between 50 % and 70 % of the organism, in contrast to carbohydrates and lipids as well as other resistant substances of higher plants (represented by carbon), are preferentially degraded. Selective degradation of nitrogen over carbon in the water column and in the sediment results in a decline in the element ratio. The C_{org}/N_{total} ratio of surface water is 4 - 7, increasing to 10 - 12 in deeper water layers (e.g. Hollerbach, [162]).

In the water column, particulate organic carbon (POC) occurs in the form of small, suspended particles (1 μm - 53 μm) up to large, rapidly sinking aggregates (> 0.5 mm).

In the photic zone, suspended particles clump together i) by physical processes such as collision and stickiness, and ii) biological activity (scavenging and bio-aggregation) [171] and sink to the ocean floor. During descent, they catch more suspended particles and free-living bacteria, which they partially release during the descent. This aggregation and disaggregation cycle is responsible for the presence of suspended particles at greater depths [172].

From the euphotic zone, only a small fraction of dead OM that could potentially reach and be stored in the surface sediment sinks to the ocean floor. Most of the OM flux is integrated in the food web or re-mineralised by photo oxidation, strongly affecting/reducing the carbon flux to the sea floor. Two sinking processes can be distinguished, either as a particulate fraction (POM, POC or "marine snow") or in "dissolved" form (DOM) with compounds < 45 μm, the transitions between the two states being dynamic [173]. The faster the particles sink, the higher is their potential for preservation, as they are less affected by mineralisation or modification by bacterial degradation processes within the water column [162] and in the upper oxic, bioturbated sediment layers [174].

2.1.1 Analytical procedures

The total carbon and nitrogen content in sediments is determined using the CHN elemental analyser (CARLO ERBA NA-1500) [175].

Before determining the total N and total C content of the samples to be analysed, the CHN elemental analyser was calibrated. For this purpose, three tin cartridges containing about 0.2 mg - 0.3 mg acetanilide (C_8H_9NO) as standard with the known carbon and nitrogen contents of C = 71.09 % and N = 10.36 % were prepared, sealed and placed in the autosampler (sample tray), which ensures automatic delivery to the CHN elemental analyser. In order to be able to asses any measurement errors, an empty tin cartridge is always included as blank in the calibration.

To determine the total C and total N contents of the sample, ~ 1.5 mg are weighed into the tin cartridges for analysis. The sample is combusted while adding a defined amount of oxygen at 1020 °C to the oxidation reactor. A complete oxidation of the sample is achieved by the addition of pure oxygen and by catalytic action of the chromium (III) oxide and silver-coated cobalt oxide in order to extract the halogen compounds in the sample material. The CO_2 and nitrogen oxides (NOx) produced during combustion are passed under helium flow (80 ml / min) into a reduction reactor filled with reduced copper

as a catalyst. The nitrogen oxides are reduced by removing the oxygen at about 600 °C, to N_2.

Any remaining water is collected using magnesium perchlorate ($Mg(ClO_4)_2$) in a water trap. In a gas chromatographic separation column, N_2 and CO_2 are separated. For the qualitative and quantitative analysis of the gases, they are passed through a heat conductivity detector.

To determine the total organic carbon (TOC) of the samples, total carbon is separated into calcium carbonate and organic carbon. In a silver cartridge, the sample is drizzled with 1N HCl until no more CO_2 evolution occurs. The sample is then dried and analysed using the CHN elemental analyser. The method allows rapid and routine analysis of marine sediment with a relative error quotient of ± 0.3 % for TOC and ± 1.6 % for nitrate [176].

2.1.2 Calculation: C_{org}/N_{total}

The C_{org}/N_{total} ratio is calculated as follows

Equation 1) Calculation of Carbon/Nitrogen ratio

$$C_{org}/N_{total} = {}^{TOC}/_{12.011u} \times {}^{N_{total}}/_{14.007u}$$

2.2 $\delta^{13}C_{org}$

Carbon has two stable isotopes, ^{12}C, and ^{13}C. ^{12}C is represented with approximately 98.9 % in the land-ocean-atmosphere system (see e.g. Wagner et al. [177]). ^{13}C accounts for ~ 1.1 % [178]. The ratio of stable isotopes serves to quantify various parameters and to temporal classification of climatic changes (e.g. Galfetti et al. [179]) as well as to analyse food network relationships (e.g. Traugott et al. [180]). Lighter isotopes are energetically more favourable due to their lower mass in chemical reactions and accumulate in equilibrium reactions in the final product. For this reason, the reaction product is always lighter than the starting material. For the determination of the source of organic material in the sediment, $\delta^{13}C_{org}$ values are often used. The $\delta^{13}C_{org}$ values for recent natural samples typically give negative values, since the isotope ratio of the reference material Pee Dee Belemnite (PDB) or Vienna Pee Dee Belemnite (VPDB) is higher than that of the biomass on land and in the ocean in recent days. If a plant is operating photosynthesis, the lighter ^{12}C is preferred. This results in different $\delta^{13}C_{org}$ values for different plant types. C_3 plants, which make up the largest proportion of the terrigenous flora, have $\delta^{13}C_{org}$ values of -26 ‰, C_4 plants (including grasses) have an

average $\delta^{13}C_{org}$ value of -13 ‰ [181], whereas marine phytoplankton is at a $\delta^{13}C_{org}$ value between -19 ‰ - 21 ‰ [182].

The original Belemnite no longer exists, so that the International Atomic Agency (IAEA, Vienna) defined an alternative standard, the VPDB. The isotope ratio is slightly depleted in the VPDB compared to the PDB. The VPDB gives a mean ^{12}C / ^{13}C ratio of 0.0111802 [183]. The comparison between standard and isotope ratio is calculated according to the following formula [182, 184]:

Equation 2) Calculation of $\delta^{13}C_{org}$

$$\delta^{13}C\ [‰] = \left(\frac{R_{sample} - R_{standard}}{R_{standard}}\right) \times 1000$$

R = isotope ratio of the sample or the standard

The here presented data were obtained at Iso-Analytical Ltd, Cheshire UK, an external service laboratory. The laboratory procedure for sample processing is described below.

Weighed samples are placed in universal tubes, acidified with 2M hydrochloric acid, mixed, oven heated at 60 °C for 2 hours and left for 24 hours to allow all carbonate to be liberated as CO_2. The sample fractions are then isolated by centrifugation and the acid is decanted. The samples are then washed twice using distilled water and centrifuged again. After acid washing, the fractions are oven dried at 60 °C.

The samples are then analysed using an Elemental Analyser - Isotope Ratio Mass Spectrometry (EA-IRMS). In brief, tin capsules containing sample or reference material are loaded into an auto-sampler on a Europa Scientific elemental analyser, from where they were dropped in sequence into a furnace held at 1,000 °C, where they are combusted in an oxygen rich environment, raising the temperature to ~1,700 °C. The gases produced on combustion are swept in a helium stream over combustion catalyst (Cr_2O_3), copper oxide wires to oxidise hydrocarbons and silver wool to remove sulphur and halides. The resultant gases, N_2, NO_x, H_2O, O_2, and CO_2 are swept through a reduction stage of pure copper wires held at 600 °C. This step removes O_2 and converts NO_x species to N_2. A magnesium perchlorate chemical trap removes water. CO_2 is separated from nitrogen by a packed column gas chromatograph held at an isothermal temperature of 100 °C. The resultant CO_2 chromatographic peak enters the ion source of the Europa Scientific 20-20 IRMS where it is ionised and accelerated. Gas species of different mass are separated in a magnetic field, then simultaneously measured using a Faraday cup collector array to measure the isotopologues of CO_2 at *m/z* 44, 45, and 46.

2.2.1 Reference Standards and Quality Control

The reference material used during $\delta^{13}C$ analysis of the samples is IA-R001 (wheat flour, $\delta^{13}C_{V\text{-}PDB}$ = of -26.43 ‰).

IA-R001 is calibrated against and traceable to IAEA-CH-6 (sucrose, $\delta^{13}C_{V\text{-}PDB}$ = -10.43 ‰). IAEA-CH-6 is an inter-laboratory comparison standard distributed by the International Atomic Energy Agency (IAEA), Vienna.

The total ion beam data was used to determine the percentage carbon of the acid washed samples. The weight loss data recorded at the acid washing stage was used to calculate the percentage TOC values from these percentage carbon values.

2.2.2 Calculation of relative fractions of terrigenous and marine OM based on bulk carbon isotopes

Isotopic measurements of natural samples mostly deviate from the stated reference values. Therefore, first the marine and terrigenous "end-members" have to be determined, adjusted to the study region. The relative proportion of marine and terrigenous OM can then be modelled by assuming that the measured isotope ratio of the sediment is composed of the isotopic ratios of the proportionate marine and terrigenous end-members. The percentage of marine OC (C_{marine} %) from TOC can be calculated as follows [185]:

Equation 3) Calculation of the relative marine OM fraction based on carbon isotopes

$$C_{marine}\,\% = \left(\frac{(\delta^{13}C_s - \delta^{13}C_t)}{(\delta^{13}C_m - \delta^{13}C_t)}\right) \times 100$$

$\delta^{13}C_s$ = isotope ratio of the total sediment
$\delta^{13}C_m$ = isotope ratio of the marine end-member
$\delta^{13}C_t$ = isotope ratio of the terrigenous "end-member"

The percent terrigenous fraction ($C_{terrigenous}$) of the total sediment is calculated according to the formula:

Equation 4) Calculation of the relative terrigenous OM fraction based on carbon isotopes

$$C_{terrigenous} = 100 - C_{marine}$$

2.2.3 Calculation of terrigenous and marine proportions

The absolute terrigenous and marine parts of the samples are to be calculated according to the following equation:

Equation 5) Calculation of terrigenous and marine proportions

$$C_{org_{at}} = \left(\frac{tA}{100}\right) \times C_{org}$$

$C_{org_{at}} = C_{org}$ *absolute terrigenous share*
$tA =$ *percentage terrigenous portion*

2.3 Mineral Surface Area (SA)

The general relationship between grain size and TOC is commonly that smaller grain sizes show higher TOC [186, 187]. The positive correlation between TOC and fine grain-size-fraction is attributed to clay minerals and their properties. Clay minerals are efficient in binding with OM (e.g. Kleber et al. ; Blair and Aller, [188, 189]) and due to their sheet silicate structure higher SA to volume ratios. In non-ideal or natural systems, the slope between TOC and SA can be variable [189–191].

The SA analysis was carried out using the BET-method according to **B**runauer, **E**mmett and **T**eller [192] at ETH Zurich. It is based on nitrogen gas adsorption to calculate the specific surface area or surface area per unit mass of a sample. The BET surface area is determined by the number of adsorbed nitrogen gas molecules. The SA analysis sample (1 g) is placed in a vial of known volume. Samples are first heated to 350 °C for 12 h, after which they are freeze dried for 12 h, to remove OM, and then degassed at 200 °C. The "bulbs" at the bottom of the vials containing the sediments are dipped into liquid nitrogen, using a NOVA 4000e Surface Area & Pore Analyzer from Quantachrome. Then, Isothermal conditions are established. The resulting isotherm is used to calculate the SA, and uncertainties are typically < 0.1 %. The isothermal multi point regression is typically linear.

2.4 Radiocarbon Analyses: ^{14}C- dating

In 1946 developed by Willard Frank Libby (1908-1980), the radiocarbon method for dating samples between 1,000 to 50,000 years was established. A recently written summary can be found in e.g. Encyclopedia of Marine Geosciences [193].

Neutron bombardment of ^{14}N in the upper atmosphere results in the production of ^{14}C by proton ejection from the ^{14}N. The newly formed ^{14}C is radioactive, with a half-life time of ca. 5,730 years. Libby [194] proposed that the rate of production and mixing of ^{14}C from the atmosphere and e.g. the ocean remained constant over several thousands of years, which permits us to exploit the ^{14}C as a chronometer. The radiogenic ^{14}C constitutes about 1.2 x 10^{-10} % of total carbon, requiring extremely precise determination

of isotope ratios. The ^{14}C in the atmosphere is absorbed as CO_2 by plants and may finally be accumulated in animal organisms. Ultimately, the constant production of ^{14}C in the atmosphere results in equilibrium between the atmospheric carbon isotopic composition and the carbon isotopic composition of living organisms. Upon the death of living organisms, the OM is isolated from the equilibration process and the ^{14}C content follows the predictions from radiogenic decay [194]. From the measurement of the specific activity (which is determined individually for each sample) of a sample and comparison to that of recent carbon isotopic composition, the time since the sample was removed from the carbon cycle may be determined [194]. It may be noted, however, that fluctuations in cosmic ray activity will introduce oscillations in the ^{14}C production rate and this was first documented and described by De Vries [195]. He demonstrated discrepancy between the radiocarbon date and calendar age of trees may be related to the climate changes or cosmic ray activity, which was further supported by the study of Suess [196]. Stuiver, [197] had previously demonstrated that these radiocarbon date discrepancies correlated directly with cosmic ray activity.

Prior to analysis of carbon isotopes, the samples need to be purified. Acidification of sample material by exposure to an acid vapour is the gentlest method to preserve the sample while dissolving unwanted carbonate without the loss of water soluble carbon [198]. The presence of carbonate artificially increases $\delta^{13}C$ and $\Delta^{14}C$ values [199] and results in incorrect measured ratios. Furthermore, ^{14}C dating can be biased by component mixing. Therefore, removal of $CaCO_3$ by an acid gassing process is essential to avoid mixed component $\delta^{13}C$ values. Ground samples are weighed relative to their TOC content into Ag capsules and stored in glass vials. To dissolve the unwanted carbonate, the samples are placed into a dissector under an acid vapour atmosphere. The acidic environment is obtained by heating fuming 36 % HCl in a closed system, in an oven up to 60 ˚C for 72 h. To neutralise and dry the samples the HCl is exchanged by addition of NaOH pellets and placed in the oven for another 96 h. This step is necessary to prevent degradation of the capsules during storage/transit and corrosion of the mass spectrometer during measurements. After decarbonisation, samples are transferred into Sn capsules [10, 200].

The samples were measured with the Elemental Analyser – Isotope Ratio Mass Spectrometer – Accelerator Mass Spectrometer (EA-IRMS-AMS) at ETH in Zurich, the AMS is a mini radiocarbon dating System (MICADAS) [201]. Although Brodie et al. [202] note that results of samples preparation with acid fumigation are

inconsistent and less reproducible, acid fumigation is the preferred method. The liquefaction of carbonates leaches DOM, which leads to even larger uncertainties in radiocarbon analyses as compared to the acid fumigation method. Larson et al. [203] also note that the sample material must be wet during the acid fumigation under vacuum conditions; otherwise, salt precipitation can be an issue. To prevent this, deionised water is added to the samples. In this study, the acid fumigation was modified not involving any vacuum. The humidity in the desiccator during fumigation is found sufficient to prevent salt precipitation. Furthermore, the humidity will allow more rapid diffusion of the acid fumes through the sample matrix.

The $\Delta^{14}C$ value represents the ratio between the isotopes ^{14}C and ^{12}C and the additional normalisation factor (standard reference material). The $\Delta^{14}C$ notation is calculated according to the equation:

Equation 6) Calculation of radiocarbon $\Delta^{14}C$ values

$$\Delta^{14}C = \left[Fm * e^{\lambda(1950-Y_c)} - 1\right] * 1000$$

Fm = fraction modern
Y_c = sampling year
λ = 1/ (true mean-life) of radiocarbon = 1/8267 = 0.00012097

where fraction modern (F_m) is a measurement of the deviation of the samples radiocarbon content from that of the modern standard (e.g. VPDB or NBS Oxalic Acid II). Modern is defined as 95 % of the radiocarbon concentration (in A.D. 1950) of NBS Oxalic Acid II, normalised to $\delta^{13}C_{VPDB}$ = -19 ‰ [204] and λ is the half-life time of carbon.

The experimental setup involving an EA-IRMS-AMS permits the sequential analysis of all C isotopes, at the expense of lower (ca. 1 %) precision on the ^{14}C measurement. The $^{13}C/^{12}C$ ratio is determined with high precision by the IRMS and the results are carried over to the evaluation of the ^{13}C and ^{14}C analysis by the AMS (0.3 % uncertainty). This permits precise correction for fractionation of C isotopes, which is found to be ca. twofold higher for ^{14}C relative to ^{13}C.

2.5 Introduction and definition of $\Delta^{14}C$ terms used in this study

For the purpose of discussion of $\Delta^{14}C$ data, this study introduces and defines three terms, i.e. potent, recalcitrant, and inert:

The discussion of bulk ^{14}C dates obtained from surface sediment (marine and terrestrial) demands clarification of the origin(s) of radiocarbon reservoirs and their respective

composition. Such clarification can be obtained from identification of discrete radiocarbon reservoirs in sediments, and key processes that may influence the interpretation of $\Delta^{14}C$ signatures. A simple conceptual model of three carbon pools and their effects on bulk $\Delta^{14}C$ are illustrated in figure 9. In this concept, carbon reservoirs are not defined by their origin, but by their reactivity and/or state of decomposition, which illustrates the discussion of degradation effects on bulk sediment radiocarbon ages. The first scenario considers that the amount of potent and recalcitrant OM is reduced because of degradation and transport, converting potent OM to recalcitrant and finally inert, while recalcitrant is converted to inert, resulting in a consistent and effective increase of the inert fraction, at the expense of the other two fractions. Alternatively, or in addition, if transport not only facilitates degradation but also removal of a TOC fraction, by e.g. microbial consumption and/or remineralisation, the inert fraction will grow over proportionally. This en-route removal will bias the bulk $\Delta^{14}C$ signature of the sink/host sediment towards the inert OM fraction (Fig. 9). The outcome of both processes would be similar, an increase in the inert OM fraction, but the level of increase will differ, affecting the age of the bulk OM pool.

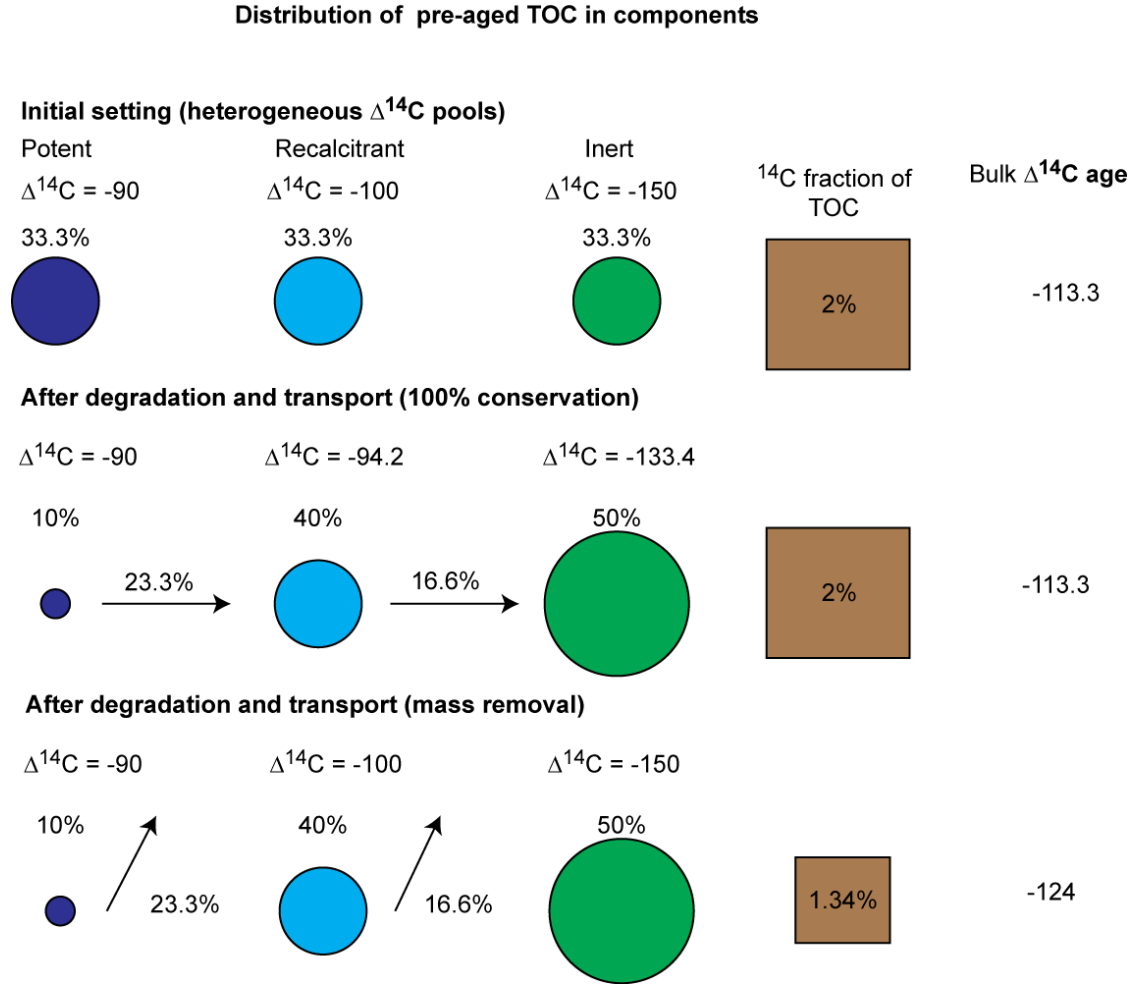

Figure 9) The response of the $\Delta^{14}C$ systematics of bulk sediment samples is modelled under the assumption that three C pools are participating (potent, recalcitrant and inert), which exhibit contrasting $\Delta^{14}C$ dates. The three pools form the uniform bulk age of -113.3 when the proportions between the reservoirs are equivalent (section A). In a first scenario, degradation and transport of the sediment and organic carbon (OC) result in modification of the proportions between the pools. The potent fraction diminishes, and part of the degradation products of the potent fraction now contribute to the recalcitrant fraction. Some components of the recalcitrant fraction degraded and now contribute to the inert fraction, but the addition of degradation products from the potent group result in a net growth of the proportion recalcitrant *vs.* potent. However, if the system remains closed during this transport and degradation process, the $\Delta^{14}C$ of the potent, recalcitrant, and inert fractions will be partially equilibrated (section B). While the proportion of the inert fraction has grown, its initial $\Delta^{14}C$ signature now more closely resembles that of the recalcitrant and potent fraction, subsequently, the bulk sediment $\Delta^{14}C$ signature has not changed, although the sediment has matured/degraded. It should be noted that with progressing degradation, eventually all of the OC would be found in the inert fraction. If during the process of degradation and transport, degraded OC departs the bulk sediment (loose of TOC), the $\Delta^{14}C$ signature of the bulk sediment shifts towards the date of the inert OC fraction, assuming that no degraded OC is retained (section C)

For the discussion of bulk sediment radiocarbon composition, two additional key variables were defined, namely 'pre-aged' and 'fossil' carbon. This study considers that 'pre-aging' begins as soon as an organism dies, after which no new radiocarbon incorporation into the respective OM occurs. This term also covers the time elapsed during transport from the source to the final burial site, after death of the organism (e.g. during river or marine current transport and sediment remobilisation/resuspension).

Futhermore, it is considered that OM is older than about 10 half-lives of ^{14}C (~50,000 yrs.) to be 'fossil' or radiocarbon dead. The following classifications introduced here are used in the subsequent text:

i. 'Potent' pre-aged carbon consists of OM with intact functional groups with heteroatoms, such as alcohols (R–OH) or carboxylic acids (R–COOH).
ii. 'Recalcitrant' pre-aged carbon, comprising partial defunctionalisation of heteroatoms and/or unsaturated bonds as compared to co-occurring 'potent' carbon. As such, 'recalcitrant' carbon is more resistant to further degradation than 'potent' carbon since less stable moieties have already been removed.
iii. 'Inert' pre-aged carbon, which is effectively graphitic carbon, made of de-functionalised hydrocarbon ring structures.

All three classes of pre-aged carbon can contain terrestrial, marine and/or petrogenic material in any proportion, as controlled by local biogeochemical factors and geologic context. While an organism is dead, its OM still interacts with the environment because of its functional groups. It is assumed that 'potent' carbon dominates recent fresh OM (*i.e.* minimal loss of functionalisation [limited degradation]).

Transport can influence the amount (*i.e.*, concentration) of 'potent' OM in sedimentary environments. Amid transport, both abiotic and biological factors (*e.g.*, oxygen and bacteria, respectively) interact with the OM, causing partial defunctionalisation (degradation) of its chemical structure. If one assumes all three sedimentary ^{14}C pools having discrete ages, and because any 'potent' OM must be fresh, 'recalcitrant' OM has to be more degraded and slightly older, while 'inert' OM will be even further degraded and, in most cases, much older (or ^{14}C dead). This concept forms a framework that may explain the negative correlation observed between $\Delta^{14}C$ and 1/TOC of the Vietnamese Shelf data (Fig. 10). Another consideration is that the relating pre-aged bulk carbon pools have initially different ages, imposing the possibility that 'potent' OM could actually be older than the 'recalcitrant' or even 'inert' OM pools. Such a scenario may be the consequence of, for instance, input from wood/forest fires (thermal alteration and defunctionalisation).

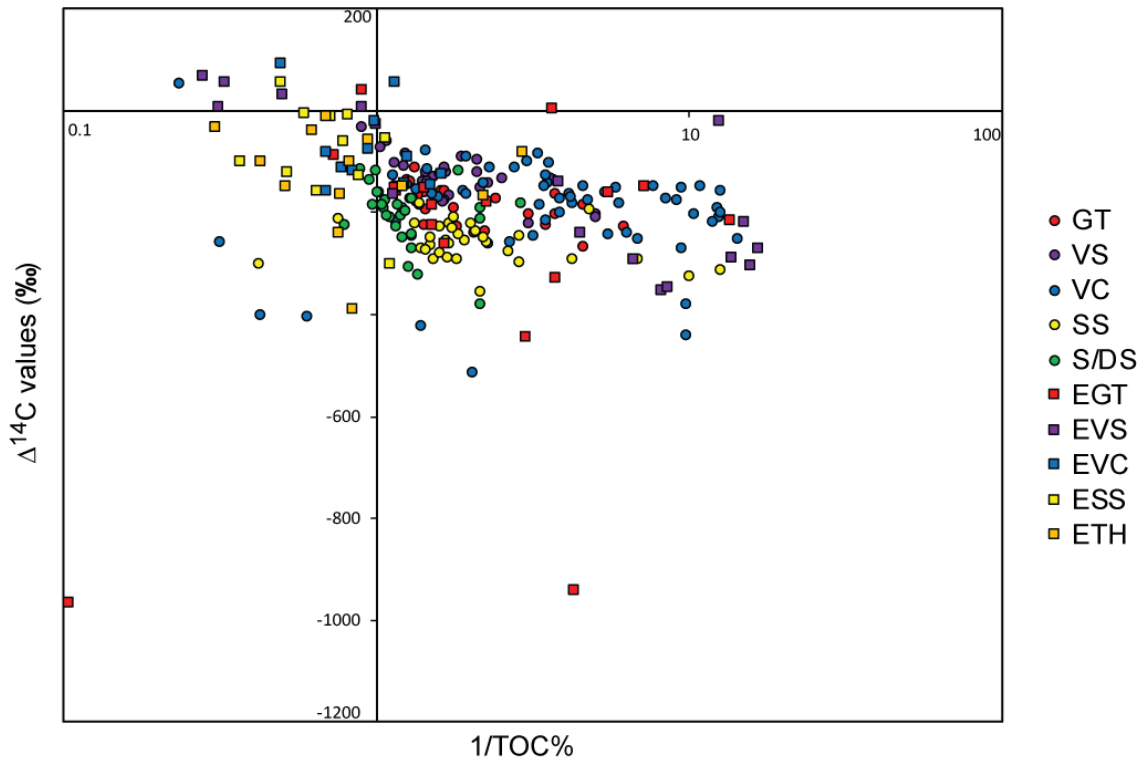

Figure 10) Correlation between bulk sediment organic carbon $\Delta^{14}C$ (radiocarbon) values and 1/TOC % values, as in Bianchi et al. [205]. Organic carbon rich sediments seemingly inherit younger dates, and most riverine samples have younger $\Delta^{14}C$ values, relative to their respective regions (marine sediments). Some outlier riverine samples, that display more negative $\Delta^{14}C$ values than their marine sediments, are likely enriched in petrogenic C, which causes shifts towards older values. Abbreviations: GT = Gulf of Tonkin, VS = Vietnamese Shelf, VC = Vietnamese Coast, SS = Sunda Shelf, S/DS = Slope/Deep Sea, EGT = Estuaries Gulf of Tonkin, EVS = Estuaries Vietnamese Shelf, EVC = Estuaries Vietnamese Coast, ESS = Estuaries Sunda Shelf, ETH = Estuaries Thailand.

The first scenario shown in figure 9 considers that the amount of potent and recalcitrant OM is reduced as a result of degradation and transport, converting potent OM to recalcitrant and finally inert, while recalcitrant is converted to inert, resulting in a consistent and effective increase of the inert fraction, at the expense of the other two fractions. Alternatively, or in addition, if transport not only facilitates degradation but also removal of a TOC fraction, by e.g. microbial consumption and/or remineralisation, the inert fraction will grow over proportionally. This en-route removal will bias the bulk $\Delta^{14}C$ analysis of the sink/host sediment towards the inert OM fraction (Fig. 9). The outcome of both processes would be similar, an increase in the inert OM fraction, but the level of increase will differ, affecting the age of the bulk OM pool.

The introduction and widespread use of these definitions are designed to clarify ongoing discussion in the literature (e.g. Trumbore et al. [206]), where the term pre-aged carbon can have several meanings. The terms here were used for a better comparison of $\Delta^{14}C$ data from riverine and marine sediments, some of which do not exhibit correlations that can be explained with conventional terminology.

2.6 Biomarkers (*n*-fatty acids, FA)

Biomarkers are natural products preserved in sediments and rocks that can be traced to a particular biological source. A wide variety of biomarkers are established and subject to research, including *n*-alkanes, hopanes, sterols, triterpanes or, in the case of this study, fatty acids (FA).

Carboxylic acids with long aliphatic chains and carboxyl groups (-COOH) are FA.

Two groups of FA are found, saturated or unsaturated. Most naturally occurring FA have an unbranched chain of an even number of carbon atoms, but also branched FA are theoretically possible. Most FA show a strong even over odd number predominance. FA are usually derived from triglycerides or phospholipids. In marine sediments and in particulate matter of seawater, straight chain FA often are the most abundant lipids. FA are significant components of animals, higher plants, marine fauna, and other microorganisms, like bacteria or microalgae. Each of these sources has a diagnostic FA profile. However, some FA are ubiquitous; examples include hexadecanoic (*n*-$C_{16:0}$) acid or octadecanoic (*n*-$C_{18:0}$) acid. To differentiate between marine and terrestrial-derived FA, the carbon chain length is commonly used. In ocean and deltaic sediments, marine sourced short-chain FA dominate, while even-numbered longer-chain FA (*n*-C_{20} - *n*-C_{30}) are associated with terrestrial higher plants [207]. Plant-derived long-chain FA with odd C-numbers are the result of metabolic processes or environmental degradation [208]. However, microalgae and bacteria also serve as a minor source of long-chain odd numbered FA [207]. Short-chain FA are more reactive and prone to degradation than long-chain FA, and saturated FA are more reactive than unsaturated FA [209, 210].

FA were extracted from the SCS surface sediment via accelerated solvent extraction (ASE).

2.7 Accelerated solvent extraction (ASE)

Accelerated solvent extraction (ASE) is a rapid technique for OM extraction or/and the chromatographic separation of complex mixtures of lipids in environmental matrices (e.g., sediments or soil) for molecular characterisation and isotope analysis [211]. For this study, stock extraction cells (33 ml volume) were initially packed with a microfiber glass filter followed by 1 g of sand to prevent clogging [212] and then filled with 2 g – 10 g of sediment. The remaining volume was filled with quartz sand. Once filled, the cells were extracted with dichloromethane (DCM) and methanol (MeOH) in a

volumetric ratio of 85:15 with 70 % rinse volume [213] in 3 cycles of 5 min. each at 100 °C (10.3 MPa) on a Dionex ASE 350 system. The resultant total lipid extract (TLE) was gently dried under nitrogen (e.g. Denis et al. [214]). Subsequently, the dried TLE was reconstituted in increasingly polar solvents to separate individual lipid fractions (i.e., [un]saturated hydrocarbons and polar lipids) using gravity "flash" column chromatography [215, 216].

2.8 Gravity columns

Gravity columns are constructed from a short-necked Pasteur pipette with a glass wool plug. Thereafter, about 2 g of activated silica gel is added to the pipette [216] and then provided with a thin layer of sand, to prevent the column drying. Combined hydrocarbons were eluted with 8 ml of Hexane and the polar lipid fraction was eluted with 8 ml of Methanol. Through the natural behaviour of the polar lipid fraction and the used mid-polar DB-5 column for measurements, the free FA need to be methylated, to form methyl-esters.

2.9 Methylation

The methylation of carboxylic acids to form methyl-esters (of fatty acid methyl-esters) is required for GC-FID and GC-MS analyses of fatty acids. The esterification reaction is an acid-catalysed equilibrium between carboxylic acid and an alcohol:

$$ROOH+R'OH \leftrightarrow ROOR'+HOH$$

Because of this equilibrium reaction, the yield of the ester can be increased by using an excess of the carboxylic acid or the alcohol, and/or by removing water from the reaction mixture, as it forms. In this procedure, an excess of the alcohol is allowed to react with carboxylic acids. Here, a Boron-trifluoride (BF_3) solution is used as an acid reagent. The BF_3 fails to methylate some fatty acids, such as wax esters or triacyl glycerol's, instead only free fatty acids are methylated. This permits a more targeted sample extraction.

In preparation of the sample extraction, samples are transferred to Teflon lined 8 ml screw cap vials, using either an aprotic or a protic solvent. The solvent is then evaporated under a low flow N_2 stream. After dryness is achieved, the sample is re-dissolved in DCM. Then ca. 100 µl of BF_3 / MeOH is added, in proportion the total amount of organic acids. The vial is gently filled with N_2 and capped, to provide a non-reactive environment. The vials are then placed in an oven at 60 ^oC -80 ^oC for 15 min. after 15 min., the vials are removed from the oven and left to cool down to ambient temperature. Then, 1.5 ml of

Millipore water and then 1.5 ml of Hexane are added to each vial and well mixed. The upper layer is extracted, containing the free methylated fatty acids. This procedure is repeated four times. The now methylated samples are dried again under a nitrogen environment and re-dissolved in Hexane prior to analysis.

2.10 GC-FID and GC-MS

The organic compounds were measured, quantified and identified with Gas Chromatograph-Flammable-Ionization-Detector (GC-FID) and a Gas Chromatograph-Mass-Spectrometer (GC-MS), a Thermo Scientific Trace 1310 and Thermo Scientific Trace 1300 respectively at the Lyell Centre, Heriot-Watt University Edinburgh. In case of the GC-FID, the column is connected to a flammable ion detector. In case of the GC-MS the column is connected to an ISQ LT quadrupole MS. Both instruments are equipped with a split/splitless injector operated in splitless mode at 320 °C and are equipped with a 30 m Agilent DB-5 fused-silica column, with an inner diameter of 0.250 mm and a polymer film thickness of 0.25 µm. The flow rate was 1 ml/min and helium was used as a carrier gas. Oven temperature in both instruments is held at 60 °C for 1 min, then ramped to 320 °C at 6 °C/min and held at 320 °C for 20 min and 40.2 s. The Injector temperature is 320 °C for the GC-FID and GC-MS. The GC-MS is operated with a scanning mass range of *m/z 50 - 600* at 3 scans per second and ionization energy of 70 eV. The Ion Source temperature operated with 300 °C, while the transfer-line is at 310 °C.

3 Assessment of transport and accumulation of organic matter in the western South China Sea – implications from estuary and marine surface sediments

3.1 Introduction

The transfer of organic carbon (OC) from land to ocean is a multi-facetted process, where continued transformation of organic matter (OM) results in a variety of compositions by e.g. mixing and/or physical and (bio-)chemical decomposition. A comprehensive evaluation of these processes is challenging due to the complex interactions from different OM sources and the gradual homogenisation and degradation prior to longer term deposition in modern coastal, shelf and deep sea sediments.

The transport of OC from land to ocean via rivers is known to have lasting impact on bioactivity in the marine environment, through export of critical nutrients, including carbon, nitrogen, and phosphorus. Furthermore, once OM is remineralised to CO_2, N_2O and CH_4, it is a principle source of greenhouse gas that can potentially enter the atmosphere and impact climate (e.g. Houghton et al. [217]). Once deposited and preserved in marine sediments, OM can act as a sensitive recorder of changes in the local environment, including climatic change and the impact of anthropogenic activity on ecosystems [218–221].

In the western SCS, the transport distances of river systems range from just several hundreds of meters, to several hundreds of kilometres, or more. For example, the Mekong River travels almost 4,900 km, allowing riverine waters to drain a large variety of carbon sources from the hinterland to the marine environment. However, long transport distances and subsequent physical and (bio-) chemical processes modify the OM cargo of rivers to an extent where the initial source composition and isotopic signature are strongly modified [222].

The amount of carbon, which enters the oceans via rivers, is therefore only a fraction of the original carbon input into the river systems [223]. The estimate of carbon preserved from its original introduction to the riverine system is in the range of ~ 30 % to 40 % for a case study on the Congo River, with evidence that other major river systems preserving similar amounts of OM prior to deposition in marine sediments [224]. Most of this riverine carbon is returned to the atmosphere as CO_2 before reaching the oceans or is

stored within river corridors as sedimentary OC after erosion and transport from distant sites [223].

In addition, the physical and chemical abrasion and weathering of bedrock lithology can mobilise inorganic carbon (IC) that mixes with OC in aqueous and terrestrial systems. This mixing of carbon pools complicates the approach to apply commonly used proxy variables, such as stable carbon isotopes, to identify bulk sources of OC and its changes through the depositional system. The range of $\delta^{13}C$ isotopic compositions for potential source reservoirs is summarised in Clark and Fritz [225], e.g. carbon in metamorphic rocks can have $\delta^{13}C$ isotopic compositions ranging from ~ 0 ‰ to 8 ‰, and limestone $\delta^{13}C$ ranging from ~ -2 ‰ to 2 ‰. Typical biogenic sources (e.g. C_3, C_4 and CAM plants) range from -8 ‰ to -32 ‰ [177, 225].

Other biophysical factors modifying the bulk OM composition on its way from land to ocean include natural filtration systems, such as dense mangrove root networks in coastal regions, e.g. those of the Red River area [226]. The interface between rivers and coastal oceans are also subject to cyclic processes of variable magnitude, summarised as 'tidal force'. As a consequence of tide intrusions with marine coastal waters, a salinity and temperature gradient is built up in estuary/coastal areas with direct impact on alternating biochemical and physical conditions (e.g. presence or absence of algae, bacteria etc.). These tidal effects are well studied in the Mekong River estuary/delta [71]. Tidal Force is responsible for significant amounts of sediments discharge into the coastal SCS [99]. In essence, the combination of inland riverine and tidal effects can heavily overprint any initial evidence of OM input to coastal systems from higher plants (e.g. C_3 and C_4) in the source hinterland, making its reconstruction based on marine sediment proxy variables challenging, if not in places impossible.

Any improved assessment of the carbon cycle therefore requires a detailed characterisation of carbon abundance, variability, composition, and source reservoirs. This can be achieved by using bulk geochemical proxies, such as stable carbon isotopes (e.g. $\delta^{13}C_{org}$) and the elemental ratio of C_{org}/N_{total} (e.g. Lamb et al. [220]), complemented by a detailed component analysis by means of molecular characterisation (e.g. Naafs et al.; Pancost and Boot; Volkman [61, 227, 228]). For the SCS, a potentially useful molecular marker is the group of FA, which have great potential to differentiate between bacteria, microalgae, higher plants and marine fauna [228]. FA are formed by most organisms, whereby longer chain FA are typically produced by terrestrial plants [228]

and shorter chain FA preferentially by algae [229] [230] [231]. Furthermore, uneven carbon chain length is the product of plant enzymatic splitting or more generally the result of FA decomposition. This diversity in the FA origin requires careful evaluation and normalisation to identify reliable correlations (e.g. negative excursions after normalisation of chain length abundance, or changes in abundance between short and long-chain FA). One example from modern environments can be the appearance or disappearance of plants and domesticated cattle. More abundant pentadecanoic acid (n-$C_{15:0}$) can be indicative for either increased domination or disappearance of *Durio graveolens* (which is a plant, native in Southeast Asia, [78] or cow milk [232]). Normalisation strategies to resolve such appearance or disappearance require a temporal or spatial element. In the case of the SCS, for example, the patterns obtained by normalisation using Slope/Deep Sea sediments *vs.* riverine sediments can be indicative for changes in vegetation. If the Slope/Deep Sea sediments are older or younger than the riverine samples, a temporal timescale can be established. Additionally, the enrichment or depletion of FA compared to the normalisation is anticipated to give clues to the distribution of specific plant coverage, such as *Durio graveolens*. These observations can then be brought into the wider geological context, by comparison with other relevant evidence on e.g. the appearance or disappearance of species.

Previous studies have combined bulk and molecular strategies with success to identify changes in terrestrial supply of C_3 and C_4 plants through glacial-interglacial climate cycles (e.g. Huang et al. [233]) by correlating detailed records of lipids (*n*-alkanes, *n*-acids and *n*-alcohols) from higher plant remnants with the fractionation of carbon isotopes related to C_3 and C_4 plants. Evidence from the record of C_3 and C_4 plants during glacial periods can be combined with observations from Wang and Sun [234], who suggested that the sea level in the SCS dropped during the glacial maximum. Furthermore, Wang and Sun [234] suggested that the regional air temperatures in past glacial winters were on average 6 ^{o}C – 10 ^{o}C cooler, resulting in a more pronounced seasonality, compared to today. This is considered to cause changes in the vegetation cover, which would suggest that the occurrence of C_3 and C_4 plants in the SCS region and their export to the marine environment might have been variable over time. However, the reconstruction of OM source characteristics could have been further complicated if significant amounts of OM produced during these past glacial conditions were remobilised at a later stage but prior to modern-day burial, resulting in a time offset between production and mobilisation and burial of OM. Wang and Sun [234] concluded that vegetation zones in the SCS

experienced a southward shift, possibly resulting in the temporarily disappearance of monsoonal rainforests in the south of China (affecting parts of the coastal area of the Gulf of Tonkin and Hainan). These conclusions were corroborated by the study of Wang et al. [235], who presented independent evidence of pollen records in sediment cores from the former Sunda Land (now Sunda Shelf; Chapter 1 - General Introduction). These pollen data indicate a massive change in coastline (specifically to the present-day shelf break marking the transition from shelf to deep sea), but do not support a notable change in humidity. These observations from previous studies can be compared with observations from FA data from time equivalent sediments to cross validate or expand their interpretation.

Aim and outcome of Chapter 3:

Chapter 3 acquires a large region-specific dataset of $\delta^{13}C_{org}$, C_{org}/N_{total} and FAME, with the aim to identify source variability and in-situ production of OM. The mobilised and terrestrial OM fraction is approximated, creating a highly diversified and well-resolved regional overview of its distribution. FAME biomarkers have been selected as they are more sensitive indicators for preservation than e.g. *n*-alkanes [218] and, unlike other lipid compounds, they occur in higher abundances in the SCS [236, 237]. One critical assumption is that FAMEs can be evaluated based on their linear ageing trend, which assumes a simple correlation between abundance, transport distance and time. FAME data primarily record the transition the riverine to marine environment, but with greater target specific resolution compared to conventional bulk $\delta^{13}C_{org}$ and C_{org}/N_{total} data. A key focus of this chapter is to evaluate OM source variability (e.g. allochthones and autochthonous), homogenisation of terrestrial OM during deposition, and the identification of efficient OM storage sites. One important observation is that short-chain FA of likely marine origin are dominant, supporting interpretations from $\delta^{13}C_{org}$ and C_{org}/N_{total}. Despite the general agreement between molecular and bulk data, a secondary aim explores other factors that may cause minor discrepancies between the three proxy data sets.

3.2 Methods

Marine surface sediments have been recovered from the SCS during several sampling campaigns mainly with the Research Vessel (RV) Sonne (SO) (cruises: SO-115; SO-140; SO-187-3; SO-220 (for more details see Cruise reports)). The surface samples were measured for Total Organic Carbon (TOC), $\delta^{13}C_{org}$, C_{org}/N_{total} and FAME as detail in the

introduction of this PhD thesis (Chapter 1 - General Introduction). For convenience, a brief description of the analytical approach is provided below. Bulk $\delta^{13}C_{org}$ was measured at an external service laboratory (Iso-Analytical Limited, Cheshire, UK). Samples were acidified in universal tubes for 24 hr (to remove carbonate), washed twice in distilled water, air-dried, and (re)homogenised *in situ*. Samples were measured by conventional Elemental Analysis - Isotope Ratio Mass Spectrometry (EA-IRMS). The TOC was measured by partners at the Tongji University Shanghai and the University of Hamburg. Most (n = 296 of 320) TOC data were measured at University of Hamburg using a CARLO ERBA NA-1500 EA. The standard deviation of reference material analyses was 0.15 % for TOC. During combustion for TOC analyses, CO_2, and NO_x oxides are formed, the latter requiring an oxidation step to produce N_2 prior to analysis. The remaining 24 samples of the total sample set were measured at Tongji University Shanghai with an Elementar Vario ISOTOPE EA equipped to a CNHS element analyser.

For the FA analyses, the samples were extracted and afterwards fractionated with gravity columns into three fractions (non-polar, mid-polar, and polar). The polar fraction contains the FA and were methylated with BF_3 (to FAME) and measured with a GC-MS, using a Thermo Scientific Trace 1310 and Thermo Scientific Trace 1300 on a DB 5 column in Hexane.

The full details of the analytical procedure are described in Chapter 2 (Material and Methods).

3.3 Results

The following section reports the results of TOC, $\delta^{13}C_{org}$, C_{org}/N_{total} and FAME, which are summarised in table 1 and illustrated in figure 12.

3.1.1 Total organic carbon (TOC) in marine surface and estuary sediments

The TOC concentrations of the 319 surface sediments were determined, and grouped as marine surface sediments (table 1) and estuary samples (table 2). This is done to highlight the concentration differences of the marine and estuary systems and to allow for more readily extractable and depictable differences on regional scales.

Table 1) TOC (%) values of marine surface sediments

Region	Max. value	Min. value	Average	*n*
Gulf of Tonkin	0.9 %	0.2 %	0.5 %	41
Vietnamese Shelf	1.1 %	0.1 %	0.5 %	32
Vietnamese Coast	4.3 %	0.1 %	0.5 %	75
Sunda Shelf	2.4 %	0.1 %	0.5 %	53
Slope/ Deep Sea	1.3 %	0.2 %	0.8 %	31

TOC in river estuary samples ranges from 0.1 % to 9.7 %, in shelf sediments from 0.1 % to 3.2 %, and in Slope/Deep Sea sediments from 0.7 % to 4.3 % (Fig. 12a and b).

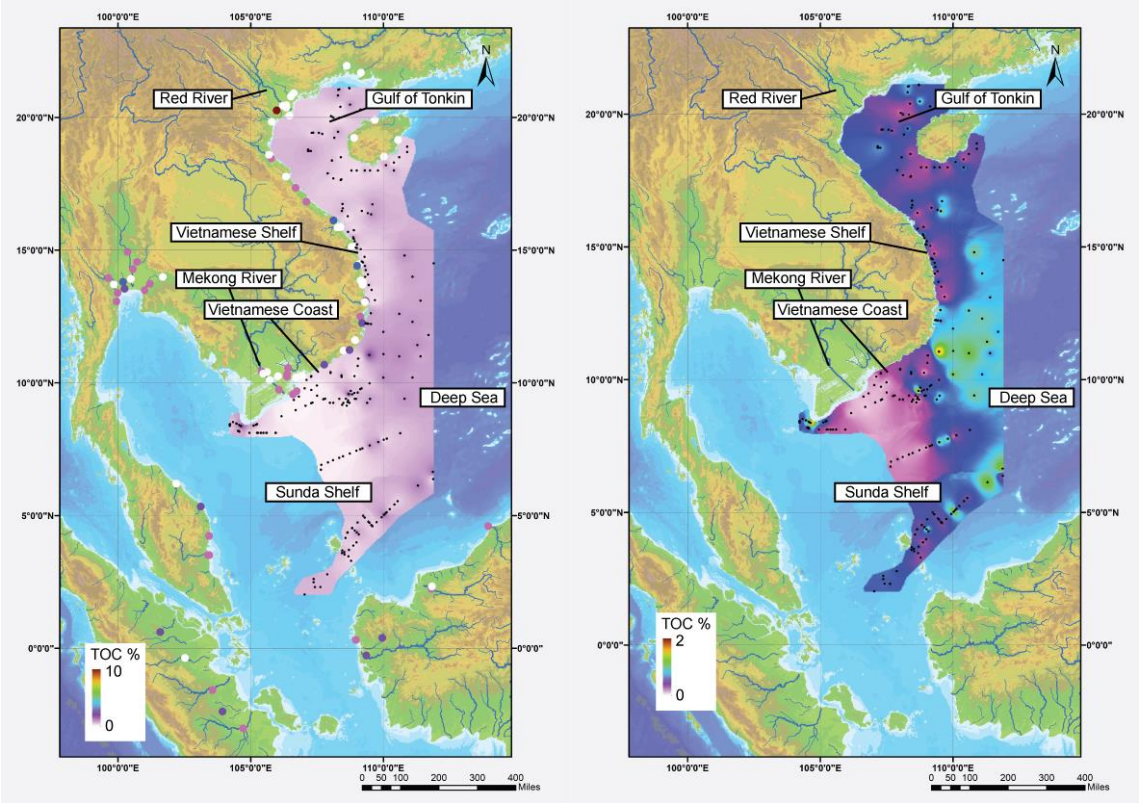

Figure 11) Interpolated (Inverse distance weighting) total organic carbon map of the study area. Available river data plotted as individual spots. Map a (left) shows the TOC distribution of 0-10 %, b (right) shows the TOC distribution from 0-2 %, river samples excluded. Low TOC content (pink colours) is predominantly observed in proximity to the Mekong River delta and parts of the Sunda Shelf. High TOC content (green colours) is predominant in the Deep Sea area. River samples represent the highest TOC contents (up to 9 %, Red River)

The regional ranges of TOC in the defined sub-domains of the study area are as follows: Gulf of Tonkin from 0.2 % to 0.9 % (average 0.5 %; n = 41), Vietnamese Shelf from 0.1 % to 1.1 % (average 0.5 %; n = 32), Vietnamese Coast from 0.1 % to 4.3 % (average 0.5 %; n = 75); Sunda Shelf from 0.1 % to 2.4 % (average 0.5 %; n = 53). Excluding

unsupported outlier values, the TOC for the Sunda Shelf ranges from 0.1 % to 0.8 % (average 0.5 %; *n* = 51) and the Slope/Deep Sea values range from 0.2 % to 1.3 % (average 0.8 %; *n* = 31).

Table 2) TOC (%) concentration of estuary samples

Region	Max. value	Min. value	Average	*n*
Estuaries from the Gulf of Tonkin area	9.7 %	0.1 %	1.1 %	18
Estuaries from the Vietnamese Shelf area	3.6 %	0.1 %	1.1 %	23
Estuaries from the Vietnamese Coast area	2.6 %	0.1 %	1.1 %	17
Estuaries from the Sunda Shelf area (Indonesia and Malaysia)	2.8 %	0.9 %	1.7 %	16
Estuaries from Thailand	3.3 %	0.4 %	1.4 %	13

The estuarine TOC for the respective subareas are: Gulf of Tonkin from 0.1 % to 9.7 % (average 1.1 %; *n* = 18); this range includes one outlier, sample VN-63, from close to the Red River Delta (20°15.600'N; 105°58.800'E) containing 9.7 % TOC. Without the outlier, TOC values in the Gulf of Tonkin estuary samples range from 0.1 % to 1.4 % (average 0.5 %; *n* = 17). Vietnamese Shelf estuaries TOC range from 0.1 % to 3.6 % (average of 1.1 %; *n* = 23), Vietnamese Coast estuaries from 0.1 % to 2.6 % (average 1.1 %; *n* = 17) and Sunda Shelf estuaries from 0.9 % to 2.8 % (average 1.7%; *n* = 16). Thailand estuary samples TOC ranges from 0.4 % to 3.3 % (average 1.4 %; *n* = 13).

Marine shelf sediments are generally <1 % TOC, with only five samples showing significant higher concentrations from 1.7 % to 4.3 %, these samples are not region specific.

3.1.2 C_{org}/N_{total}

The C_{org}/N_{total} ratio is an indicator for marine and terrestrial signatures, and the data are pre-separated into marine surface sediment samples and estuary samples in tables 3 and 4 to make differences more readily visible.

Table 3) C_{org}/N_{total} ratios of marine surface sediments

Region	Max. value	Min. value	Average	*n*
Gulf of Tonkin	10.8	6.6	7.8	29
Vietnamese Shelf	9.3	3.2	6.4	32
Vietnamese Coast	11.8	2.3	8.0	54
Sunda Shelf	6.4	2.3	4.3	9
Slope/ Deep Sea	9.4	4.1	6.5	12

The C_{org}/N_{total} ratios of the 136 marine surface sediments samples were calculated and range from 2.3 to 11.8. On regional scales, the C_{org}/N_{total} ratios in the defined sub-domains ranges are: Gulf of Tonkin from 6.6 to 10.8 (average 7.8; *n* = 29), Vietnamese Shelf from 3.2 to 9.3 (average 6.4; *n* = 32), Vietnamese Coast from 2.3 and 11.8 (average 8.0; *n* = 54), Sunda Shelf from 2.3 and 6.4 (average 4.3; *n* = 9) and the Slope/Deep Sea ratios range from 4.1 to 9.4 (average 6.5; *n* = 12).

Table 4) C_{org}/N_{total} ratios of estuary samples

Region	Max. value	Min. value	Average	*n*
Estuaries from the Gulf of Tonkin area	43.4	4.7	12.7	18
Estuaries from the Vietnamese Shelf area	24.9	2.0	15.9	23
Estuaries from the Vietnamese Coast area	20	3.2	11.6	17
Estuaries from the Sunda Shelf area (Indonesia and Malaysia)	49.8	11.3	17.7	16
Estuaries from Thailand	16.0	11.3	13.6	13

The estuarine sample C_{org}/N_{total} ratios for the respective subareas are: Gulf of Tonkin from 4.7 to 43.4 (average 12.7; *n* = 18), Vietnamese Shelf estuaries from 2 to 24.9 (average of 15.9; *n* = 23), Vietnamese coastal estuaries from 3.2 to 20.0 (average 11.6; *n* = 17), Sunda Shelf estuaries from 11.3 and 49.8 (average 17.3; *n* = 16) and Thailand estuaries from 11.3 to 49.8 (average 13.6; *n* = 13).

3.1.3 $\delta^{13}C_{org}$

The $\delta^{13}C_{org}$ isotopic composition of OM is a useful indicator for potential source reservoirs (Chapter 1 - General Introduction), and the samples are pre-grouped into marine and estuary samples (tables 5 and 6).

Table 5) $\delta^{13}C_{org}$ (‰) values of marine surface sediments

Region	Max. value	Min. value	Average	*n*
Gulf of Tonkin	-21.3 ‰	-24.4 ‰	-22.3 ‰	41
Vietnamese Shelf	-21.7 ‰	-24.5 ‰	-22.9 ‰	32
Vietnamese Coast	-20.3 ‰	-27.7 ‰	-23.1 ‰	75
Sunda Shelf	-21.6 ‰	-25.5 ‰	-22.9 ‰	51
Slope/ Deep Sea	-20.6 ‰	-23.5 ‰	-21.9 ‰	31

The marine surface sediments from all shelf samples for $\delta^{13}C_{org}$ range between -27.7 ‰ to -20.3 ‰ (*n* = 230), as shown in figure 13.

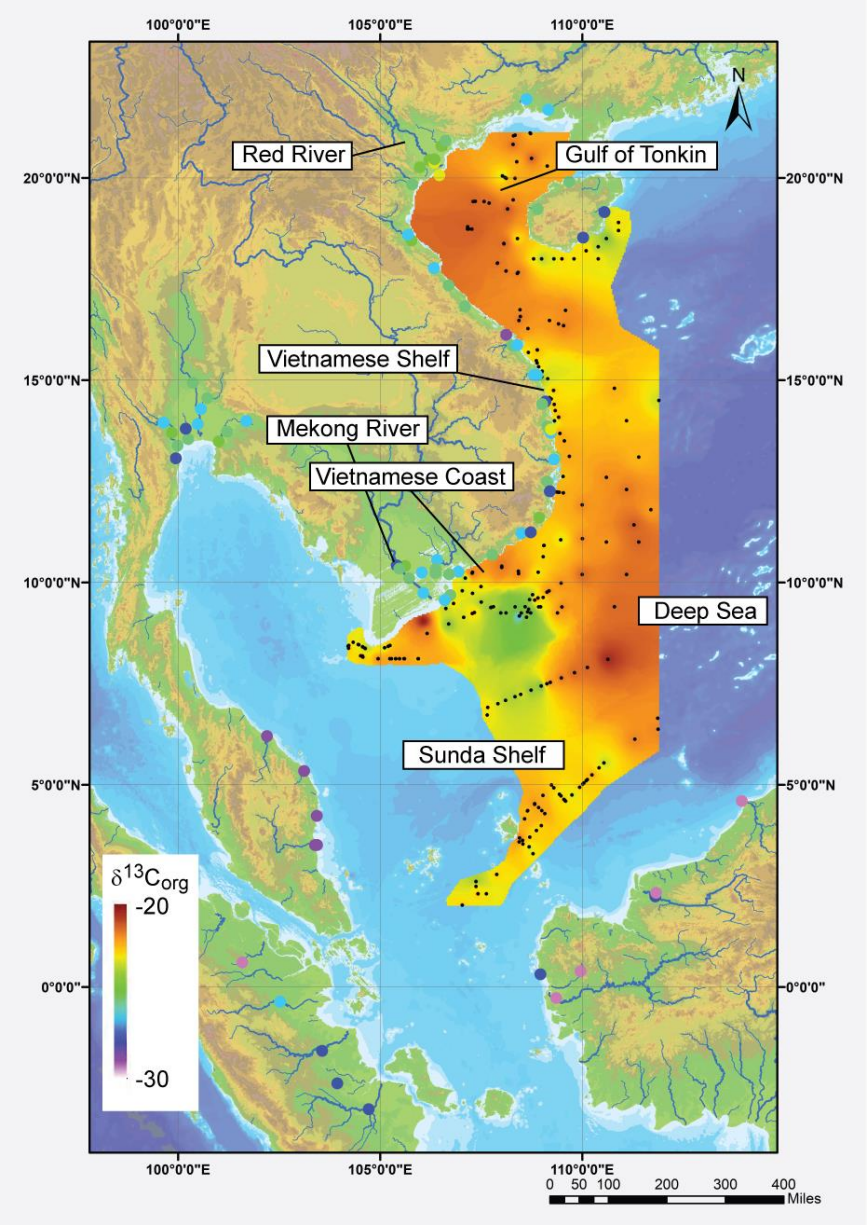

Figure 12) Interpolated (Invers distance weighting) $\delta^{13}C_{org}$ map of the study area. Available river data plotted as individual spots. The area proximal to the Mekong River is characterised by the lightest $\delta^{13}C_{org}$ isotopic composition of marine surface sediments. Rivers in the south appear to carry the lightest $\delta^{13}C_{org}$ isotopic composition, with rivers towards the north being isotopically slightly heavier

The Gulf of Tonkin has $\delta^{13}C_{org}$ ranging from -24.4 ‰ to -21.3 ‰ (average of -22.3 ‰; n = 41), the narrow Vietnamese Shelf has $\delta^{13}C_{org}$ ranging from -24.5 ‰ to -21.7 ‰, (average of -22.9 ‰; n = 32), the southern Vietnamese Coast $\delta^{13}C_{org}$ range from -27.7 ‰ to -20.3 ‰ (average of -23.1 ‰; n = 75), the Sunda Shelf has $\delta^{13}C_{org}$ range of -25.5 ‰ to -21.6 ‰ (average of -22.9 ‰; n = 51) and the Slope/Deep Sea samples show $\delta^{13}C_{org}$ values of -23.5 ‰ to -20.6 ‰ (average of -21.9 ‰; n = 31).

Table 6) $\delta^{13}C_{org}$ (‰) values of estuary samples

Region	Max. value	Min. value	Average	*n*
Estuaries from the Gulf of Tonkin area	-23.8 ‰	-27.6 ‰	-25.4 ‰	18
Estuaries from the Vietnamese Shelf area	-23.9 ‰	-28.7 ‰	-26.0 ‰	23
Estuaries from the Vietnamese Coast area	-24.6 ‰	-27.2 ‰	-26.1 ‰	17
Estuaries from the Sunda Shelf area (Indonesia and Malaysia)	-26.1 ‰	-29.5 ‰	-28.2 ‰	16
Estuaries from Thailand	-24.7 ‰	-27.6 ‰	-25.9 ‰	13

Estuary samples around the Gulf of Tonkin show $\delta^{13}C_{org}$ values from -27.6 ‰ to -23.8 ‰, (average of -25.4 ‰; n = 18). Vietnamese Shelf estuaries have $\delta^{13}C_{org}$ values from -28.4 ‰ to -23.9 ‰, (average of -26.0 ‰; n = 23). The $\delta^{13}C_{org}$ values of estuary samples of the Vietnamese Coast range from -27.17 ‰ to -24.58 ‰; (average of -26.06 ‰; n = 17). Estuaries of the Sunda Shelf range between -29.5 ‰ to -26.1 ‰, (average of -28.2 ‰; n = 16). River samples from Thailand range between -27.6 ‰ to -24.7 ‰ (average: -25.9 ‰; n = 13).

3.1.4 FAME distribution

The abundance of FAME is analysed in marine surface sediments and estuary samples, to investigate potential applications of FAME data in the interpretation of carbon processes (Fig. 14 and 15, tables 7 and 8).

Table 7) FAME (µg/g) concentration of marine surface sediments

Region	Max. value	Min. value	Average	*n*
Gulf of Tonkin	390 µg/g	2.65 µg/g	75.8 µg/g	41
Vietnamese Shelf	150 µg/g	2.99 µg/g	28.6 µg/g	31
Vietnamese Coast	134 µg/g	5.18 µg/g	27.4 µg/g	74
Sunda Shelf	179 µg/g	1.74 µg/g	31.5 µg/g	55
Slope/ Deep Sea	733 µg/g	6.23 µg/g	129 µg/g	28

In the Gulf of Tonkin the concentrations of FAME per gram sediment range from 2.65 µg/g to 390 µg/g (average of 75.8 µg/g; n = 41). The Vietnamese Shelf samples have values from 2.99 µg/g to 150 µg/g (average of 28.6 µg/g; n = 31). On the Vietnamese Coast values range between 5.18 µg/g to 134 µg/g (average of 27.4 µg/g; n = 74). The Sunda Shelf shows values from 1.74 µg/g to 179 µg/g (average of 31.5 µg/g; n = 55). In the Slope/Deep Sea area, the values range from 6.23 µg/g to 733 µg/g (average of 129 µg/g; n = 28).

Table 8) FAME (µg/g) concentration of estuary samples

Region	Max. value	Min. value	Average	*n*
Estuaries from the Gulf of Tonkin area	693 µg/g	2.87 µg/g	139 µg/g	18
Estuaries from the Vietnamese Shelf area	2333 µg/g	57.3 µg/g	505 µg/g	23
Estuaries from the Vietnamese Coast area	2120 µg/g	24.1 µg/g	474 µg/g	17
Estuaries from the Sunda Shelf area (Indonesia and Malaysia)	499 µg/g	15.6 µg/g	132 µg/g	15
Estuaries from Thailand	1236 µg/g	18 µg/g	266 µg/g	13

The estuaries for the sub areas are showing values: For the Gulf of Tonkin from 2.87 µg/g to 693 µg/g (average of 139 µg/g; *n* =18). Estuaries in the Vietnamese Shelf area are ranging between 57.3 µg/g to 2333 µg/g (average of 505 µg/g; *n* = 23). Samples from respective estuaries of the Vietnamese Coast sub-area show values from 24.1 µg/g to 2120 µg/g (average of 474 µg/g; *n* = 17). Estuaries respective to the Sunda Shelf have values ranging between 15.6 µg/g to 499 µg/g (average of 132 µg/g; *n* = 15). Estuaries of Thailand show values from 18.0 µg/g to 1236 µg/g (average of 266 µg/g; *n* = 13). The distribution of FAME in the study area is illustrated in figure 14 and 15. The data show typical even over odd frequency distribution, with the highest overall concentration for the $C_{16:0}$ and $C_{18:0}$ saturated FAME (Fig. 14).

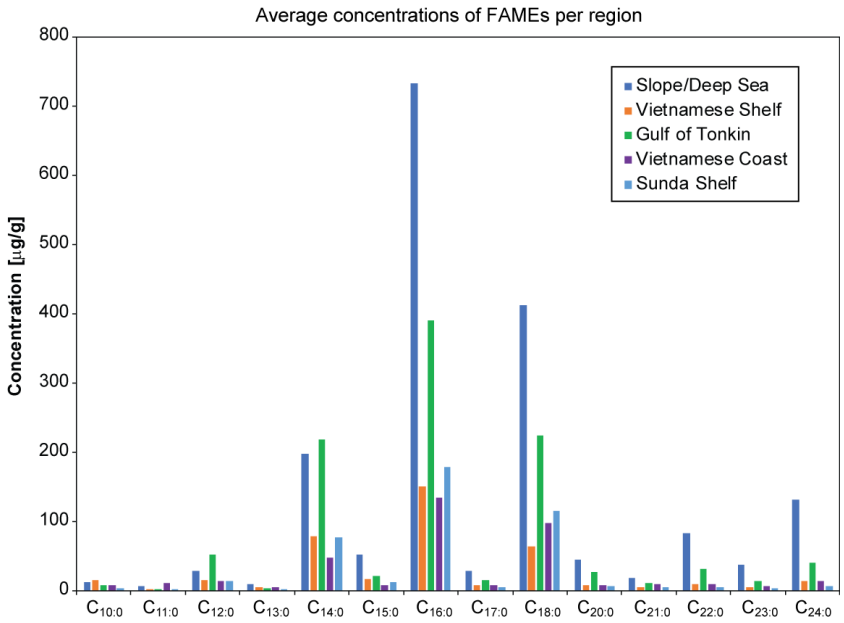

Figure 13) The average abundance of FAME of the Slope/Deep Sea, Gulf of Tonkin, Vietnamese Shelf, Vietnamese Coast and Sunda Shelf region for carbon chain lengths from $C_{10:0}$ to $C_{24:0}$, with the exception of $C_{19:0}$

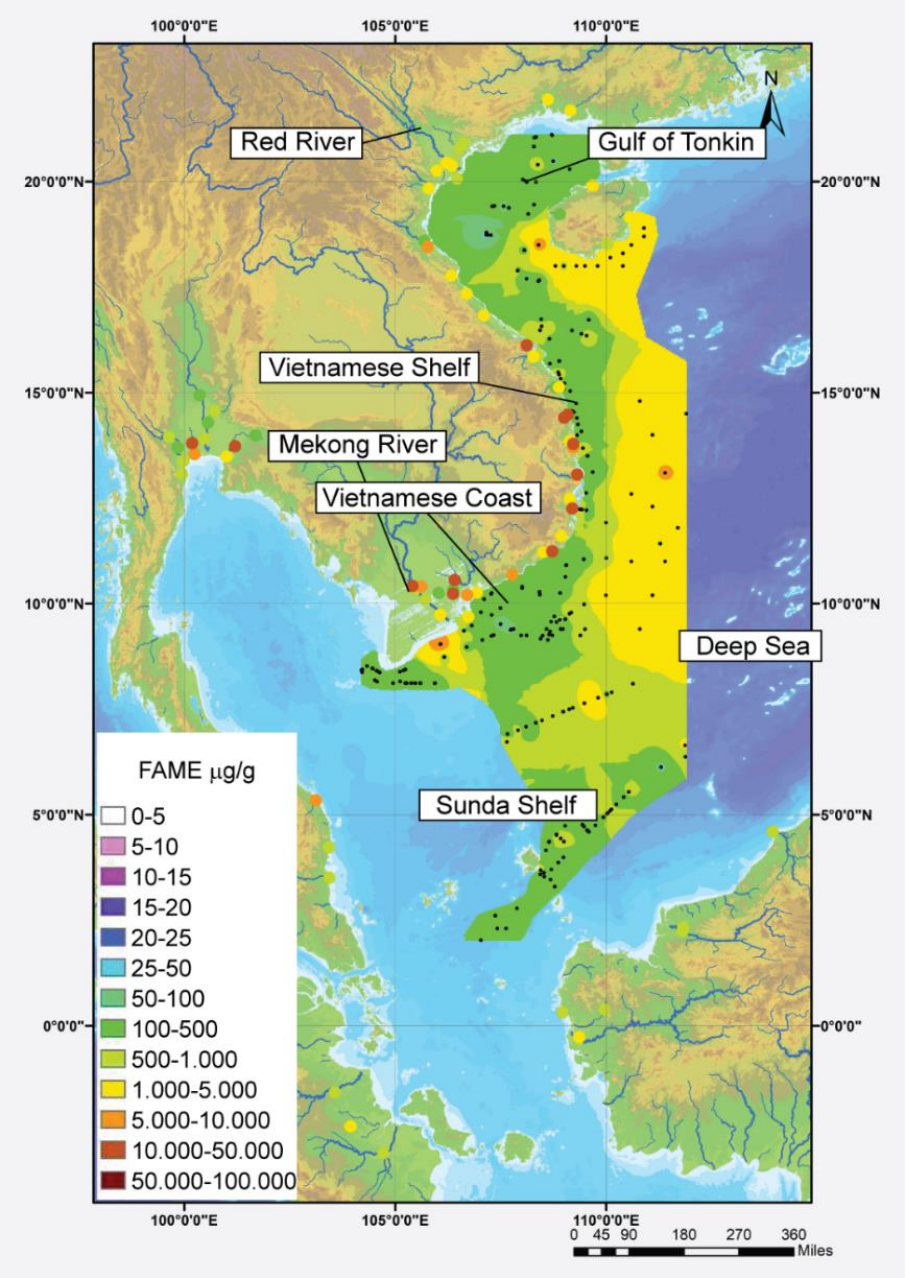

Figure 14) Interpolated (Invers distance weighting) FAME distribution map (µg/g) of the study area. Available river data plotted as individual spots. Areas of FAME accumulation are rivers, slope/deep sea sediments, and sediments to the south of Hainan

3.1.5 FAME (%) TOC normalised

Since the FAME fraction is part of the TOC, normalisation against the TOC content possibly allows for better inter-sample comparison of FAME data obtained in this study (Fig. 16, tables 9 and 10). It must however be noted that the spread in TOC between the investigated samples is relatively low, so that any normalisation effect based on TOC is expected to be relatively moderate.

Table 9) TOC normalised FAME concentration (µg/[%]) of marine surface sediments

Region	Max. value	Min. value	Average	*n* =
Gulf of Tonkin	35.8 µg/[%]	0.18 µg/[%]	6.84 µg/[%]	41
Vietnamese Shelf	16.4 µg/[%]	0.36 µg/[%]	3.05 µg/[%]	31
Vietnamese Coast	7.58 µg/[%]	0.05 µg/[%]	4.31 µg/[%]	73
Sunda Shelf	16.3 µg/[%]	0.13 µg/[%]	2.85 µg/[%]	55
Slope/ Deep Sea	162 µg/[%]	1.08 µg/[%]	27.9 µg/[%]	28

In the Gulf of Tonkin the TOC normalised FAME values range between 0.18 µg/[%] to 35.8 µg/[%] (average of 6.84 µg/[%]; *n* = 41), in the Vietnamese Shelf show values from 0.36 µg/[%] to 16.4 µg/[%] (average of 3.05 µg/[%]; *n* = 31). The Vietnamese Coast have values of 0.05 µg/[%] to 7.58 µg/[%] (average of 1.34 µg/[%]; *n* = 73), exclusive one outlier, which is sample SO-187-3-87-2 (09°02.558'N; 106°04.533'E) located very close to the coast; this sample shows high TOC values of 4.31 %. Including this one sample the values range from18.1 µg/[%] to 400 µg/[%] (average of 89.28 µg/[%]). The outlier sample is not considered in further discussions of this chapter, in absence of an interpretational framework. The Sunda Shelf shows values from 0.13 µg/[%] to 16.3 µg/[%] (average of 2.85 µg/[%]; *n* = 55). In the Slope/Deep Sea the values range from 1.08 µg/[%] to 162 µg/[%] (average of 27.9 µg/[%]; *n* = 28). The overall range for the TOC normalised FAME for the entire study area is from 0.05 µg/[%] to 162 µg/[%] with an average of 8.40 µg/[%]. The normalised data show typical even over odd frequency distribution, with the highest overall concentration for the $C_{16:0}$ and $C_{18:0}$ saturated FAME.

Table 10) TOC normalised FAME concentration (µg/[%]) of estuary samples

Region	Max. value	Min. value	Average	*n* =
Estuaries from the Gulf of Tonkin area	287 µg/[%]	1.06 µg/[%]	73.4 µg/[%]	18
Estuaries from the Vietnamese Shelf area	2743 µg/[%]	43.6 µg/[%]	539 µg/[%]	23
Estuaries from the Vietnamese Coast area	1678 µg/[%]	19.4 µg/[%]	361 µg/[%]	17
Estuaries from the Sunda Shelf area (Indonesia and Malaysia)	299 µg/[%]	10.8 µg/[%]	88.4 µg/[%]	15
Estuaries from Thailand	2044 µg/[%]	21.9 µg/[%]	435 µg/[%]	13

The TOC normalised estuary samples show for the Gulf of Tonkin values from 1.06 µg/[%] to 287 µg/[%] (average of 73.4 µg/[%], *n* = 18). In estuary samples of the Vietnamese Shelf sub-area values are ranging between 43.6 µg/[%] to 2743 µg/[%] (average of 539 µg/[%]; *n* = 23). The estuary samples of the Vietnamese Coast sub-area

show values from 19.4 µg/[%] to 1678 µg/[%] (average of 361 µg/[%], *n* = 17). Estuary samples ascribed to the Sunda Shelf have values ranging between 10.8 µg/[%] to 299 µg/[%] (average of 88.4 µg/[%]; *n* = 15). In Thailand, estuary samples show values from 21.9 µg/[%] to 2044 µg/[%] (average of 435 µg/[%]; n =13). The estuary samples (all, *n* = 86) show an overall range from 1.06 µg/[%] to 2743 µg/[%] (average of 299 µg/[%]). The estuary data also show characteristic even over odd distribution, with highest FAME concentration in $C_{16:0}$ and $C_{18:0}$.

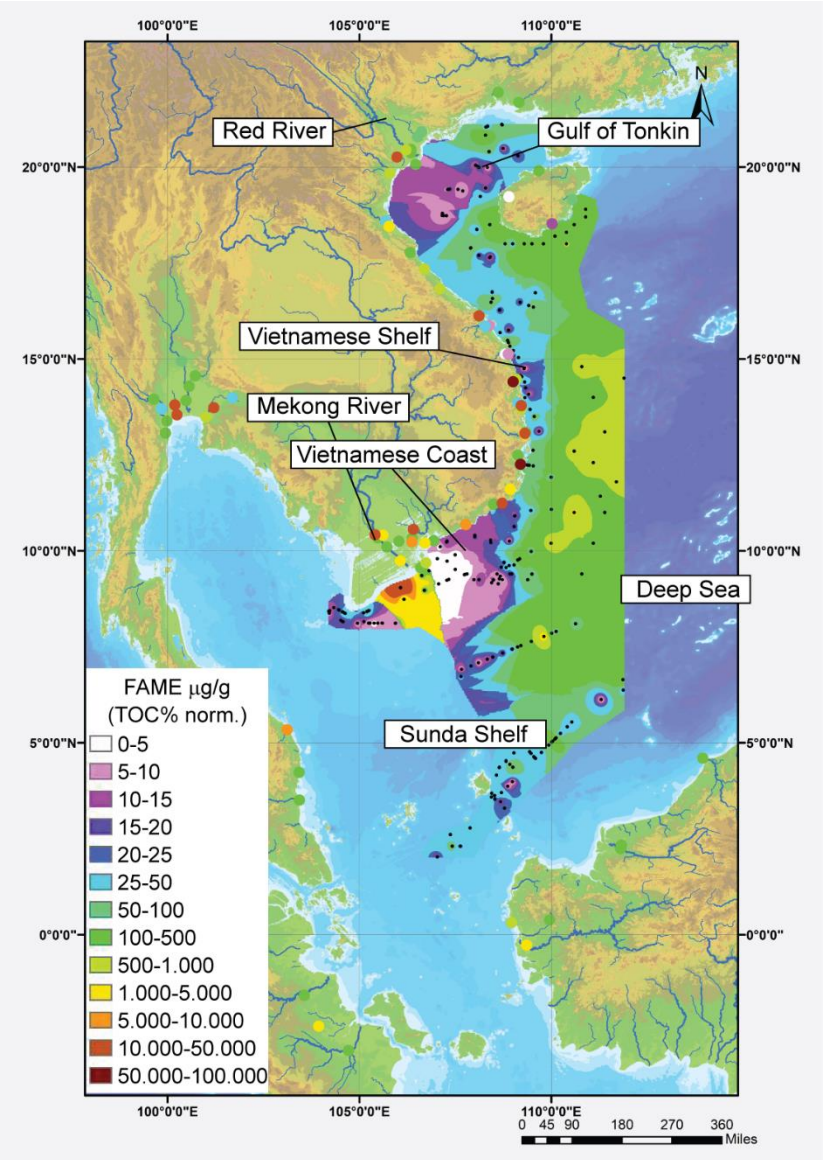

Figure 15) Interpolated (Invers distance weighting) FAME distribution map TOC (%) normalised of the study area. Available river data plotted as individual spots

3.4 Discussion

3.4.1 Origin of organic carbon in the westernmost South China Sea

OM in marine and riverine surface sediments is accumulated from a variety of different sources, of variable proportions. The different sources of OM typically are C_3 and C_4 plants, fresh and sea-water algae and bacteria, each having distinctly different $\delta^{13}C$ and C_{org}/N_{total} compositions [220] (Fig. 17). Bulk organic $\delta^{13}C$ and C_{org}/N_{total} should therefore reflect the relative contributions of the source OM [238]. Using the $\delta^{13}C_{org}$ and C_{org}/N_{total} geochemical proxies (Fig. 17), a first step is to identify possible sources and secondly make statements of which type of source contribution (e.g. C_3, C_4, or Crassulacean acid metabolism (CAM) plants) is dominant.

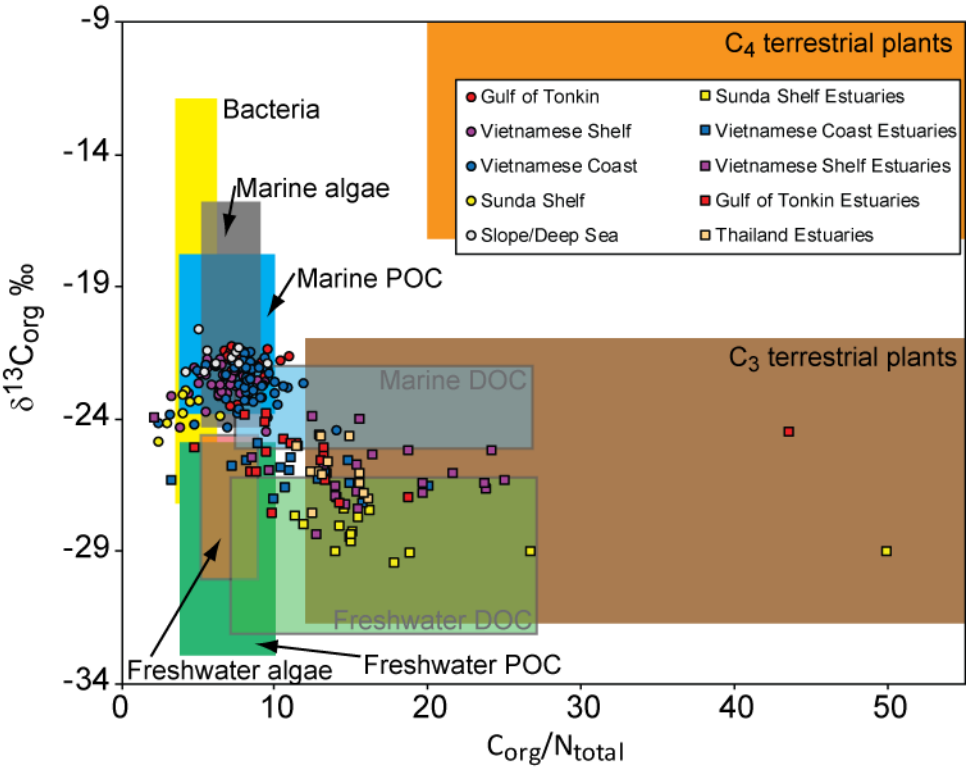

Figure 16) The $\delta^{13}C_{org}$ and C_{org}/N_{total} ratios of marine surface sediments (coloured spheres), correlating river/estuary (coloured squares) and Slope/Deep Sea samples (grey spheres). The fields illustrated are taken from Lamb et al. [220]. Uncertainties for $\delta^{13}C_{org}$ values are smaller than symbol size. Some samples with C_{org}/N_{total} ratios lower than the boxes defined by Lamb et al. could indicate local variability

The range in $\delta^{13}C_{org}$ and C_{org}/N_{total} of some of the potential sources (e.g. C_3 and C_4 plants, algae) is discussed in Lamb et al. [220] and adopted in this study for the evaluation of samples from the SCS (Fig. 17). Lamb et al. [220] reviewed a wide range of coastal environments that have utilised several techniques to distinguish $\delta^{13}C_{org}$ and C_{org}/N_{total} ratios of various sources of carbon and its wide use as a tracer of carbon pathways and storage. The review also discusses alteration pathways of geochemical signatures due to

e.g. decomposition of primary material leading to changes in $\delta^{13}C_{org}$ and C_{org}/N_{total} (lower $\delta^{13}C_{org,}$ values due to decomposition of labile OC [239] and lower C_{org}/N_{total} ratios due to decomposition of OM in very low TOC samples [240]).

For terrestrial plants, Lamb et al. [220] uses ranges for C_3 plants of $\delta^{13}C_{org}$ from -21 ‰ to -32 ‰ [65], freshwater aquatic plants with values from -11 ‰ to -50 ‰ [241, 242] and C_4 plants with a range between -9 ‰ to -17 ‰ [65]. The C_{org}/N_{total} ratios for terrestrial plants are >12, which is considered relatively high [243], as it contains higher contributions of lignin and cellulose, which are nitrogen depleted. The threshold value of 12 must be considered with some flexibility to account for local variability over large-scale regions. In addition, specific C_3 vascular plants (e.g. sweetcorn) have C_{org}/N_{total} ratios of around 12 and higher [244], whereas C_4 plants (e.g. grasses) typically have C_{org}/N_{total} ratios of above 30 [245]. Plant C_{org}/N_{total} values can further be highly variable in a small area due to large fluctuations in the nitrogen content of plants [220]. In summary, C_{org}/N_{total} is a bulk OM source proxy that must be taken with caution and should always be combined with independent, supporting evidence.

Aquatic plants, like freshwater algae in C_3 dominated environments, have $\delta^{13}C_{org}$ values of -26 ‰ to -30 ‰ [245, 246], which is distinct from marine algae that show lower $\delta^{13}C$ values from -16 ‰ to -23 ‰ [245, 247]. Freshwater and marine algae in catchments dominated by C_4 plants instead have relatively high $\delta^{13}C_{org}$ values <-16 ‰ [248]. Bacteria in coastal environments have $\delta^{13}C_{org}$ values from -12 ‰ to -27 ‰ [249], while swamp lands in the deep continental interior can have values of -66.1 ‰ ± 5 ‰ [250]. The C_{org}/N_{total} ratios for bacteria and algae are relatively low and are between 4-6 and <10, respectively [244, 245]. The POC in aquatic settings is a mixture of OM sources, including diatoms, dinoflagellates, green algae, euglenoides, and zooplankton. Marine particulate OM is characterised by $\delta^{13}C_{org}$ values that range from -21 ‰ to -18 ‰ and is dominated by phytoplankton input [251]. It is the phytoplankton which drives the C_{org}/N_{total} value towards 5 to 7, since it is nitrogen rich [244]. The threshold for marine organic C_{org}/N_{total} is defined at <8 [252]. Different from that, sediments dominated by terrestrial sources are typically rich in C_3 plant components, which exhibit $\delta^{13}C_{org}$ ranging from -25 ‰ to -33 ‰. More positive $\delta^{13}C_{org}$ values are expected with the admixture of isotopically positive/heavy C_4 plants [220]. Weiguo et al. [253] found $\delta^{13}C_{org}$ values to be a function of the relative proportion of C_3 and C_4 plants in POC.

The estuary samples from the SCS have TOC > 0.1% and most likely reflect a mixture of C_3 plant signal and freshwater POC, consistent with independent observations from Eiche et al., [226]. This interpretation is strengthened by the classification diagram in figure 17 [220], where $\delta^{13}C_{org}$ values lower than -24 ‰ and C_{org}/N_{total} ratios of 8 to 16 describe the majority of estuary samples. Based on $\delta^{13}C_{org}$ and C_{org}/N_{total} no clear distinction can be made between the estuaries of the Gulf of Tonkin, Vietnamese Shelf, and Vietnamese Coast. The Sunda Shelf estuaries represent an exception with lower $\delta^{13}C_{org}$ values but similar C_{org}/N_{total} ratios (-29.5 ‰ to -26.1 ‰ and 2.3 to 6.4 respectively, Fig. 17) compared to the other estuary samples. While the Sunda Shelf marine surface sediments have very low C_{org}/N_{total} ratios (2.3 to 6.4), clearly separating them from the Gulf of Tonkin, some of the Vietnamese Shelf and Coast samples show similar signatures ($\delta^{13}C_{org}$ from -27.7 ‰ to -20.3 ‰, C_{org}/N_{total} from 2.3 to 11.8). This observation suggests a gradual change in OM source from north to south, linked to latitudinal variations in e.g. coastal vegetation supply (e.g. less/more mangrove), variable bacteria, and phytoplankton activity along the N-S shelf transect.

There is an apparent relationship between the composition of estuary samples and marine surface sediment samples from the Sunda Shelf. Sunda Shelf marine surface sediment samples are isotopically heavier than their estuary counterparts, and exhibit lower C_{org}/N_{total} values. This transition of geochemical composition likely reflects source to sink processes such as decomposition, mixing of sources or transport distances and timescales. This observation is also made for samples from marine and estuary systems of the Gulf of Tonkin, Vietnamese Shelf, and Vietnamese Coast. Between these regions, the minimum and maximum $\delta^{13}C_{org}$ isotopic composition appears to be restricted to different ranges, e.g. the Sunda Shelf is distinctly lighter on average, while the Vietnamese Shelf is isotopically heavier on average. This can be related to vegetation cover and OM composition introduced to the riverine systems.

It is observed that the bulk composition of estuary and marine surface sediments provide no evidence for a significant contribution of C_4 plants. This comes surprising, since farm crops such as sweetcorn (C_4 plant) are documented. The study of Eiche et al. [226] has also demonstrated that samples close to the Red River exhibit a geochemical composition that forms a loose array between the range of C_4 plants and marine POC [226]. It therefore appears that any C_4 plant signal in proximity to the Red River is only preserved for few hundreds of meters transport distance, interpreting the data presented by Eiche et al. [226]. Since the majority of the vegetation cover in the study region is characteristic of

C_3 plants, the data presented in this study reflects the expected ranges and compositional transition.

The marine surface sediments from the SCS are almost exclusively characterised by marine POC and bacteria signatures, using $\delta^{13}C_{org}$ and C_{org}/N_{total} (Fig. 16), and the estuary/river samples form an array from the range ascribed to C_3 plants. Previous studies have suggested that these differences in OM composition are attributed to variations in the role of different sources, i.e. an increased influx of material from freshwater POC [226] from the Red River into the Gulf of Tonkin or other (marine) sources.

The coastal mangrove belts near Ba Lat of the Red River delta range in $\delta^{13}C_{org}$ from -25.9 ‰ to -28.1 ‰ and in C_{org}/N_{total} from 11.6 to 27.1 [254, 255]. The mangrove belts probably are the last C_3 plant source contributing to the OM signatures, before mixing with the marine source materials. The marine surface sediment C_{org}/N_{total} ratio in the data from this study are typically <12, which is wider than ranges observed by Eiche et al., [226], suggesting that terrestrial components contribute significantly to the C_{org}/N_{total} signature.

Overall, the data reflect the expected gradual transition of terrestrial OM (i.e. C_3 plants) towards marine OM signatures using $\delta^{13}C_{org}$ isotopic composition and C_{org}/N_{total} values.

3.4.2 Total abundance of FAME in surface sediments

Information on the origin of OM is obtained from both the composition of sedimentary lipids and their abundance. Comparison of total FAME abundances is known to identify carbon pathways and provide constraints on degradation processes. FA are abundant in most organisms and thus they are the most common lipid type in recent sediments [256]. Different chain lengths are typical for different sources, such as bacteria, microalgae, higher plants, and marine fauna. The long-chain alkanoic acids ($>C_{22:0}$) reflect a source from terrigenous higher plants [231, 257] whereas FA in the lower carbon number range (*n*-$C_{14:0}$– *n*-$C_{22:0}$) are derived mainly from algae [229–231], making them a proxy for marine productivity. However, some FA are ubiquitous (*n*-$C_{16:0}$; *n*-$C_{18:0}$) and common in both microorganisms and higher plants, and highest concentrations are observed for *n*-$C_{16:0}$ and *n*-$C_{18:0}$ in marine surface sediment samples.

The average distribution patterns of *n*-alkanoic FAME in the SCS sub-areas are presented in figure 14 and 15. All sub-areas exhibit a monomodal to weak bimodal distribution with a strong even-numbered carbon chain predominance, maximising at *n*-$C_{14:0}$, *n*-$C_{16:0}$

or *n*-$C_{18:0}$ (Fig. 14). In the Slope/Deep Sea and Gulf of Tonkin areas *n*-$C_{22:0}$ and *n*-$C_{24:0}$ are elevated relative to the remaining areas and are interpreted to reflect accumulation of terrestrial material. Slope/Deep Sea sediments show overall the highest FAME content of sediments studied, except for *n*-$C_{12:0}$, followed by samples from the Gulf of Tonkin. This suggest that the Slope/Deep Sea and the Gulf of Tonkin serve as storage sites for terrestrial derived OM, while the Vietnamese Shelf, Vietnamese Coast and Sunda Shelf are either limited in their capacity to accumulate OM, or transport mechanisms (e.g. current dynamics) are more efficient than those processes which govern fixation in sediments (e.g. SA).

While the abundance of FA did reveal differences between sub-regions of the SCS, the identification of sources and their quantitative contribution is limited, since the most abundant chain lengths are representative of marine and terrestrial origins (*n*-$C_{14:0}$, *n*-$C_{16:0}$ and *n*-$C_{18:0}$). While the high abundance of longer (>*n*-$C_{22:0}$) chain FA in the Gulf of Tonkin and the Slope/Deep Sea area imply an increased terrestrial component, comparison of *n*-$C_{10:0}$/ *n*-$C_{24:0}$ ratios between different regions of the SCS does not suggest localised enrichment of terrestrial OM (Appendix 4). The application of a TOC normalisation to total FAME abundances did not reveal any notable differences in the aforementioned patterns. This is expected from the spread of TOC in the samples and simply verified and reported here for consistency.

3.4.3 Transition of sediment composition from Estuary to Deep Sea signatures – implications from fatty acid methyl esters (FAME)

The abundance of FA in nature is characterised by higher proportions of even number carbon chains compared to their corresponding odd numbered carbon chains [61], as observed in the SCS by Hu et al. [236]. This relationship is related to the fact that even chain FA are built in living organisms. For example, the human body produces only even chain FA since the enzymes exclusively process carbon-carbon chains. It is only in plants where these newly constructed long-chain FA are split by enzymatic processes, resulting in an uneven number of total carbon atoms in the chains. This opens the opportunity to distinguish plant *vs.* non-plant input in a natural sample. In order to compare data of different samples using the abundance and chain length of FA by qualitative means, the data must be normalised against potential dominant source reservoirs (e.g. average river or deep sea sediment) to reduce scatter between even and uneven chain lengths. In this study, the two main source reservoirs are i) average river/estuary and ii) Slope/Deep Sea

sediments. This normalisation step also allows to better reveal the presence and/or absence of typical terrestrial (long-chain, C_n >20 [228]) or marine (short-chain to mid chain, *n*-$C_{10:0-20:0}$ [256]) signals.

3.4.3.1 Identification of region-specific patterns after normalisation

A quantitative separation of FA chain length between terrestrial and marine source is not straight forward, since biodegradation results in the decomposition of long-chain terrestrial FA into short-chain FA, which could be misinterpreted as marine origin. By comparing any sample from the estuary-shelf-deep sea SCS with either the terrestrial or the marine dominated 'end-member' reservoir, the degree of mixing of the OM can be determined. Differences observed in samples from the same region can be indicative of changing conditions, including transport efficiency (e.g. primary marine *vs.* terrestrial production, oxygenation, physical force during transport), or, for estuary samples, river flow/land use perturbations (e.g. through damming) in the hinterland. Normalisation against a defined reservoir (in this case study "deep" marine) removes scatter and anomalies, if i) the average values of the reservoir selected for the normalisation are representative, ii) the samples have not undergone excessive physical- or bioturbation, and iii) bulk OM composition post deposition is not artificially fractionated.

Figure 17 shows that most of the surface sediment samples in the Gulf of Tonkin are depleted in FA relative to the estuaries (y-axis values below 1 in figure 17). Most samples show a pronounced negative *n*-$C_{14:0}$ anomaly. This negative anomaly can have two origins, i) higher production and/or preservation of *n*-$C_{14:0}$ in the reference samples used to normalise the unknown samples or ii) lower production and/or preservation of *n*-$C_{14:0}$ in the unknown samples at present day relative to the normalisation factor. Since the Slope/Deep Sea normalisations samples are assumed older than the unknown samples, this could reflect changes in vegetation cover, which can result in compositionally different OM transported and deposited in the study area. Furthermore, some samples from the Gulf of Tonkin are characterised great similarity to the estuary sample composition (values close to one, see indication figure 17). Samples which exhibit this feature were taken close to the coast of Hainan, in an upwelling area [258], which is an area of high bio productivity. This high productivity area can be responsible for the higher abundance of measured FAME content, thus explaining some of the observed spread in figure 17. Intriguingly, those samples from the upwelling area do not exhibit a

negative *n*-$C_{14:0}$ anomaly, which could mean, the deficit of *n*-$C_{14:0}$ is linked to marine bio production, rather than terrestrial vegetation cover.

In the Vietnamese Shelf samples, marine reservoir normalisation results in a flat correlation for shelf deposits, without pronounced negative anomalies (Fig. 18). The Vietnamese Shelf samples are depleted in all FAME abundances, when normalised to the regional estuary samples (Fig. 17). Some FAME reveal both negative (*n*-$C_{16:0}$ and *n*-$C_{18:0}$) and positive (*n*-$C_{21:0}$) anomalies, with a restricted range in abundance (Fig. 17). A lower abundance of long-chains FAME (*n*-$C_{10:0}$ > *n*-$C_{24:0}$) and weakly defined positive anomalies for *n*-$C_{14:0}$, *n*-$C_{16:0}$ and *n*-$C_{18:0}$ are noted (Fig. 18).

The normalisation of Vietnamese Shelf samples to the marine end-member reservoir reveals an enrichment of short-chain (≤10) FAME to the expense of long-chain FAME. A general negative trend from short-chain to long-chain FAME is noted for most samples with a weakly defined negative anomaly for *n*-$C_{16:0}$ and *n*-$C_{18:0}$. Some of the samples from the Vietnamese Shelf show an enrichment of total abundance of *n*-$C_{10:0}$ FAME (SO-140-27; SO-140-30; SO-140-37; SO-140-50; SO-140-52).

Similar patterns for the Vietnamese Coast sediments are observed, except for two samples. Most of the samples exhibit a negative anomaly at *n*-$C_{14:0}$, and a positive anomaly at *n*-$C_{21:0}$. Samples SO-187-3-87-2 (9.04 N; 106.08, 20 m water depth off the Mekong River delta) and SO-140-22 (9.79N; 109.18 E, 183 m water depth and close to the continental slope) are enriched in FAME in comparison to other samples from the region. Sample SO-187-3-87-2 has to be evaluated with care, and observations made while taking the sample can possibly account for observed data. The extraordinary high abundance of FAME is in correlation with the high TOC value (4.3 %), which is exceptional high compared to the other samples (max ~2 %). During sample processing, strong organic odours were noticeable, as well as chunks of OM that resembled of grass or seaweed leaves. Intriguingly, the general patterns are of striking similarity to the other samples, suggesting that this an effect related to OM preservation only. The sample SO-140-22 is visually different in figure 17 and 18, as it does not exhibit any significant anomalies. In particular, the similarity with the Slope/Deep Sea normalisation factor (values close to one, figure 18) is intriguing.

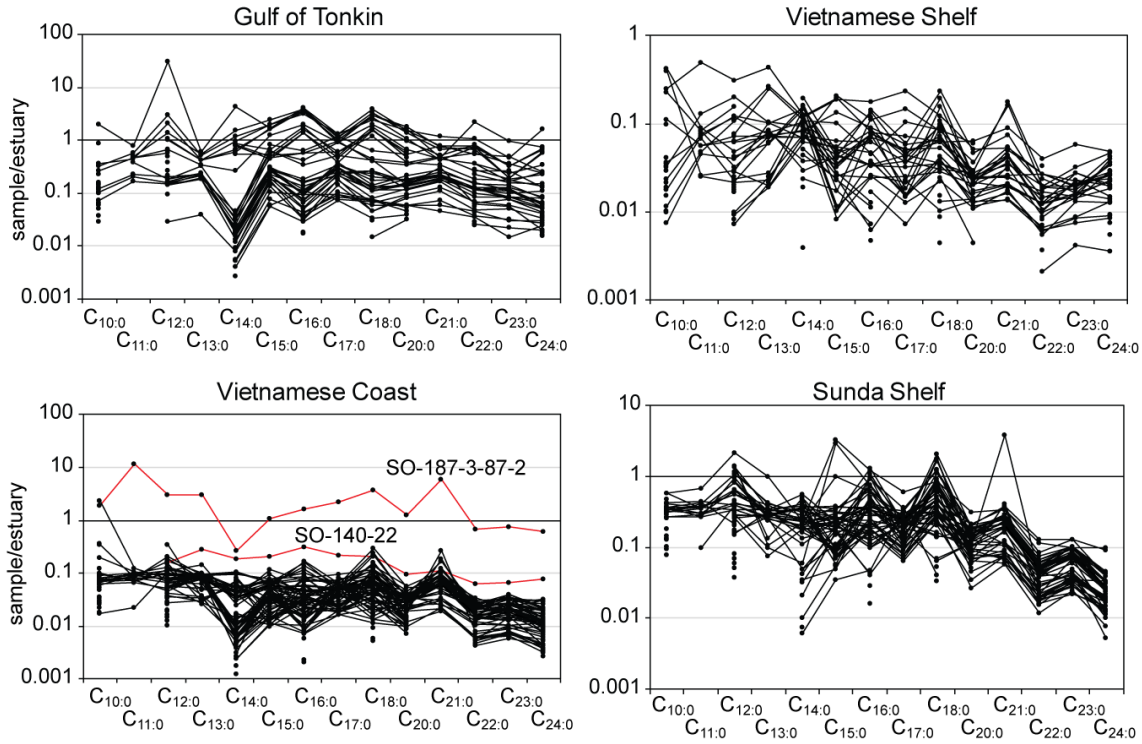

Figure 17) Marine surface sediments FAME values normalised against the respective average river/estuary sediment FAME composition from the Gulf of Tonkin, Vietnamese Shelf, Vietnamese Coast, and Sunda Shelf

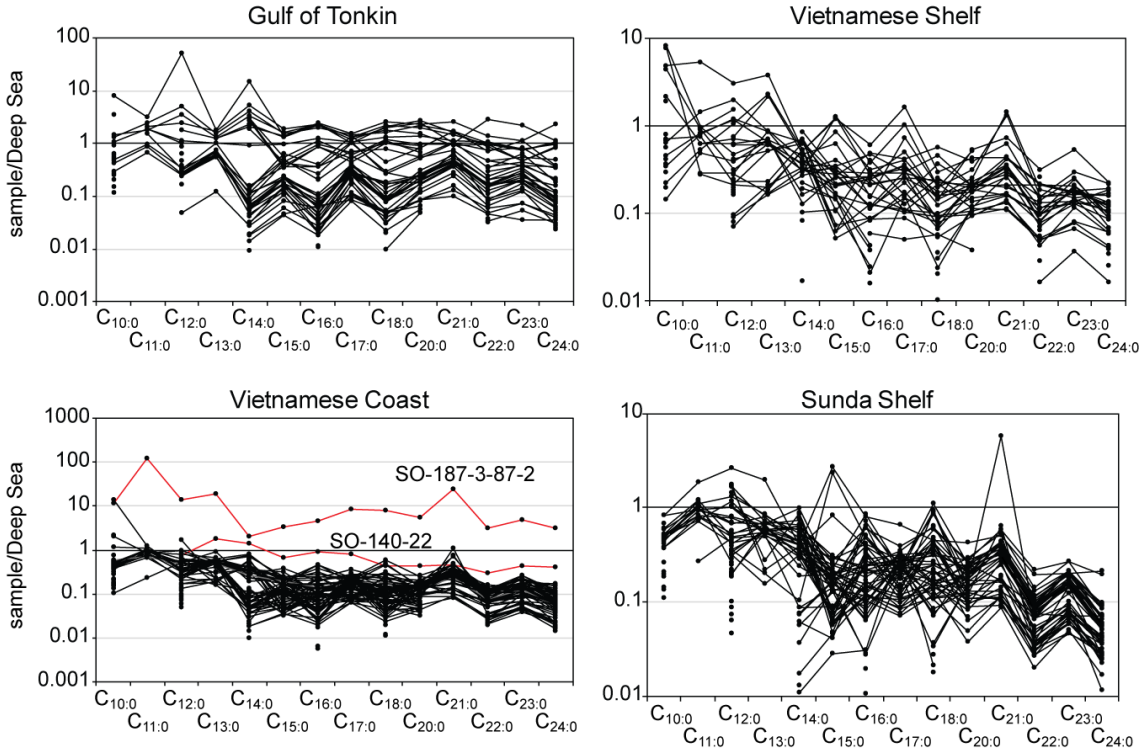

Figure 18) Marine surface sediments fatty acid methyl esters values normalised against the average slope/Deep Sea sediment fatty acid methyl ester composition. The terms enriched refer to values >1, depleted to values <1 and anomaly describes the low abundance of a fatty acid relative to the fatty acids one-carbon longer and shorter (e.g. $C_{13:0}$ is lower than $C_{12:0}$ and $C_{14:0}$), after normalisation. In this study the assumption is made that the Slope/Deep Sea samples reflect older OM relative to the estuary sample composition, which are considered to be recent/modern

Upon investigating the geographic location, proximity to the boundary between shelf and slope (at 200 m depths) is observed, as evident from water depth (sample at 183 m) and bathymetric maps. It is hypothesised that the sample might not represent pure shelf sediment composition, but instead is a hybrid in the transition zone, constituting FAME composition intermediate between a typical shelf value (the shallower samples of the Vietnamese Coast) and the Slope/Deep Sea normalisation factor. A more speculative interpretation could be based on the total concentration of FAME data. Samples SO-187-3-87-2 and SO-140-22 are enriched in FAME (>1,300 µg/g), while the next highest samples from the shelf contain ~700 µg/g. This would make the lower concentration samples more susceptible to selective decomposition processes, which are volume, or rate limited, which could increase the observed roughness in the spectra. Both samples with higher FAME content exhibit smooth spectra, which could be evidence supporting this hypothesis. However, more data is needed to investigate this phenomenon.

Open marine samples from the southernmost area of this study, the Sunda Shelf, were normalised to estuaries of Malaysia and Sumatra and show a general depletion of FAME abundance relative to estuary samples. It should be noted that the extent of the Sunda Shelf requires a much larger estuary data coverage, than what is available at present. Those estuary samples studied are strongly enriched in long-chain (*n*-$C_{18:0}$ and longer) FAME (Fig. 17), consistent with a stronger terrestrial origin.

3.4.3.2 Interpretation of observed anomalies after normalisation of FAME

FA allow better resolution between marine and terrestrial components, and their sensitivity to degradation allow a more region-specific estimation of fresh OM preservation [259]. The observations made from FA tracers can be compared to bulk sediment observation, testing the differences and similarities of each approach. The comparison of both datasets will also allow to test how robust each finding is, and how bulk and molecular level analyses should be weighed in their interpretation.

The introduced normalisation factors (average estuaries and average Slope/Deep Sea) are set to decipher processes, which have modified the OM FAME signatures during transfer from land to ocean. The estuaries are treated locally, since changes in vegetation, human settlement density and climate may affect sedimentary FAME signature stronger than in open marine settings. This approach allows identifying, which FAME components experience the strongest depletion or enrichment due to terrestrial processes.

Technically, the riverine normalisation should result in a deficiency of FAME in all unknown marine surface sediments (simply speaking, values lower than one). The normalisation using Slope/Deep Sea values is expected to result in values greater than one for unknown marine surface sediments, assuming that progressive decomposition from the riverine to deep marine environment is in effect. Any deviation from these expectations could be related to e.g. constant influx of FAME from e.g. marine bio-productive activity or mixing of different source materials in the transitional zone. Additional complexity can be introduced, if TOC content from land to deep ocean does not decrease in a linear fashion, and instead accumulation occurs in the deep sea area. In fact, in the SCS study area the TOC content for the riverine and deep ocean systems are on average higher than the unknown shelf sediments, which will technically result in normalisation values lower than one, regardless of the chosen normalisation factor.

FA are particularly diverse in their ability to record several processes, since they are present in all living organisms and comprise the most abundant component of lipids [260]. Several FA have been described in the literature, and here a focus on *n*-$C_{15:0}$ (pentadecanoic acid) of both plant (e.g. *Durio graveolens* [78]) or animal [261] sources is pursued, while it is acknowledged that many more sources are possible. The FA record in this study might be a sensitive indicator to changes in OM composition preserved in marine surface sediment samples. Possible factors changing the OM composition are manifold (e.g. climate or nutrition related, etc.), but cannot be isolated at present. Of all of the FA compounds some are only slowly degraded or some are transformed to more stable chemical structures (e.g. Gagosian et al. and Kohnen et al. [262, 263]), and thus they can be used as tracers of degradation, if initial concentrations are known. The best approach to this is comparing the abundance of several FA from a given sample, but it is important to note that some compounds are more widely distributed in the biosphere than others [256].

Selective preservation of FA can possibly be reinforced by the fact that the Gulf of Tonkin does not exchange significant mass of water or suspended material [264] with the main area of the SCS. This i) prevents addition of significant amounts of marine OM from further offshore areas, ii) prevails changes in wind direction and strength [146] might reduce the overall impact of marine production over several seasons and iii) favours shallow marine currents within the Gulf that result in efficient and repetitive circulation of OM in the region rather than transport away to the deep basin or Vietnamese Shelf.

The data suggest that across the Vietnamese Coast a positive anomaly of *n*-$C_{21:0}$ is present, possibly attributed to either plants (*cleome viscosa*, [265], animals (chicken skin lipid, [266], human milk fat [267] or marine algae and organisms [229]. Chicken skin and human milk fat are likely transported by wastewater, while *cleome viscosa* has applications in the farming industry [268]. However, the quantity of external input cannot be determined and assessed, making it impossible to evaluate if a positive anomaly is related to higher algae and microorganism activity or anthropogenic activity. With the available data, a correlation with anthropogenic sources seems unlikely, but cannot be rule out entirely. The amount of biomass produced by vegetation is likely to outweigh the anthropogenic contribution, and this can possibly be tested when investigating another FAME.

Some of the Sunda Shelf samples exhibit a negative anomaly for *n*-$C_{15:0}$, a compound that is known to have origins in: i) cows' milk fat [261], ii) hydrogenated mutton fat [269] and iii) the plant *Durio graveolens* [78]. The latter is found across Sumatra, Southern Thailand, Borneo and the Malayan peninsula [270] in great abundance. *Durio graveolens* flourishes at high humidity and heat conditions, which are found at present day in southern parts of the SCS. Assuming that *Durio graveolens* is the primary cause for the observed *n*-$C_{15:0}$ negative anomaly, this can indicate i) the possibility that climate conditions have changed in the past impacting abundance of *Durio graveolens*, or ii) that transport mechanisms were more effective in the past (e.g. change in transport distance). The discussion of the scenario outlined requires a preservation of OM signatures accumulated ca. 21 BP to 12 ka BP. Based on previous documentation of relict sands from the sample area [271], it is reasonable to assume that such sediment is exposed at present day ocean floor surface. For this purpose, an isolated set of samples is investigated, which exhibits a pronounced negative *n*-$C_{15:0}$ anomaly and originates from the Molengraaff Palaeoriver (Chapter 1 – General Introduction, Fig. 8), which is partly comprised of relict sands (Fig.19).

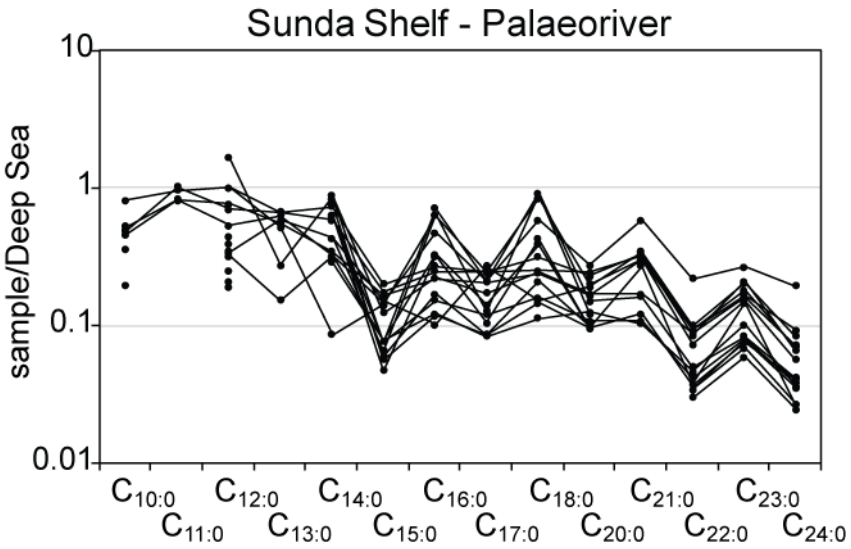

Figure 19) Marine surface sediments fatty acid methyl esters values normalised against the average slope/Deep Sea sediment fatty acid methyl ester composition. The terms enriched refer to values >1, depleted to values <1 and anomaly describes the low abundance of a fatty acid relative to the fatty acids one-carbon longer and shorter (e.g. $C_{13:0}$ is lower than $C_{12:0}$ and $C_{14:0}$), after normalisation. In this study, the assumption is made that the Slope/Deep Sea samples reflect older OM relative to the estuary sample composition, which are considered recent/modern. Here an isolated set of samples, which represents a palaeo-river, exhibits a negative *n*-$C_{15:0}$ anomaly

Previous climate studies have suggested a colder period in the SCS (~20 BP - 10 ka BP), which resulted in a sea level change [152]. Furthermore, during past colder periods the transport way of *Durio graveolens* might have been shorter than today, if the landmass reconstruction of Hanebuth et al. [152] is accurate. The transfer distance between shallow shelves to deep sea would have been shorter by hundreds of miles compared to present day, for large parts of the SCS. Importantly, if the colder climate has caused a reduction or disappearance of *Durio graveolens*, the sediments formed at this time will contain reduced amounts of *n*-$C_{15:0}$, relative to present day samples which contain more abundant *n*-$C_{15:0}$ from *Durio graveolens.* Therefore, this approach of normalisation of FAME data can be very useful to investigate relict sand samples, samples taken from stratigraphically older sediments, and highlight immediate differences in local, regional or over regional data sets.

As for animal derived origin of *n*-$C_{15:0}$, this is difficult to test due to lack of data, but overall considered an unlikely source. Cows' milk fat is rarely used in South East Asia, compared to Europe, and dense vegetation is unusual for mutton and goat farming. Additionally, human and domesticated cattle populations were lower to non-existent in the past (up to 20 ka BP).

Concluding, in this study the FAME *n*-$C_{15:0}$ appears to be a sensitive recorder of past changes in vegetation, likely related to climate and sea level change, making the study of

FAME records a useful tool in understanding present and past processes in marine geoscience in the SCS. Yet, these interpretations can be further reinforced by using multiple normalisation factors, to test consistency.

In a next step it is tested if the data are sensitive to comparison with a normalisation factor derived from both recent samples (estuary) and a normalisation factor derived from older (Slope/Deep Sea) samples, based on radiocarbon timescales (see Chapter 2 – Material and Methods). The appearance/disappearance of the anomaly related to the choice of either older or recent normalisation factor implies that variable climate conditions, mobilisation, transport, and burial mechanisms can be responsible for this feature. If the climate conditions in the SCS were variable, as suggested by Hanebuth et al. [152], postulating that parts of the Sunda Shelf were above sea level during the last glacial maximum (around 21 Kyrs BP), the FA anomaly could be a result of changes in palaeoclimate, which could be partly preserved in the studied surface sediments. This hypothesis can be tested, by investigating the Sunda Shelf samples for an anomaly in *n*-$C_{15:0}$, when normalised against the regional estuary samples, which are inferred to be young/modern (see Chapter 4). If the anomaly of *n*-$C_{15:0}$ is due to the more widespread occurrence of *Durio graveolens* from past glacial conditions, no anomaly in *n*-$C_{15:0}$ should be observed when normalised against the estuary, as confirmed for the samples examined (Fig. 17). This makes normalisation against chronologically older and younger material a useful indicator to probe for potential changes in palaeoclimate and palaeoenvironment.

The application of a modern normalisation factor, such as recent river and estuary compositions, can also be sensitive to identify short-term changes in bio-production, anthropogenic influence, and rates and length of transport pathways from OM sources to marine sinks. On the topic of land-use, the sedimentary FAME record in parts of the SCS could indeed be affected by the extensive production of palm oil for economic purposes across the SE Asian region. Such contributions from commercial agriculture may potentially explain the observed negative anomaly in *n*-$C_{14:0}$ and *n*-$C_{16:0}$ in the Gulf of Tonkin and along the Vietnamese Coast. However, this conclusion is not straight forward, as other sources may contribute to the total abundance of *n*-$C_{14:0}$, most prominent from gram-negative bacteria [272, 273], including cyanobacteria. Cyanobacteria are abundant across the study area [274–276], consistent with high concentrations in other shelf regions (e.g. Chesapeake Bay, [277]). Data on the FAME composition of cyanobacteria, their abundance, and temporal variability are to current knowledge

unavailable in the study area. The negative excursion of *n*-$C_{14:0}$ might therefore be either an indicator for the absence of palm oil, or large-scale cyanobacterial activity for the time-period representing the deposition of the surface sediment, or a combination of both.

Different to the Gulf of Tonkin and Vietnamese Coast, samples from the Vietnamese Shelf and Sunda Shelf do not show any positive or negative anomalies when normalised against their estuary compositions, suggesting different controls on FAME supply and preservation in the southern and more open marine sector of the study area. A depletion in long-chain FA relative to short-chain FA in this southern region is recognised (Fig. 18). This depletion may reflect i) degradation of OM during transport and settling and ii) mixing of marine and terrestrial OM, where marine OM is rich in short-chain FAME [256], in combination shifting the bulk composition towards higher abundance of short-chain FAME.

While these FAME specific interpretation help to resolve multi-scale variations in temporal space and vegetation, the total abundance of FAME allow a better understanding, which regions serve as accumulation areas of OM. Since long-chain FAME are considered terrestrial markers, a higher abundance of these in a marine environment suggests that terrestrial derived OM is preferentially supplied and stored in such regions. Alternatively, or in addition, the marine FAME counterparts may be subject to faster degradation before burial, which would result in a sedimentary signature that is biased towards terrestrial components. A better identification and quantification of these competing processes are a remaining central task that, once achieved, will allow a better evaluation of the regional carbon cycle.

Finally, to contribute to this challenge, the region under investigation is examined for its average frequency of FAME from *n*-$C_{10:0}$ to *n*-$C_{24:0}$. To avoid sampling bias, each region's sum is normalised to the number of samples, without rejecting outliers. While this sacrifices some spatial resolution, it allows for a robust regional scale comparison and interpretation of data. The normalised sum of FAME is highest for the Slope/Deep Sea sediments (Fig. 13), which likely serves as the final and long-term storage area of OM in the SCS. This conclusion is supported by generally higher TOC in the Slope/Deep Sea samples, relative to the shelf and estuary systems. The *n*-$C_{14:0}$, *n*-$C_{16:0}$ and *n*-$C_{18:0}$ FAME are the most abundant, consistent with observations from other studies (e.g. Eglinton et al.; Volkman et al. and Hu et al. [236, 256, 278]), but the SCS Slope/Deep Sea also shows a significant enrichment in long-chain FAME. This observation supports

the conclusion that the Slope/Deep Sea rather than the shelf acts as a long-term reservoir of OM transported across the SCS, at least under modern conditions. From the four coastal regions, the Gulf of Tonkin shows the highest abundance of normalised FAME abundance (Fig. 13); it is proposed that this pattern is related to the unique geographical setting and marine surface circulation pattern that efficiently prevents the exchange and loss or gain of OM to/from the other regions of the SCS. A similar trend of enrichment of long-chain FAME is observed in the Slope/Deep Sea across the SCS. This argues that water depth is not a dominant factor in the accumulation and burial of OM. Instead, current dynamics and/or other factors such as river discharge, relict sands, and vegetation/land use may be significant. Steep shelf systems, e.g. Vietnamese Shelf and Coast and the Sunda Shelf, may therefore play a less important role in storage of labile/reactive carbon than commonly assumed. More research is needed to constrain the different rates of OM degradation within transitional transport systems and their effects on sedimentary OM burial in deep marine settings.

Therefore, normalisation of a range of FAME (and likely *n*-alkanes, *n*-alcohols, sterols and hopanes, etc.) against older reservoirs can be a useful indicator for changes in e.g. vegetation and climate over time. Secondly, further studies might find normalisation against young reservoirs useful in reconstructing short-term changes, which can be of anthropogenic origin.

The diverse number of sources and processes are related to the record of FAME in the SCS necessitates a data reduction process capable to perform cross evaluation/weighing of several tracers that can result in cohesive results. This can be achieved by stepwise building of more complex interpretations, starting with binary mixing models that consider restricted number of sources and processes. Building on that, computational modelling following e.g. Bayesian statistics (or any other statistical approach) can be utilised, to create a statistically valid model, assuming sufficient data density and quality is available. Bayesian modelling also allows incorporating qualitative and semi-quantitative observations, a useful flexibility in geological modelling.

3.5 Conclusion

Based on literature as well as own, newly established data the following conclusions are made for the SCS:

1) The abundance of FAME decreases from riverine/estuary samples towards shelf and then increases from the shelf to deep sea surface sediments, which is

interpreted to reflect degradation and decomposition of OM derived from the terrestrial reservoir and accumulation prior to final fixation and deposition. This implies that terrestrial carbon likely is an important source of nutrients to the shallow coast and estuary regime, and that marine bio-production is an essential source of carbon prior to burial in deep sea sediments.

2) The composition of FAME in the SCS normalised against end-member reservoirs, such as the Slope/Deep Sea or estuary/river, are sensitive indicators for recent changes in FAME supply and composition (e.g. related to *Durio graveolens* abundance) in the study area. The observed patterns indicate a deficiency in long-chain (*n*-C > 13) FA stored in the marine surface sediment samples, which is interpreted to reflect a diminishing component of terrestrial origin during alteration of OM prior to fixation and deposition.
3) The Gulf of Tonkin FAME signature and abundances are of high similarity to those observed from Slope/Deep Sea marine sediments, and notably enriched in long-chain (*n*-C > 18) FA, when compared to the other shelf regions studied. The most striking features of the Gulf of Tonkin are i) geographic isolation (semi-enclosed basin), ii) circular current systematics with negligible water mass exchange with the adjacent region and iii) comparatively shallow water depths relative to the Slope/Deep Sea reservoir. This similarity between isolated shelf and deep basins implies that water depth is not the dominant control in carbon burial in the SCS, but local current systematics and geographic isolation of shallow ocean currents are favourable for OM deposition and retention.
4) Here it is suggested that FAME are more sensitive to changes in the contribution of terrestrial OM than the bulk sediment composition (compared to e.g. C_{org}/N_{total} and/or $\delta^{13}C_{org}$). Classically, the C_{org}/N_{total} or $\delta^{13}C_{org}$ isotopic composition have been considered as robust tracers to the identification of marine and terrestrial contribution to the bulk OM. However, the lower abundance of FAME in combination with its often unique origin (e.g. enzyme specific generation or organism specific origin) reduce the potential for mixing effects to mask the origin of FAME, compared to bulk C_{org}/N_{total} and $\delta^{13}C_{org}$. While the number of sources for specific FAME (e.g. *n*-$C_{15:0}$) is smaller than for e.g. $\delta^{13}C_{org}$, many combinations are possible and substantial research is necessary to conclusively recommend ideal FAME tracers. Future research should be directed to the identification of FAME that are diagnostic of e.g. C_3, C_4 and CAM plants, to better estimate minuscule contributions to bulk sediment composition. An example in

the current dataset includes *Durio graveolens* (*n*-$C_{15:0}$), which might be a diagnostic plant and climate indicator in the study area. At present, no empirical evidence for C_4 plants is available, yet the presence of C_4 plants is well documented from land use (farming), so it might be interesting to understand why no C_4 signatures are present.

5) The C_{org}/N_{total} and $\delta^{13}C_{org}$ of the estuary and river samples from the SCS are dominantly characterised by C_3 plants, with no evidence for impact by C_4 crop farming. A mixing array between the estuary/river samples and the marine shelf sediments is observed, suggesting a gradual change in OM composition within the marine and terrestrial environment, but also with a sharp boundary at the land-ocean interface.

4 Controls on regional mixing and degradation of organic matter in the South China Sea – implications from mineral surface area, $\Delta^{14}C$, $\delta^{13}C_{org}$ and total organic carbon in riverine and marine surface sediments

4.1 Introduction

The understanding, quantification, and prediction of modern OC systems are a fast developing and diverse field of research, with relevant impacts on anthropogenic, climatic, and geologic applications. Many processes including mixing, decomposition, and (re)mineralisation of carbon are contemporaneously active, with highly variable magnitudes and rates, and locations. Deconvolution of these co-occurring processes in a spatiotemporal context demand tailored data sampling and interpretive approaches.

Previous studies have shown that riverine systems are a primary source and transport pathway of terrestrial particulate POC, globally accounting for ~200 Tg C/year of all carbon inputs into the ocean [189, 279–281]. Estimates of remineralisation of OC during transport from the continent to coastal regions are not well constrained, but maybe on the order of ~55 % - 80 % as estimated for the Gulf of Mexico and the Washington Continental Shelf [189, 282]. The remaining terrestrial OC (e.g. lipids, sugars, proteins etc. produced onshore) is mixed with fresh biogenic (organic), fossil (organic) and petrogenic (inorganic) carbon prior to introduction into river deltas and subsequently to the shelf systems. This newly mixed OC pool is ultimately introduced into the sedimentary system in delta sediments and then moved along coastlines and continental margins [282–284] before some of it may transfer into the deep ocean basins. In the SCS, the riverine POC input is estimated at 16.03 Tg/year ± 2.87 Tg/year (based on 52 rivers) [285]. Rates of deposition, decomposition and burial in shelf-margin environments are highly heterogeneous and region-specific [189]. With this in mind, the geographic extent of the SCS harbours multiple changes in shelf-types (isolated, narrow, wide) in a single interconnected system, representing the majority of shelf types found in the modern ocean [51].

To create an interpretational framework that describes carbon-cycling processes in the SCS, terrestrial source lithologies must first be considered. This is because they serve as the primary source of bedrock-derived OC classed as petrogenic carbon [11]. This petrogenic carbon, in turn, affects the radiocarbon composition (‘age’) in marine surface sediments. Bianchi et al. [205] document that increasing proportions of petrogenic carbon

in sediments correlate with older radiocarbon dates (Taiwan, northern California, Bay of Bengal).

In this study, the aim is to test if this same observation also applies to the SCS, since this might be a function of the rate of fresh, biogenic to old petrogenic carbon exported from land to sea, and local source characteristics. Furthermore, decomposed OC (re)mobilised from soils and eventually mixed with petrogenic carbon and fresh terrestrial, lacustrine/riverine and microbial biomass, may result in variable but typically low radiocarbon content ('young' age) OM. This high degree of complexity in OC radiocarbon content requires careful evaluation of bulk analyses, to be able to use radiocarbon content as a geochemical tool.

The continental source regions of the SCS are extensive and riverine transport (sediment and POC discharge) is dominated by two large river systems, the Red River (138 mil. M.T.) in the north and the Mekong River (166 mil. M.T.) in Vietnam [16], with numerous small and intermediate size rivers contributing to regional/local transport and export. River types behave differently, based on the river continuum concept [286]. Large river systems exhibit longitudinal patterns, from source to delta [286], and receive significant quantities of fine particulate OM from upstream processing of e.g. dead leaves and woody debris. The effect of riparian vegetation is insignificant, but primary production may often be limited by depth and turbidity [286]. In contrast, small headwater streams often exhibit variable chemical characteristics reflecting geomorphology and ecology in individual watersheds. These catchment properties are consistent with the river discontinuum theory that recognises the uniqueness of small streams draining dramatically different catchments and gaps in downstream patterns that occur as tributaries merge [287]. Mountainous rivers are different with variable biogeochemical characteristics when altitudinal changes in terrestrial ecosystems are reflected in streams [288]. Rivers drain large sources of freshwater, mineral matter and nutrients [223, 289], known to affect the salinity at the interface of the delta towards the coastal ocean [290].

River-water-redox condition is another environmental variable to consider. The Red River maintains an oxygenated environment in the Gulf of Tonkin, while the Mekong River carries lower amounts of dissolved oxygen [291] to the northern Sunda Shelf, both impacting shelf carbon cycling. The export of oxygen-rich river water in the Gulf of Tonkin is important, as low surface current dynamics within the Gulf compared to the western part of the SCS [57] reduce oxygen exchange at the water-atmosphere interface.

A more turbulent water surface in contrast favours gas exchanges with the atmosphere [292, 293].

The study of Rojana-anawat et al. [291] concluded that this discrepancy of dissolved oxygen between both Vietnamese rivers is related to colder temperatures in the Red River, compared to the Mekong River. It has also been shown that the higher dissolved oxygen input, e.g. from the Red River into the Gulf of Tonkin, increases the rates of degradation on the enclosed shelf, based on laboratory experiments [294]. This effect of oxygen enrichment propagates several tens of kilometres from the Red River Delta into the Gulf of Tonkin [291]. The excess supply of dissolved oxygen can also contribute to higher bioactivity (microbial and more complex organisms), potentially increasing bio-production compared to other regions with similar climatic, topographic and oceanographic conditions.

The tropical to sub-tropical climate across the study region results in high bio-production both on land and offshore which results in a unique ecosystem, including mangrove belts covering nearly the entire coastline (for more information see Chapter1 – General Introduction). Mangrove belts play a critical role in retaining larger plant debris from river loading through their dense network of roots and branches, and are also important for specialised biospheres such as coral reefs, buffering them from excessive sedimentation [69]. Subsequently, intact coastal mangrove belts actively contribute to differences in OC loads of riverine sediments and corresponding coastal/shelf sediments.

It has been shown that the sediment capacity to store OC is closely controlled by its clay mineralogy, more specifically their mineral surface area (SA), which provides binding sites for OM [164, 188, 295, 296]. Furthermore, the mineral SA of a sediment typically correlates positively with TOC, with regional variations in the relationship between both variables [189–191].

Scope and outcome summary of this Chapter

In an effort to account for the extensive spatial extent of the SCS, this work focusses on identifying pertinent data (including mineral SA analysis, radiocarbon $\Delta^{14}C$, stable $\delta^{13}C_{org}$ and TOC) to constrain (sub)regional details and patterns of the carbon cycle within the SCS.

In this study, regional-to-local scale variations in radiocarbon composition are linked to ocean current patterns and on-shore surface exposures. The interpretation of radiocarbon

data requires detailed knowledge of terrestrial source compositions; a primary source of petrogenic OC released from soils and bedrock that may vary considerably in its carbon isotopic composition. Significant impact of local surface lithology on OC composition is recognised here, highlighting the need for high spatially resolved and diversified end-members, when interpreting radiocarbon data. Marine sediments have radiocarbon dates younger than expected, which can be explained by the fast net loss of "old" terrestrial OM. A notable difference between the radiocarbon record of terrestrial and marine samples further strengthens the conclusions from Chapter 3, that terrestrial matter is decomposed in quick succession at the land-ocean interface, with young and marine OM dominating in the marine settings.

4.2 Methods

Surface-sediment samples were recovered from the SCS (RV Sonne Cruises: SO-115; SO-140; SO-187-3; SO-220 (for more details see Chapter 1- General Introduction and Methods or Cruise reports) for measurements of bulk $\delta^{13}C$, TOC, mineral surface area (SA) and $\Delta^{14}C$, as described in more detail in the Material and Methods (Chapter: 2). For convenience, a short summary is provided here. Bulk organic $\delta^{13}C$ was measured through Iso-Analytical Limited (Cheshire, UK), before which sediments were acidified in universal tubes for 24 h (to remove carbonate), washed twice in distilled water, air-dried, and (re)homogenised *in situ*. Samples were measured by conventional Elemental Analysis - Isotope Ratio Mass Spectrometry (EA-IRMS). The TOC was measured by partners at the Tongji University Shanghai and the University of Hamburg. Most (n = 296 of 320) TOC data were measured at University of Hamburg using a CARLO ERBA NA-1500 EA. The standard deviation of reference material analyses was 0.15 % for TOC. During combustion for TOC analyses, CO_2, and NO_x oxides are formed, the latter requiring an oxidation step to produce N_2 prior to analysis. The remaining 24 samples of the total sample set were measured at Tongji University with an Elementar Vario ISOTOPE EA equipped to a CNHS element analyser.

Mineral SA data are derived from nitrogen gas sorption to calculate the specific- or mass normalised SA. BET (**B**runauer, **E**mmett and **T**eller [192]) SA is determined by the number of sorbed nitrogen molecules divided by mass. Sediment OM was removed from samples by heating to 350 °C, and then samples were degassed at 200 °C. SA data were measured with a NOVA 4000e Surface Area & Pore Analyzer from Quantrochrome (Quantrochrome; at ETH Zurich) under isothermal conditions.

For $\Delta^{14}C$ measurements, carbonate was removed with acid fumigation prior to measurement by Elemental Analyser – Isotope Ratio Mass Spectrometer – Accelerator Mass Spectrometer (EA-IRMS-AMS) at the ETH Zurich (detailed description see Chapter 2 - Material and Methods). The $\Delta^{14}C$ value represents the ratio between the isotopes ^{14}C and ^{12}C and the normalisation factor (Oxalic acid II, standard reference material).

4.3 Results

The following section reports the results of $\delta^{13}C$, TOC, SA and $\Delta^{14}C$. A summary of the results is presented in table 11-13 and figures 20 and 21. Geographic regions are defined as: Gulf of Tonkin, Vietnamese Shelf, Vietnamese Coast, Sunda Shelf, and Slope/Deep Sea (see Fig. 2 in Chapter 1 - General Introduction).

4.3.1 Mineral surface area of marine and riverine surface sediments

The mineral SA for marine surface sediments in the SCS range from 0.38 m^2g^{-1} – 23.7 m^2g^{-1} (n = 203) (Fig. 20).

Table 11) Mineral surface (m2 g-1) area values of marine surface sediments

Region	Max. value	Min. value	Average	*n*
Gulf of Tonkin	23.5 m^2 g^{-1}	4.05 m^2 g^{-1}	14.4 m^2 g^{-1}	29
Vietnamese Shelf	17.3 m^2 g^{-1}	2.49 m^2 g^{-1}	10.7 m^2 g^{-1}	32
Vietnamese Coast	23.7 m^2 g^{-1}	1.33 m^2 g^{-1}	7.35 m^2 g^{-1}	75
Sunda Shelf	19.9 m^2 g^{-1}	0.38 m^2 g^{-1}	7.66 m^2 g^{-1}	54
Slope/ Deep Sea	22.3 m^2 g^{-1}	3.90 m^2 g^{-1}	8.84 m^2 g^{-1}	13

In the Gulf of Tonkin, mineral SA ranges between 4.05 m^2g^{-1} – 23.5 m^2g^{-1} (average of 14.6 m^2g^{-1}, n = 29). The narrow Vietnamese Shelf area shows lower values between 2.49 m^2g^{-1} – 17.3 m^2g^{-1} (average of 10.7 m^2g^{-1}, n = 33), comparable with the southern Vietnamese Coast (n = 75), which ranges between 1.33 m^2g^{-1} – 23.7 m^2g^{-1} (average of 7.35 m^2g^{-1}). Mineral SA in the Sunda Shelf samples (n = 55) ranges between 0.38 m^2g^{-1} – 19.9 m^2g^{-1} (average of 7.66 m^2g^{-1}). Slope/Deep Sea samples with a water depth up to 1974 m range between 3.90 m^2g^{-1} – 22.8 m^2g^{-1}, average of 8.84 m^2g^{-1} (n = 13). Mineral SA for river-estuary samples could not be measured because of insufficient sample material.

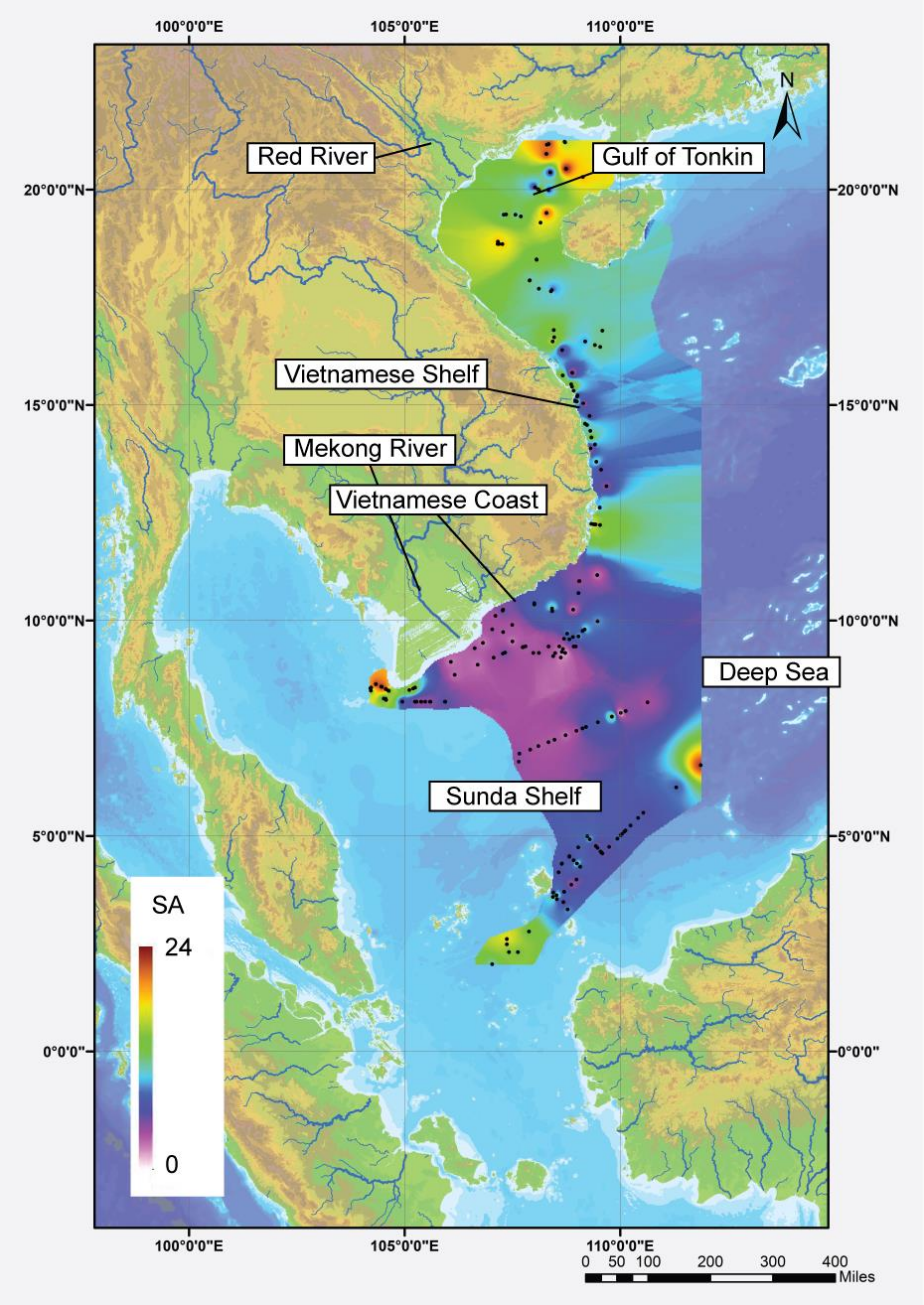

Figure 20) Inverse distance weighing (IDW) graphical illustration of mineral surface area m-2g-1 data from the SCS marine surface sediments, using ARC GIS version 10.6. The data suggest a gradual transition from high SA in the northern part, to low SA further south.

4.3.2 Total organic carbon in marine and estuary sediments in the South China Sea

The distribution of TOC concentration of marine surface sediments and estuary samples is described in detail in Chapter 3. Concentrations for marine surface sediments range between 0.1 % to 4.3 %, in estuary samples the TOC values range from 0.1 % to 9.7 % (n = 319). Key features include low TOC areas in proximity to the Mekong River delta, while higher TOC contents are typically observed in the Slope/Deep Sea areas and some parts of the southern Sunda Shelf investigated in this study (Fig. 11a and b).

4.3.3 Bulk $\delta^{13}C_{org}$ values in estuary and marine surface sediments in the South China Sea

The marine surface sediments from all shelf samples range between -27.7 ‰ to -20.3 ‰ (n = 230), estuary samples show $\delta^{13}C_{org}$ values between -23.8 ‰ to -29.5 ‰ (n = 87). The regions are described in more detail in Chapter 3. Key features include more negative $\delta^{13}C_{org}$ values in proximity of the Mekong River delta (Fig. 12), some parts of the Vietnamese Shelf, where small mountainous rivers reach the ocean interface, and parts of southern Hainan, as well as the southernmost part of the Sunda Shelf.

4.3.4 $\Delta^{14}C$ values of riverine and marine surface sediments

Calculated $\Delta^{14}C$ values (Fig. 21 and tables and 13), which reflect values relative to the 1950 bomb event (for calculation of $\Delta^{14}C$ values see Chapter 2 – Material and Methods, section 2.4), show values including pre-bomb (negative) and post-bomb (positive) dates in estuary samples (n = 70), ranging from -966 ‰ to +93.9 ‰ (Fig. 21).

Table 12) $\Delta^{14}C$ (‰) values of marine surface sediments

Region	Max. value	Min. value	Average	*n*
Gulf of Tonkin	-111 ‰	-265 ‰	181 ‰	27
Vietnamese Shelf	-31.6 ‰	-220 ‰	-130 ‰	26
Vietnamese Coast	54.7 ‰	-511 ‰	-193 ‰	63
Sunda Shelf	-182 ‰	-354 ‰	-257 ‰	34
Slope/ Deep Sea	-112 ‰	-378 ‰	-203 ‰	28

Marine surface sediments on all shelf regions of the SCS show a collective $\Delta^{14}C$ range of -512 ‰ to +54.7 ‰, including one outlier of +54.7 ‰ next to the Vietnamese Coast (SO-187-3-87-2 [09°02.558'N; 106°04.533'E]). Positive $\Delta^{14}C$ values are the product of contamination from nuclear weapons radiation signature and technically record future $\Delta^{14}C$ composition. Excluding this contaminated outlier leads to a $\Delta^{14}C$ range between -32.6 ‰ to -512 ‰ with an average of -196 ‰.

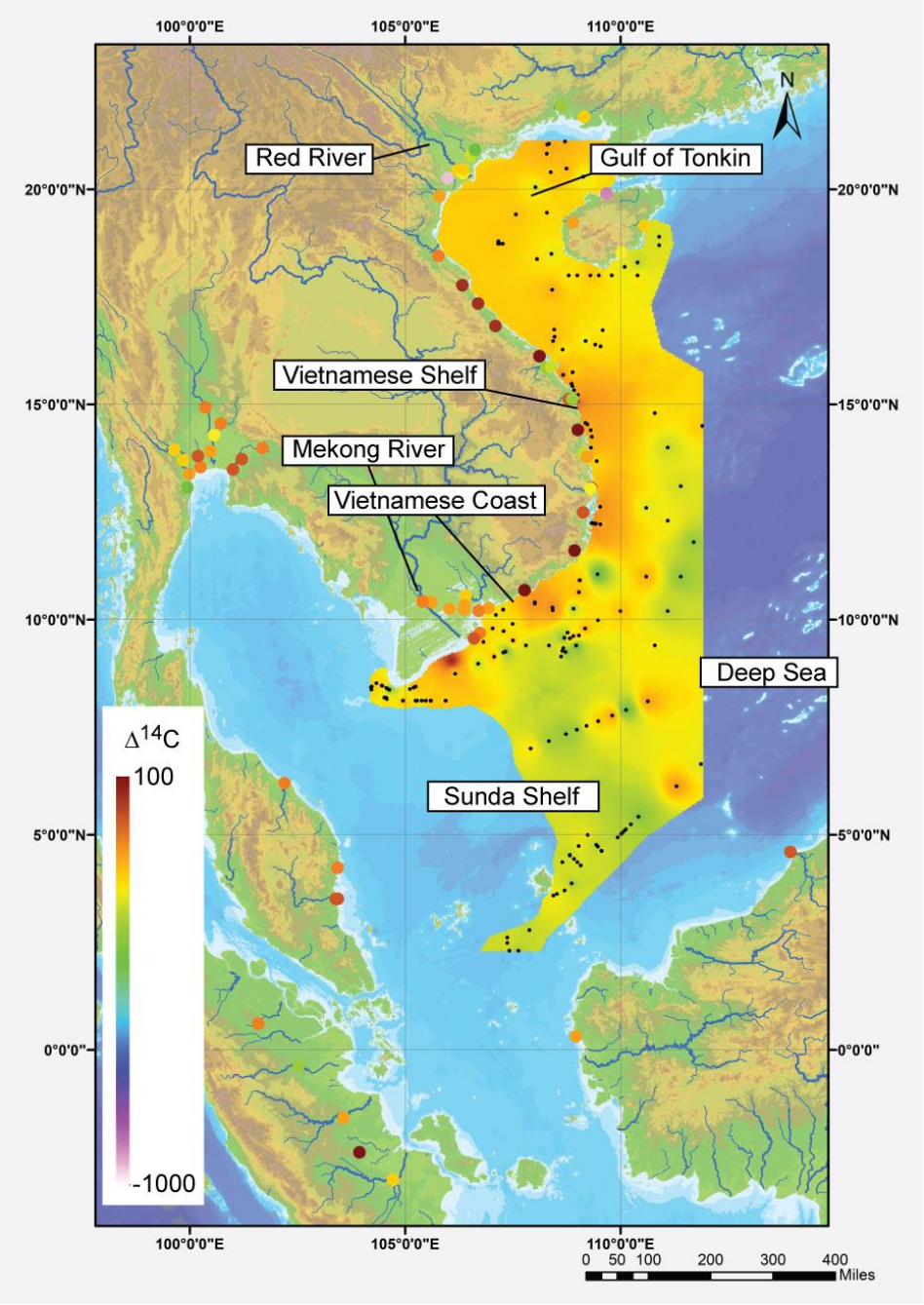

Figure 21) Inverse distance weighing (IDW) using ARC GIS version 10.6. Radiocarbon $\Delta^{14}C$ interpolation of marine surface sediments, and highlighted (circles) $\Delta^{14}C$ data of river sediment samples

The Gulf of Tonkin has $\Delta^{14}C$ ranging from -111 ‰ to -265 ‰ (average of -181 ‰, n = 27), the narrow Vietnamese Shelf has $\Delta^{14}C$ ranging from -31.6 ‰ to -220 ‰ (average of -130 ‰, n = 26). $\Delta^{14}C$ along the southern Vietnamese Coast ranges from +54.7 ‰ to -512 ‰, (average of -193 ‰ (including the outlier), n = 63). Excluding the already mentioned outlier data, $\Delta^{14}C$ values range from -76.4 ‰ to -512 ‰ (average of -197 ‰, n = 62). The Sunda Shelf has $\Delta^{14}C$ ranging from -182 ‰ to -355 ‰, (average of -257 ‰, n = 34). The Slope/Deep Sea show values ranging between -378 ‰ and -112 ‰, (average of -203 ‰, n = 28).

Table 13) $\Delta^{14}C$ (‰) values of estuary samples

Region	Max. value	Min. value	Average	*n*
Estuaries from the Gulf of Tonkin area	40.7 ‰	-966 ‰	-267 ‰	17
Estuaries from the Vietnamese Shelf area	69.8 ‰	-353 ‰	146 ‰	17
Estuaries from the Vietnamese Coast area	93.9 ‰	-155 ‰	-75.4 ‰	12
Estuaries from the Sunda Shelf area (Indonesia and Malaysia)	56.5 ‰	-300 ‰	-79.6 ‰	11
Estuaries from Thailand	-10.7 ‰	-389 ‰	-128 ‰	13

Respective estuary samples for the Gulf of Tonkin range from -966 ‰ to 40.7 ‰ (average of -267 ‰, n = 17); these estuary samples include two samples with very negative values, VN-63: -964 ‰ (20°15.600'N; 105°58.800'E) and sample HN-02: -941 ‰ (19°54.000'N; 109°40.800'E). Sample VN-63 is derived from the Red River Delta and sample HN-02 from Hainan. Estuaries of the Vietnamese Shelf sub-area have values between -353 ‰ and 69.8 ‰, (average of -146 ‰, n = 17). Values of estuaries, which are respective to the Vietnamese Coast range from -155 ‰ to 93.9 ‰ (average of -75.6 ‰, n = 12). Samples for estuaries respective for the Sunda Shelf area show values from -300 ‰ to 56.5 ‰, (average of -79.6 ‰, n = 11). Samples of estuaries from Thailand show values from -389 ‰ to -10.7 ‰, (average of -128 ‰, n = 13).

4.4 Discussion

4.4.1 Assessing the role of clay minerals in adsorption of OM – surface area and total organic carbon

Mineral SA for marine sediment has been shown to play an essential role in OC cycling for different shelf systems around the globe. This is related to the capacity of SA to bind OM, as confirmed by positive correlation of SA with TOC [164, 188, 295, 296]. Strong, positive linear correlation of SA and TOC is also observed in the sediment samples from the SCS (Fig. 22).

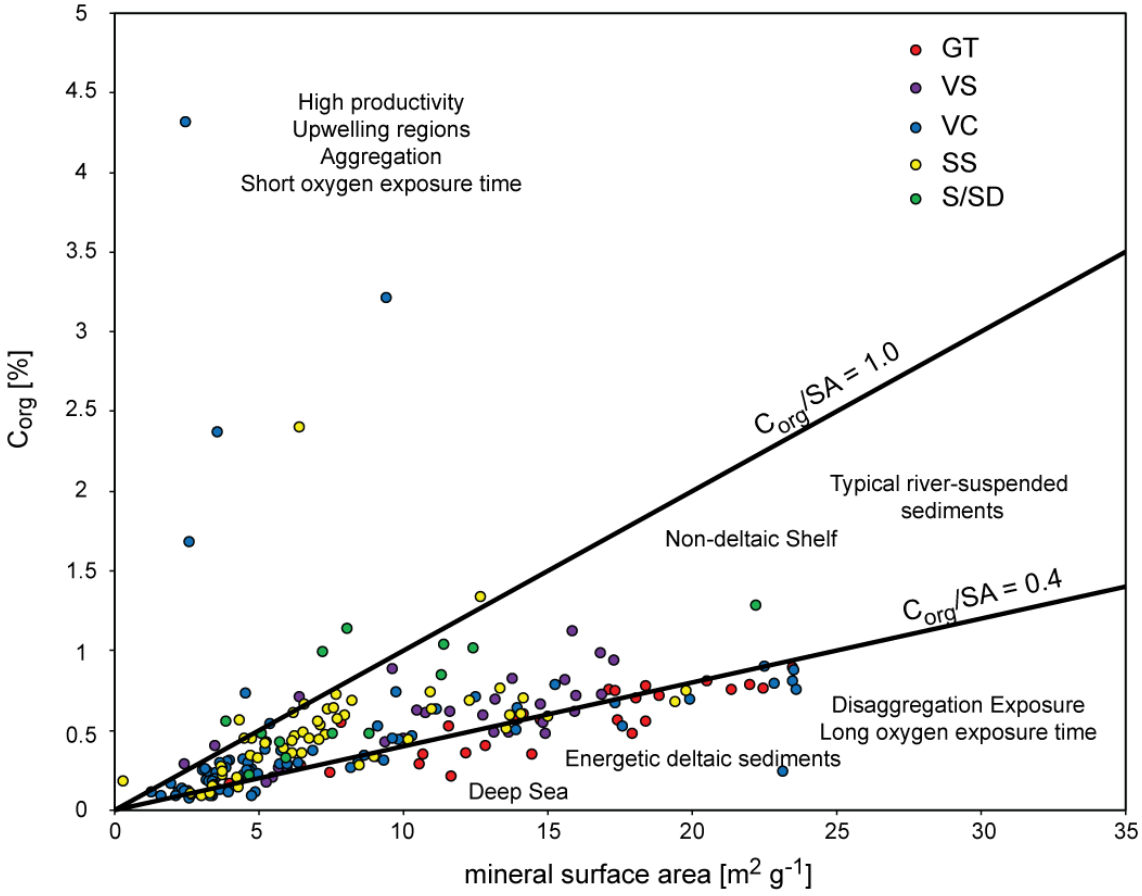

Figure 22) Total organic carbon (TOC) contents generally correlate with the mineral surface area, which is consistent with a high binding capacity of fine (clay) material for organic carbon. Blair and Aller [189] defined several distinctive ranges of surface loading (C_{org}/SA) which are characteristic for sedimentary environments, which have implications for net balance between supply and remineralisation reactions. Abbreviations: GT = Gulf of Tonkin, VS = Vietnamese Shelf, VC = Vietnamese Coast, SS = Sunda Shelf, S/DS = Slope/Deep Sea

This observation is interpreted to reflect the abundance of fine-grained (<63 µm) particles with larger SA (i.e. clay minerals) that are known to have good binding sites for OM [191, 284]. The SA analysed samples from the SCS range from 0.38 m^2g^{-1} – 23.9 m^2g^{-1}, which are overall low compared to other shelf areas. For comparison, SA from the Amazon-Guianas mud-belt range between ~16 m^2g^{-1} – 50 m^2g^{-1} [297] and for the coast off Papua New Guinea between ~16 m^2g^{-1} – 31 m^2g^{-1} [298].

Depending on mineral type (e.g. smectite *vs.* kaolinite), the efficiency of OM fixation varies and the order for the binding capacity is kaolinite < illite < smectite [299]. Within the SCS, smectite is the dominant clay mineral (Fig. 15 in Liu et al. [16]). In general, regions with similar SA properties often share similarities in the abundance and distribution of TOC, given that physical parameters are comparable. Examples include the Yangtze River [300, 301], the Pearl River (e.g. Yu et al. [302]), the Ayeyarwardy Shelf [303], and the Amazon River [304]. One critical external control on SA of marine sediments is the strength of ocean currents and tides, as they can preferentially remove

high-SA particles in the sortable silt fraction or prohibit the settling of fine material [305] leaving more coarse-grained sediments behind (lag deposits).

Besides SA, other aspects that have been shown to affect the sedimentary TOC budget are dissolved oxygen availability in the water column (e.g. Dauwe and Middelburg, [306]) and pore waters, the formation of aggregates (e.g. Drake et al. and Wefer, [307, 308]), the variability in the clay mineral composition and post depositional mixing (e.g. in tempestite and/or by bioturbation) (e.g. Stein et al. Ding et al. and Kennedy et al. [309–311]). The latter two are described for the SCS [16, 312–315] but no correlation is found with SA.

In a next step, the potential impact of SA, variation in clay mineralogy and post depositional mixing on the SCS are explored. This analysis is then compared with other shelf areas worldwide to identify what conditions might favour unexpectedly high or low carbon burial efficiency in the southern SCS.

Low SA is attributed to either higher proportion of sand components, and/or the formation of aggregates. Therefore, a first test is to analyse the relationship between grain size fraction (clay, silt, and sand) and SA. The assumption is that if clay minerals are the primary agent in OM fixation, SA should correlate positively with clay and possibly silt, but negatively with sand fractions. An evaluation for the Gulf of Tonkin samples where grain size analyses are available shows that SA and TOC correlate positively (Fig. 22), as well as the clay and silt fractions (Fig. 23).

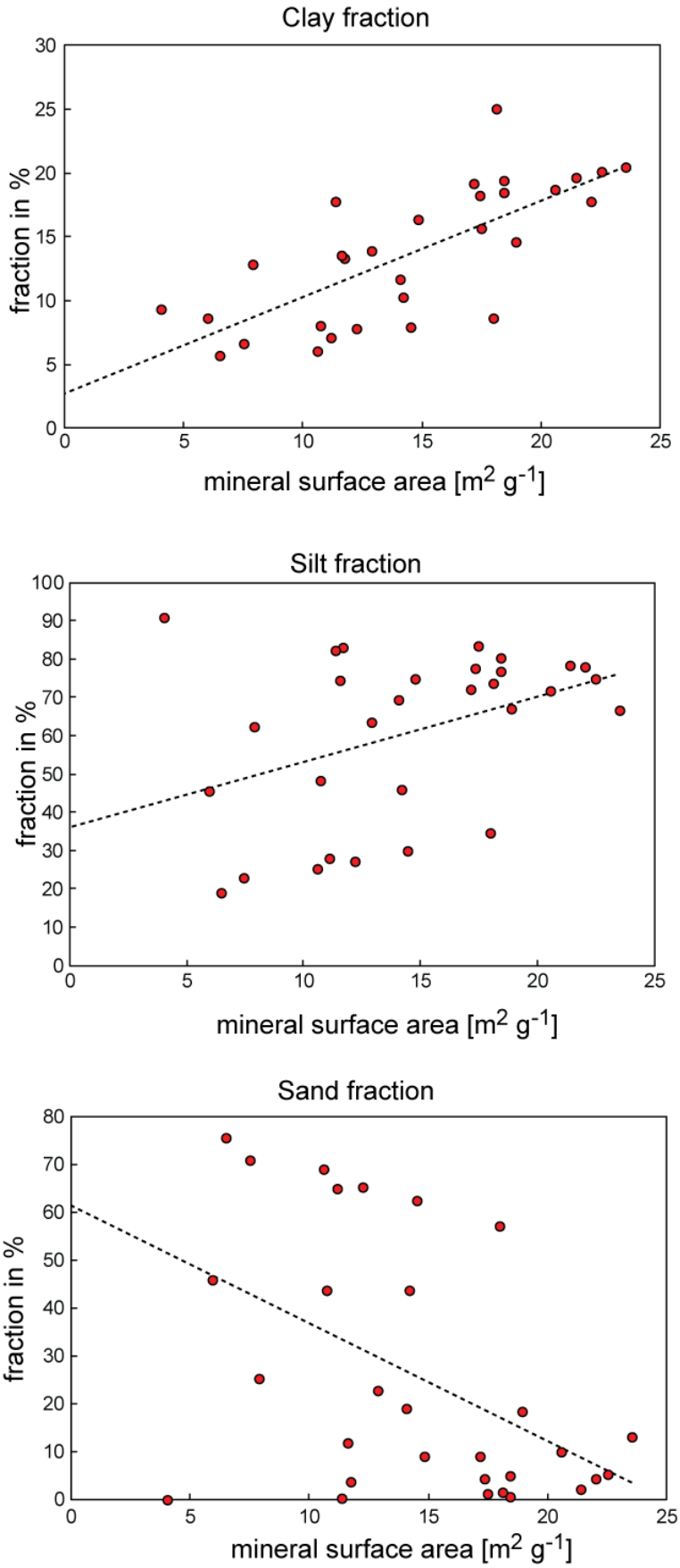

Figure 23) Correlation between grain-size fractions (clay, silt and sand) and mineral surface area for samples from the Gulf of Tonkin, demonstrating that SA is a function of grain size distribution

In contrast, the sand fraction significantly scatters without any relevant relationship. It is assumed that the SA scatter for sand fractions originate from variable grain shapes (grains with cracks have larger surfaces compared to completely round shapes, or plates, which result in higher surface to volume ratios), but cannot be identified with certainty in the frame of this study. Another peculiar feature of the Gulf of Tonkin dataset is the intercept between clay mineral fraction and TOC (Fig. 22), close to zero (<0.08 %, Fig. 23). This implies that the clay size fraction has a dominant control on TOC in this region. Within the SCS, the clay mineral ratio between kaolinite, chlorite, smectite, and illite is highly variable (e.g. smectite / chlorite range is 0.4 – 44.5) [16]. However, the Gulf of Tonkin, Vietnamese Coast, Vietnamese Shelf and Sunda Shelf, which are representative for ~50 % of the SCS, are remarkably similar in their clay mineral ratios [16].

By comparing SA with TOC (Fig. 22), a positive linear correlation (R^2 0.5 - 0.76) within all regions of the SCS is apparent, although the slope of the correlation is variable between regions, including some scatter. This correlation underlines the importance of physical properties of the sediments concerning fixing and preserving OC. Variations in the slope and scatter of the data probably indicate regional differences in e.g. TOC supply, current dynamics and TOC fixation rates are present throughout the SCS. These do not influence the SA but OC fixation and preservation. Other physical factors that can affect the settling and binding of OC are current velocities and variable rates of preservation. These factors are evaluated below.

The shallowest slope in SA *vs*. TOC is observed for samples from the Gulf of Tonkin and from the Vietnamese Coast (Fig. 22) areas, which are in part affected by the deltas of the Mekong River and Red River, respectively. This hinges to lower OC binding efficiency in proximity to freshwater outflow areas (higher current velocities), or faster decomposition (e.g. oxygen availability). Higher current velocities could also play a role in marine sediment OC content. Firstly, higher velocities could prevent the settling of finer sediment (e.g. clay minerals), which limits the carbon binding efficiency. Secondly, transport the OC away from the sediment could occur at rates faster than OC fixation. Such conditions would be consistent with the observation that in the southern Vietnamese Coast area, higher TOC at low SA is observed with increasing distance from the Mekong River delta (samples with TOC > 0.7 %).

In the Sunda Shelf region, two groups of samples are distinguished (Fig. 22). The first group has a steep slope in SA *vs.* TOC with SA values <10 m^2g^{-1}, while a second group

with SA values >10 m^2g^{-1} shares similarities with the river-impacted Gulf of Tonkin and Vietnamese Coast. High SA values of samples from the Sunda Shelf are located across the Molengraaff Palaeoriver depth transect (see Chapter 1- General Introduction), which is known to be composed of finer material [316], Cruise report RV Sonne 115, core samples SO-115-20, -21, -50, -60, -62, -63, -65, -66, -68, -76). This observation is supported by other studies on palaeorivers, which found that finer sediment fractions settle with increasing distance to the river deltas [317]. The comparatively low TOC at higher SA in the Sunda palaeoriver channel could therefore be attributed to increased decomposition of OM during past deposition, fuelled by abundant dissolved oxygen in bottom waters and an active benthic layer. These conditions may cause the TOC/SA ratios in the Molengraaff River to be slightly elevated, relative to other samples from the Sunda Shelf (0.083 versus 0.071). The study by Keil et al. [318] interpreted higher OC/SA ratios to reflect higher burial efficiency of terrestrial OM (Amazon River and Delta [318]), due to sea level low stands during glaciations and a more direct transport pathway [319]. The samples from the Vietnamese Shelf behave differently and generally show a positive correlation in SA *vs*. TOC, with a slope intermediate between the steep slope of the Sunda Shelf and the river delta regions of the Gulf of Tonkin and the southern Vietnamese Coast. The Vietnamese Shelf is strongly affected by small-scale mountainous rivers, which have shorter transport distances and possible shorter transit timescales. Another interesting observation from the SA vs. TOC data is low OC storage in sediments close to the two large rivers (Mekong River and Red River), even though they are expected to discharge large amounts of continental OM [285]. It is likely that these high amounts of continental OM is strongly diluted at the interface of the river delta and the ocean, if e.g. marine primary production is low or water mass exchange is rapid. The SA/TOC relationship (steep slope) is consistent with other areas in proximity to smaller rivers (Fig. 22), suggesting that a close proximity to rivers, in general, inhibits effective OM burial. It therefore seems crucial to interpret marine sediment data with proximity to freshwater inflows carefully, and ideally characterise the rivers and sediments discharged to coastal and inner shelf regions.

The narrow Vietnamese Shelf region is very different with its numerous small, mountainous rivers compared to the rest of the Vietnamese shelf (see e.g. Liu et al. [16]). Milliman and Farnsworth [99] and Larsen et al. [320] report that globally steep and wet mountains deliver 62 % of all sediment to the ocean. In these settings sediment mobilisation occurs through chemical and physical weathering, to result in soil creep,

sheet wash, gulling, debris flows and landslides, including mobilisation of POC from above and below ground biomass, soils and sedimentary rocks [319]. Furthermore, POC from biomass and plant litter tends to be more concentrated, younger (in ^{14}C age) and more reactive [319] relative to e.g. petrogenic carbon. A major factor that influences erosion and the mobilisation of material on land is the hydrological regime, i.e. precipitation and runoff patterns, both surface and sub-surface. Low frequency, high magnitude precipitation events have been shown to be responsible for a disproportional large portion of sediment and POC mobilisation in mountainous areas [319, 321]. For example, in the Leiwu catchment on Taiwan (adjacent to the study area of this study) 77 - 92 % of biospheric POC transport occurs during cyclone-triggered floods, that occur about three times per year [322–324]. Importantly, these authors also noted that the biospheric OC fraction of POC was only 30 %, with the remaining 70 % deriving from petrogenic carbon. Similar relationships have been reported from other steep mountainous regions, such as the headwaters of the Amazon River in Peru, with up to 80 % of the total POC being petrogenic [325]. Since the SCS is the largest marginal sea of the Pacific Ocean, these observations made in Peru and Taiwan support that, the SCS potentially plays an important role in the global carbon budget.

Finally, marked reductions in TOC between riverine and marine sediments, observed in all regions from the SCS warrant further discussion. These drop to the overall low TOC across the entire SCS shelf region and challenge the common perception that shelf systems function as key storage regions of OC [284]. TOC in riverine sediments indeed can be as high as 3.61 % in the study area (Tra Khuc River St. 1b), but corresponding open marine sediments are generally <1 %. This discrepancy may in part be related to the presence of and widespread occurrence of coastal mangrove forests along eastern Vietnam and northern Indonesia, which are known to catch not only significant amounts of sediment [69] but also POC. The efficiency in which mangrove retain sediment in northern Vietnam depends on spatial geomorphology, hydrodynamics and vegetation [326]. These factors are highly variable throughout the SCS and no conclusive assessment for mangrove-controlled sedimentation is currently available. The only quantitative estimate proximal to the SCS is discussed in Victor et al. [69], with data from the Palau islands. Victor et al. [69] estimated sediment entrapment of up to 30 % of the discharged sediment. However, higher rates are necessary to explain the discrepancy between river TOC and marine sediment TOC content in the SCS (requires sediment

entrapment of ca. 40 % - 60 %). In the absence of further data to quantify the mangrove effect, other factors such as biomass decomposition are also considered important.

4.4.2 The relationship between $\delta^{13}C_{org}$ and TOC – identification of decomposition of OM in estuary and marine sediments

To explore the degree of decomposition it is crucial to investigate the relationship between TOC loading and bulk $\delta^{13}C$ isotopic composition. Conceptually, one expects a net loss of terrestrial C_{org} to be accompanied by a drop in isotopic composition (e.g. heavier $\delta^{13}C$ values), as demonstrated in the global review by Blair and Aller [189]. The lighter isotopic $\delta^{13}C$ values are characteristic for terrestrial C_3 plants, which are more resistant to decomposition compared to marine biomass [3], that is characterised by heavier $\delta^{13}C$ values. The samples from the Gulf of Tonkin, Vietnamese Coast and Shelf and the Sunda Shelf show a clear trend of terrestrial C_{org} depletion (c.f. negative correlation in Fig. 24), and fall into a narrow range (TOC/SA has max 0.16, with five outliers above 0.3), overall. The SCS marine sediment data are characterised by low TOC/SA, relative to the maximum value of ~0.7 (Amazon River) presented by Blair and Aller [189]. Yet, the slopes of the regression lines are based on a high amount of data and assumed reliable and robust. When directly comparing the SCS region with the Amazon data [297, 318], the slope of the regression line of the SCS data is seemingly shallower than the amazon data (Fig. 24). The restricted range of the SCS data implies that the terrestrial C_{org} budget in the SCS is relatively low, compared to other shelf systems (e.g. Amazon [318] and French Guiana [297]). This could indicate that terrestrial C_{org} is more readily decomposed in the SCS, compared to the Amazon [297] and Amazon-French Guiana [318] system. Since the SCS and Amazon reflect two regions with distinctively different vegetation and climate conditions, it cannot be ruled out that physical and chemical processes control or affect the rates at which terrestrial sourced OM is decomposed. Furthermore, the initial ratio between marine and terrestrial OM might vary between those two regions and requires further investigation. Nonetheless, the assumption that the data indeed reflect net loss of terrestrial C_{org} receives further support from observations in FAME composition of bulk sediments discussed in Chapter 3. The FAME record indicates a deficit in long-chain FAME, which are diagnostic for terrestrial sourced OM, and interpreted as decomposition of terrestrial C_{org}.

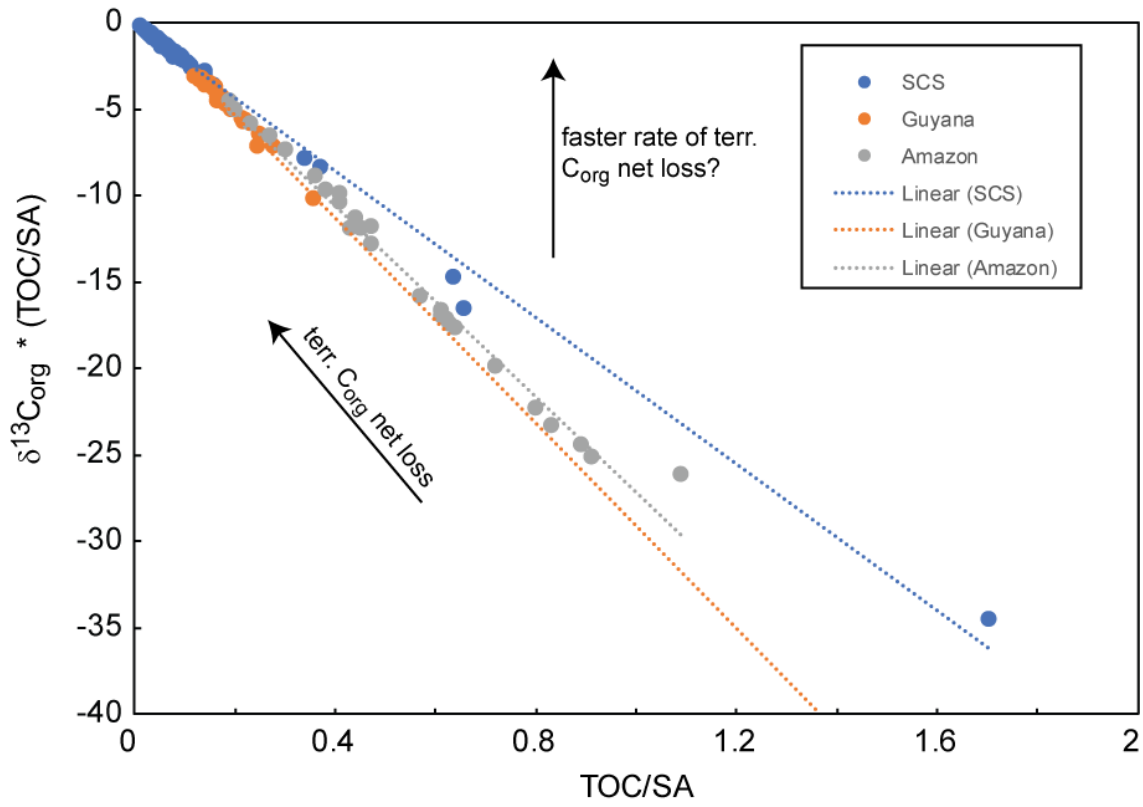

Figure 24) Relationship between C_{org} loading and bulk carbon $\delta^{13}C$ isotopic composition for marine surface sediments from the SCS, which show a trend of net loss of C_{org}. The similar slope between different regions is indicative of similar processes (e.g. degradation) responsible for the modification of sediment isotopic and physical signatures. The slope of the SCS data regression line is unaffected by the five data points with TOC/SA values greater than 0.3

Dissolved oxygen availability is efficient for the decomposition of OM by microbial processes, and regional variations in oxygen abundance are related to TOC abundances in marine sediments [327–329]. The study of Rojana-anawat et al. [291] demonstrate for the Gulf of Tonkin, Vietnamese Coast and Vietnamese Shelf strong variability in available dissolved oxygen from north to south.

Rojana-anawat et al. [291] found, that oxygen availability drops with increasing water depth and distance to the river mouth, with surface current dynamics determining regional variations. If dissolved oxygen is a dominant factor in the decomposition of TOC, the Gulf of Tonkin is expected to yield low TOC, since it has the greatest amount of dissolved oxygen availability in the study area. However, TOC content in the Gulf of Tonkin is relatively high (Fig. 22) indicating that the role of oxygen availability is secondary, relative to factors such as SA.

The Gulf of Tonkin also preserves significant amounts of FA (Chapter 3), which are expected to rapidly decompose, owing to their functional groups. This would require the Gulf of Tonkin to have i) high primary production rates and/or ii) shielding of OM by

adsorption to clay minerals, which are known to retard degradation [330]. A similar degree of preservation of TOC abundance relative to the Gulf Tonkin is only achieved in the Slope/Deep Sea area, but features different framework conditions, such as greater water depth, lower water temperature, lower primary production detritus and significantly higher water current velocities and large scale current structures, all seasonally dependent.

4.4.3 Transition of OM radiocarbon dates during transport and decomposition

The composition of OC transported by riverine systems to the coastal ocean is controlled by the composition of different source regions (e.g. variation in bedrock lithology and soil type and abundance, vegetation change such as C_3, C_4 and CAM plants) and the variation of relative proportions of source material constituting the OM. The bulk sediment OC also reflects properties of the watershed and the residence time of OC and sediments therein [189].

The Red River and the Mekong River transport large volumes of water and sediment, which are sourced from the hinterland with contributions from the coastal regions. Both river systems exhibit C_{org}/N_{total} ratios of around 10 - 12 typical of terrestrial components (see Chapter 2 – Material and Methods), which argue for a strong hinterland component. However, tidal forces cause a reversal in stream dynamics of the Mekong River delta (see Chapter 1- General Introduction) which increases the weight of coastal contributions. In eastern Vietnam, numerous small mountainous rivers are the principal transport pathway from land to ocean [331]. In these small mountainous rivers the drainage regions are small and often effected by rapid erosion, particularly during the monsoonal season [205]. The steep topography naturally accelerates water streams, which reduce the time for potential mixing with other sources, making mixing less likely and if so, less pronounced. As a result, the proportion of petrogenic carbon can be highly variable over time and space and be dominant over fluvial transported potent terrestrial OM and/or recalcitrant OM. Furthermore, the residence time of OC transported by these mountainous rivers across and along the inner shelf areas is crucial for the preservation of their original isotopic composition [332]. This has important implications for the bulk radiocarbon content of both riverine and marine POC. While both large and small rivers can be sources of old carbon, their OC age distribution can be highly variable [205]. Typically, rivers in active margin systems are bimodal in their ^{14}C carbon composition due to mixing of inert petrogenic carbon from weathering processes and potent biospheric OC. More

complex mixing relations are however observed in large river systems, such as the Red River and the Mekong River. Here, the mixing may not only carry potent biospheric OC and small proportions of inert petrogenic carbon, but also significant amounts of recalcitrant OC of variable ^{14}C composition, sourced from diverse soils in the drainage areas [12, 332, 333]. Bianchi et al. [205] suggest that bulk OC radiocarbon ages vary with river discharge. Low river flows carry predominantly low-density materials, e.g. plant debris and algal OC, which are rich in ^{14}C. On the contrary, heavy precipitation events can erode denser and older sedimentary or soil material which are typically ^{14}C poor [321]. This cannot be tested here, in absence of necessary data, but it is a possible explanation.

Bianchi et al. [205] found that the correlation between OC and radiocarbon values ($\Delta^{14}C$) and 1/TOC are indicative that organic rich sediments generally have younger ages in various regions (e.g. Amazon Shelf [297, 318, 334–339], Northern Gulf of Mexico [340–348] Pan-China Sea [10, 12, 349–354] on earth, with only one exception (Pan-Arctic). Bianchi et al. [205] concludes that the variability in $\Delta^{14}C$ age across a given system is dominantly controlled by the variable contribution of petrogenic carbon. For the investigated samples in the SCS, the same observation is made in $\Delta^{14}C$ vs. 1/TOC space (see Fig. 10 in Chapter 2 – Material and Methods), suggesting variations in the petrogenic carbon component dominantly control $\Delta^{14}C$ dates in the SCS. The simple, yet scattered correlation does not provide evidence for significant addition of autochthonous (marine, algal) material transported from other regions. Instead, the investigated samples seem to form a principle two-component mixing system with petrogenic carbon and radiocarbon sourced carbon from local reservoirs as end-members.

Furthermore, bulk shelf sediments tentatively have older $\Delta^{14}C$ ages than their respective riverine feeder systems, owing to lateral transport distances of undetermined duration and speed. Figure 25 identifies that riverine and marine samples from the SCS are distinct in their $\delta^{13}C$ isotopic signature, with the marine samples being heavier (approximately 2 ‰ – 6 ‰ units) in $\delta^{13}C$ relative to the riverine samples (red circles, figure insert in Fig. 25). In the case of the Sunda Shelf and the Vietnamese Coast, riverine samples have $\Delta^{14}C$ compositions younger than marine samples from the respective areas (Fig. 25). This discrepancy between riverine and marine apparent $\Delta^{14}C$ age can be the result of preferential removal of the youngest riverine components and fresh marine production, relatively enriching less reactive and isotopically older carbon [355].

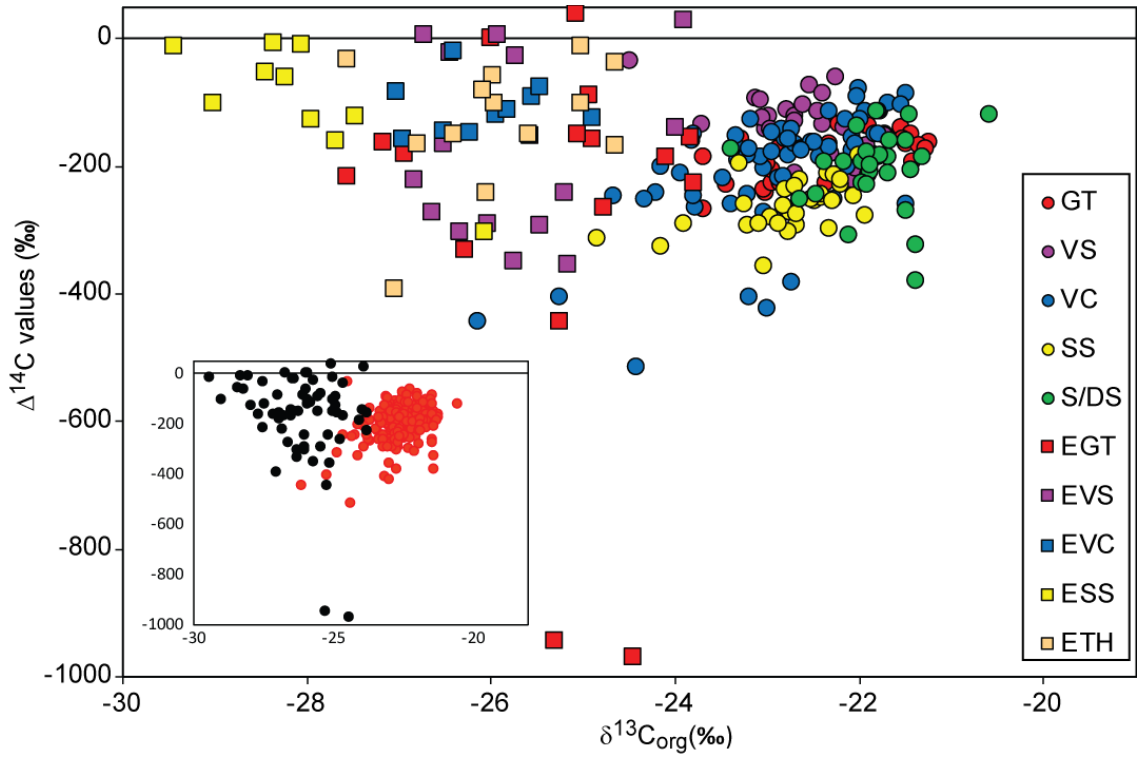

Figure 25) Correlation between bulk sediment organic carbon $\delta^{13}C$ (stable) values and $\Delta^{14}C$ values, as in Bianchi et al. [205]. Riverine samples exhibit more negative values, characteristic of terrestrial source substrate, while marine sediments have values typical of marine environments. The inset differentiates only between riverine (black) and marine (red) samples to illustrate the sharp transition between riverine and marine samples. Abbreviations: GT = Gulf of Tonkin, VS = Vietnamese Shelf, VC = Vietnamese Coast, SS = Sunda Shelf, S/DS = Slope/Deep Sea

However, some riverine samples from both the Gulf of Tonkin and Vietnamese Shelf exhibit $\Delta^{14}C$ values, which span younger and older ranges than their marine counterpart samples (Fig. 25). Following the conclusions of Bianchi et al. [205], this can be attributed to the variable proportions of petrogenic carbon, which can cause apparent older dates in bulk sediment $\Delta^{14}C$ analyses. A possible explanation for this inconsistency in petrogenic carbon mass fraction can be seasonality in precipitation on the Vietnamese mainland (see Chapter 1 - General Introduction), which temporarily result in increased proportions in petrogenic carbon (remobilisation by weathering) mobilisation [319]. Whether this is a seasonal effect (e.g. monsoonal) or an event or multi-annual effect cannot be resolved with the available sample set, as this would require additional seasonal sampling at a finer spatial resolution. In the case of the Gulf of Tonkin, the Red River is the dominant source of terrestrial OC, which is more resistant to the petrogenic carbon, as discussed above.

Yet some of the riverine samples show significantly older values than any marine surface sediment samples studied in the Gulf of Tonkin (VN-63 and HN-02). Speculatively, anthropogenic activities might provide an explanation. The Red River passes through the Quang Ninh coal basin, responsible for over 90 % of Vietnams coal mining [356]. It is

therefore plausible to assume that high mobilisation of coal tailings and industrial activity may comprise the ancient and inert carbon load from the catchment bedrock, shifting the radiocarbon signal to older ages of the bulk marine shelf sediments. This effect is not observed in other areas of this study, and potentially restricted to short transport pathways and small areas. Additional inert carbon source is also identified off north-eastern Hainan by some outlier samples (Fig. 25, sample VN-63). The northern part of Hainan Island has significant exposure of basic volcanic rocks, which are a source of petrogenic carbon (Fig. 3 (in Chapter 1 – General Introduction), HN-02). The study of Blattmann et al. [11] recently demonstrated for the Taiwan system that the source rock geology can project into POC offshore, causing a shift towards older dates. It is therefore well possible that the same process controls the radiocarbon signatures observed around northern Hainan, and any other regions with significant exposure of volcanic lithology.

Other studies have demonstrated that bioturbated sediments can produce similar evidence where benthic macrofauna are relatively enriched in $\Delta^{14}C$ as a result of preferential feeding on labile sediment detritus [357, 358]. Mixing of locally produced marine OC (heavier $\delta^{13}C_{org}$ isotopic signatures) with older sedimentary OC bearing a terrestrial signature will still result in selective remineralisation of the labile marine material, which can produce dissolved inorganic carbon signatures mirroring marine environments [189, 359, 360].

The data presented here, support the conclusion that marine surface-sediments of the SCS consist of mixtures from reservoirs with distinct $\delta^{13}C$ and $\Delta^{14}C$ compositions. A tendency towards preservation of organic carbon with older $\Delta^{14}C$ signatures can be observed, as evident from older bulk marine sediments compared to riverine sediments. This conclusion is consistent with previous findings in other coastal margin regions [205].

The OC derived from terrestrial reservoirs may also be subject to remineralisation, but the available data do not permit a robust evaluation of this process. Previous studies have shown that the bulk sediment OC is often dominated by isotopically lighter and older components [205, 298], but within the SCS, data on the source regions is essentially absent. This paucity of well-calibrated end-member data needed to reconstruct and understand the carbon transfer from land to ocean can potentially be resolved using an inversion approach, where the data correlation of the final sediment from the deep sea through the shelf is used to constrain the most likely source reservoir compositions. In

the next section, this option is used to reconstruct potential $\delta^{13}C_{org}$ and $\Delta^{14}C$ source reservoir compositions

4.5 Conclusions

1) The mineral SA and the TOC content of marine surface sediments correlate positively throughout the SCS, albeit variations in the slope between different regions and special locations (e.g. Sunda Shelf palaeo-channels) are observed. The different slopes are controlled by the clay fraction, determining TOC concentration. Highest amounts of TOC are found with increasing distance to river deltas. Some of the Vietnamese Coast samples have the highest TOC/SA and another area with consistently high TOC/SA is the Slope Deep/Sea, which is the area of accumulation of OM in the study area. Within the Sunda Shelf, two trends emerge, of which one returns lower TOC/SA values for samples in proximity to palaeoriver beds. The Gulf of Tonkin is characterised by lowest TOC/SA values, suggesting that low current velocities permit both the settling of clay fraction and OM. Seemingly, current dynamics (speeds and structures formed) significantly affect the composition of marine sediments, possibly regardless of the amount and composition imported from the terrestrial interface by e.g. rivers.
2) The transformation of OM $\delta^{13}C_{org}$ signatures from terrestrial sources towards the Slope/Deep Sea sediments is related to several processes: i) decomposition of OM, as evident from gradual changes (increase) in $\delta^{13}C_{org}$ isotopic composition with increasing distance to the source, ii) mixing of terrestrial sourced OM with marine bio-produced matter, causing shifts towards heavier $\delta^{13}C_{org}$ values. In particular, a net loss of terrestrial C_{org} is evident from relationships in $\delta^{13}C_{org}$ *vs.* TOC/SA, consistent with observations for other shelf and delta systems worldwide. Additionally, coastal mangrove belts can reduce transfer of sediments from the terrestrial source regions towards the oceans by up to 30 %, as documented previously for areas of Japan [69]. This will increase the weight of marine OM in bulk composition. Detailed transect sampling through a river-mangrove-ocean segment is required to accurately quantify and characterise this process.
3) The $\Delta^{14}C$ radiocarbon dates of riverine sediments are generally younger than those of the corresponding marine sediments. However, some outliers are observed. Special circumstances can cause anomalous apparent older dates in some cases,

which in the literature are generalised by long storage times in the transport system prior to final deposition, and not to source specific features. In this case, these anomalous older river dates can be traced back to localised geographic features, such as the entry of coal carbon through mining and related processes. Other examples include rivers that drain mafic bedrocks, where substantial amounts of petrogenic carbon appear to be mobilised, shifting the radiocarbon date of marine sediments to less radiogenic compositions. These details highlight the importance of high spatial resolution mapping in the interpretation of regional data sets.

5 Model estimates of OC pools and process in the SCS: Comparing simulation and calculation-based approaches

5.1 Introduction

Numerical models are a powerful tool in the decryption and interpretation of larger datasets, set to interpret geological questions and conundrums. At foremost this study is concerned to identify theoretical bulk sediment compositions related to a mixture of different sources. The preservation of terrestrial sourced OM from source to sink has important implications for the interpretation of carbon processes connecting the land ocean transition zone and could have implications for the storage of carbon. Therefore, an accurate assessment of bulk sediment composition and the identification of contributing sources is a fundamental framework parameter.

Mixed terrestrial reservoirs can be de-convoluted using e.g. geochemical proxies C_{org}/N_{total} $\delta^{13}C_{org}$ and $\Delta^{14}C$ measurements of bulk organic carbon in marine and riverine surface sediments (e.g., Foster and Walling, and Rowntree and Foster, [361, 362]). Furthermore, this study introduces a statistical Bayesian inversion model to estimate relative carbon-source contributions in marine surface sediments of the SCS, and to approximate source signatures currently uncharacterised. The goal is to create an average reservoir reference for larger scale models, which can be applied to any given marine surface sediment sample from the SCS and discuss implications and limitations of this approach.

At the same time, the scepticism of Müller, [164] concerning the C_{org}/N_{total} ratio and its use in mixing models is investigated and evaluated using Bayesian statistic style approach. Additionally, the performance of binary single proxy models with multi variance models is compared to make a recommendation as to which will return the most probable accurate data.

The comparison of these methods highlights the potential of Bayesian statistics, particularly in the validation of theoretical end-members when combined with iterative refinement. In particular, the ability of the Bayesian statistics approach to incorporate unquantifiable data by means of prior knowledge definitions make this tool extremely potent in geological and environmental studies. This is consistent with the observation, that any model applied to the study area is subject to local conditions (e.g. variations in bedrock), which can easily be incorporated in Bayesian statistics. It is demonstrated that

end-members are regional specific and consequently may lead to a bias or even erroneous interpretations when general endmembers are applied. The performance and suitability of geochemical tracers such as the C_{org}/N_{total} ratio is subject to debate. Here it is found to reduce the performance of the models tested, suggesting that it is an unsuitable geochemical tracer to reconstruct or validate end-member compositions. Following the findings of this approach, a modification is suggested to incorporate linear equations in the non-linear Bayesian simulations to improve model *vs.* data fit. This approach will permit the identification of underestimated and/or unrecognised OM source end-members through the iterative component, while the Bayesian statistics permit a mathematical estimate for size fractions.

5.2 Methods

5.2.1 Estimates of marine and terrestrial components based on an end-member mixing model using the $\delta^{13}C_{org}$ isotopic composition

The proportion of OM bearing a marine origin can be estimated using the bulk sediment $\delta^{13}C_{org}$ isotopic composition using the equations of Craig, [184]. The first model boundary parameters used here are taken from reported data of the Changjiang River [363]. A second model run uses the data generated in this study as boundary parameters (using samples with most terrestrial/marine signatures as limits). The value for the marine end-member from the Changjiang River study is $\delta^{13}C_{org}$: -19.2 ‰ [363] and for the terrestrial end-member $\delta^{13}C_{org}$: -24.9 ‰ [363]. For comparison, the value for the marine end-member extracted from the presented study is $\delta^{13}C_{org}$: -20.3 ‰ and for the terrestrial end-member is -29.5 ‰.

5.2.2 Bayesian statistics – using qualitative and quantitative data in geological models

Bayesian statistic is based on the Bayes-Theorem, which incorporates discrete *a priori* information about multidimensional data (signal) distributions and their uncertainty ("prior probabilities" of the end-members) to estimate compositional information (for instance, mixing proportions of the end-members) for samples with unknown composite signals ("posterior probability"), including geological data [364].

Bayesian statistics differ from classical, frequentist statistic in four ways:

I) Frequentists estimate the probability of data occurring given an explicit hypothesis [P(Y|H)]. In contrast, Bayesian inference offers a quantitative estimate

of the likelihood that an explicit hypothesis is true in light of the available data [P(H|Y)] [364]. This approach is useful in many geoscience disciplines wherein data are often sparse, and boundary parameters derived from secondary data (e.g. proxies) are used for constraining global solutions and theoretical hypotheses (i.e. computer models).

II) Differences in defining probability: frequentists define it in terms of long-run (infinite) frequencies of events in a relative sense, and Bayesians define it from an individual's degree of confidence in the likelihood of an event [364]. This permits the application of Bayesian statistics to size limited data sets, while retaining a mathematical sense of uncertainty that can be expressed numerically.

III) Bayesian statistics use *a priori* information (e.g., prior knowledge) along with the sample data, whereas classic statistics use sample data alone [364]. This permits the inclusion of e.g. qualitative data or observations, into quantitative models.

IV) Bayesian statistics consider model boundary-parameters as random variables, whereas classic statistics consider them to be estimates of fixed (true) values [364].

The "**F**ood **R**econstruction **U**sing **I**sotopic **T**ransferred **S**ignals" (FRUITS) model [365] uses Bayesian statistics to constrain most likely proportions of end-member sources (e.g. marine, terrestrial and petrogenic carbon fractions), using measured geochemical proxies to constrain the algorithms (e.g. $\delta^{13}C_{org}$ and F_m). It should be noted, that any Bayesian modelling approach, such as the algorithm used by FRUITS, is inherently nonlinear for systems with multiple end-members, although 'large scale' (global) nonlinearities can appear almost linear at fine (local) scales [366]. The FRUITS model generates the most likely probability proportion (distributions) of the end-member sources or compositional fractions, as informed by given end-member source and data-distribution constraints. FRUITS can be further refined through boundary parameters or conditional requirements that need to be fulfilled (also described as prior or *a priori* knowledge); for instance, a condition that fraction A is bigger than fraction B, or any other adaptable qualitative information.

In the absence of *a priori* information, FRUITS implements a Gaussian (beta) distribution constructed from source-reservoir compositional boundary parameters and their uncertainties. In contrast, incorporating prior information essentially guides model development to create sharper resolution data output [365]. Prior information can include observations from previous studies (e.g., A is bigger than B but smaller than C), region-

specific features such as climate variability or extreme event frequencies or previous model results.

5.2.3 Quantitative modelling of source signatures using a Bayesian statistic approach (FRUITS model)

5.2.3.1 Model estimates for $\delta^{13}C_{org}$ and C_{org}/N_{total} input data

Bayesian statistics are used to calculate theoretical mixing between multiple end-members, representing the composition of i) continental signal and ii) marine cumulate sediment. This study uses C_{org}/N_{total} ratio and $\delta^{13}C_{org}$, as they are commonly used tracers to differentiate terrestrial and marine source composition. The model is restrained to not consider isotopic fractionation and concentrations. The model output is reported in section 5.3.2 table 18 and 19.

5.2.3.2 Model estimates for $\delta^{13}C_{org}$ and $\Delta^{14}C$ input data

Bayesian statistics are used to calculate theoretical mixing between multiple end-members, representing the composition of i) continental signal and ii) marine cumulate sediment. This study uses $\delta^{13}C_{org}$ and $\Delta^{14}C$, as they are carbon specific tracers used to differentiate terrestrial and marine source composition. It is important to note that radiocarbon ($\Delta^{14}C$) records can be decoupled from stable carbon isotopes in some cases, e.g. if transport timescales vary significantly in the region of interest. The model is restrained to not consider isotopic fractionation and concentrations. The model output is reported in section 5.3.3 table 20 and 21.

5.2.4 Increasing model complexity by addition of source reservoirs and numerical refinement through iterative calculations

The output of Bayesian models is non-linear, since the data density and data composition determine the spread, but this offers the flexibility to introduce additional variables. The first aim was to estimate/calculate the proportion of petrogenic carbon to complement the FRUITS model estimate for marine and terrestrial proportions (Fig. 26 step 1). The outcome can be compared to conventional estimates from stable isotopes and C_{org}/N_{total} ratios (see section 5.3.1 and 5.3.2). The first step calculates the relative proportion of petrogenic carbon, using the ratios of marine and terrestrial from FRUITS as start-parameters, and an arbitrarily chosen starting estimate for petrogenic carbon (e.g. 5 %). The choice of starting estimate is not of relevance, as the equation used in the model solves the unknown variable based on the known variable input. The output is tested by

calculating new bulk $\delta^{13}C_{org}$ and $\Delta^{14}C$ values and comparing them against the actual measured values.

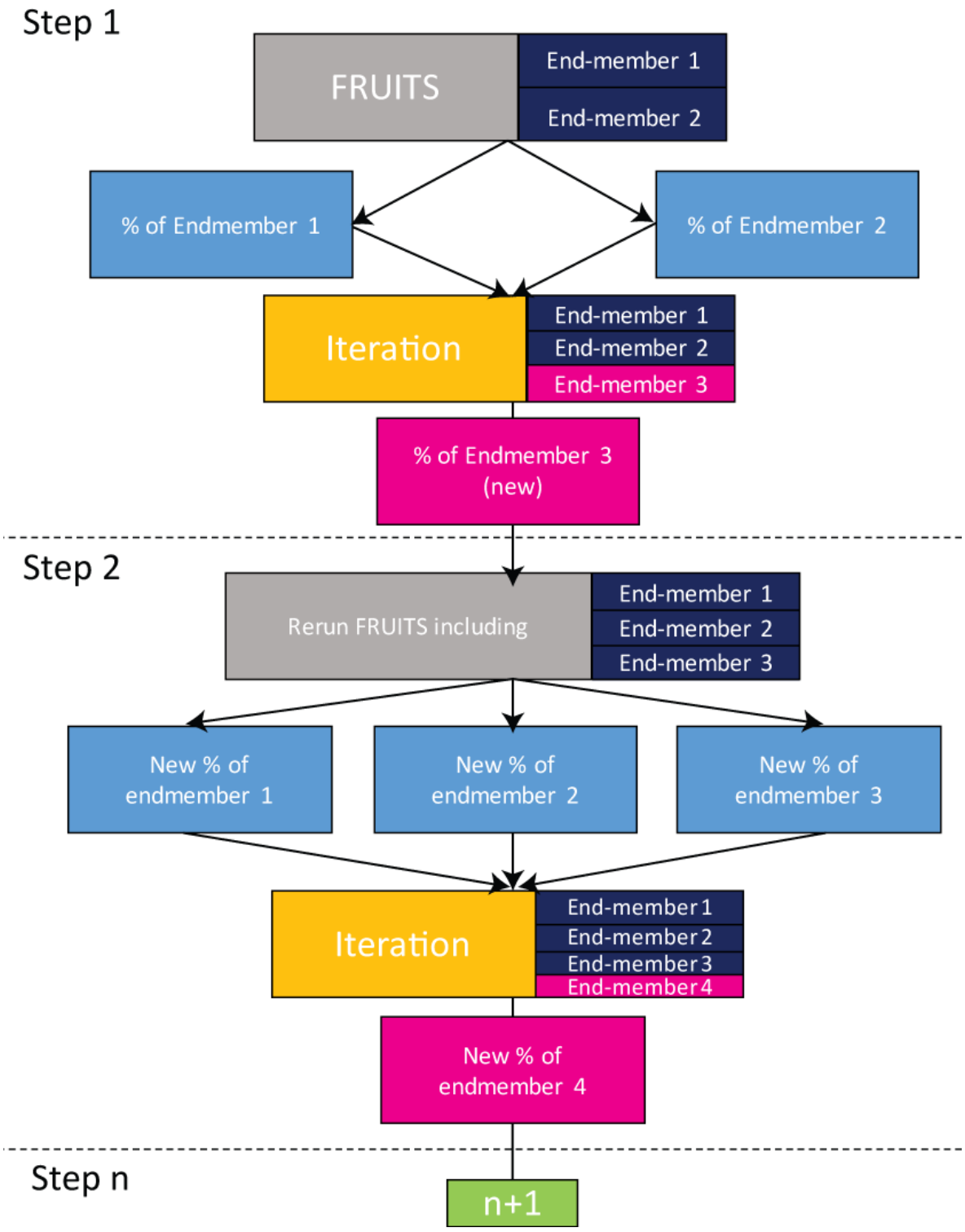

Figure 26) Schematic illustration of the inversion model workflow (using FRUITS version 2.1.1. Beta). Individual end-members are stepwise resolved, starting with two end-members (marine and terrestrial), utilising carbon isotope data ($\delta^{13}C_{org}$ and $\Delta^{14}C$). Each new step represents a model run with an additional end-member (e.g. petrogenic carbon in step 1, carbon dead in step 2). FRUITS requires the input of the assumed reservoir composition and sample compositions, to perform Bayesian simulations. The results from step 1 are used to construct the model run parameters of step 2, and the model can be expanded infinitely. However, a reasonable number for steps is proportionate to the

number of tracers utilised, and significantly, amounts of uncertainty in the model output must be expected if the number of sources is larger than the number of geochemical proxies plus one

As explained in Chapter 3 and 4, the prior knowledge about the overall composition and diagnostic signature of each carbon source is rather limited and based on assumptions derived from the literature. Prior knowledge is only available for marine and terrestrial end-member calculations, but it is to expect that two sources mixing models do not account for the overall system and the contributing factors, which play a role in the carbon cycle.

Following the initial calculation cycle, FRUITS outputs for terrestrial, marine and petrogenic mixing proportions reveal a discrepancy between measured and modelled bulk $\delta^{13}C_{org}/\Delta^{14}C$ for SCS surface sediment samples. To resolve these discrepancies, iterative calculations were performed using Microsoft Office Excel functionality, gradually adjusting pools of marine, terrestrial and petrogenic carbon until an acceptable match between measured and model data is observed (>90 % for $\delta^{13}C_{org}$ and visual fit of total data in Fig. 27). For this, marine, terrestrial and petrogenic carbon reservoirs/end-members are given specific $\delta^{13}C_{org}$ and fraction modern values. End-member $\delta^{13}C_{org}$ values were compiled from recent literature from locations nearby or with comparable depositional features (c.f., the marine bio-production $\delta^{13}C_{org}$ value of -19.2 ‰ has been adopted from Wang et al. [363]. This end-member $\delta^{13}C_{org}$ value yields an almost 1:1 correlation between measured and modelled data output, however the linear regression does not have a zero intercept. Attribute this to minor regional differences in marine $\delta^{13}C_{org}$ the Changjiang River, which is distal to the study area, is influenced by compositionally different sources. Wang et al. [363] reported eutrophication of the Changjiang River, which is ascribed to intensive farming and the use of fertilisers. Excessive farming in the Changjiang River catchment will therefore create a markedly different vegetation cover (on shore) compared to the SCS study area, likely explaining the observed offset in $\delta^{13}C_{org}$ data.

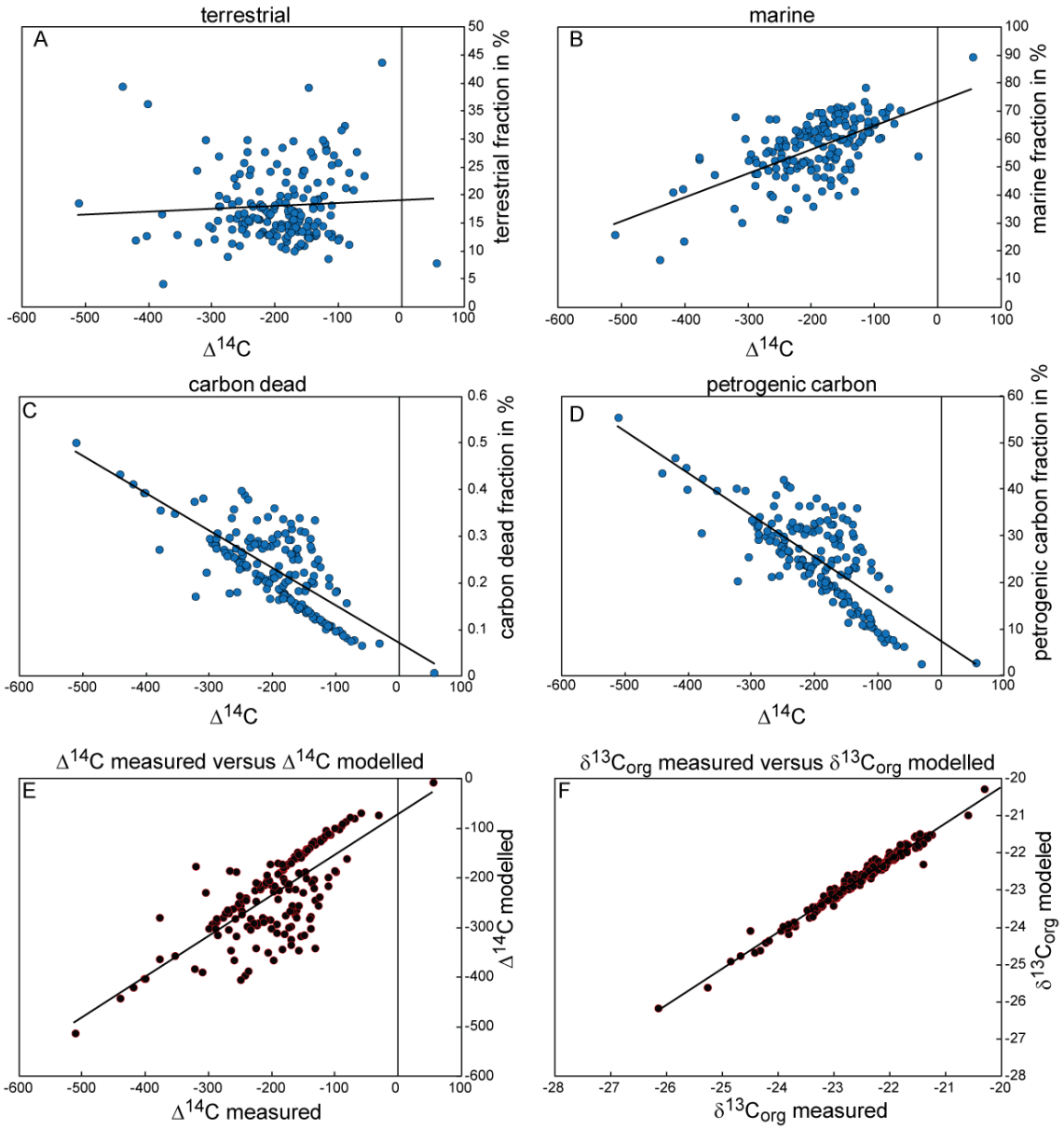

Figure 27) Model output of FRUITS optimised by iterative refinement to increase the fit between observed and modelled data. The dependence of measured $\Delta^{14}C$ and modelled fraction is illustrated in A, B, C and D, testing the robustness of the model output. Scatter can be caused by incorrect choice of source compositions or underestimation of sample complexity. The $\Delta^{14}C$ system is revealed to be more sensitive relative to the $\delta^{13}C$ (E and F), expressed by higher degrees of scatter in measured *vs.* modelled data. Some of the scatter in $\Delta^{14}C$ can be related to the radiogenic nature of the $\Delta^{14}C$ system, which can result in non-linear mixing relations.

For the terrestrial bio-production a value of -30 ‰ has been selected, based on observations that for terrestrial C_3 plants $\delta^{13}C_{org}$ ranges between -21 ‰ and -32 ‰ [220]. By picking this specific end-member for C_3 plants, based on the observations from Chapter 3 and that for the $\delta^{13}C_{org}$ distribution only C_3 plants have an impact in the region. In the simulations the value of -30.0 ‰ for the terrestrial C_3 reservoir [367] in combination with a value of -19.2 ‰ for the marine reservoir result in a good fit between model estimates and measured data (Fig. 27). Lamade et al. [367] found $\delta^{13}C_{org}$ values of oil palm leaves for bulk OM in the autotrophic stage of -29.01 ‰ ± 0.9 ‰ in northern

Sumatra our lowest measurements is -29.45 ‰ , also in northern Sumatra which reinforces the choice of -30 ‰ for the terrestrial end-member.

For the $\delta^{13}C_{org}$ value of the petrogenic carbon an end-member of -25.4 ‰ was selected based on the findings of Blattmann et al. [11], who investigated sediment traps in the shelf close to Taiwan, which is in proximity to the study area. It can be observed that the F_m model *vs.* measured data display higher amounts of scatter compared to the $\delta^{13}C_{org}$ data. This is likely attributed to the fact that:

i) $\Delta^{14}C$ is a radiogenic system that is more sensitive to mixing effects and variable source region compositions, as well as carbon transfer and cycle times
ii) unrecognised heterogeneity in the source regions in terms of $\Delta^{14}C$ composition.

To improve the fit of the $\Delta^{14}C$ model *vs.* measured data the next step was to introduce a fourth reservoir in the model iteration, i.e. 'carbon dead'.

For the carbon dead fraction a $\delta^{13}C_{org}$ end-member of -25 ‰ [225] was used, assuming that this carbon is sourced from geologically old material, such as coal. Coal mining is significant in e.g. the delta of the Red River and coal particles (aeolian and/or fluvial transported) might be introduced to the carbon cycle by burning of coal in e.g. power plants or through mining activity and subsequent processing.

For the marine bio-production a F_m value of 1.04 was chosen, which represents the average value of all samples with a post-bomb signal and which is close to the atmospheric F_m value. The marine bio-production was chosen to represent the post-bomb signal because the ocean surface readily exchanges carbon with the atmosphere and most marine bio-production occurs near the surface.

For the terrestrial bio-production a $F_m = 0.851$ is selected, representing the average of all measured F_m values in the studied samples. The terrestrial reservoir $\Delta^{14}C$ value is -155 ‰ (sampling year 2012).

For the petrogenic carbon an $F_m/\Delta^{14}C$ value of 0.12/-880 ‰ was used, consistent with Rosenheim and Galy., [368]. They reported that any given riverine sample carrying petrogenic carbon also carries a young component, which possibly derives from mixing of truly old sediment OC with relatively young sediment OC. Rosenheim and Galy, [368] report a value of - 880 ‰ for the Ganges river system. It is to assume that this is an

acceptable approximation of the petrogenic carbon reservoir composition, when draining both ancient and more recent sediments.

Assuming that the simulations approximate reality, the Bayesian model output can be refined using simplified mixing equations in iterative steps. The iterative models were performed stepwise and always used the FRUITS model output of initial estimates for marine and terrestrial proportions as a foundation. Below is about the calculation that results in what it is to consider the best estimate for the number of reservoirs and their composition in the SCS with the available data. In order to perform calculations, it is used a simple equation that can be adjusted for any number of variables (e.g. number of sources). The equation expressed below is set to solve for petrogenic carbon (*c*):

Equation 7) Calculation of bulk composition

$$bulk\ M = (a * x) + (b * y) + (c * z)$$

Bulk M = measured bulk value
a = marine [%]
b = terrestrial [%]
c = petrogenic carbon [%]
x = end-member marine $\delta^{13}C_{org}$ composition
y = end-member terrestrial $\delta^{13}C_{org}$ composition
z = end-member petrogenic carbon $\delta^{13}C_{org}$ composition

The petrogenic carbon [%] (*c*) in this example is the unknown, so it has to reorder the equation to solve for the factor *c*:

Equation 8) Calculation of petrogenic carbon

$$c = \frac{bulk\ M - (a \times x) - (b \times y)}{z}$$

To avoid the problem of negative values it has to calculate with absolute values in Microsoft Office Excel and the final sum is calculated to 100 %.

In preparation of the introduction of petrogenic carbon into the total sum, the fractions of marine and terrestrial are reduced in equal proportions. This is done for both marine and terrestrial (%) as follows:

Equation 9) Reduction of marine and terrestrial proportions

$$u = (a/100) \times (100 \times q)$$

u = new part of ratio
q = starting point for contamination (random pick)
a = fraction of marine or terrestrial [%].

Since *u* gives the new fraction estimate based on the size of *q*, this needs to be performed for all starting values (here marine and terrestrial estimate from the FRUITS model). The estimate for the newly introduced component can be picked at random, although it cannot exceed 100. In our case, a starting point in the range of 0 % to 20 % is advisable for the fraction estimate of petrogenic carbon, based on the reservoir definitions. Preceding further with the iteration, the next *q* would be the first calculation of equation 10. Now it is possible to iteratively calculate new *bulk M* values and compare model *vs.* measured values of e.g. $\delta^{13}C_{org}$ or $\Delta^{14}C$ until an acceptable fit is obtained using the equation:

Equation 10) Calculation of the new bulk composition

$$new\ bulk\ M = (a * u) + (b * v) + (c * w)$$

New bulk M = model calculated new bulk signal
w = new calculated petrogenic carbon [%] (in first equation, chosen contamination, in further iterations result of equation 1). Sums are calculated to 100 %. Below the progress is described and documented in detail.

The petrogenic carbon reservoir estimate is refined taking the results from the first calculation adjusted for mass balance to preserve system sum of 100 %. Five iterations were performed, after which insignificant change is observed.

A new bulk $\delta^{13}C_{org}$ and F_m value is calculated, using the fraction proportions from the last iteration (marine, terrestrial and petrogenic carbon). This calculated value is compared with the measured value (Fig. 27 and 28).

Potential sources of uncertainty are

i) incorrect reservoir definition,
ii) underestimation of the total number of reservoirs,
iii) reworking of carbon in the marine environment during transport.

The fit is generally good for $\delta^{13}C_{org}$ (>90 %) and estimates for petrogenic carbon can range from 1 % to 20 %. The fit of F_m is acceptable (qualitatively, Fig. 28, but typically better than 70 %), but contains significant amounts of scatter, even after five iterations. However, performing additional iterations for F_m returns insignificant change. This might indicate that the model does not cover enough complexity in the F_m systematics. This observation leaves two options: first, to rerun the FRUITS model with the new validated end-member composition or secondly, add more diagnostic tracer data (e.g. other stable isotope data).

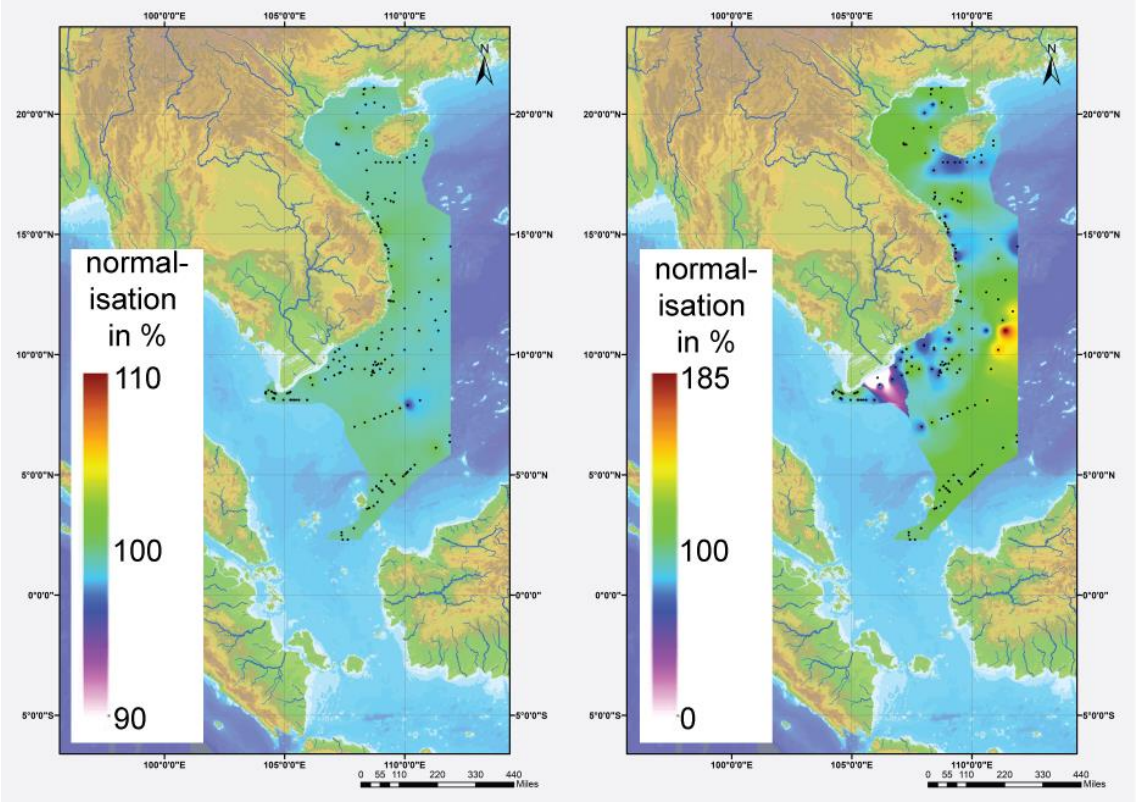

Figure 28) The model fit between model output and measured data is illustrated graphically by IDW interpolation. A) The $\delta^{13}C$ interpolation reveals areas that consistently over- or underestimate the model, and that data are regionally constrained, e.g. at ca. 15°N $\delta^{13}C$ model values overestimate relative to measured values. B) The $\Delta^{14}C$ interpolation reveals significant heterogeneity in the model fit, with up to 85% deviation for some samples, reflecting the scatter in Fig. 27E

The second step was to estimate a fourth reservoir – carbon dead – to improve the fit in F_m model versus measured data, but not changing the $\delta^{13}C_{org}$ model result.

For the estimation of the % fraction of carbon dead a reservoir age of zero for F_m is used, which is equivalent to a $\Delta^{14}C$ value of -1000 ‰ (~>10 half live times of carbon, [194]). $\Delta^{14}C$ was used because of the mathematical error produced when division through zero is performed. This can be circumvented using $\Delta^{14}C$ values rather than the F_m values. The F_m values are preferred since they are more accurate when comparing with other samples and were used in the FRUITS model prior to the introduction of the carbon dead reservoir.

Technically an unknown sample can still have a $\Delta^{14}C$ value of zero but is absent in the modelled data here.

Since carbon dead is assumed to be part of petrogenic carbon, the amount of carbon dead is important to calculate the bulk $\Delta^{14}C$.

The first attempted model is based on the approach that the bulk sample is a mixture of all four components. To calculate the carbon dead amount, five iterative calculations were made to create a fit between actual measured bulk $\Delta^{14}C$ against calculated bulk $\Delta^{14}C$,

as well as measured bulk $\delta^{13}C_{org}$ to calculated $\delta^{13}C_{org}$. Using this approach, both systems show a good fit (Fig. 28). Technically, the actual FRUITS model can be used to calculate the amount of carbon dead by itself, but the outcome shows a poorer fit, than the refined iterative approach (iFRUITS).

The third and final step was to refine the model further, by considering a fifth component, the marine reservoir effect. However, no qualitative improvement occurred. Scatter is still observed, which occurs probably because of reworked sediment, which cannot be accounted for in the absence of a reliable composition and proxy needed in quantitative modelling. While the scatter could not be resolved completely, the fit between modelled and observed data improved to >90 % on average, and the likely source composition and size fraction of two previously uncharacterised reservoirs are estimated.

5.3 Results

5.3.1 Estimates of marine and terrestrial components based on end-member mixing model using the $\delta^{13}C_{org}$ isotopic composition

The proportion of OM bearing a marine origin can be estimated using the bulk sediment $\delta^{13}C_{org}$ isotopic composition using the equations of Craig, [184]. End-member compositions for $\delta^{13}C_{org}$ defined here for binary-mixing models are employed in all simulations, including the multi-variable FRUITS model simulations (section 5.3.1). One binary mixing model to constrain model parameters is based on reported data from the Changjiang River [363]. A second model run uses the data generated in this study as parameters (using samples with most terrestrial/marine signatures as boundaries). The value for the marine end-member from the Changjiang River study is $\delta^{13}C_{org}$: -19.2 ‰ [363] and for the terrestrial end-member $\delta^{13}C_{org}$: -24.9 ‰ [363] (Fig. 29, table 14 and 15).

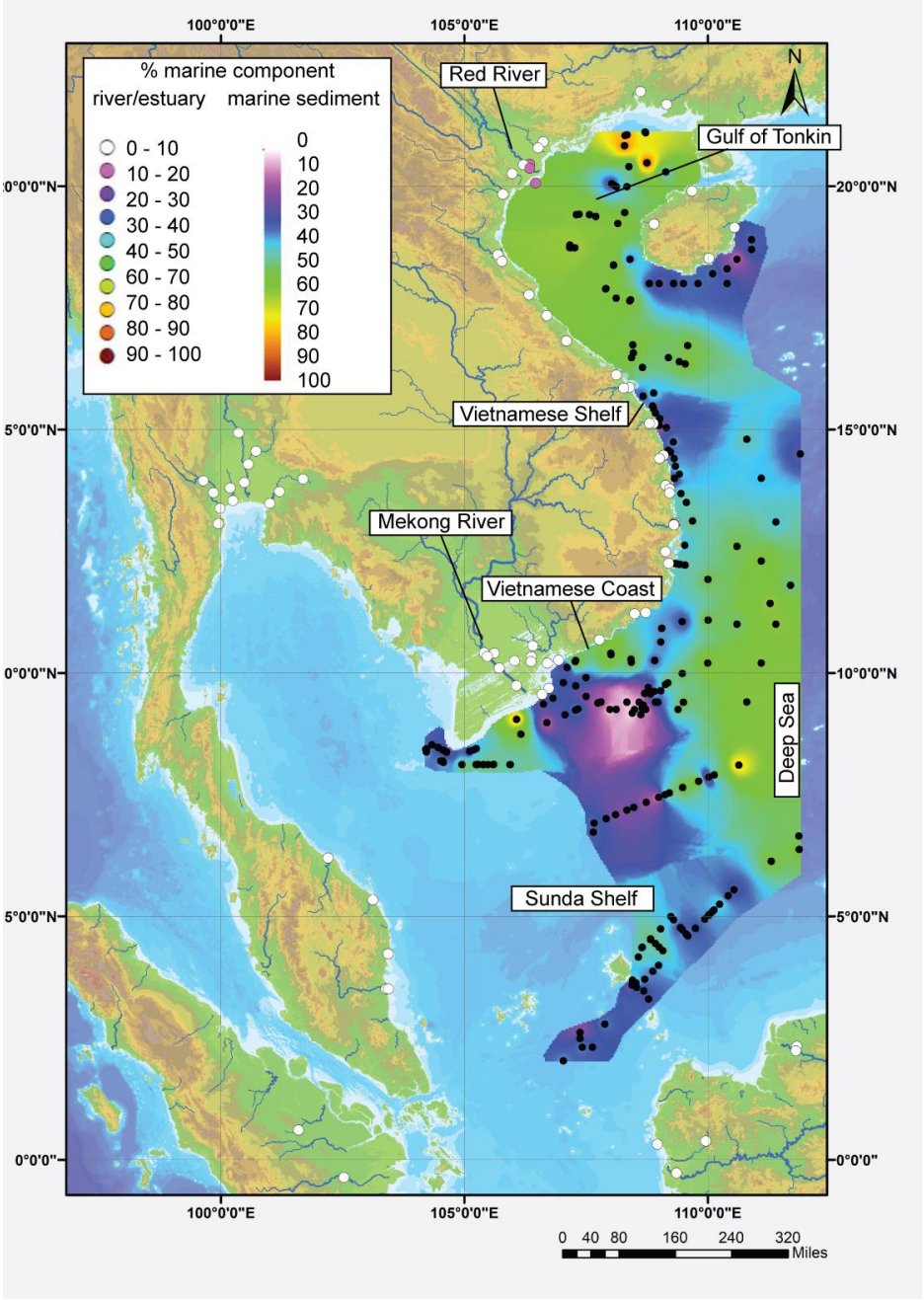

Figure 29) Estimate of the marine component of marine surface and river/estuary sediment samples from the SCS, based on the $\delta^{13}C_{org}$ isotopic record using literature end-members for terrestrial (-24.9‰) and marine (-19.2‰) reservoirs [363]. The model assumes simple two component mixing. River samples (coloured spheres) are not interpolated but the colour of the sphere relates to the value as indicated in the legend. Black spheres indicate marine surface sediment sample locations. The marine surface sediment samples are interpolated using an inverse distance weighting model using ArcGIS v.10.6.

For comparison, the value for the marine end-member extracted from the presented study is $\delta^{13}C_{org}$ -20.3 ‰ and for the terrestrial end-member -29.5 ‰ (Fig. 30a, tables 16 and 17).

The percent estimate of the marine component is reported, based on a binary mixing model (first with literature values, see figure 29).

Table 14) Calculated marine proportions for marine surface sediments with a binary single component $\delta^{13}C_{org}$ model based on literature end-member (marine: $\delta^{13}C_{org}$: -19.2 ‰; terrestrial: $\delta^{13}C_{org}$: -24.9 ‰ [363]

Region	Max. value	Min. value	Average	*n*
Gulf of Tonkin	64.0 %	9.47 %	46.6 %	41
Vietnamese Shelf	55.8 %	7.02 %	38.9 %	32
Vietnamese Coast	80.5 %	0.00 %	32.1 %	75
Sunda Shelf	57.4 %	0.00 %	34.9 %	51
Slope/ Deep Sea	24.7 %	75.4 %	52.2 %	31

For the Gulf of Tonkin the marine component estimates range from 9.47 % to 64.0 % (average: 46.6 %, $n = 41$). In the Vietnamese Shelf the estimates of the marine proportion range from 7.0 % to 55.8 % (average: 38.9 %, $n = 32$). On the Vietnamese Coast the marine component ranges from 0 % to 80.5 % (average: 32.1 %, $n = 75$). In the Sunda Shelf the marine component ranges between 0 % and 57.4 % (average: 34.9 %, $n = 51$). In the Slope/Deep Sea the estimates for the marine component range from 24.7 % to 75.4 % (average: 52.2 %, $n = 31$).

Table 15) Calculated marine proportions estuary samples with a binary single component $\delta^{13}C_{org}$ model based on literature end-member (marine: $\delta^{13}C_{org}$: -19.2 ‰; terrestrial: $\delta^{13}C_{org}$: -24.9 ‰ [363])

Region	Max. value	Min. value	Average	*n*
Estuaries from the Gulf of Tonkin area	0.0 %	13.9 %	3.42 %	18
Estuaries from the Vietnamese Shelf area	17.3 %	0.0 %	2.15 %	23
Estuaries from the Vietnamese Coast area	2.6 %	0.0 %	0.33 %	17
Estuaries from the Sunda Shelf area (Indonesia and Malaysia)	0.0 %	0.0 %	0.0 %	16
Estuaries from Thailand	4.27 %	0.0 %	0.65 %	13

In the study area for the respective estuaries, the marine component estimates range from 0.0 % to 19.3 % (average: 3.42 %, $n = 18$) in the Gulf of Tonkin. In the Vietnamese Shelf the respective estuaries show estimates of the marine proportion ranging from 0 % to 17.3 % (average: 2.15 %, $n = 23$). In the Vietnamese Coast the marine component ranges from 0 % to 5.53 %, with values being zero except for one sample (average: 0.33 %, $n = 0.33$ %). Estuary samples from the Sunda Shelf region show no exception 0.0 % for a marine proportion. Estuary samples from Thailand have values from 0.0 % to 4.27 % (average: 0.65 %, $n = 13$).

The second model run is performed with the suggested end-members as documented above. The percentage estimate of the marine component is given, where the model sum is 100 % between marine and terrestrial component.

Table 16) Calculated marine proportions of marine surface sediments with a binary single component $\delta^{13}C_{org}$ model based on internal end-member (marine: $\delta^{13}C_{org}$: -20.3 ‰; terrestrial: $\delta^{13}C_{org}$: -29.5‰)

Region	Max. value	Min. value	Average	*n*
Gulf of Tonkin	89.7 %	55.7 %	78.8 %	41
Vietnamese Shelf	84.6 %	54.2 %	74.1 %	32
Vietnamese Coast	100 %	19.2 %	69.8 %	75
Sunda Shelf	85.6 %	43.5 %	71.6 %	51
Slope/ Deep Sea	96.8 %	65.2 %	82.3 %	31

For the Gulf of Tonkin the marine component estimates range from 55.7 % to 89.7 % (average: 78.8 %, $n = 41$). In the Vietnamese Shelf the estimates of the marine proportion range from 54.2 % to 84.6 % (average: 74.1%, $n = 32$). In the Vietnamese Coast the marine component ranges from 19.2 % to 100 % (average: 69.8 %, $n = 75$). In the Sunda Shelf the marine component ranges between 43.5 % and 85.6 % (average: 71.6 %, $n = 51$). In the Slope/Deep Sea the estimates for the marine component range from 65.2 % to 96.8 % (average: 82.3 %, $n = 31$).

Table 17) Calculated marine proportions of estuary samples with a binary single component $\delta^{13}C_{org}$ model based on internal end-member (marine: $\delta^{13}C_{org}$: -20.3 ‰; terrestrial: $\delta^{13}C_{org}$: -29.5‰)

Region	Max. value	Min. value	Average	*n*
Estuaries from the Gulf of Tonkin area	61.8 %	20.6 %	44.4 %	18
Estuaries from the Vietnamese Shelf area	60.6 %	11.7 %	37.7 %	23
Estuaries from the Vietnamese Coast area	53.2 %	24.9 %	0.33 %	17
Estuaries from the Sunda Shelf area (Indonesia and Malaysia)	36.9 %	0.0 %	13.4 %	16
Estuaries from Thailand	52.4 %	20.6 %	38.6 %	13

For the respective estuaries, in the Gulf of Tonkin the marine component estimates range from 20.6 % to 61.8 % (average: 44.4 %, $n = 18$). In the Vietnamese Shelf the respective estuaries show estimates of the marine proportion ranging from 11.7 % to 60.6 % (average: 37.7 %, $n = 23$). In the Vietnamese Coast the marine component ranges from 24.9 % to 53.2 % (average: 37.1 %, $n = 17$). Estuary samples from the Sunda Shelf region values range from 0.0 % to 36.9 % (average: 13.4 %, $n = 16$). Estuary samples from Thailand have values from 20.6 % to 52.4 % (average: 38.6 %, $n = 13$). The binary single

compound mixing model result based on selected end-members is illustrated in figure 30a.

5.3.2 Quantitative modelling of source signatures using a Bayesian statistics approach (FRUITS model)

Bayesian statistics are used to calculate theoretical mixing between multiple end-members, representing the composition of i) pure continental signal and ii) marine cumulate sediment. This study uses C_{org}/N_{total} ratio and $\delta^{13}C_{org}$ (Fig. 30a and b), as they are commonly used tracers to differentiate terrestrial and marine source composition. The model is restrained to not consider isotopic fractionation and concentrations.

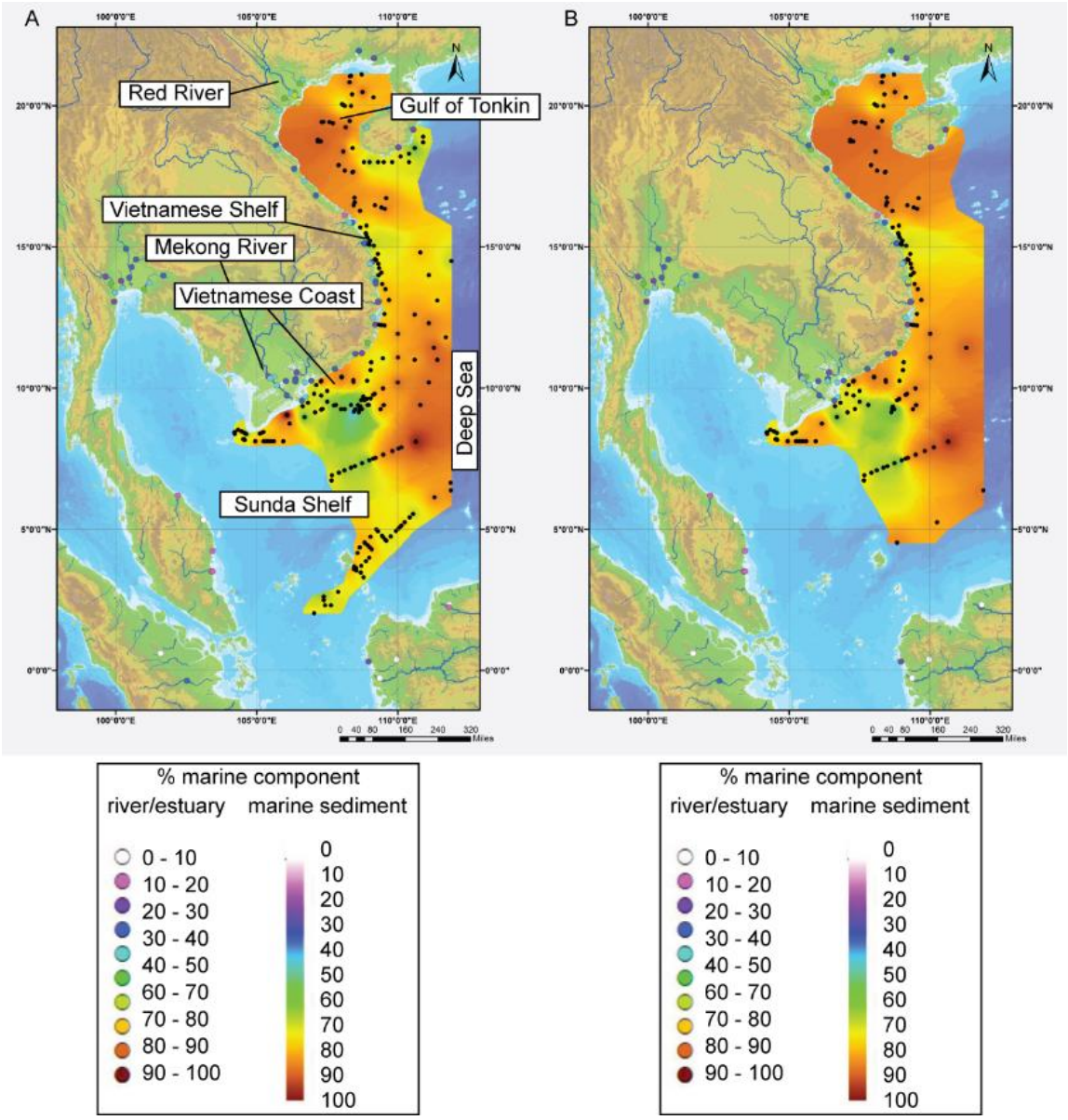

Figure 30) a (left): Estimate of the marine component of marine surface and river/estuary sediment samples from the SCS are estimated to be based on the $\delta^{13}C_{org}$ isotopic record using internal end-members for terrestrial (-29.45 ‰) and marine (-20.31 ‰) reservoirs. The model assumes simple two component mixing. River samples (coloured spheres) are not interpolated but the colour of the sphere relates to the value as indicated in the legend. Black spheres indicate the marine surface sediment samples locations. The marine surface sediment samples are interpolated using an inverse distance weighting model using ArcGIS v.10.6.

b (right): Estimate of the marine component of marine surface and river/estuary sediment samples from the SCS, estimated based on the $\delta^{13}C$ isotopic record and C_{org}/N_{total} data, using theoretical end-members for terrestrial ($\delta^{13}C_{org}$ = -29.45‰, C_{org}/N_{total} 49.8) and marine ($\delta^{13}C_{org}$ = -20.31‰, C_{org}/N_{total}=2.33) reservoirs. The model assumes simple two-component mixing and employs Bayesian statistics (Fernandes et al. [365]). River samples (coloured spheres) are not interpolated but the colour of the sphere relates to the value as indicated in the legend. Black spheres indicate the marine surface sediment samples locations. The marine surface sediment samples are interpolated using an inverse distance weighting model using ArcGIS v.10.6

The model estimate proportions are reported in percent values and are strictly binary mixing results.

Table 18) Model estimates for marine proportions using C_{org}/N_{total} ratio and $\delta^{13}C_{org}$ (a Bayesian approach) for marine surface sediments

Region	Max. value	Min. value	Average	*n*
Gulf of Tonkin	93.3 %	70.7 %	88.4 %	29
Vietnamese Shelf	98.5 %	79.9 %	93.2 %	32
Vietnamese Coast	98.8 %	52.3 %	69.8 %	75
Sunda Shelf	98.8 %	89.9 %	95.9 %	11
Slope/ Deep Sea	98.1 %	79.5 %	92.6 %	16

In the Gulf of Tonkin, the proportion of marine OM ranges from 70.7 to 93.9 % (average: 88.4 %, n = 29). In the Vietnamese Shelf, the marine components comprise for 79.9 % to 98.5 %, (average: 93.2 %, n = 32). In the Vietnamese Coast, the marine proportions range from 52.3 % to 98.8 % (average: 85.6 %, n = 56). In the Sunda Shelf, marine proportions are estimated to range from 89.9 % to 98.8 %, (average: 95.9 %, n = 11). Calculations of the marine proportions from samples of the Slope/Deep Sea range from 79.5 % to 98.1 %, (average: 92.6 %, n = 16).

Table 19) Model estimates for marine proportions using C_{org}/N_{total} ratio and $\delta^{13}C_{org}$ (a Bayesian approach) for estuary samples

Region	Max. value	Min. value	Average	*n*
Estuaries from the Gulf of Tonkin area	97.8 %	1.48 %	63.5 %	18
Estuaries from the Vietnamese Shelf area	98.9 %	1.80 %	31.8 %	23
Estuaries from the Vietnamese Coast area	98.6 %	3.28 %	60.3 %	17
Estuaries from the Sunda Shelf area (Indonesia and Malaysia)	79.1 %	0.54 %	19.5 %	16
Estuaries from Thailand	67.1 %	5.5 %	41.3 %	13

In the respective estuary samples the proportion of marine component ranges from 1.48 % to 97.8 %, (average: 63.5 %, n = 18) in the Gulf of Tonkin. In the Vietnamese Shelf estuary, the marine components comprise for 1.80 % to 98.9 %, (average: 31.8 %, n = 32). In the Vietnamese Coast estuary, the marine proportions range from 3.28 % to 98.6 %, (average: 60.3 %, n = 17). In the Sunda Shelf estuary, marine proportions are estimated to range from 0.54 % to 79.1 %, (average: 19.5 %, n = 16). Estuary samples from Thailand range from 5.5 % to 67.1 % (average: 41.3 %, n = 13), but cannot be related

directly to a marine region with the available data set and are only reported to complement further research in the area.

5.3.3 Model estimates for source region compositions from $\delta^{13}C_{org}$ and F_m space

The composition of three potential source reservoirs (petrogenic carbon, marine and terrestrial bio-production) has been identified and quantified, using a multiple end-member Bayesian statistics and inversion modelling approach. This model includes only marine surface sediments, estuaries/riverine samples need a different approach and different end-member. The model was tuned using a $\delta^{13}C_{org}$ and F_m composition of petrogenic carbon of -25.4 ‰ [11], and 0.12 for marine bio-production -19.2 ‰ [363] and 1.04, for terrestrial bio-production -30 ‰ and 0.851, and for carbon dead -25 ‰ and 0 (no radiogenic carbon present), respectively.

The calculated proportions (n = 176) of marine component in the SCS surface sediments range from 17.7 % to 87.9 % (average: 53.3 %), terrestrial component ranges from 4.8 % to 42.3 % (average: 15.2 %), petrogenic carbon ranges from 2.2 % to 30.3 % (average: 15.8 %), and carbon dead ranges from 1.8 % to 28.9 % (average: 15.8 %) (Fig. 31 and 32, tables 20-31).

In detail:

Table 20) Model estimates for marine proportions using $\delta^{13}C_{org}$ and F_m (a Bayesian approach) for marine surface sediments

Region	Max. value	Min. value	Average	*n*
Gulf of Tonkin	72.0 %	33.2 %	54.7 %	27
Vietnamese Shelf	69.9 %	32.7 %	58.2 %	26
Vietnamese Coast	87.9 %	17.7 %	49.5 %	63
Sunda Shelf	65.0 %	20.3 %	50.5 %	32
Slope/ Deep Sea	77.4 %	37.3 %	59.4 %	28

The proportion of the marine component ranges in the Gulf of Tonkin from 33.2 % to 72 % (average: 54.7 %, n =27). On the Vietnamese Shelf values range 32.7 % to 69.9 % (average: 58.2 %, n = 26). On the Vietnamese Coast the marine component shows values from 20.3 % to 77.4 % (average: 50.5 %, n =32). In the Slope/Deep Sea region the marine proportion ranges from 37.3 % to 77.4 % (average: 59.4 %, n = 28).

Table 21) Model estimates for terrestrial proportions using $\delta^{13}C_{org}$ and F_m (a Bayesian approach) for marine surface sediments

Region	Max. value	Min. value	Average	*n*
Gulf of Tonkin	19.9 %	8.23 %	12.6 %	27
Vietnamese Shelf	42.3 %	8.83 %	19.3 %	26
Vietnamese Coast	41.6 %	7.56 %	16.9 %	63
Sunda Shelf	27.4 %	9.15 %	14.8 %	32
Slope/ Deep Sea	16.1 %	4.75 %	10.3 %	28

The terrestrial proportion calculated from the FRUITS model approach shows values in the Gulf of Tonkin from 8.23% to 19.9 % (average: 12.6 %, n = 27). On the Vietnamese Shelf the proportion ranges from 8.83 % to 42.3 % (average: 19.3 %, n = 26). The percentages of the terrestrial component on the Vietnamese Coast range from 7.56 % to 41.6 % (average: 16.9 %, n = 63). In the Sunda Shelf region values range from 9.15 % to 27.4 % (average: 14.8 % n = 32). The Slope/Deep Sea shows values from 4.75 % to 16.1 % (average: 10.3 %, n = 28).

Table 22) Model estimates for petrogenic carbon proportions using $\delta^{13}C_{org}$ and F_m (a Bayesian approach) for marine surface sediments

Region	Max. value	Min. value	Average	*n*
Gulf of Tonkin	24.4 %	6.96 %	16.1 %	27
Vietnamese Shelf	25.2 %	2.20 %	11.3 %	26
Vietnamese Coast	29.1 %	2.40 %	16.8 %	63
Sunda Shelf	30.3 %	10.9 %	17.8 %	32
Slope/ Deep Sea	24.0 %	6.93 %	14.8 %	28

Calculated petrogenic carbon values range in the Gulf of Tonkin from 6.96 % to 24.4 % (average: 16.1 %, n = 27). The Vietnamese Shelf shows proportions for the terrestrial component from 2.20 % to 25.2 % (average: 11.3 %, n = 63). The Vietnamese Coast shows values from 2.40 % to 29.1% (average: 16.8 %, n = 63). In the Sunda Shelf, percentages of the terrestrial component range from 10.9 % to 30.3 % (average: 17.8 %, n = 32). In the Slope/ Deep Sea area values range from 6.93 % to 24.0 % (average: 14.8 %, n = 28).

Table 23) Model estimates for carbon dead proportions using $\delta^{13}C_{org}$ and F_m (a Bayesian approach) for marine surface sediments

Region	Max. value	Min. value	Average	*n*
Gulf of Tonkin	27.3 %	6.04 %	16.6 %	27
Vietnamese Shelf	26.7 %	1.83 %	11.3 %	26
Vietnamese Coast	28.6 %	2.11 %	16.9 %	63
Sunda Shelf	28.9 %	9.32 %	16.9 %	32
Slope/ Deep Sea	24.0 %	6.02 %	15.5 %	28

The calculated proportions for carbon dead range in the Gulf of Tonkin from 6.04 % to 27.3 % (average: 16.6 %, n = 27). Values on the Vietnamese Shelf range from 1.83 % to 28.6 % (average: 11.3 %, n = 26). The proportions for the carbon dead component range on the Vietnamese Coast from 2.11 % to 28.6 % (average: 16.9 %, n = 63). In the Sunda Shelf values range from 9.32 % to 28.9 % (average: 16.9 %, n = 32). Proportions range in the Slope/Deep Sea from 6.02 % to 24.0 % (average: 15.5 %, n = 28).

The iFRUITS (iteration) based on the $\delta^{13}C_{org}$ data (n = 176) results in values of the marine component ranging from 16.8 % to 90.7 % (average: 60.4 %). The corresponding terrestrial component ranges from 3.6 % to 39.0 % (average: 14.7 %), petrogenic carbon ranges from 2.8 % to 55.9 % (average: 23.9 %) while carbon dead ranges from 0.8 % to 1.0 % (average: 1.0 %) (Fig. 31, tables 24 - 27).

Table 24) Model estimates for marine proportions using $\delta^{13}C_{org}$ and F_m (a Bayesian approach) for marine surface sediments combined with an iterative

Region	Max. value	Min. value	Average	*n*
Gulf of Tonkin	73.6 %	43.2 %	62.0 %	27
Vietnamese Shelf	72.6 %	44.2 %	64.3 %	26
Vietnamese Coast	90.7 %	16.8 %	57.4 %	63
Sunda Shelf	67.8 %	30.6 %	56.0 %	32
Slope/ Deep Sea	79.4 %	49.2 %	67.3 %	28

The marine proportions from the iteration for the $\delta^{13}C_{org}$ component range in the Gulf of Tonkin from 43.2 % to 73.6 % (average: 62.0 %, n = 27). Values range from 44.2 % to 72.6 % on the Vietnamese Shelf. On the Vietnamese Coast the marine proportion ranges from 16.8 % to 90.7 % (average: 57.4 %, n = 63). The Sunda Shelf have values from 30.6 % to 67.8 % (average: 56.0 %, n = 32). The marine proportions range in the Slope/Deep Sea area from 49.2 % to 79.4 % (average: 67.3 %, n = 28).

Table 25) Model estimates for terrestrial proportions using $\delta^{13}C_{org}$ and F_m (a Bayesian approach) for marine surface sediments combined with an iterative

Region	Max. value	Min. value	Average	*n*
Gulf of Tonkin	20.0 %	6.81 %	13.3 %	27
Vietnamese Shelf	38.5 %	10.9 %	17.8 %	26
Vietnamese Coast	39.0 %	5.75 %	16.4 %	63
Sunda Shelf	27.9 %	7.85 %	13.8 %	32
Slope/ Deep Sea	18.1 %	3.56 %	10.5 %	28

The terrestrial proportions in the Gulf of Tonkin range from 6.81 % to 20.0 % (average: 13.3 %, n = 37). The Vietnamese Shelf show values from 10.9 % to 38.5 % (average: 17.8 %, n = 27). The proportions for the terrestrial component range from 5.75 % to 39.0 % on the Vietnamese Coast (average: 16.4 %, n = 63). The Sunda Shelf show values from 7.85 % to 27.9 % (average: 13.8 %, n = 32). In the Slope/Deep Sea area values range from 3.56 % to 18.1 % (average: 10.5 %, n = 28).

Table 26) Model estimates for petrogenic carbon proportions using $\delta^{13}C_{org}$ and F_m (a Bayesian approach) for marine surface sediments combined with an iterative

Region	Max. value	Min. value	Average	*n*
Gulf of Tonkin	36.5 %	12.1 %	23.8 %	27
Vietnamese Shelf	34.9 %	3.13 %	17.1 %	26
Vietnamese Coast	55.9 %	2.81 %	25.3 %	63
Sunda Shelf	40.5 %	20.0 %	29.3 %	32
Slope/ Deep Sea	42.4 %	12.5 %	21.3 %	28

The calculated proportions of petrogenic carbon range in the Gulf of Tonkin from 12.1 % to 36.5 % (average: 23.8 %, n = 27). The Vietnamese Shelf show values from 3.13 % from 34.9 % (average: 17.1 %, n = 26). The calculated proportion of petrogenic carbon ranges on the Vietnamese Coast from 2.81 % to 25.3 % (average: 25.3 %, n = 32). In the Sunda Shelf values range from 20.0 % to 40.5 % (average: 21.3 %, n = 32). Calculated proportion ranges in the Slope/ Deep Sea are from 12.5 % to 42.4 % (average: 21.3 %, n = 28).

Table 27) Model estimates for carbon dead proportions using $\delta^{13}C_{org}$ and F_m (a Bayesian approach) for marine surface sediments combined with an iterative

Region	Max. value	Min. value	Average	*n*
Gulf of Tonkin	0.93 %	0.83 %	0.87 %	27
Vietnamese Shelf	0.93 %	0.84 %	0.87 %	26
Vietnamese Coast	1.03 %	0.79 %	0.89 %	63
Sunda Shelf	0.97 %	0.85 %	0.88 %	32
Slope/ Deep Sea	0.91 %	0.81 %	0.85 %	28

The calculated proportions of carbon dead range in the Gulf of Tonkin from 0.83 % to 0.93 % (average: 0.87 %, *n* = 27). On the Vietnamese Shelf values range from 0.84 % to 0.93 % (average: 0.87 %, *n* = 26). Calculated values range on the Vietnamese Coast from 0.79 % to 1.03 % (average: 0.89 %, n = 63). In the Sunda Shelf the calculated proportions for carbon dead range from 0.81 % to 0.91 % (average: 0.85 %, *n* = 28).

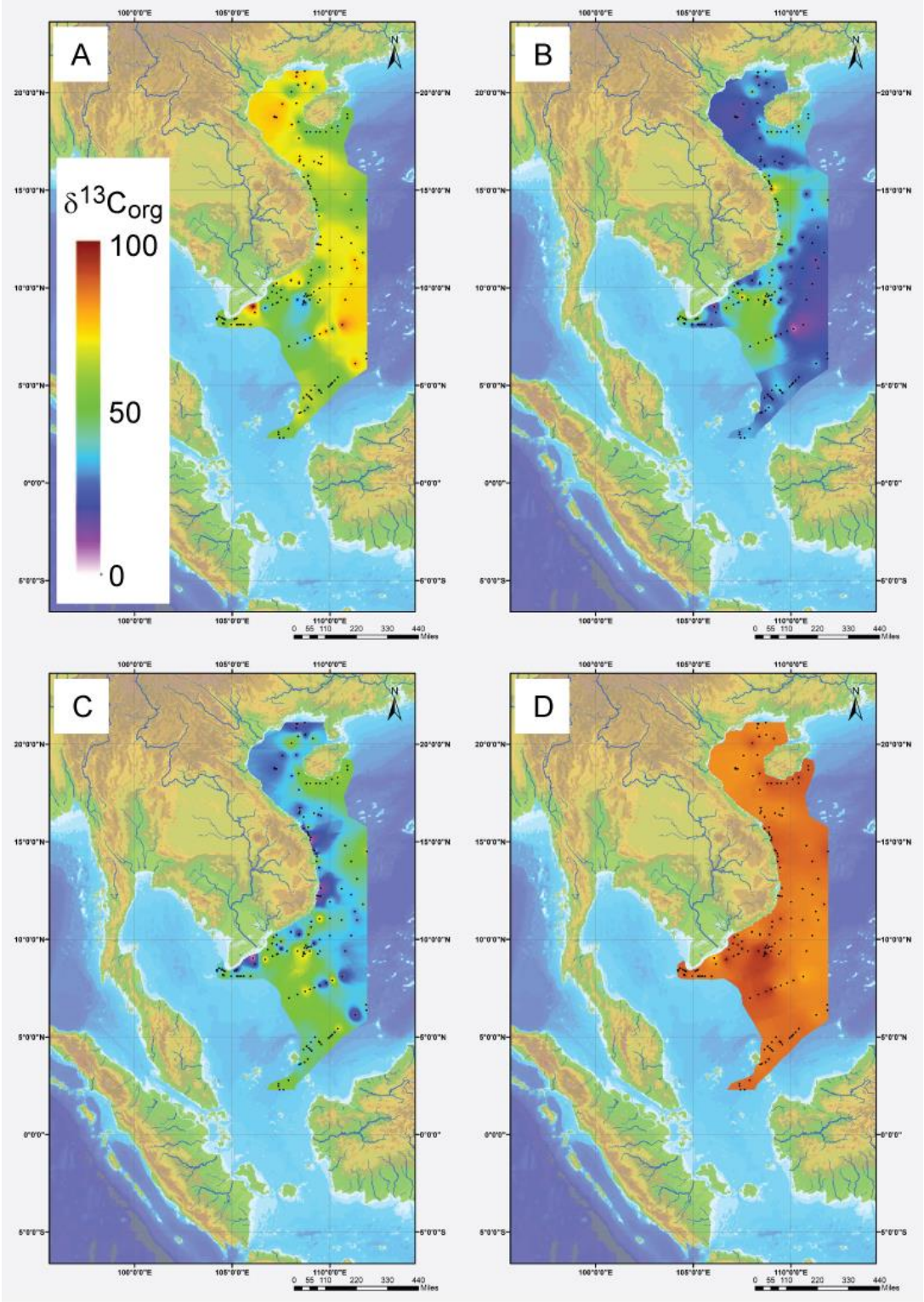

Figure 31) The model estimates using δ^{13}Cdata for marine, terrestrial, petrogenic carbon and carbon dead are normalised to 100, to reveal regional differences. A) Marine estimates are high in the Gulf of Tonkin and the Slope/Deep Sea areas, but also display some heterogeneities. B) Terrestrial estimates are high in areas where marine components are low, particularly in the Vietnamese Shelf and Vietnamese Coast. C) Estimates for petrogenic carbon are heterogeneous throughout the SCS and highly variable. D) The carbon dead fractions are essentially homogenous, suggesting no link with any geographic features

The iFRUITS (iteration) based on Δ^{14}C (n = 176) data produces values of the marine component range 16.9 % to 91.4 % (average: 60.8 %). The terrestrial component ranges

from 3.6 % to 39.2 % (average: 14.8 %), petrogenic carbon component ranges from 2.8 % to 56.2 % (average: 24.1 %), while the calculated proportion of carbon dead ranges from 0.0 % to 0.5 % (average: 0.2 %) (Fig. 33, tables 28 - 31).

Table 28) Model estimates for marine proportions using $\delta^{13}C_{org}$ and F_m (a Bayesian approach) for marine surface sediments combined with an iterative

Region	Max. value	Min. value	Average	*n*
Gulf of Tonkin	74.1 %	43.5 %	62.4 %	27
Vietnamese Shelf	73.2 %	44.4 %	64.7 %	26
Vietnamese Coast	91.4 %	16.9 %	57.8 %	63
Sunda Shelf	68.2 %	30.8 %	56.4 %	32
Slope/ Deep Sea	80.0 %	49.5 %	67.7 %	28

Calculated proportions of the $\Delta^{14}C$ iteration range in the Gulf of Tonkin from 43.5 % to 74.1 % (average: 62.4 %, n = 27). On the Vietnamese Shelf values range from 44.4 % to 73.2 % (average: 64.7 %, n = 26). Calculated proportions range on the Vietnamese Coast from 16.9 % to 91.4 % (average: 57.8 %, n = 63). The Sunda Shelf shows values from 30.8 % to 68.2 % (average: 56.4 %, n = 32). In the Slope/Deep Sea values range from 49.5 % to 80.0 % (average: 67.7 %, n = 28).

Table 29) Model estimates for terrestrial proportions using $\delta^{13}C_{org}$ and F_m (a Bayesian approach) for marine surface sediments combined with an iterative

Region	Max. value	Min. value	Average	*n*
Gulf of Tonkin	20.1 %	6.86 %	13.4 %	27
Vietnamese Shelf	38.9 %	11.0 %	17.9 %	26
Vietnamese Coast	39.2 %	5.79 %	16.6 %	63
Sunda Shelf	28.1 %	7.89 %	13.9 %	32
Slope/ Deep Sea	18.2 %	3.58 %	10.6 %	28

The calculated terrestrial proportions range in the Gulf of Tonkin from 6.86 % to 20.1 % (average: 13.4 %, n = 27). Values range on the Vietnamese Shelf from 11.0 % to 38.9 % (average: 17.9 %, n = 26) and on the Vietnamese Coast from 5.79 % to 39.2 % (average: 16.6 %, n = 16.6 %). Terrestrial proportions range in the Sunda Shelf from 7.89 % to 28.1 % (average: 13.9 %, n = 32). The Slope/Deep Sea show values from 3.58 % to 18.2 % (average: 10.6 %, n = 28).

Table 30) Model estimates for petrogenic carbon proportions using $\delta^{13}C_{org}$ and F_m (a Bayesian approach) for marine surface sediments combined with an iterative

Region	Max. value	Min. value	Average	*n*
Gulf of Tonkin	36.7 %	70.7 %	88.4 %	27
Vietnamese Shelf	35.1 %	3.16 %	17.2 %	26
Vietnamese Coast	56.2 %	2.83 %	25.4 %	63
Sunda Shelf	40.8 %	20.1 %	29.5 %	32
Slope/ Deep Sea	42.6 %	12.5 %	21.5 %	28

The percentages of the calculated petrogenic carbon proportion show values in the Gulf of Tonkin from 70.7 % to 36.7 % (average: 88.4 %, n = 27). Proportions range on the Vietnamese Shelf from 3.16 % to 35.1 % (average: 17.2 %, n = 26). The Vietnamese Coast shows values from 2.83 % to 56.2 % (average: 25.4 %, n = 63). The marine surface sediments from the Sunda Shelf shows values from 20.1 % to 40.8 % (average: 29.5 %, n = 32) for the calculated petrogenic carbon. The Slope/Deep Sea range from 12.5 % to 42.6 % (average: 21.5 %, n = 28).

Table 31) Model estimates for carbon dead proportions using $\delta^{13}C_{org}$ and F_m (a Bayesian approach) for marine surface sediments combined with an iterative

Region	Max. value	Min. value	Average	*n*
Gulf of Tonkin	0.34 %	0.10 %	0.21 %	27
Vietnamese Shelf	0.32 %	0.07 %	0.16 %	26
Vietnamese Coast	0.50 %	0.0 %	0.23 %	63
Sunda Shelf	0.39 %	0.17 %	0.26 %	32
Slope/ Deep Sea	0.36 %	0.10 %	0.18 %	28

Calculated percentages for the carbon dead component show values in the Gulf of Tonkin from 0.10 % to 0.34 % (average: 0.21 %, n = 63). Proportions for carbon dead range on the Vietnamese Shelf from 0.07 % to 0.32 % (average: 0.16 %, n =26). On the Vietnamese Coast values range from 0.0 % to 0.50 % (average: 0.23 %, n = 63). The Sunda Shelf shows values from 0.17 % to 0.39 % (average: 0.26 %, n = 32). Marine surface sediments of the Slope/Deep Sea show calculated proportions from 0.10 % to 0.36 % (average: 0.18 %, n = 28).

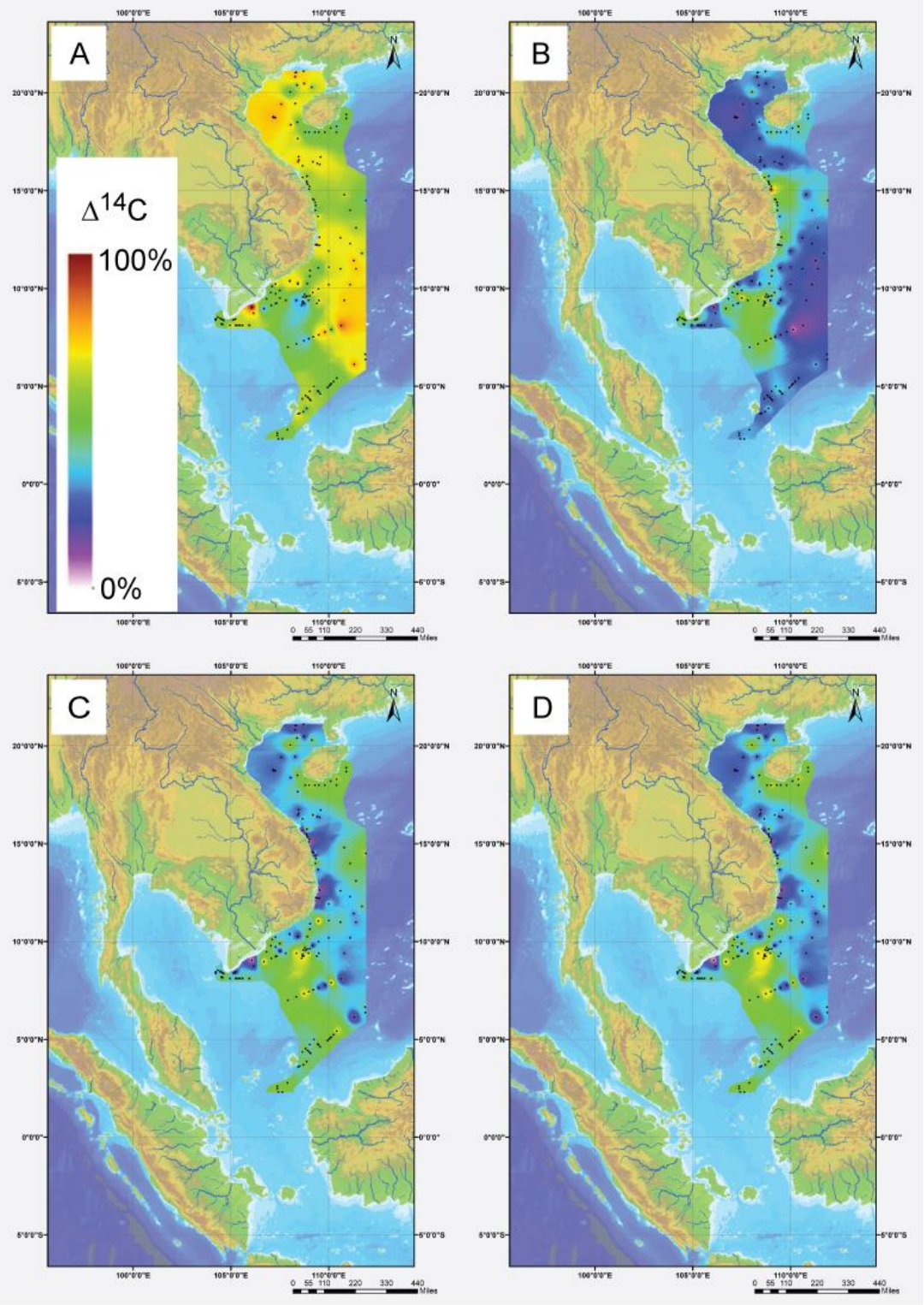

Figure 32) The model estimates using $\Delta^{14}C$ data for marine, terrestrial, petrogenic carbon and carbon dead are normalised to 100, to reveal regional differences. A) Marine estimates are high in the Gulf of Tonkin and the Slope/Deep Sea areas, but also display some heterogeneities. B) Terrestrial estimates are high in areas where marine components are low, particularly in the Vietnamese Shelf and Vietnamese Coast. C) Estimates for petrogenic carbon are heterogeneous throughout the SCS and highly variable. D) Distribution of carbon dead reveals heterogeneity, analogous to petrogenic carbon, contrary to estimates from $\delta^{13}C$ in Fig. 31

5.4 Discussion

5.4.1 Advantages and Limitations of computational modelling FRUITS (Bayesian) iterative refinement model (iFRUITS) performance

Before starting to use computational model outputs to interpret complex geological relationships, it is necessary to evaluate strengths and weaknesses of the model and its output data. The origin of strength and weakness can be either technical (e.g. input data related) or geological (e.g. underestimation of complexity). During model development the following strengths and limitations were identified, some of which might only be relevant to this study:

Limitations of the model:

I. Difficulty of defining the appropriate end-member compositions, to represent a whole system is always hard, but it is noticed that the difference between a marine and terrestrial end-member always must be ~11 ‰, to achieve an intercept through zero. This can in part be related to underestimation of the depositional complexity, e.g. more end-members need to be introduced.

II. The approach to equally decrease proportions of each component to mass balance for the newly introduced component might not be accurate and cause artificial bias. This approach is chosen, because this allows to preserve the ratio between sources from the FRUITS model output. This is the mathematically most neutral approach to refining existing and calculating additional sources, but might not be the most appropriate. In this study however, it is assumed that the unaccounted source "petrogenic carbon" is compositionally very similar to the fraction "terrestrial". Therefore, it might be more plausible that only the terrestrial fraction should be reduced.

III. The iterative approach of the model respects the individual proxies independently of each other. This can result in conflicting fraction size estimates, when comparing the estimates from the different proxies. The potential discrepancy heavily depends on point I). If the end-members are chosen incorrectly, the discrepancy should increase.

IV. Bayesian inversion modelling, like any other modelling approach, relies on the quality and quantity of data used. Secondly, the ability to solve for multiple unknown values is governed by the availability of tracer tools (e.g. stable isotope data or elemental ratios) (see e.g. Phillips and Gregg, [369]). In many cases,

model behaviour can be unexpected, if the number of sources exceeds the number of tracer tools, plus one. In this study, two tracers are used, $\delta^{13}C_{org}$ and $\Delta^{14}C$, theoretically robust model estimates can only be expected when three or less sources are used in the model

V. The generalisation of end-members might be an oversimplification, which will negatively influence the model performance. However, with the given data density and diversity of data, some simplifications must be performed. It might however not be appropriate, to assume that homogenous end-members are representative, if the investigated study area spans several thousands of miles.

VI. The model in its current iteration does not account for carbon loss/degradation/remineralisation during transport, which is unlikely to reflect conditions in nature. However, no robust framework is available for riverine transport mechanisms in the study area, that quantifies the rates of carbon degradation and isotopic signature modification, which can be implemented. Generally, it is expected that >50 % up to 80 % [297, 319] of the original terrestrial OM can be re-mineralised during transport. This process can be counteracted by continuous addition of OM from near river sources and requires a study in itself, to assess and evaluate accurately potential rates of change.

VII. The use of $\Delta^{14}C$ data as a tracer depends on the requirement that the different sources are characterised by distinct $\Delta^{14}C$ values, as $\Delta^{14}C$ is insensitive to modification transport processes (see section 5.4.3). It is plausible and commonly observed, that terrestrial OM is typically older, simply because transport from land to oceans requires time while *in-situ* produced marine OM has short transfer times relative to terrestrial OM.

Advantages of the model:

I. Bayesian statistics allow all proxies to be included and contributing to the results, including those that are of qualitative nature. This essentially allows the geologists observations to be included in mathematical operations.

II. The model allows infinitely additions of end-member to refine the outcome and final source identification, as long as these can be distinguished by tracer tools.

III. The model is able to perform calculations including uncertainties, which helps to introduce flexibility as well accurately value aspects such as analytical uncertainty and precision.

IV. The model can identify the proportions of different sources (e.g. OM pools) relative to each other, based on bulk measurements and assumed source regions compositions (Fig. 31 and 32), which permits more detailed insight into the preservation and fate of OM during transport prior to burial.

V. Prior knowledge concerning the system of interest can be included, but is not strictly required (in the absence of previous knowledge, a Gaussian (beta) distribution will be used to identify the ratios of source compounds).

5.4.2 Testing the applicability of the model by use of qualitative expectations

Considering the numerous discussed limitations, the application of the model to unknown data can only be evaluated and interpreted, if a pre-existing framework is present to validate or compare model *vs.* nature. In case of the study presented herein, geographical features (on land and off shore) and fundamental observations from previous studies to compare the model output and logical expectations are used.

First, previous studies using $\delta^{13}C_{org}$ and C_{org}/N_{total} data have demonstrated that in the marine environment, the proportions of marine components are large, typically dominant over any other modelled component [282], where marine primary production is high. In the SCS, the Gulf of Tonkin and the Vietnamese Shelf are characterised by higher Chlor-α abundances, which are evidence for higher bio-production. These areas also show higher model estimates for marine components. Secondly, upwelling areas, which are nutrient rich and favour higher bio-production, are expected to yield higher marine proportions. Liu et al. [55] identified two upwelling areas in the SCS that are relevant to this study. The first is located at the NE edge of the Sunda Shelf and Slope/Deep Sea and the second off SE-Vietnam at the southern end of the narrow Vietnamese Shelf. Both of these areas also yield higher marine model estimates (Fig. 31 and 32).

Areas that could return lower estimates for marine components can be those that have hydrodynamic settings, which inhibit TOC accumulation and sediment settling. In the SCS, the current dynamics are variable, but some re-occurring features are well documented. For example, in the Sunda Shelf the presence of a gyre could either prohibit the accumulation of OM during periods of high bio-production or enhance accumulation. Regardless of the actual effect, it would be expected that some deviation from the regional average is plausible. This receives support from the lower than average model estimates for a part of the Sunda Shelf (Fig. 31 and 32).

The bedrock geology on-shore can be a source of carbon that carries an isotopically distinct composition, if e.g. carbonates are compared with igneous rocks [225]. From the lithological map provided by Hartmann and Moosdorf, [44], in central Vietnam a sharp transition in exposed lithology is documented (carbonates *vs.* igneous rocks) (Fig. 3 Chapter 1 - General Introduction). Rivers sourcing carbon and other matter from these areas are expected to potentially obtain distinct isotopic compositions ($\delta^{13}C_{org}$ and $\Delta^{14}C$), and therefore, estimates for terrestrial and petrogenic carbon can be variable in these regions (Fig. 31 and 32). This is consistent with the model outputs (Fig. 28).

A binary $\delta^{13}C_{org}$ mixing model yielded outputs (Fig. 29 and 30a) that are consistent with the aforementioned observations, suggesting that the model outputs from FRUITS and iterative refinement are robust and that interpretations drawn can be geologically meaningful. Two sets of end-members were employed, testing the relevance of local source compositions, by using internal (local) and external (distal) source composition estimates (Fig. 29 and 30a). The estimate of marine proportions directly depends on the choice of end-members as dictated by the simplicity of the model. Subsequently further evidence is needed to validate and test the accuracy of the binary single proxy mixing model. This can the achieved by more diverse proxy data, and choice of model with greater variance (e.g. equations based on the Bayes-Theorem).

5.4.3 A quantitative model for organic matter composition transition during transport from the Shelf to the Deep Sea

The determination of OM composition in the SCS, a setting which is subject to constant influx and loss of mass of variable composition, is challenging and requires robust proxies to obtain sensible results. The most traditional proxies are either bulk carbon isotope ratios (e.g. $\delta^{13}C_{org}$) or the elemental ratio of C_{org} to N_{total}, either used individually or in conjunction.

For the quantification of the composition of bulk OM in terms of marine and terrestrial components, two different models were employed. As with any numerical model, setting the boundary parameters presents a key challenge, as the choice of main reservoirs will strongly affect the model outcome. To approach this challenge, it is necessary to test if modelled variability between sub-regions of the SCS is persistent throughout i) boundary parameters selected based on average values from the literature and ii) boundary parameters selected from data obtained in this study (i.e., using values of most extreme riverine and marine sediment samples). An initial, conservative model is a two-end-

member mixing model using the $\delta^{13}C_{org}$ composition of bulk OM [182]. The $\delta^{13}C_{org}$ end-members have been selected from the literature (of a comparable region [363]) and are viewed as a limiting factor in the model performance. This emphasises the need for more region-specific calibration data, making inter-comparison and refined modelling challenging on large scales, such as the westernmost part of the SCS.

The discussion of the results of this single component two-end-member mixing model is done first. The available literature data resulted in the selection of $\delta^{13}C_{org}$ of -24.9 ‰ for terrestrial, and -19.2 ‰ for the marine end-members. The literature data have been filtered with the condition that these are above the thermocline (at ~80 m - 120 m depths [370]), and then averaged. The estimates of the marine component from the $\delta^{13}C_{org}$ mixing model are presented in figure 29. In the Gulf of Tonkin, the model reveals some heterogeneity in the relative marine distribution, with a tendency towards higher proportions of marine OM compared to the western part of the Gulf of Tonkin. Additionally, a sudden change towards a reduced marine fraction at the boundary of the Gulf of Tonkin and the Vietnamese Shelf is observed (Fig. 29). Samples from the most eastern and deepest part of the study area, associated with the Slope/Deep Sea area, have a higher proportion of marine component, relative to all shelf areas studied (Fig. 29). The lowest estimates for marine component are observed in proximity to the Mekong River delta, identifying significant loads of continental sediment discharge and POC from the mainland into coastal areas [16]. However, some samples from the Mekong River delta have $\delta^{13}C_{org}$ values which fall well outside the defined range for marine and terrestrial samples, i.e. their $\delta^{13}C_{org}$ composition is lighter/more negative than the terrestrial reservoir end-member. This observation requires either a re-evaluation of the suspect reservoir compositions outside of the so far documented range of data, or a two-component mixing model, which is better suited for higher complexity (e.g. influx and loss of mass of variable composition) in front of major rivers. For this purpose, the combination of $\delta^{13}C_{org}$ and the elemental C_{org}/N_{total} ratio is tested, which has a well-defined range of marine and terrestrial values, which satisfy the range observed in the estuary samples.

A Bayesian mixing model is used in a second step to optimise the results of the two-component model [365] with the results illustrated in figure 30b. The model returns overall higher estimates of marine components, with the majority of the estimates above 80 % marine signature, when using average values from the literature. The Gulf of Tonkin retains high values for marine proportions, consistent with the $\delta^{13}C_{org}$ model, and

a sharp change at the boundary between Gulf of Tonkin and Vietnamese Shelf is observed as in the previous $\delta^{13}C_{org}$ binary mixing model (Fig. 29). However, in proximity to the Mekong River delta the majority of samples now implies a marine fraction of >80 %, and even some of the Mekong River and estuary samples have high estimates for a marine signature (spheres in the Mekong River delta, Fig. 30b). This would imply that tidal forces exert strong control over the geochemical C_{org}/N_{total} signature of the Mekong River delta, but do not significantly modify the carbon isotopic composition. This Bayesian model therefore implies that the geochemical proxies $\delta^{13}C_{org}$ and C_{org}/N_{total} suggest much stronger homogenisation in the marine environment, even in the tidal impacted estuary regions, which is unnoticed in the single end-member ($\delta^{13}C_{org}$) model. When using the internally selected values as boundaries in the mixing model, the estimate of marine components is lower (based on a combined C_{org}/N_{total} and $\delta^{13}C_{org}$ model), but regional variations are persistent (Fig. 30b) when compared to e.g. the $\delta^{13}C_{org}$ end-member mixing model.

It can be concluded that any model attempting to estimate the marine and terrestrial proportions of unknown samples is highly sensitive to the choice of reservoir end-members and the number of tracers used. In this study, the $\delta^{13}C_{org}$ model offers better spatial resolution due to higher data density, and regional differences become more visible (Fig. 29). However, this hinges on the assumption that a single end-member is representative to the investigated sample set. Comparison of geological bedrock features suggest that some regional variability in the terrestrial $\delta^{13}C_{org}$ composition must be assumed, particularly where bedrock lithology change from e.g. carbonate to igneous rocks (as seen in northern/central Vietnam, Fig. 29). Other factors that need consideration are the local vegetation and farming activity, as plants can cause shifts in the $\delta^{13}C_{org}$ isotopic composition (i.e. C_3 *vs.* C_4 plants). This model dependence on regional features seems to diminish upon the introduction of additional tracers (here C_{org}/N_{total}), which are seemingly insensitive to processes affecting the $\delta^{13}C_{org}$ isotopic composition. This emphasises the use of large scale, high resolution and high tracer tool diversity data sets, as performed in the here presented study.

5.4.4 Incorporation of radiocarbon values in simulation-based models and iterative linearisation of model output data

The mixed use of isotopic and elemental data can result in un-expected model behaviour, such as over or underestimation of source contributions. Therefore, a third model

calculation is performed, where the proxy data is comprised of carbon isotope data only. The previously used C_{org}/N_{total} ratio (section 5.3.2) potentially creates a bias towards N specific processes and sources, although C_{org}/N_{total} has experienced widespread use in the literature. However, by working with carbon specific values a greater consistency could be achieved and ultimately compared with the output of the mixed carbon and nitrogen (section 5.3.2) and carbon only (this section and 5.3.1 and 5.3.3) proxies in a final step.

The spatial distribution of marine OC proportions, based on the iterative data, suggests the presence of zones that are enriched or depleted within the SCS (see Fig. 31 and 32). The Gulf of Tonkin and Slope/Deep Sea samples are seemingly most enriched in marine component (Fig. 31 and 32), when using the iterative refinement data and FRUTIS model data. In the coastal part of central Vietnam, the FRUITS model shows weak evidence for lower proportions of marine component (Fig. 31 and 32). When evaluating the iterative refinement maps for $\delta^{13}C_{org}$ and $\Delta^{14}C$, the central Vietnamese Shelf area consistently implies lower proportions of marine component. In proximity of the Mekong River delta, several samples yield low proportions of marine OC components. This observation is consistent for maps, which display the FRUITS multi component model results and the iterative refined $\delta^{13}C_{org}$ and $\Delta^{14}C$ model results (Fig. 31 and 32).

Petrogenic carbon distribution is variable, but zones of enrichment are observed in proximity to the island of Hainan and to the delta of the Mekong River and some parts of the Sunda Shelf (Fig. 31 and 32). In the Hainan area, increased proportion of petrogenic carbon is consistent with decrease in marine proportions, while no significant variation in terrestrial component is observed (Fig. 31 and 32).

The distribution of carbon dead material is highly variable (Fig. 31 and 32), and notable enrichment is observed close to the Hainan island such as the area between the Mekong River delta and the Sunda Shelf (Fig. 31 and 32). It is important to note that the estimate for the fraction that is carbon dead is highly dependent on the model parameter choice. Iterative calculations result in significantly lower estimates of carbon dead, compared to FRUITS model estimates (average FRUITS ($\delta^{13}C_{org}$ and $\Delta^{14}C$) = 15.8 %, average iterative ($\delta^{13}C_{org}$) = 0.9 %, average iterative ($\Delta^{14}C$) = 0.2 % (Fig. 31 and 32)). However, relative differences between regions are seemingly unaffected, preserving information of regional enrichment/depletion within the SCS.

In the following discussion, the outcomes of the five numerical models (as described above) are compared. This will be used to evaluate the usefulness of the geochemical

proxies C_{org}/N_{total}, $\delta^{13}C_{org}$, $\Delta^{14}C$ and determine if C_{org}/N_{total} is a reliable tracer in carbon models or if indeed nitrogen specific processes control the C_{org}/N_{total} ratio as Müller, [164] suggested. For this purpose, the model outputs relative to the $\delta^{13}C_{org}$ model and the $\delta^{13}C_{org}$ + $\Delta^{14}C$ FRUITS are compared.

In figure 33a, the model outputs are normalised against the $\delta^{13}C_{org}$ model (see section 5.2.4). The figure shows some linearity between the $\delta^{13}C_{org}$ model and the FRUITS, $\delta^{13}C_{org}$ iFRUITS, $\Delta^{14}C$ iFRUITS and the $\delta^{13}C_{org}$ (literature based) models. The literature based $\delta^{13}C_{org}$ model shows the greatest amount of deviation, while behaving linear. The FRUITS model (C_{org}/N_{total} + $\delta^{13}C_{org}$) is characterised by a high degree of scatter, which implies that the assumption of Müller [164], that C_{org}/N_{total} can be an unsuitable tracer for carbon processes is accurate for the study area. The two iFRUITS model outputs show the greatest degree of resemblance with the $\delta^{13}C_{org}$ model (own parameters). However, while most of the data appear to behave linearly, a moderate amount of scatter is observed. This could be due to insufficient model complexity, such as lack in spatial resolution or number of geochemical proxies. The FRUITS model based on refined source compositions does not resolve the discrepancies with the $\delta^{13}C_{org}$ model; instead, it implies the development of two distinct groups in the dataset.

Figure 33b shows the model outputs normalised against the most complex and evolved model data, which is the FRUITS model with redefined end-members based on the iFRUITS output. The C_{org}/N_{total} + $\delta^{13}C_{org}$ model shows a high degree of scatter, persistent with observations in figure 33b, suggesting that it is the most inaccurate. The $\delta^{13}C_{org}$ binary models show both some amount of linearity. Notable differences are that the $\delta^{13}C_{org}$ model based on the here presented dataset has a positive offset and the $\delta^{13}C_{org}$ binary model, based on literature data, has a negative offset. However, the $\delta^{13}C_{org}$ model based on literature data show similarity with the normalisation data. Yet, the amount of scatter is higher compared to the two iFRUITS model outcomes. The best fits are based on the iFRUITS models, with the highest linearity and less amount of scatter. Seemingly, two parallel trends develop in the iFRUITS data, reinforcing the need for refined model complexity and/or proxy data.

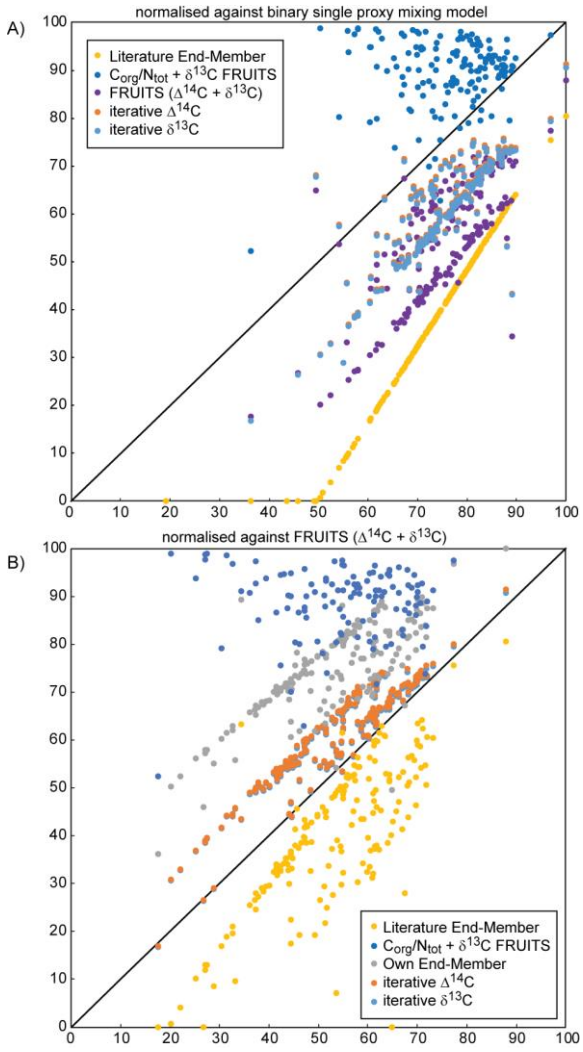

Figure 33) The results of the discussed numerical models are normalised against the output of the most simplistic model (A), and against the model with the highest degree of complexity and refinement (B). The black line represents the ideal fit between modelled and observed data. Residual scatter might originate from insufficient model complexity (e.g. number of sources or geochemical proxies). The iterative solutions using $\Delta^{14}C$ and $\delta^{13}C$ are almost identical on the selected scales. Model output based on C_{org}/N_{total} results in the greatest amount of scatter. The literature end-member is taken from an adjacent region (Western China Sea)

Both figures illustrate the complexity of the study area and the difficulties to recapitulate sources/reservoirs making it challenging to recommend ideal model parameters and model choices. To resolve complexity issues in numerical modelling, a multiple end-member model is considered the appropriate way forward, ideally using Bayesian statistics. Ultimately, it appears that localised variability in source reservoir compositions can be a plausible explanation for scatter in large-scale datasets.

5.5 Conclusion

1) The simplicity of a binary single proxy mixing model ($\delta^{13}C_{org}$) results in an immediate dependence on the choice of model boundary parameters, which limits the application to smaller scale regions (essentially single source and single

deposition environments). It is crucial to use study area specific parameters as demonstrated in the comparison between literature-based end-member mixing models and local-based end-members.

2) Presumably, a model incorporating two geochemical proxies and using Bayesian statistics should yield more accurate model output relative to the binary single proxy model. Yet, when using C_{org}/N_{total} + $\delta^{13}C_{org}$ parameters in the FRUITS model, significant amounts of scatter are observed. In comparison, models based on $\delta^{13}C_{org}$ and/or $\Delta^{14}C$ yield more linear correlations. Therefore, here it must be assumed that nitrogen processes control the C_{org}/N_{total} parameter, which is in conflict with the aim to investigate carbon processes.
3) The comparison of different model output leads to the conclusion that two distinct groups are present in the study area, which would mandate at least two sets of end-members to achieve internally consistent model outputs. The parameters $\delta^{13}C_{org}$ and $\Delta^{14}C$ appear to be the most reliable in the computational modelling of carbon processes in the study area.
4) Bulk measurements make it difficult to predict the source composition of the OM, the number of relevant sources and the proportions of the sources contributing to the bulk sediment. Inverse mixing models offer a solution to de-convolute such bulk data, and allow estimating a larger number of source reservoirs and their relative contributions. Here, at least four source reservoirs are successfully resolved, which contributed to the bulk sediment, suggesting that geochemical proxies such as $\delta^{13}C_{org}$ and $\Delta^{14}C$ are of high value and reliability. Variations in the complexity of the model parameters returned qualitative consistent results, suggesting a high robustness of the data set and model output. The FRUITS model output revealed more detail in the study area relative to the binary $\delta^{13}C_{org}$ model. The details revealed by the model are furthermore consistent with e.g. changes in bedrock lithologies and proximity to river deltas. Through this cross validation, it is to conclude that the following source region parameters are representative for the westernmost SCS. These are for the study area i) marine end-member $\delta^{13}C_{org}$ = -19.2 ‰, $\Delta^{14}C$ = 33.3‰; ii) terrestrial end-member $\delta^{13}C_{org}$ = -30 ‰, $\Delta^{14}C$ = -155.4 ‰; iii) petrogenic carbon $\delta^{13}C$ = -25.4 ‰, $\Delta^{14}C$ = -880.2 ‰; iv) carbon dead $\delta^{13}C_{org}$ = -25.0 ‰, $\Delta^{14}C$ = -1000 ‰. These values are recommended to be used in carbon models for the SCS.

6 Distribution patterns and transport mechanisms of synthetic halocarbons in the SCS – tracing man-made pollution

6.1 Introduction

The pollution of the oceans by anthropogenic activity is rapidly expanding topic of research activity. Documentation of the discharge and secondary mobilisation of e.g. herbicides applied on land is essentially non-existent in the SCS, but studies have begun to document the presence of synthetic compounds in the marine environment (e.g. Zhong et al. and Zhong et al. [4, 371]). Some other persistent organic pollutants (POPs), e.g. plasticisers and/or flame retardants, are known to be mildly/non-toxic in the terrestrial environment, but highly toxic in aquatic systems. Subsequently they are considered contaminants of potential concern (COPC). Therefore, it is immediate concern to establish occurrence and distribution patterns of POPs in the marine environment, particularly in those systems in proximity to centres of anthropogenic activity, such as the SCS.

One emerging group of compounds identified in westernmost marine SCS sediments are organophosphate esters [c.f. tris (2-chloroethyl) phosphate, tris (2-chloroisopropyl) phosphate] (TCPP) together with compounds called thiocarbamates (c.f., triallate). These compounds derive from anthropogenic origins and testify pollution of open marine surface environments. This study gives a first impression about the dimension of organic pollutants in the environment. Furthermore, they may hint to transport pathways and the coupling or decoupling from natural carbon pathways.

Both TCPP and triallate are unambiguously products of large-scale manufacturing production that function as industrial flame-retardants and herbicides, respectively. Due to their widespread distribution and frequent farm applications, such compounds are diagnostic tracers of OM transport routes and transport times from source-to-sink. Indeed, both TCPP and triallate were only produced and dispersed since the 1960s, such that their occurrence in marine sediments must be restricted to the past 60 years, in stratigraphically undisturbed sediments.

Further, understanding how synthetic anthropogenic compounds react (e.g. POPs) in aquatic environments is crucial to direct conservation efforts in marine and terrestrial settings alike. Since many synthetic and halogenated compounds used on land have highly toxic effects in the environment, including the marine habitat, their identification

and distribution require immediate attention. As such, the main POPs objective of this work is to establish i) distribution patterns of selected POPs, and ii) to correlate relevant POPs distributions with findings (e.g. role of SA and deep sea setting as accumulation factors) reported in Chapters 3 and 4. This single coherent database allows to immediately assess if the same physical parameters govern the fixation, distribution, and accumulation of triallate and TCPP.

6.2 Background information of organosulfates and organophosphates

6.2.1 Triallate - a Thiocarbamate organosulfur compound

Triallate is an organosulfur compound (thiocarbamate) first produced and dispensed in the 1960s [372] for application in weed control. Associated triallate thiocarbamates occur with two isomeric forms: *O*-thiocarbamates, $ROC(=S)NR_2$, and *S*-thiocarbamates, $RSC(=O)NR_2$, although triallate is an *S*-isomer also known as [S-(2,3,3-trichloroallyl)diisopropylthiocarbamate].

The primary path through, which triallate controls weed growth is via selective inhibition of lipid (fatty acid) biosynthesis [373]. The commercial herbicide, which includes triallate, is Fargo®. Fargo® is used to control wild oats in various crop plants (e.g. peas, corn, wheat, flax and beets) [374, 375].

Importantly, triallate is reported highly toxic to fish and other aquatic organisms [376, 377], including crustacean [377] and algae [376]. The Monsanto Company [376] reported that triallate concentrations measured in bluegill sunfish and rainbow trout over a 7-week trial period experienced significant bioaccumulation. Stopping the application of triallate resulted in a rapid removal of measurable traces triallate in both kinds of fish [376]. Triallate is documented to be a neurotoxin and carcinogenic [378]. The same study postulated, that triallate concentrations in aquatic systems are unlikely to reach the level of toxic conditions, but these have only concerned systems in close proximity to triallate sources (e.g. farmland), and do not consider re-mobilisation within the river-ocean environment.

6.2.2 Organophosphate Esters – an introduction

Organophosphate esters (OPEs) are exclusively produced by industrial processes and thus do not occur naturally. Structurally, OPEs are organic compounds with a phosphorous atom in their centre [4]. The OPEs are widely used as flame-retardants (c.f. TCPP) and as plasticisers in a variety of products, such as electronic equipment, furniture, varnishes,

polyurethane foams, and many more [4, 379, 380]. OPEs are differentiated into the following types:

i) chlorinated, such as tris (2-chloroethyl) phosphate,
tris (2-chloroisopropyl) phosphate (TCPP), and
tris (1,3-dichloropropyl) phosphate, and

ii) non-halogenated, such as tri-n-butyl phosphate,
tris(2-butoxyethyl) phosphate, triphenyl phosphate,
2-ethylhexyl diphenyl phosphate, and tricresyl phosphate [381].

Increasing industrialisation since about 1950 has resulted in high production of OPEs, globally. OPEs are processed by physical mixing and, as far as known, are not chemically bound to matrix or surrounding product materials, making them susceptible to release by leaching and volatilisation into the surrounding environment [382]. Subsequently, a multitude of sources of OPEs to the natural environment exists and several hypotheses have been formulated, albeit quantitative studies are sparse (e.g. Zhang et al. Salamova et al. and Sühring et al. [159, 383, 384]). Their widespread application has resulted in extensive diffusion and ubiquitous distribution in the environment, both terrestrial and marine.

Urban areas, as centres of human activities and infrastructure, have elevated concentrations of OPEs. Available studies on OPE distribution suggest that they occur in detectable concentrations throughout the biosphere, hydrosphere and atmosphere for example in air [381, 385–388] wastewater and sludge [389, 390], surface water, fresh and marine water face [160, 161, 390–395], groundwater [393], terrestrial and marine sediments [4, 371, 379, 380, 396–399], soil [400], and even the human body [401–403]. OPEs were also detected in precipitation, an indicator of their atmospheric deposition processes [160, 161].

The study of Zhang et al. [159] predicted that OEPs have a half-live in the atmosphere of <2 days. This conclusion is challenged by recent studies that reported OPEs in atmospheric particles in remote European and Canadian Arctic sites [383, 384]. The presence of OPEs at these remote locations indicate prolonged transport times and subsequently much longer half-life times than 2 days. This notion is strongly supported by marine studies that report OPEs in the open ocean (airborne particles), including the northern Pacific and Indian Ocean, the Arctic [404], the tropical and subtropical Atlantic, Pacific and Indian Ocean [405], and the Mediterranean, Black and North Seas [406, 407].

All these observations demonstrate that OPEs are capable of long-atmospheric transport distances and times [399]. However, little research has focused on the fate of OPEs in remote offshore and deep marine settings. Similar to that of traditional POPs (**Pesticides**: aldrin, chlordane, DDT, dieldrin, endrin, heptachlor, hexachlorobenzene, mirex, toxaphene; **Industrial chemicals**: hexachlorobenzene, polychlorinated biphenyls (PCBs); and **By-products**: hexachlorobenzene; polychlorinated dibenzo-p-dioxins and polychlorinated dibenzofurans (PCDD/PCDF), and PCBs, (http://www.pops.int)). The net flux of OPEs in the offshore marine environment typically follows the air−surface water-deeper-water route followed by burial in benthic sediments, where the deep ocean basins seem to be the long-term sedimentary repository of these artificial chemicals [399, 408, 409]. Furthermore, some studies have shown that chlorinated OPEs are particularly persistent in the environment [160, 410], implying a filtering/selected preservation mechanism of OEPs with distance to source.

OPEs are mostly lipophilic and difficult to dissolve in water [411] and tend to bind to suspended particulate matters and accumulate in river sediments. Sediment therefore acts as a relevant sink of OPEs in the environment [380]. This makes the study of OEPs in SCS sediments interesting, in particularly when combined with other geochemical proxies (C_{org}/N_{total}, $\delta^{13}C_{org}$, $\Delta^{14}C$ and FAME), summarised in Chapters 3 and 4, and published information on clay minerals. Since OPEs are associated with sinking particles and lateral advective processes, their presence in the offshore sediments of the SCS confirm that carbon transfer from land to the study sites must occur rather quickly, on time scales of ~60 yr. or less (the time of widespread production and introduction of OPEs). The settling of OPEs could theoretically be driven by the "biological pump", describing the settling flux of particle organic carbon (POC) associated with primary production in the photic zone [408, 412], making OPEs directly comparable with observations from carbon cycling studies (e.g. Chapter 3 and 4). From previous studies it is known that halogenated OPEs have greater water stability relative to non-halogenated OPEs, which potentially results in different transport distances [413]. Zhong et al. [4] observed the accumulation of OPEs in muddy areas of the Bohai and Yellow Sea, which would suggest a correlation with higher SA values in the current dataset. To the authors current knowledge there is no study which correlates the distribution of natural OM with the here observed POPs. It should be noted that there might be many other POPs or chemical substances in the sediments, which have not been traced.

6.3 Methods

For molecular analyses, freeze-dried bulk sediment (~1g - 10 g) was extracted before open-column chromatographic separation of total lipid extract (TLE) into three fractions (non-polar, mid-polar, and polar). The polar fraction contained TCPPs and triallate. All fractions were measured by Gas Chromatograph-Mass Spectrometry (GC-MS), using a Thermo Scientific Trace 1300 with an ISQ TL mass spectrometer. A detailed description is provided in Chapter 2- Material and Methods.

For the identification of triallate (Fig. 34) the major ion *m/z 86* together with a secondary (qualifier) ion *m/z 277* that is abundant in TCPP1–2 isomers [414] is used.

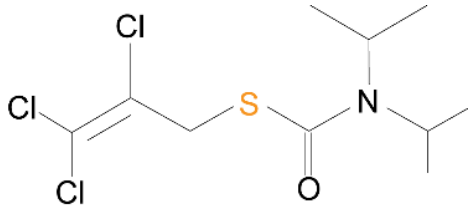

Figure 34) Illustration of the chemical structure of triallate. Abbreviations, S = Sulphur, N = Nitrogen. Cl = Chlorine, O = Oxygen. Parallel lines indicate double bonds. Carbon not illustrated but present at the connection between lines

The *m/z 277* is used to calculate composition ratios of TCPP1/TCPP2 (Fig 35); this approach removes complications with attempting quantification in absence of calibrated and appropriate standards since response factors of both compounds are almost identical and therefore, challenging to be neglected [415].

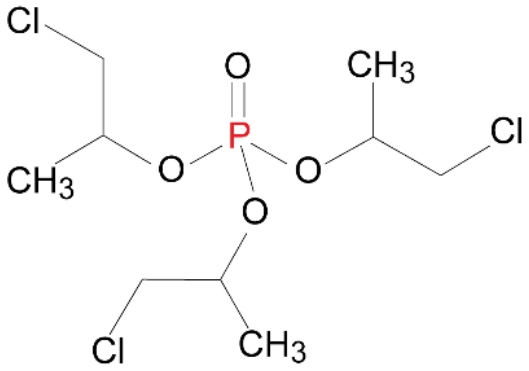

Figure 35) Illustration of the chemical structure of tris (2-chloroethyl) phosphate (TCPP1)

In the absence of true standards, the sample with the highest peak area of triallate is used to semi-quantify and normalise the remaining samples. The normalised data is then multiplied by a factor of 10, for better readability. In this study we used sample SO-187-3-98-1 from west of the Mekong River delta, offshore Cà Mau peninsula, as the maximum reference sample against which all samples across the SCS were normalised.

6.4 Results

In the following, semi-quantification of triallate (section 6.4.1), TCPP1 and TCPP2, together with ratios of TCPP1/TCPP2 (Section 6.4.2) are reported. The results are illustrated in figure 36 - 39 and table 23 - 39.

6.4.1 Triallate

In total, 212 SCS surface sediment samples were analysed for triallate. As such, samples without detectable *m/z 86* have a relative abundance of zero. The average relative abundance of triallate across all the samples equal 0.88 (Fig. 36, table 32 and 33).

Table 32) Samples normalised (SO-187-3-98-1) triallate distribution in marine surface sediments

Region	Max. value	Min. value	Average	*n*
Gulf of Tonkin	0.11	0.00	0.03	32
Vietnamese Shelf	5.46	0.00	1.30	31
Vietnamese Coast	10.0	0.00	0.92	74
Sunda Shelf	8.74	0.00	1.21	52
Slope/ Deep Sea	3.05	0.00	0.62	23

In the Gulf of Tonkin, triallate abundances are overall low to absent (Fig. 36), with a range of 0.00 – 0.11 (average: 0.03, n = 32). Normalised *m/z 86* values increase southwards along the Vietnamese Shelf to a maximum of 5.46 (average: 1.30, n = 31). Peak value of ten is observed on the Vietnamese Coast (average: 0.92, n = 74, red circle on Fig. 3). On the Sunda Shelf values range from 0.00 to 8.74 (average: 1.21, n = 52). In Slope/Deep Sea environments, relative abundance values range from 0.00 to 3.05 (average: 0.62, n = 23). Concentrations in proximity to rivers (Mekong River, Red River, Chao Phraya) are overall lower than in offshore surface sediments (Fig. 36).

Table 33) Samples normalised (SO-187-3-98-1) triallate distribution of estuary samples

Region	Max. value	Min. value	Average	*n*
Estuaries from the Gulf of Tonkin area	2.25	0.00	0.33	7
Estuaries from the Vietnamese Shelf area	3.57	0.00	1.19	14
Estuaries from the Vietnamese Coast area	0.84	0.00	0.24	12
Estuaries from the Sunda Shelf area (Indonesia and Malaysia)	2.36	0.00	0.76	15
Estuaries from Thailand	0.60	0.14	0.35	10

In addition to marine surface-sediment, 58 estuarine samples were analysed. Triallate shows the same overall range as for marine sediments (0.00 to 3.57, average: 0.63). Estuarine sediment from the Gulf of Tonkin region ranges from 0.00 to 2.25 (average: 0.33, *n* = 7). Riverine samples connected to the Vietnamese Shelf have values of 0.00 to 3.57 (average: 1.19, *n* = 14). Samples connected to the Vietnamese Coast range from 0.00 to 0.84 (average: 0.24, *n* = 12). Samples from Indonesia, Sumatra and Malaysia, which are connected via the Sunda Shelf to the main study area of this study, show values of 0.00 to 2.36 (average: 0.76, *n* = 15). Riverine samples of Thailand have values from 0.14 to 0.60 (average: 0.35, *n* = 10).

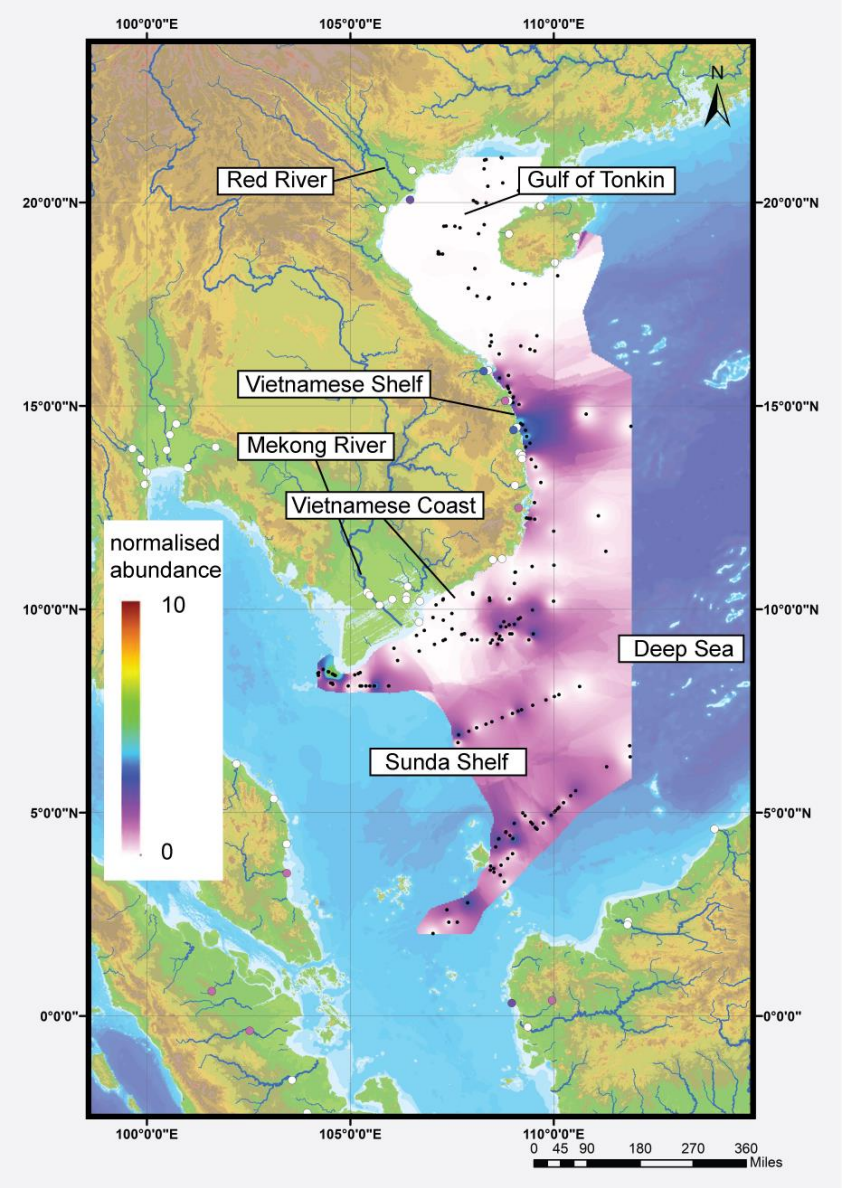

Figure 36) Interpolated (IDW) distribution of triallate in the study area. Noteworthy are the low concentrations in proximity to the deltas of the Mekong River and Red River. River samples are not interpolated

Some parts of the Vietnamese Shelf are notably enriched (between 15°N and 14°N) which are in proximity to the outflow of small-scale mountainous rivers.

6.4.2 TCPP1 and TCPP2

6.4.2.1TCPP1

The same marine sediment samples analysed for triallate were also analysed for TCPP isomers. Normalisation is performed using sample SO-187-3-98-1, which yielded the highest abundance of triallate. While this allows a more straightforward comparison of triallate and TCPP, this also results in normalisation values greater than 1, since sample SO-187-3-98-1 does not represent the highest measured concentration of TCPP. The highest overall normalisation value of TCPP1 is therefore 6.163 (SO-115-22-2), the lowest value is 0.00 (average: 2.86, Fig.37, table 34 and 35).

Table 34) Samples normalised (SO-187-3-98-1) tris (2-chloroethyl) phosphate (TCPP1) distribution in marine surface sediments

Region	Max. value	Min. value	Average	*n*
Gulf of Tonkin	1.73	0.00	0.35	32
Vietnamese Shelf	27.3	0.01	5.18	31
Vietnamese Coast	14.7	0.00	2.98	74
Sunda Shelf	61.6	0.00	3.20	52
Slope/ Deep Sea	11.5	0.03	2.07	23

In the Gulf of Tonkin, values ranges from 0.00 to 1.73 (average: 0.35, n = 32). The Vietnamese Shelf shows values from 0.01 to 27.3 (average: 5.18, n = 31). On the Vietnamese Coast values range from 0.00 to 14.7 (average: 2.98, n = 74). The Sunda Shelf has values range from 0.00 to 61.6 (average; 3.20, n = 52) and in the Slope/Deep Sea, area values range from 0.00 to 11.5 (average: 2.07, n = 23). Distribution of TCPP1 indicates irregular to patchy enrichment in proximity to coastal areas, whereas deep sea areas record low concentrations.

In addition to the marine sediment samples, 58 estuary samples were analysed and normalised against sample SO-187-3-98-1. The highest overall value of TCPP1 for estuarine samples is 4.82; the lowest value is 0.00 (average: 0.70).

Table 35) Samples normalised (SO-187-3-98-1) tris (2-chloroethyl) phosphate (TCPP1) distribution of estuary samples

Region	Max. value	Min. value	Average	*n*
Estuaries from the Gulf of Tonkin area	4.82	0.00	1.53	7
Estuaries from the Vietnamese Shelf area	3.75	0.00	0.94	14
Estuaries from the Vietnamese Coast area	3.46	0.00	0.72	12
Estuaries from the Sunda Shelf area (Indonesia and Malaysia)	1.00	0.00	0.40	15
Estuaries from Thailand	0.49	0.03	0.19	10

The estuary samples in the area of the Gulf of Tonkin range from 0.00 to 4.82 (average: 1.53, $n = 7$). Riverine samples connected to the Vietnamese Shelf have values of 0.00 to 3.75 (average: 0.94, $n = 14$). Samples connected to the Vietnamese Coast show values from 0.00 to 3.46 (average: 0.72, $n = 12$). Samples from Indonesia, Sumatra and Malaysia which are connected via the Sunda Shelf show values of 0.00 to 1.00 (average: 0.40, $n = 15$). Riverine samples of Thailand show values which range from 0.03 to 0.49 (average: 0.19, $n = 10$).

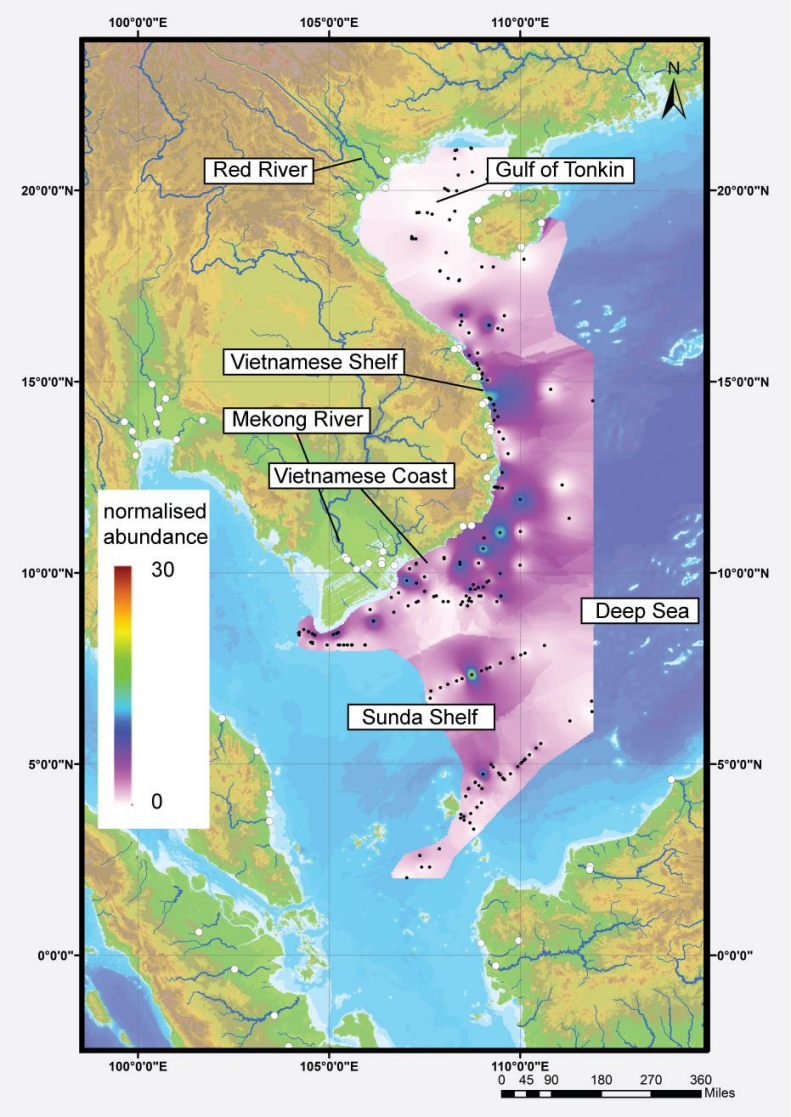

Figure 37) Interpolated (IDW) distribution of tris (2-chloroethyl) phosphate in the study area. River samples are not interpolated

6.4.2.2 TCPP2

TCPP2 was analysed on 212 marine sediment samples, and samples are normalised to sample SO-187-3-98-1. The highest overall value for TCPP2 is 28.2, the lowest value is 0.00 (average: 0.61), using internal standardisation (Fig. 38, table 36 and 37).

Table 36) Samples normalised (SO-187-3-98-1) tris (2-chloroethyl) phosphate (TCPP2) distribution in marine surface sediments

Region	Max. value	Min. value	Average	*n*
Gulf of Tonkin	0.22	0.00	0.03	32
Vietnamese Shelf	2.49	0.00	0.64	31
Vietnamese Coast	2.38	0.00	0.35	74
Sunda Shelf	28.2	0.00	1.02	52
Slope/ Deep Sea	14.2	0.00	1.30	23

The Gulf of Tonkin show values ranging from 0.00 to 0.22 (average: 0.03, *n* = 32). On the Vietnamese Shelf the normalised values range from 0.00 to 2.49 (average: 0.64, *n* = 31). On the Vietnamese Coast values range from 0.00 to 2.38 (average: 0.35, *n* = 74). The Sunda Shelf has values from 0.00 to 28.2 (average; 1.02, *n* = 52) and in the Slope/Deep Sea values range from 0.00 to 14.2 (average: 1.30, *n* =23, (Fig. 38)).

Estuary samples (*n* = 58) were analysed for TCPP2. The abundance of TCPP2 is nearly non-detectable.

Table 37) Samples normalised (SO-187-3-98-1): tris (2-chloroethyl) phosphate (TCPP2) distribution of estuary samples

Region	Max. value	Min. value	Average	*n*
Estuaries from the Gulf of Tonkin area	0.70	0.00	0.22	7
Estuaries from the Vietnamese Shelf area	0.51	0.00	0.15	14
Estuaries from the Vietnamese Coast area	0.56	0.01	0.11	12
Estuaries from the Sunda Shelf area (Indonesia and Malaysia)	0.14	0.00	0.05	15
Estuaries from Thailand	0.06	0.00	0.02	10

The estuary samples in the area of the Gulf of Tonkin range from 0.00 to 0.70 (average: 0.22, *n* = 7). Riverine samples of the Vietnamese Shelf have values of 0.00 to 0.51 (average: 0.15, *n* =14). Estuary samples of the Vietnamese Coast range from 0.01 to 0.56 (average: 0.11, *n* = 12). Samples from Indonesia, Sumatra and Malaysia which are connected to the Sunda Shelf show values of 0.00 to 0.14 (average: 0.05, *n* = 15). Riverine samples of Thailand show values which range from 0.00 to 0.06 (average: 0.02, *n* = 10). Overall, slight enrichment in proximity to the coast is observed; with some samples in the Sunda Shelf, being strongly enriched (Fig. 38).

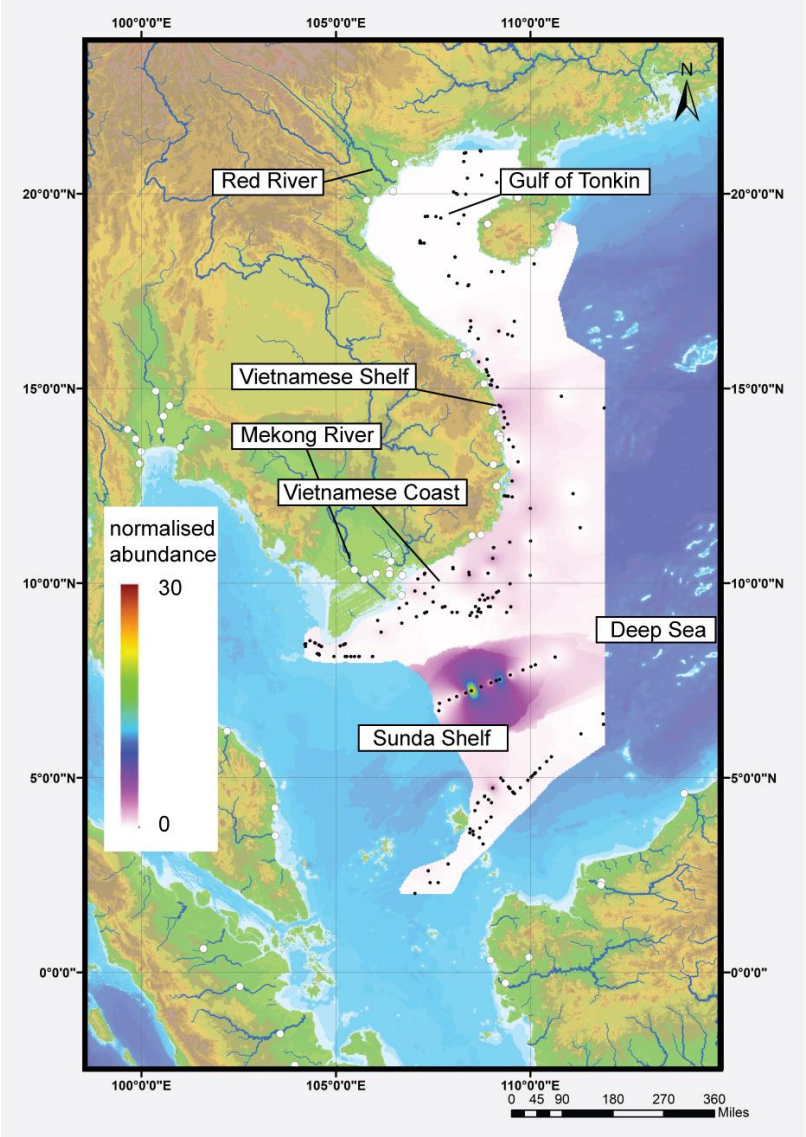

Figure 38) Interpolated (IDW) distribution of tris (2-chloroisopropyl) phosphate in the study area. River samples are not interpolated

6.4.2.3 TCPP1/TCPP2 ratios

The overall TCPP ratios in the marine sediment (n = 212) samples of the SCS are ranging from 0.01 to 17.5 with an average of 8.34. For a graphical illustration, see figure 38, table 38 and 39.

Table 38) Ratio of tris (2-chloroethyl) phosphate (TCPP1) and tris (2-chloroethyl) phosphate (TCPP2) samples normalised (SO-187-3-98-1) distribution in marine surface sediments

Region	Max. value	Min. value	Average	*n*
Gulf of Tonkin	13.8	0.00	9.25	32
Vietnamese Shelf	15.7	5.12	8.33	31
Vietnamese Coast	17.5	5.59	8.80	74
Sunda Shelf	15.0	0.02	7.52	52
Slope/ Deep Sea	9.73	0.01	7.38	23

In the Gulf of Tonkin, the TCPP1/TCPP2 ratio ranges from 0.00 to 13.8 (average: 9.25, *n* = 32). The Vietnamese Shelf shows ratios ranging from 5.12 to 15.7 (average: 8.33, *n* = 31). TCPP1/TCPP2 ratios on the Vietnamese Coast are ranging from 5.59 to 17.5 (average: 8.80, *n* = 74). On the Sunda Shelf the TCPP1/TCPP2 ratios have a minimum value of 0.02 and a maximum value of 15.0 (average: 7.52, *n* = 52). In the Slope/Deep Sea ratios range from 0.01 to 9.73 (average of 7.38, *n* = 23).

The overall TCPP ratios in the estuary samples (*n* = 58) samples of the SCS are ranging from 0.07 to 23.5 (average: 8.25).

Table 39) Ratio of tris (2-chloroethyl) phosphate (TCPP1) and tris (2-chloroethyl) phosphate (TCPP2) samples normalised (SO-187-3-98-1) distribution of estuary samples

Region	Max. value	Min. value	Average	*n*
Estuaries from the Gulf of Tonkin area	16.2	6.07	9.47	9.47
Estuaries from the Vietnamese Shelf area	9.30	0.07	7.18	14
Estuaries from the Vietnamese Coast area	9.47	5.96	7.81	12
Estuaries from the Sunda Shelf area (Indonesia and Malaysia)	23.5	7.23	8.83	15
Estuaries from Thailand	9.18	8.11	8.51	10

In the estuary samples of the Gulf of Tonkin the TCPP1/TCPP2 ratio ranges from 6.07 to 16.18 (average: 9.47, *n* = 7). Samples of the Vietnamese Shelf have ratio values ranging from 0.07 to 9.30 (average: 7.18, *n* = 14). On the Vietnamese Coast values are ranging from 5.96 to 9.47 (average: 7.81, *n* = 12). In the Sunda Shelf the TCPP1/TCPP2 ratios have a minimum value of 7.23 and a maximum value of 23.5 (average: 8.83, *n* = 15). Estuary samples of Thailand have ratios from 8.11 to 9.18 (average: 8.51, *n* = 10).

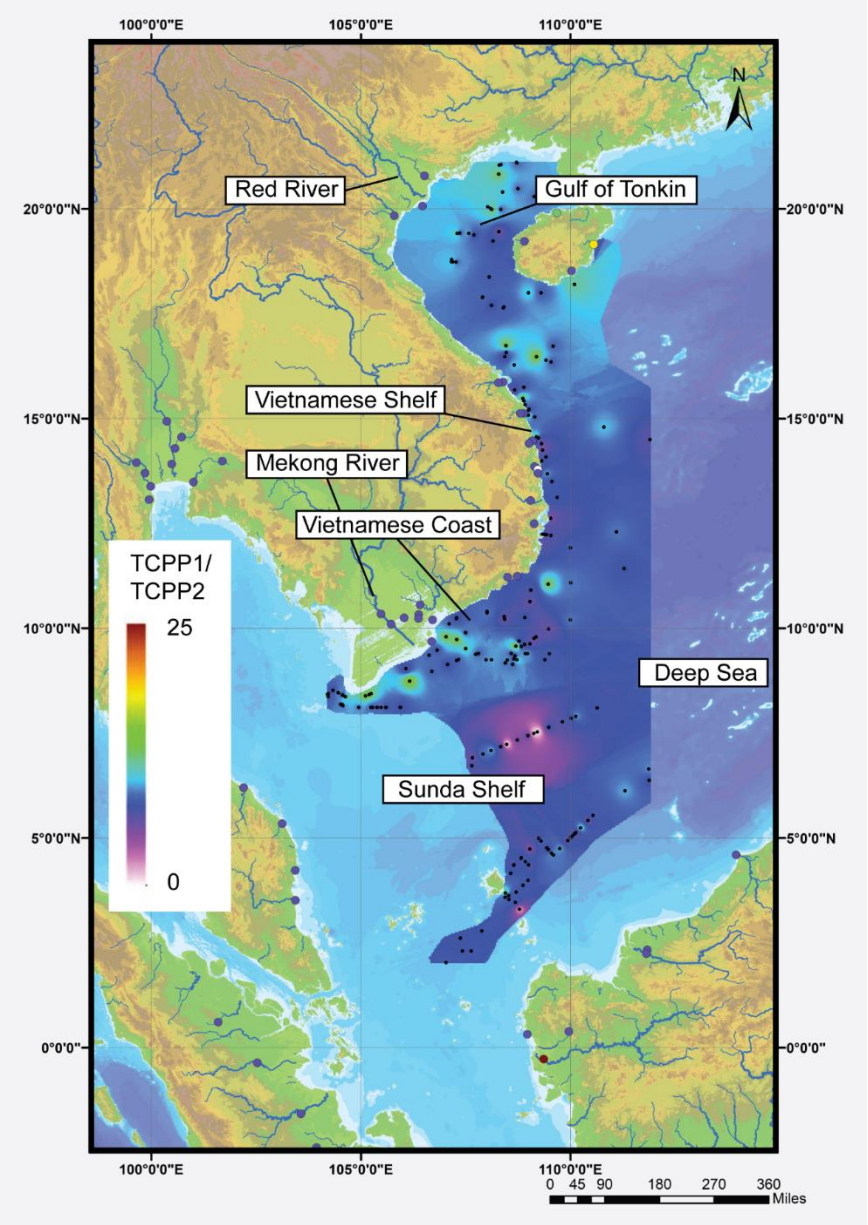

Figure 39) Interpolated (IDW) ratio of tris (2-chloroethyl) phosphate and tris (2-chloroisopropyl) phosphate. River samples are not interpolated

6.5 Discussion

The distribution and base-abundance of anthropogenic compounds – providing compelling evidence of marine pollution or COPC – in the SCS is variable across space, as evidenced by triallate and TCPP isomers (Fig. 36, 37 and 38). In general, triallate and TCPP abundances – especially TCPP1 and TCPP2 – are higher in marine surface-sediments as compared to estuarine samples (Fig. 40).

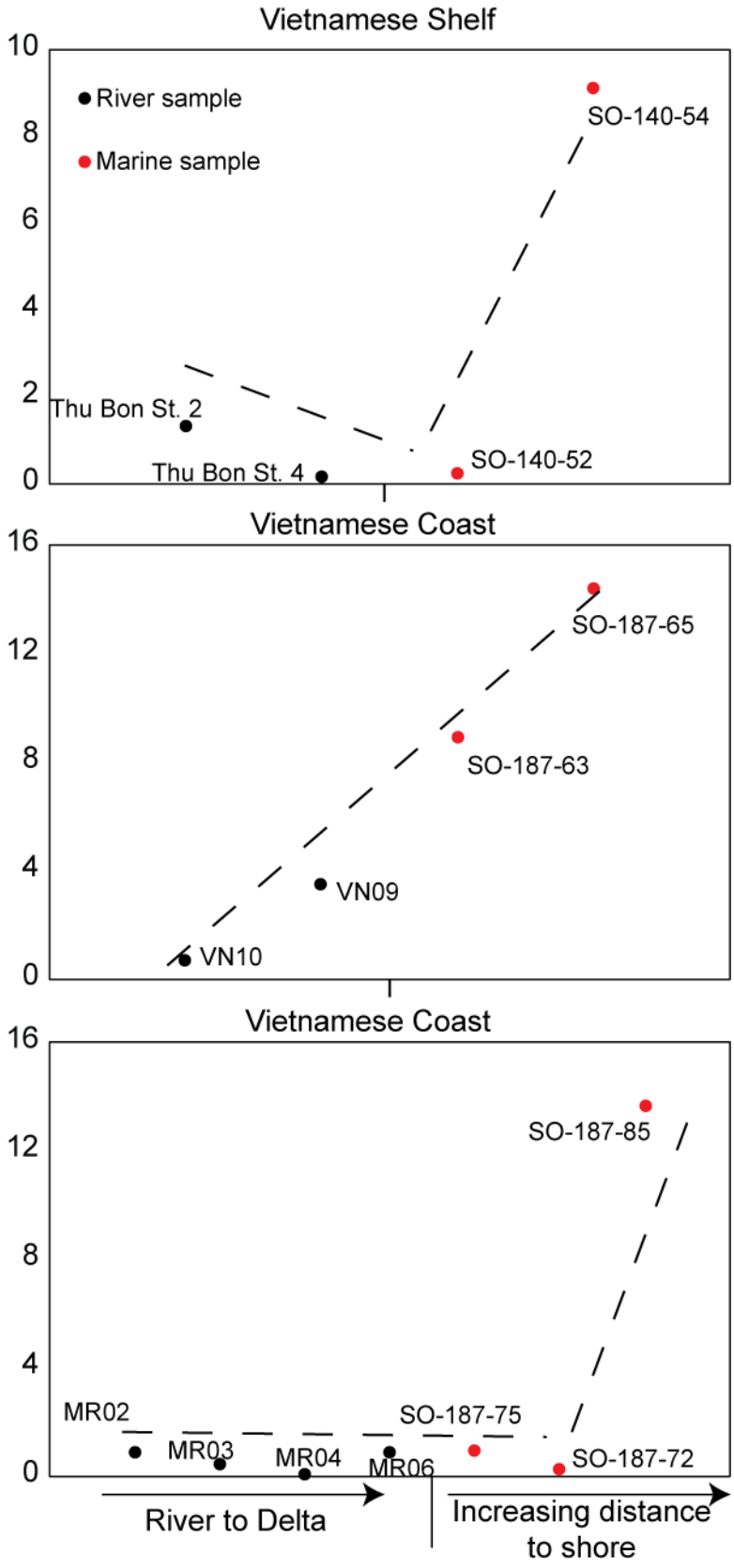

Figure 40) Selected transects representing the transition from shallow estuarine rivers (black circles) to the marine shelf (red circles) with increasing distance to shore and increasing water depths

This observation has important implications for the storage of anthropogenic pollutants and COPC in the environment, as it provides evidence that marine sediments far off the coast and even in deep basins act as a sink for POPs. This apparent gradient between land

(estuary) and ocean abundances is lower when investigating triallate. Particularly the Vietnamese Shelf and some part of the Red River Delta show a tendency towards homogenisation of abundances. Lower concentrations in estuary samples possibly reflect fluctuations in production quantity in the hinterland or can imply that transport pathways other than riverine play important roles, such as airborne particle transfer, making marine sediment a more efficient accumulator compared to riverine sediments. In the absence of reliable data, other mechanisms such as influence of current dynamics (e.g. cyclonic gyres *vs*. downstream transport) could possibly affect the accumulation within the water column prior to fixation in sediments can only be speculated about. Alternatively, the POPs could be bound to OM, which progressively decomposes while being transported towards the marine environment. If the OM is decomposed in the marine environment, the POPs could be released past the estuarine environment, explaining the higher abundance in the marine environment.

In order to predict and make accurate assessments about the accumulation and fixation of POPs (TCPPs and triallate) it is first evaluated if these compounds behave similar or equivalent to OM. A first objective is to qualitatively compare POPs distribution maps with other available data (e.g. TOC and/or SA), to establish potential links (Chapters 3 and 4).

Qualitatively, no correlation is found between POPs and SA, clay mineral distribution, TOC, summer current patterns, and carbon isotopes. Furthermore, the distributions of triallate and TCPP do not correlate (Fig. 36, 37 and 38), which indicate that either the processes controlling transport and fixation in sediment differ, or that differences in physicochemical properties (e.g. van der Waals bindings) dictate the distribution of the investigated POPs in the study area. Some studies have investigated the adsorption of POPs to plastic debris and resin pellets [416, 417], and if these are dispersed in the oceans, POPs distribution are probably following these patterns. If POPs are found to be accumulated with other anthropogenic materials such as plastic, the SCS might be the most important study area for this topic. The amount of potential plastic waste entering the oceans was estimated by [418], and countries bordering the SCS have the highest potential to introduce plastic waste. Therefore, coupled plastic and POPs analysis might prove itself important to understand POPs distribution in the oceans.

Conceptually, triallate should be elevated in regions with extensive agricultural farming because it is a potent herbicide and readily available to farmers [376]. The Ministry of

Agriculture & Rural Development (2010) (https://ipad.fas.usda.gov/rssiws/al/seasia_cropprod.aspx) published a map of the distribution of the agriculture of corn and other farm crops. Comparison of this map with the triallate findings of this study confirm short transport pathways of farmland agriculture signatures close to the coastal ocean, especially along mountainous coastal regions (Vietnamese Shelf). This match of high triallate content in marine surface sediments seems to represent winter surface current patterns (see Fig. 6b Chapter 1- General Introduction) and wet seasonal conditions when herbicides are preferentially applied to cropland. Furthermore, higher precipitation in mountainous areas, such as Central Vietnam, can result in greater mobilisation of sediment and soil matter, explaining the observed higher triallate concentrations in these the river estuaries (Fig. 36). To note is that TOC and SA (Chapters 3 and 4) do not translate into obvious correlations with triallate, suggesting a decoupling of these variables. The accumulation of triallate therefore seems largely unrelated to sedimentary properties (e.g. percentage clays) consistent with earlier studies showing that triallate is not adsorbed to clay minerals [419].

The isomer ratio of TCPP1/TCPP2 is illustrated in figure 39. In the studied samples, several off-shore samples yield lower TCPP1/TCPP2 ratios (Fig. 39). Truong et al. [414] suggested that TCPP1 and TCPP2 can be fractionated by evaporation on the basis of different vapour pressures. Other reasons could be mixing of sources with variable TCPP1/TCPP2 values, but no sources are identified in the literature, albeit any item treated with flame retardant is a potential source. A logical continuation to the quest of understanding TCPP distribution must therefore be the analysis of items such as furniture, building material, flooring, and clothing, to create an interpretational framework.

When the content of triallate is compared with TOC data, the predominate feature can be described as scatter, with very little qualitative and quantitative evidence for correlation with TOC (Fig. 40). The same observation is made for TCPP where no correlation with TOC can be established. Since the overall TOC content in the discussed dataset is moderately low (generally <1 %), a final conclusive statement if TOC and POPs correlate positively cannot be made, but the discussed data oppose the observation made by [4], who reported very similar range in TOC. Experiments investigating the adsorption of POPs to OM are needed to better comprehend the potential relation between TOC content of marine sediments and POPs.

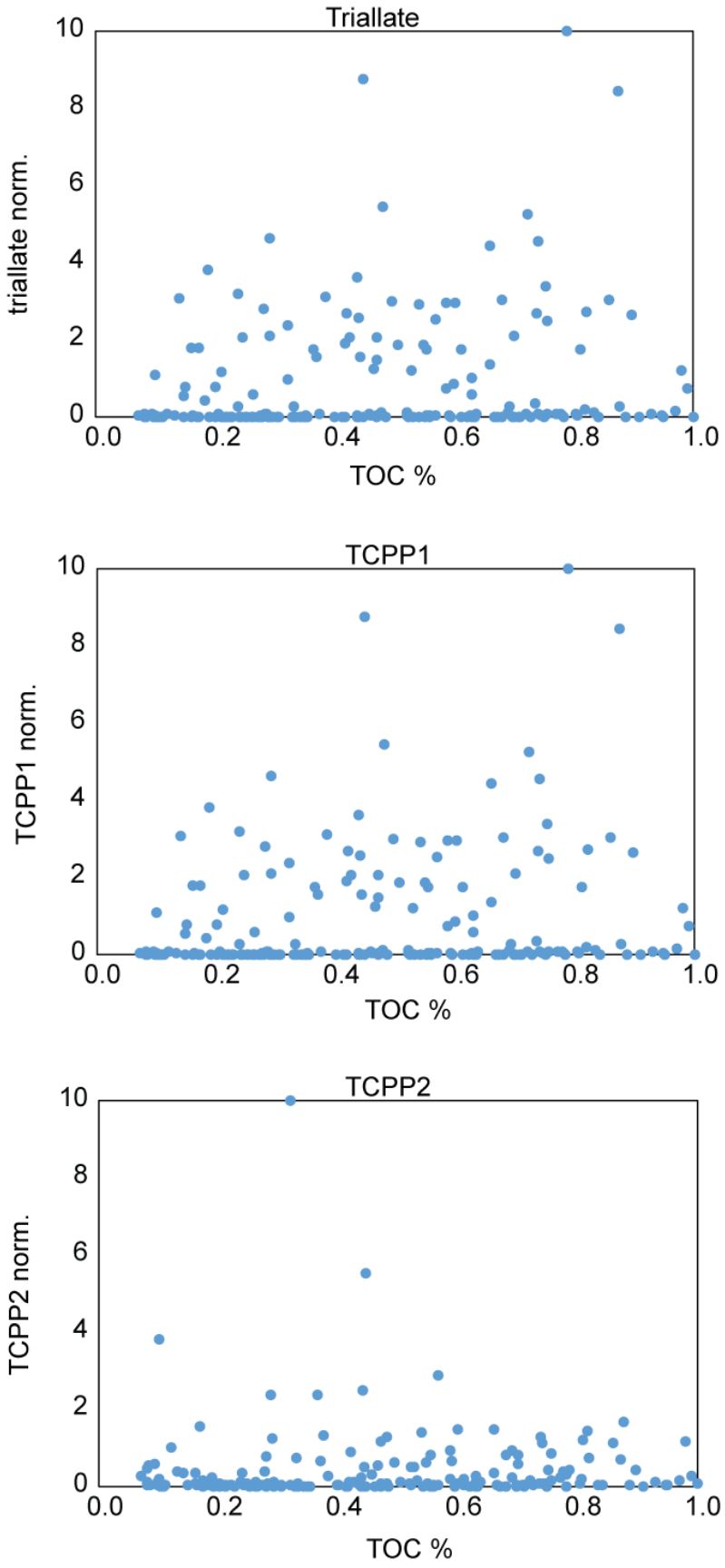

Figure 41) The abundance of anthropogenic compounds (triallate, tris (2-chloroethyl) phosphate (TCPP1) and tris (2-chloroisopropyl) phosphate (TCPP2)) is compared with total organic carbon (TOC [%]), to establish if pollutant and contaminants of potential concern transit is governed by the same mechanisms and processes

The nature of TCPP and triallate distribution cannot conclusively be evaluated with the here available data and require more fundamental research on the adsorption and mobilisation of POPs.

6.6 Conclusion

The widespread occurrence of anthropogenic organic pollutants and COPC in marine surface sediments documents fast distribution rates and poses an uncharacterised risk for the coastal-offshore environment. Based on the here presented and discussed data, following conclusions and observations can be made:

1) OPE and OSE fixation and transport are decoupled relative to OM, as evident from riverine sediments and marine surface sediments data. The role of riverine transport is difficult to assess in the absence of knowledge of concentrations of the source of OPE and OSE compounds. In mountainous regions with farming activity (central Vietnam), the compound triallate is abundant in rivers draining the area, suggesting it is mobilised from farmland and effectively transported seawards in aqueous solutions. Larger river systems such as the Mekong River and Red River yield only low concentrations of TCPP and triallate, which could mean that large rivers carry diluted amounts of POPs and that up-concentration occurs only in the marine environment, controlled by unknown processes. Airborne transportation of these compounds is documented, and precipitation into the oceans could be an important source of POPs in marine waters prior to fixation in sediment.
2) Sediment properties such as clay mineralogy and mineral surface area do not correlate with POPs content, making it difficult to establish links to known and characterised transport pathways and mechanisms.
3) Some localised enrichment of POPs in marine surface sediment is supported by seasonal current patterns, but in the absence of a characterisation of processes, which govern long-term fixation of POPs in sediment; this observation should be considered carefully. Circular gyre structures appear to correlate with areas of increased POPs concentrations.

7 Conclusions and Future work

7.1 Conclusion Summary

The South China Sea (SCS) is investigated using estuary and marine bulk surface sediments, characterising its TOC, $\delta^{13}C_{org}$, $\Delta^{14}C$, C_{org}/N_{total}, mineral surface area (SA), Fatty Acid Mehtylesters (FAME) content and composition. These data were used to evaluate the composition and fate of organic carbon (OC) transported from the terrestrial to marine environment and identify regional distribution and storage patterns. Several numerical models were computed, their output interpreted and evaluated and the performance of several model approaches and parameters compared to identify most robust data treatment approaches. The data presented in this study and its evaluation have culminated in conclusions that are summarised below:

1) The characterisation of carbon processes requires large datasets, which are spatially well resolved to cover the terrestrial, terrestrial-marine interface, marine shallow shelf, and marine deep sea reservoirs. Essential data to establish an interpretational framework are: TOC, $\delta^{13}C_{org}$, $\Delta^{14}C$, FAME, SA, and C_{org}/N_{total}, which are obtained from bulk marine surface sediments. These data can then be correlated with e.g. vegetation cover (C_3, C_4, and CAM plants), bedrock geology (e.g. carbonates *vs.* mafic rocks), river delta systems (e.g. amount of discharge), and hydrodynamic settings (currents dynamics and structures).
2) FAME content diminishes gradually from estuary to marine sediment samples investigated; suggesting decomposition and degradation are a primary process in the modification of bulk sediment FAME composition and content. Instrumental to the interpretation of FAME data, normalisation occurs of several FAME members (e.g. *n*-$C_{10:0}$ to *n*-$C_{24:0}$) by use of reservoirs such as the average estuary FAME composition, which is compositionally close to terrestrial milieus, and deep marine FAME compositions, which resemble the composition of the OM prior to final deposition and burial. Overall, the FAME record presents itself as a useful indicator for smaller scale changes in vegetation, if suitable reservoir compositions are characterised. Here, the marine signal is more pronounced than the terrestrial signatures, indicating the importance of decomposition and degradation of terrestrial OM, and the input from marine primary production to bulk sediment OM composition. The chain length e.g. is a useful proxy to distinguish marine or terrestrial sources, and at a minimum, chain length from

n-$C_{10:0}$ to n-$C_{24:0}$ should be analysed, eventually even up to chain length n-$C_{30:0}$ is recommended, although the longer chains are often found to be below detection limit.

3) Besides biochemical processes, physicochemical properties are found to affect the fixation/storage of OM and synthetic organic compounds (e.g. persistent organic pollutants (POPs)). For TOC and SA positive correlation confirms the importance of sediment composition, particularly the presence of the clay fraction. Variations in the slope between TOC and SA are related to current strength and hydrodynamic patters (e.g. gyres and upwelling areas). In the interface between terrestrial and marine milieu, vegetation cover (e.g. mangrove) is found to act as a physical filter of particles and larger debris pieces. A quantitatively minor contributor to the modification of OM composition is the contribution of carbon mobilised from soils and bedrock cover, which in particular influences the $\Delta^{14}C$ systematics of samples, by addition of unradiogenic carbon. Variations in bedrock appear to relate to changes in $\Delta^{14}C$ records, which are interpreted to changes in the release of unradiogenic carbon, due to higher or lower resistance to weathering (e.g. carbonate *vs.* mafic rocks).
4) Computational models are a powerful tool in the interpretation of larger data sets, given that suitable parameters and hypotheses are used. Here, the combination of two robust geochemical proxies ($\delta^{13}C_{org}$ and $\Delta^{14}C$) is found most suitable for the characterisation of marine and terrestrial proportions, which has important implications in the assessment of OM preservation derived from the terrestrial milieu. Simulation based models, such as Bayesian statistics, offer the necessary flexibility for geological and biochemical complex settings, such as the SCS study area. Linear and simplified models result in homogenisation of results, which creates a misfit between observed and modelled data. Using the simulation based approach; inverse determination of potential source reservoirs is possible in some scenarios. In this study, this approach has been used to identify the most likely terrestrial end-member composition, and refined marine and transitional reservoir compositions based on bulk surface sediment data. These are for the study area i) marine end-member (refined) $\delta^{13}C_{org}$ = -19.2 ‰, $\Delta^{14}C$ = 33.3‰; ii) terrestrial end-member (new) $\delta^{13}C_{org}$ = -30 ‰, $\Delta^{14}C$ = -155.4 ‰; iii) petrogenic carbon (refined) $\delta^{13}C_{org}$ = -25.4 ‰, $\Delta^{14}C$ = -880.2 ‰; iv) carbon dead (new) $\delta^{13}C_{org}$ = -25.0 ‰, $\Delta^{14}C$ = -1000 ‰.

5) An important observation in the study of marine surface sediments is the accumulation of POPs, which can be either organophosphate (OPE) or organosulfate (OSE) compounds in the frame of this study. OSEs such as triallate have applications in the farming industry, and some rivers in Vietnam draining farmland have elevated contents of triallate. Other, more ambiguous sources of OPEs such as flame-retardants do not show clear correlations, suggesting that a diverse mixture of processes results in the mobilisation, transport, and accumulation of OPEs used as flame-retardants in anthropogenic products. Processes, which control the transport, distribution, and fixation of OM, do not appear to apply to POPs distribution and accumulation. The only exception to this appears to be the role of currents and hydrodynamic structures such as gyres, which overlap with area of higher POPs contents. Clearly, more research on the mobilisation, transport, and deposition of POPs is necessary to identify and prevent contamination of the marine ecosystem with these toxic compounds.

In particular, the introduction of FAME normalisation and graphical illustration as spider-diagrams has shown itself to be an interesting tool in the study OM composition evolution during transport prior to deposition and fixation in sediments. The inverse data modelling has permitted the extraction of most likely end-members for areas where samples are unavailable, which offers future research opportunities to validate and/or refine the outcomes of these models.

7.2 Future work

Despite significant progress, this project faced several challenges that could not be solved, warranting further investigations. In the following research and other gaps are identified and potential strategies to overcome these challenges recommended. Some of these recommendations are specifically targeted to the study area whereas others explore more generic/global questions.

1) The sample set available to this project has been unique but ideal for the scope of this study, with marine surface sediments obtained over a total period of 16 years during 1996 - 2012 ship expeditions. Riverine/estuary samples also not taken systematically as part of dedicated projects but rather opportunistic as opportunities emerged, all together leading to a rather diverse set of materials to work with. Furthermore, both riverine and marine sediments were taken during contrasting seasons, mixing wet and dry season signatures in one sample set.

Finally, no material has been available from any location to covering seasonal variability. This leaves a principle challenge to identify and separate processes and response mechanisms that represent the highly diverse climatic/oceanographic boundary conditions across the study region. This challenge is not easily solved; however, it would be desirable to design and deliver a targeted sampling strategy that takes spatial and temporal relationships along strategic land-ocean transects into account. Such an approach should also include river catchments in the hinterland and salinity transitions at the estuary/marine interface, to better capture the source signatures entering and leaving the river. The sample set investigated also lacked data on the actual transition zone connecting land and marine sediments, the ocean water column. It is therefore suggested that a future sampling campaign is also targeting sediment traps located intermediate to riverine outflows and marine deposition centres, water column samples and greater down-core sampling (e.g. topmost 10 cm at 1 cm intervals). In particular, some samples from the mainland source regions such as forest and farmland are interesting targets, since they help to constrain computational models by providing maximum initial values, while deep sea marine surface sediments possibly constrain the minimum values. Another underestimated factor is the composition of soils in the landmasses adjacent to the study area. Since soils are essentially mixtures of fresh and decomposed material, it is important to understand which components are remobilised from those soils, transported by the riverine system, and eventually deposited in the marine milieu.

2) Due to limitations in available sample volume for selected study locations, this project was not able to generate grain size and other data for all estuarine and marine surface sediments leaving a partly inconsistent database for the discussion. Furthermore, accurate and spatially diverse sedimentation/accumulation rates are not available at present and would need to be established to enhance the accuracy of flux calculations and transportation pathways linked with hydrodynamic data. In Chapter 4, it has been shown that TOC correlates with mineral SA and the clay fraction (where data was available). However, given the lack of sufficient sample volumes for all study sites it remains unclear if this relationship between TOC and clay fraction is consistent throughout the study area, or if there are diversions that may influence carbon fixation in selected marine environments. Here it will be important to test areas with low and high current velocities, to test if changes in the slope between TOC and the clay fraction are related to detaching of OM from

the clay fraction at higher current velocities, which could explain differences observed between regions in this study. Furthermore, the adsorption of POPs is currently poorly determined, and the combination of POPs content with the different size fractions of sediment could reveal potential dependencies.

3) A promising avenue forward would be to combine the bulk sediment analyses performed in this study with more detailed grain size specific carbon analyses (TOC, C_{org}/N_{total}, carbon isotopes, $\Delta^{14}C$, and $\delta^{13}C_{org}$). This approach is relatively novel and underexplored but has been occasionally applied since the mid- 1990s [420–422], it has large potential to greatly enhance the resolution of carbon processes as it provided additional evidence on hydrodynamic sorting, lateral displacement, and potentially decomposition of OM fractions, and ages of OM fractions in different size pools. These processes cannot be accurately addressed with the bulk sediment dataset presented. Working on grain size specific fractions will permit a more refined interpretation of data (e.g. TOC, $\delta^{13}C_{org}$, $\Delta^{14}C$, C_{org}/N_{total} and FAME). For example, increased molecular separation and analyses of compounds such as FAME or TOC could be used to test the effect of physical abrasion on OM, e.g. if coarser particles can physically affect OM when sediments are compacted periodically or re-suspended. The FAME composition and distribution in the size fractions could be used to test, if marine and terrestrial OM preferentially will allow to target hard and soft compounds (e.g. marine *vs.* terrestrial or anthropogenic origin). The combination of carbon isotope analyses ($\Delta^{14}C$ and $\delta^{13}C_{org}$) of specific grain sizes will be useful for a better understanding which part of sediments contains the "oldest" carbon, as these fractions may be critical for long-term carbon fixation.

4) This project was not initially designed to investigate anthropogenic pollutants (POPs) and other human-derived organic chemicals. More bespoke procedures will need to be established to fully explore the pool of POPs, including chemicals released during the Vietnam War (Agent Orange and related highly toxic products). Here, the consensus in the literature is that multiple suspect sources are present, but none of these has been quantified. This identifies the potential to take the question further how POPs are transported across the land-ocean continuum. The data from this study suggest that transport and accumulation processes are not directly linked to OM and clay mineralogy/SA. This may be unexpected but opens the interesting challenge to find out the primary transport mechanisms. Some previous research has suggested that POPs can adsorb to

particles of plastic. Therefore, some laboratory experiments involving different size and surface area fractions of plastics mixed with defined concentrations of POPs should be performed e.g. exposed to variable currents, water temperatures, salinity, and pH-conditions etc.. A curiosity experiment could involve the addition of algae usually found on plastics in oceans to the plastics POPs mixture, to investigate potential biochemical processes in the decomposition and/or fixation of POPs. Understanding the sources of pollutants and COPC, these can be used to accurately describe and model the degradation of these compounds, by comparing source with i) transition (i.e. water column) and ii) depositional composition. This will permit the estimation of persistence of these compounds under natural conditions, as opposed to laboratory conditions often advocated by those who produce the compounds in the first place. Furthermore, it would be relevant to investigate the impact of these chemicals on benthic and microbial ecosystems, and feedbacks to the environment.

5) Another focus developing from this research is the distinction and characterisation of OM pools (e.g. inert, recalcitrant, and potent) with their unique reactivity, degradation, transport, and burial properties. The novel modelling approach presented in Chapter 5 shows one way forward to use data and advanced modelling to better understand these pools and their fates. An emerging problem observed in this model, is the need for diverse sources to create models that can produce outputs that correlate with observed data. However, the number of sources is beginning to exceed the number of geochemical proxies, which naturally decreases the accuracy of the model. Therefore, more geochemical proxies must be identified and established to permit the identification and characterisation of more reservoirs. These new, more robust models will greatly enhance the interpretation of $\Delta^{14}C$ values, which then can be used to assume timescales for geological processes. The combination with $\delta^{13}C_{org}$ isotopes and other new tracers will then narrow down the number of potential source reservoirs, allowing a prediction of a more accurate and likely pathway for carbon from land to ocean. These findings could then be used to more accurately describe the total carbon flux from land to ocean, which has implications for climate models.
6) The transition of OM composition from land to ocean can be estimated and assessed using the $\delta^{13}C_{org}$ isotopic composition. In combination with SA and TOC data, deductions of net terrestrial C_{org} can be made, as demonstrated in Chapter 4. However, the SCS data set covers a relatively restricted range in TOC/SA,

compared to other regions such as the Amazon and Amazon French Guiana mud belt. To allow better comparison of the SCS data and the inferred net loss of terrestrial C_{org} with those regions, samples with high TOC/SA need to be identified and analysed, to verify observed differences in regression lines. Should the current regression lines be verified (Chapter 4), the SCS would be identified as a terrestrial C_{org} incinerator, relative to the Amazon system.

Further international and interdisciplinary studies are fundamentally important to solve the puzzle of carbon transfer in the biggest marginal sea of the Pacific Ocean, the SCS, and will result in a better understanding about the effects of climate change and may help to identify and prepare for future issues and challenges.

8 References

1. Su J, Sein DV, Mathis M et al. (2014) Assessment of a zoomed global model for the North Sea by comparison with a conventional nested regional model. Tellus A: Dynamic Meteorology and Oceanography 66(1): 23927. doi: 10.3402/tellusa.v66.23927

2. Bourgoin L-H, Tremblay L (2010) Bacterial reworking of terrigenous and marine organic matter in estuarine water columns and sediments. Geochimica et Cosmochimica Acta 74(19): 5593–5609. doi: 10.1016/j.gca.2010.06.037

3. Alkhatib M, Schubert CJ, del Giorgio PA et al. (2012) Organic matter reactivity indicators in sediments of the St. Lawrence Estuary. Estuarine, Coastal and Shelf Science 102-103: 36–47. doi: 10.1016/j.ecss.2012.03.002

4. Zhong M, Wu H, Mi W et al. (2018) Occurrences and distribution characteristics of organophosphate ester flame retardants and plasticizers in the sediments of the Bohai and Yellow Seas, China. Sci Total Environ 615: 1305–1311. doi: 10.1016/j.scitotenv.2017.09.272

5. FAO (2006) World Agriculture: Towards 2030/2050. Interim Report. UN Food and Agriculture Organization, Rome.

6. Inthorn M, Wagner T, Scheeder G et al. (2006) Lateral transport controls distribution, quality, and burial of organic matter along continental slopes in high-productivity areas. The Geological Society of America 34(3): 205. doi: 10.1130/G22153.1

7. Bao R, McNichol AP, McIntyre, C, P. et al. (2018) Dimensions of Radiocarbon Variability within Sedimentary Organic Matter. Radiocarbon 60(3): 775–790. doi: 10.1017/RDC.2018.22

8. Nittrouer C, DeMaster D, Eidam E et al. (2017) The Mekong Continental Shelf: The Primary Sink for Deltaic Sediment Particles and Their Passengers. Oceanog. 30(3): 60–70. doi: 10.5670/oceanog.2017.314

9. Gaye B, Nagel B, Dähnke K et al. (2013) Amino acid composition and δ^{15}N of suspended matter in the Arabian Sea: Implications for organic matter sources and degradation. Biogeosciences 10(11): 7689–7702. doi: 10.5194/bg-10-7689-2013

10. Bao R, McIntyre C, Zhao M et al. (2016) Widespread dispersal and aging of organic carbon in shallow marginal seas. Geology 44(10): 791–794. doi: 10.1130/G37948.1

11. Blattmann TM, Zhang Y, Zhao Y et al. (2018) Contrasting Fates of Petrogenic and Biospheric Carbon in the South China Sea. Geophys. Res. Lett. 38(02): 295. doi: 10.1029/2018GL079222

12. Tao S, Eglinton TI, Montluçon DB et al. (2015) Pre-aged soil organic carbon as a major component of the Yellow River suspended load: Regional significance and global relevance. Earth and Planetary Science Letters 414: 77–86. doi: 10.1016/j.epsl.2015.01.004

13. Mann PJ, Eglinton TI, McIntyre CP et al. (2015) Utilization of ancient permafrost carbon in headwaters of Arctic fluvial networks. Nat Commun 6: 7856. doi: 10.1038/ncomms8856

14. Vonk JE, Semiletov IP, Dudarev OV et al. (2014) Preferential burial of permafrost-derived organic carbon in Siberian-Arctic shelf waters. J. Geophys. Res. Oceans 119(12): 8410–8421. doi: 10.1002/2014JC010261

15. Schroeder A, Wiesner MG, Liu Z (2015) Fluxes of clay minerals in the South China Sea. Earth and Planetary Science Letters 430: 30–42. doi: 10.1016/j.epsl.2015.08.001

16. Liu Z, Zhao Y, Colin C et al. (2016) Source-to-sink transport processes of fluvial sediments in the South China Sea. Earth-Science Reviews 153: 238–273. doi: 10.1016/j.earscirev.2015.08.005

17. Komada T, Druffel ERM, Hwang J (2005) Sedimentary rocks as sources of ancient organic carbon to the ocean: An investigation through Δ 14 C and δ 13 C signatures of organic compound classes. Global Biogeochem. Cycles 19(2): 1-10. doi: 10.1029/2004GB002347

18. Hossler K, Bauer JE (2013) Amounts, isotopic character, and ages of organic and inorganic carbon exported from rivers to ocean margins: 1. Estimates of terrestrial losses and inputs to the Middle Atlantic Bight. Global Biogeochem. Cycles 27(2): 331–346. doi: 10.1002/gbc.20033

19. Goñi MA, Ruttenberg KC, Eglinton TI (1997) Sources and contribution of terrigenous organic carbon to surface sediments in the Gulf of Mexico. Nature 389(6648): 275

20. Galy V, Peucker-Ehrenbrink B, Eglinton T (2015) Global carbon export from the terrestrial biosphere controlled by erosion. Nature 521(7551): 204–207. doi: 10.1038/nature14400

21. Berner R (1982) Burial of organic carbon and pyrite sulfur in the modern ocean: its geochemical and environmental significance. American Journal of Science(282): 451–475

22. Eglinton G, Murphy MTJ (eds) (1969) Methods and Results. Springer-Verlag, New-York, Inc

23. Meyers PA, Ishiwatari R (1993) Lacustrine organic geochemistry—an overview of indicators of organic matter sources and diagenesis in lake sediments. Organic Geochemistry 20(7): 867–900

24. Hu J, Peng P, Chivas AR (2009) Molecular biomarker evidence of origins and transport of organic matter in sediments of the Pearl River estuary and adjacent South China Sea. Applied Geochemistry 24(9): 1666–1676. doi: 10.1016/j.apgeochem.2009.04.035

25. Derrien M, Yang L, Hur J (2017) Lipid biomarkers and spectroscopic indices for identifying organic matter sources in aquatic environments: A review. Water Research 112: 58–71. doi: 10.1016/j.watres.2017.01.023

26. Riboulleau A, Schnyder J, Riquier L et al. (2007) Environmental change during the Early Cretaceous in the Purbeck-type Durlston Bay section (Dorset, Southern England): A biomarker approach. Organic Geochemistry 38(11): 1804–1823. doi: 10.1016/j.orggeochem.2007.07.006

27. Winter MJ, Verweij F, Garofalo E et al. (2005) Tissue levels and biomarkers of organic contaminants in feral and caged chub (Leuciscus cephalus) from rivers in the West Midlands, UK. Aquat Toxicol 73(4): 394–405. doi: 10.1016/j.aquatox.2005.05.001

28. Xu W, Yan W, Chen Z et al. (2014) Organic matters and lipid biomarkers in surface sediments from the northern South China Sea: Origins and transport. J. Earth Sci. 25(1): 189–196. doi: 10.1007/s12583-014-0412-z

29. Killops SD, Killops VJ (2013) An Introduction to Organic Geochemistry, Second Edition. John Wiley & Sons

30. Hunt JM (1995) Petroleum geochemistry and geology, 2nd edn. Freeman, New York

31. Peters KE, Walters. CC, Moldowan JM (2005) The biomarker guide, 2nd ed. Cambridge University Press, Cambridge UK, New York

32. Bianchi TS, Canuel EA (2011) Chemical biomarkers in aquatic ecosystems. Princeton University Press

33. Lamchin M, Lee W-K, Jeon SW et al. (2017) Long-term trend and correlation between vegetation greenness and climate variables in Asia based on satellite data. Sci Total Environ 618: 1089–1095. doi: 10.1016/j.scitotenv.2017.09.145

34. Song J (2010) Biogeochemical Processes of Biogenic Elements in China marginal seas; chapter 5 south china sea. Springer

35. Chen CTA, Wang SL, Wang BJ et al. (2001) Nutrient budgets for the South China Sea basin. Marine Chemistry(75): 281–300

36. Chu PC, Li R (2000) South China Sea Isopycnal-Surface Circulation. J. Phys. Oceanogr. 30(9): 2419–2438. doi: 10.1175/1520-0485(2000)030<2419:SCSISC>2.0.CO;2

37. Chen C-C, Shiah F-K, Chung S-W et al. (2006) Winter phytoplankton blooms in the shallow mixed layer of the South China Sea enhanced by upwelling. Journal of Marine Systems 59(1-2): 97–110. doi: 10.1016/j.jmarsys.2005.09.002

38. Shi M, Chen C, Xu Q et al. (2002) The Role of Qiongzhou Strait in the Seasonal Variation of the South China Sea Circulation. J. Phys. Oceanogr. 32(1): 103–121. doi: 10.1175/1520-0485(2002)032<0103:TROQSI>2.0.CO;2

39. Wang P (1999) Response of Western Pacific marginal seas to glacial cycles: paleoceanographic and sedimentological features. Marine Geology 156: 5–39

40. Karin BR, Das I, Jackman TR et al. (2017) Ancient divergence time estimates in Eutropis rugifera support the existence of Pleistocene barriers on the exposed Sunda Shelf. PeerJ 5: e3762. doi: 10.7717/peerj.3762

41. Kang X, Zhao W, Pan Z et al. (1994) Study on architecture of sequence stratigraphic framework of Beibuwan Basin. Earth Science-J. China Univ. Geosci. (in Chinese) 19: 493–502

42. Taylor B, Hayes DE (1980) The tectonic evolution of the South China Basin. The tectonic and geologic evolution of Southeast Asian seas and islands(23): 89–104

43. Liu Z, Colin C, Huang W et al. (2007) Climatic and tectonic controls on weathering in south China and Indochina Peninsula: Clay mineralogical and geochemical investigations from the Pearl, Red, and Mekong drainage basins. Geochem. Geophys. Geosyst. 8(5). doi: 10.1029/2006GC001490

44. Hartmann J, Moosdorf N (2012) The new global lithological map database GLiM: A representation of rock properties at the Earth surface. Geochem. Geophys. Geosyst. 13(12): 119. doi: 10.1029/2012GC004370

45. Schoenbohm LM, Whipple KX, Burchfiel BC et al. (2004) Geomorphic constraints on surface uplift, exhumation, and plateau growth in the Red River region, Yunnan Province, China. Geol Soc America Bull 116(7): 895. doi: 10.1130/B25364.1

46. Leloup PH, Arnaud N, Lacassin R et al. (2001) New constraints on the structure, thermochronology, and timing of the Ailao Shan-Red River shear zone, SE Asia. Journal of Geophysical Research: Solid Earth 106(B4): 6683–6732

47. Replumaz A, Lacassin R, Tapponnier P et al. (2001) Large river offsets and Plio-Quaternary dextral slip rate on the Red River fault (Yunnan, China). Journal of Geophysical Research: Solid Earth 106(B1): 819–836

48. Liu Z, Wang H, Hantoro WS et al. (2012) Climatic and tectonic controls on chemical weathering in tropical Southeast Asia (Malay Peninsula, Borneo, and Sumatra). Chemical Geology 291: 1–12. doi: 10.1016/j.chemgeo.2011.11.015

49. Hutchison CS (1968) Dating tectonism in the Indosinian–Thai–Malayan orogen by thermoluminescence. Geological Society of America Bulletin 79(3): 375–386

50. Hennig-Breitfeld J, Breitfeld HT, Hall Rt et al. (2019) A new upper Paleogene to Neogene stratigraphy for Sarawak and Labuan in northwestern Borneo: Paleogeography of the eastern Sundaland margin. Earth-Science Reviews 190: 1–32. doi: 10.1016/j.earscirev.2018.12.006

51. Wang P, Li Q (2009) The South China Sea: Paleoceanography and Sedimentology

52. Paeth H (2006) Das Monsunklima in Asien. In: Deutsche Wetterdienst (ed) Klima und Wetter in den Tropen, 32nd edn. promet, pp 98–113

53. Chu PC, Guihua W (2003) Seasonal Variability of Thermohaline Front in the Central South China Sea. Journal of Oceanography 59(1): 65–78

54. Wang G, Chen D, Su J (2006) Generation and life cycle of the dipole in the South China Sea summer circulation. J. Geophys. Res. 111(C6): 1925. doi: 10.1029/2005JC003314

55. Liu K-K, Chao S-Y, Shaw P-T et al. (2002) Monsoon-forced chlorophyll distribution and primary production in the South China Sea: observations and a numerical study. Deep Sea Research I 49: 1387–1412

56. Gerbich C (2001) Lithogener Partikelfluß im Südchinesischen Meer: Quellen, Transport und Sedimentation.

57. Narman LS (2015) Rezente Sedimentation im Golf von Tonkin. MSc, Universität Hamburg

58. Huang R, Sun. F. (1992) Impacts of the Tropical Western Pacific on the East Asian Monsoon. Meteorological Society of Japan 70: 243–256

59. Ehleringer JR, Cerling TE, Helliker BR (1997) C 4 photosynthesis, atmospheric CO 2, and climate. Oecologia 112(3): 285–299

60. O'Leary MH (1981) Carbon isotope fractionation in plants. Phytochemistry 20(4): 553–567

61. Pancost RD, Boot CS (2004) The palaeoclimatic utility of terrestrial biomarkers in marine sediments. Marine Chemistry 92(1-4): 239–261. doi: 10.1016/j.marchem.2004.06.029

62. Still C, Rastogi B (2017) What Drives Carbon Isotope Fractionation by the Terrestrial Biosphere? J. Geophys. Res. Biogeosci. 122(11): 3108–3110. doi: 10.1002/2017JG004155

63. Arens NC, Jahren AH, Amundson R (2000) Can C3 plants faithfully record the carbon isotopic composition of atmospheric carbon dioxide? Paleobiology 26(1): 137–164. doi: 10.1666/0094-8373(2000)026<0137:CCPFRT>2.0.CO;2

64. Beerling DJ, Royer DL (2002) Fossil Plants as Indicators of the Phanerozoic Global Carbon Cycle. Annu. Rev. Earth Planet. Sci. 30(1): 527–556. doi: 10.1146/annurev.earth.30.091201.141413

65. Deines P (1980) The isotopic composition of reduced organic carbon. In: Fritz P, Fontes JC (eds) Handbook of Environmental Isotope Geochemistry, vol 1, pp 329–406

66. Marino BD, McElroy MB (1991) Isotopic composition of atmospheric CO2 inferred from carbon in C4 plant cellulose. Nature 349(6305): 127

67. Li S, Meng X, Ge Z et al. (2015) Vulnerability assessment of the coastal mangrove ecosystems in Guangxi, China, to sea-level rise. Reg Environ Change 15(2): 265–275. doi: 10.1007/s10113-014-0639-3

68. Zhu H (2017) The Tropical Forests of Southern China and Conservation of Biodiversity. Bot. Rev. 83(1): 87–105. doi: 10.1007/s12229-017-9177-2

69. Victor S, Golbuu Y, Wolanski E et al. (2004) Fine sediment trapping in two mangrove-fringed estuaries exposed to contrasting land-use intensity, Palau, Micronesia. Wetlands Ecology and Management(12): 277–283

70. Zhang J, Wang DR, Jennerjahn T et al. (2013) Land–sea interactions at the east coast of Hainan Island, South China Sea: A synthesis. Continental Shelf Research 57: 132–142. doi: 10.1016/j.csr.2013.01.004

71. Wassmann R, Hien NX, Hoanh CT et al. (2004) Sea Level Rise Affecting the Vietnamese Mekong Delta: Water Elevation in the Flood Season and Implications for Rice Production. Climatic Change 66(1/2): 89–107. doi: 10.1023/B:CLIM.0000043144.69736.b7

72. Kamoshita A, Nguyen YTB, Dinh VTH (2018) Preliminary Assessment of Rice Production in Coastal Part of Red River Delta Surrounding Xuan Thuy National Park, Vietnam, for Improving Resilience. In: Takeuchi K, Saito O, Matsuda H et al. (eds) Resilient Asia, vol 84. Springer Japan, Tokyo, pp 7–38

73. Van TT, Wilson N, Thanh-Tung H et al. (2015) Changes in mangrove vegetation area and character in a war and land use change affected region of Vietnam (Mui Ca Mau) over six decades.Mau, Vietnam. Acta Oecologica 63(12): 71–81. doi: 10.5194/bgd-10-20047-2013

74. Quartel S, Kroon A, Augustinus PGEF et al. (2007) Wave attenuation in coastal mangroves in the Red River Delta, Vietnam. Journal of Asian Earth Sciences 29(4): 576–584. doi: 10.1016/j.jseaes.2006.05.008

75. Chaiyo U, Garivait S, Wanthongchai K (2011) Carbon storage in above-ground biomass of tropical deciduous forest in Ratchaburi Province, Thailand. 58: 636–641

76. Rangsiruji A, Boonpragob K, Mongkolsuk P et al. (2016) Diversity and phylogenetic survey of cyanobacterial lichens (Collematineae, Ascomycota) in mangrove forests of eastern Thailand. The Bryologist 119(2): 123–130. doi: 10.1639/0007-2745-119.2.123

77. Lee HS, Ashton PS (1995) Population Structure and Canopy Dominance of Two Emergent Dipterocarp Species in a Tropical Rain Forest of Sarawak, East Malaysia. Tropics 4(2/3): 133–141

78. Nasaruddin MH, Noor MIQN, Mamat H (2013) Komposisi Proksimat dan Komponen Asid Lemak Durian Kuning (Durio graveolens) Sabah: Proximate and Fatty Acid Composition of Sabah Yellow Durian (Durio graveolens). Sains Malaysiana(42): 1283–1288

79. Margono BA, Turubanova S, Zhuravleva I et al. (2012) Mapping and monitoring deforestation and forest degradation in Sumatra (Indonesia) using Landsat time series data sets from 1990 to 2010. Environ. Res. Lett. 7(3): 34010. doi: 10.1088/1748-9326/7/3/034010

80. Koh LP, Miettinen J, Liew SC et al. (2011) Remotely sensed evidence of tropical peatland conversion to oil palm. Proc Natl Acad Sci U S A 108(12): 5127–5132. doi: 10.1073/pnas.1018776108

81. Ilman M, Wibisono IT, Suryadiputra N (2011) State of the Art Information on Mangrove Ecosystems in Indonesia. Wetlands International

82. Basyuni M, Putri LAP, Julayha et al. (2012) Non-Saponifiable Lipid Composition of Four Salt-Secretor and Non-Secretor Mangrove Species from North Sumatra, Indonesia. MSS 16(2). doi: 10.7454/mss.v16i2.1402

83. Basyuni M, Putri LAP, Nainggolan B et al. (2014) Growth and Biomass in Response to Salinity and Subsequent Fresh Water in Mangrove Seedlings Avicennia marina and Rhizophora stylosa. jtfm 20(1): 17–25. doi: 10.7226/jtfm.20.1.17

84. Basyuni M, Sulistiyono N (2018) Deforestation and reforestation analysis from land-use changes in North Sumatran Mangroves, 1990-2015. IOP Conf. Ser.: Mater. Sci. Eng. 309: 12018. doi: 10.1088/1757-899X/309/1/012018

85. Biemans H, Haddeland I, Kabat P et al. (2011) Impact of reservoirs on river discharge and irrigation water supply during the 20th century. Water Resour. Res. 47(3): 247. doi: 10.1029/2009WR008929

86. Pokhrel Y, Hanasaki N, Koirala S et al. (2012a) Incorporating Anthropogenic Water Regulation Modules into a Land Surface Model. J. Hydrometeor 13(1): 255–269. doi: 10.1175/JHM-D-11-013.1

87. Pokhrel YN, Hanasaki N, Yeh PJ-F et al. (2012b) Model estimates of sea-level change due to anthropogenic impacts on terrestrial water storage. Nature Geosci 5(6): 389–392. doi: 10.1038/ngeo1476

88. Vörösmarty C, Lettenmaier D, Leveque C et al. (2004) Humans transforming the global water system. Eos Trans. AGU 85(48): 509–514. doi: 10.1029/2004EO480001

89. Milliman JD, Farnsworth KL, Albertin CS (1999) Flux and fate of fluvial sediments leaving large islands in the East Indies. Journal of Sea Research 41(1-2): 97–107

90. Milliman JD, Syvitski JPM (1992) Geomorphic/Tectonic Control of Sediment Discharge to the Ocean: The Importance of Small Mountainous Rivers. The Journal of Geology 100(5): 525–544. doi: 10.1086/629606

91. Saito Y, Chaimanee N, Jarupongsakul T et al. (2007) Shrinking megadeltas in Asia: Sea-level rise and sediment reduction impacts from case study of the Chao Phraya Delta. Inprint Newsletter of the IGBP/IHDP Land Ocean Interaction in the Coastal Zone, 2 (39)

92. Huang W, Wang P (2006) Sediment mass and distribution in the South China Sea since the Oligocene. Science in China Series D: Earth Sciences 49(11): 1147–1155. doi: 10.1007/s11430-006-2019-4

93. Kondolf GM, Gao Y, Annandale GW et al. (2014) Sustainable sediment management in reservoirs and regulated rivers: Experiences from five continents. Earth's Future 2(5): 256–280. doi: 10.1002/2013EF000184

94. Berg M, Tran HC, Nguyen TC et al. (2001) Arsenic contamination of groundwater and drinking water in Vietnam: a human health threat. Environ Sci Technol 35(13): 2621–2626. doi: 10.1021/es010027y

95. Tanabe S, Saito Y, Lan V. Q. et al. (2006) Holocene evolution of the Song Hong (Red River) delta system, northern Vietnam. Sedimentary Geology 187(1-2): 29–61. doi: 10.1016/j.sedgeo.2005.12.004

96. Wang H, Saito Y, Zhang Y et al. (2011) Recent changes of sediment flux to the western Pacific Ocean from major rivers in East and Southeast Asia. Earth-Science Reviews 108(1-2): 80–100. doi: 10.1016/j.earscirev.2011.06.003

97. van Maren DS (2007) Water and sediment dynamics in the Red River mouth and adjacent coastal zone. Journal of Asian Earth Sciences 29(4): 508–522. doi: 10.1016/j.jseaes.2006.03.012

98. Rangin C, Klein M, Roques D et al. (1995) The Red River fault system in the Tonkin Gulf, Vietnam. Tectonophysics 243(3-4): 209–222. doi: 10.1016/0040-1951(94)00207-P

99. Milliman JD, Farnsworth KL (2011) River Discharge to the Coastal Ocean. Cambridge University Press, Cambridge

100. Le TPQ, Garnier J, Gilles B et al. (2007) The changing flow regime and sediment load of the Red River, Viet Nam. Journal of Hydrology 334(1-2): 199–214. doi: 10.1016/j.jhydrol.2006.10.020

101. Bauer A, Radziejewska T, Liang K et al. (2013) Regional Differences of Hydrographical and Sedimentological Properties in the Beibu Gulf, South China Sea. Journal of Coastal Research 66: 49–71. doi: 10.2112/SI_66_5

102. Cat VM, Duong BD (2006) Assessment of saline water intrusion into estuaries of Red-Thai Binh River during dry season having considered water released from upper reservoirs and tidal fluctuation. Proceeding of the Vietnam-Japan Estuary Workshop, Hanoi, Vietnam.

103. Sang PN, Liu Z, Zhao Y et al. (2018) Chemical weathering in central Vietnam from clay mineralogy and major-element geochemistry of sedimentary rocks and river sediments. Heliyon 4(7). doi: 10.1016/j.heliyon.2018.e00710

104. Kummu M, Varis O (2007) Sediment-related impacts due to upstream reservoir trapping, the Lower Mekong River. Geomorphology 85(3-4): 275–293. doi: 10.1016/j.geomorph.2006.03.024

105. Lu XX, Siew RY (2006) Water discharge and sediment flux changes over the past decades in the Lower Mekong River: possible impacts of the Chinese dams. Hydrology and Earth System Sciences 10: 181–195

106. Gugliotta M, Saito Y, Nguyen VL et al. (2018) Tide- and River-Generated Mud Pebbles from the Fluvial To Marine Transition Zone of the Mekong River Delta, Vietnam. Journal of Sedimentary Research 88(9): 981–990. doi: 10.2110/jsr.2018.54

107. Siripong H, Wirat K., Suwi T The Chao Phraya Delta: Historical Development, Dynamics and Challenges of Thailand's Rice Bowl. In: Proceedings of the International Conference: The Chao Phraya Delta: Historical Development, Dynamics and Challenges of Thailand's Rice Bowl, pp 13–15

108. Piyakarnchana T (1989) Yield dynamics as an index of biomass shifts in the Gulf of Thailand ecosystems. Biomass yields and geography of Large Marine Ecosystems: 95–142

109. Pauly D, Chuenpagdee R (2003) Development of fisheries in the Gulf of Thailand large marine ecosystem: analysis of an unplanned experiment. In: Large Marine Ecosystems (2003), pp 337–354

110. Piyakarnchana T (1999) Changing State and Health of the Gulf of Thailand Large Marine Ecosystem. In: Sherman K, Tang Q (eds) Large Marine Ecosystemsof the Pacific Rim - Assessment, Sustainability and Management. Blackwell Science, Malden US, pp 240–250

111. Ling T-Y, Soo C-L, Sivalingam J-R et al. (2016) Assessment of the Water and Sediment Quality of Tropical Forest Streams in Upper Reaches of the Baleh River, Sarawak,

Malaysia, Subjected to Logging Activities. Journal of Chemistry 2016(2): 1–13. doi: 10.1155/2016/8503931

112. Ling T-Y, Soo C-L, Phan T-P et al. (2017) Assessment of the Water Quality of Batang Rajang at Pelagus Area, Sarawak, Malaysia. JSM 46(3): 401–411. doi: 10.17576/jsm-2017-4603-07

113. Staub JR, Gastaldo RA (2003) Tropical deltas of southeast Asia: Late Quaternary sedimentation and peat development in the Rajang River delta, Sarawak, east Malaysia.

114. Staub JR, Among HL, Gastaldo RA (2000) Seasonal sediment transport and deposition in the Rajang River delta, Sarawak, East Malaysia. Sedimentary Geology 133(3-4): 249–264. doi: 10.1016/S0037-0738(00)00042-7

115. Li S, Dai Z, Mei X et al. (2017) Dramatic variations in water discharge and sediment load from Nanliu River (China) to the Beibu Gulf during 1960s–2013. Quaternary International 440: 12–23. doi: 10.1016/j.quaint.2016.02.065

116. Wang H, Xiao W, Wang Y et al. (2019) Assessment of the impact of climate change on hydropower potential in the Nanliujiang River basin of China. Energy 167: 950–959. doi: 10.1016/j.energy.2018.10.159

117. Liu T, Tao Y, Liu Y (2017) Mangrove swamp expansion controlled by climate since 1988: a case study in the Nanliu River Estuary, Guangxi, Southwest China. Acta Oceanol. Sin. 36(12): 11–17. doi: 10.1007/s13131-017-1097-9

118. Kaiser D, Kowalski N, Böttcher M et al. (2015) Benthic Nutrient Fluxes from Mangrove Sediments of an Anthropogenically Impacted Estuary in Southern China. JMSE 3(2): 466–491. doi: 10.3390/jmse3020466

119. Bonnema MG, Sikder S, Hossain F et al. (2016) Benchmarking wide swath altimetry-based river discharge estimation algorithms for the Ganges river system. Water Resour. Res. 52(4): 2439–2461. doi: 10.1002/2015WR017296

120. Li Z, Zhang Y, Li Y et al. (2010) Palynological records of Holocene monsoon change from the Gulf of Tonkin (Beibuwan), northwestern South China Sea. Quat. res. 74(01): 8–14. doi: 10.1016/j.yqres.2010.04.012

121. Manh D-V, Yanagi T (2000) A Study on Residual Flow in the Gulf of Tongking. Journal of Oceanography 56: 59–68

122. Chern C-S, Jan S, Wang J (2010) Numerical study of mean flow patterns in the South China Sea and the Luzon Strait. Ocean Dynamics 60(5): 1047–1059. doi: 10.1007/s10236-010-0305-3

123. Chen G, Hou Y, Chu X (2011) Water exchange and circulation structure near the Luzon Strait in early summer. Chin. J. Ocean. Limnol. 29(2): 470–481. doi: 10.1007/s00343-011-0198-0

124. Lüdmann T, Wong KH, Berglar K (2005) Upward flow of North Pacific Deep Water in the northern South China Sea as deduced from the occurrence of drift sediments. Geophys. Res. Lett. 32(5): 1. doi: 10.1029/2004GL021967

125. Shaw P-T, Chao S-Y (1994) Surface circulation in the South China Sea. Deep Sea Research Part I: Oceanographic Research Papers 41(11-12): 1663–1683. doi: 10.1016/0967-0637(94)90067-1

126. Qu T (2000) Upper-layer circulation in the South China Sea. Journal of Physical Oceanography(6): 1450–1460

127. Fang G, Fang WD, Fang Y et al. (1998) A survey of studies on the South China Sea upper ocean circulation. Acta Oceanographica Taiwanica 37: 1–16

128. Yuan D, Han W, Hu D (2006) Surface Kuroshio path in the Luzon Strait area derived from satellite remote sensing data. J. Geophys. Res. 111(C11): 559. doi: 10.1029/2005JC003412

129. Zhang Y, Liu Z, Zhao Y et al. (2014) Mesoscale eddies transport deep-sea sediments. Sci Rep 4: 5937. doi: 10.1038/srep05937

130. Manh D-V, Yanagi T (1997) A three-dimensional numerical model of tide and tidal current in the Gulf of Tonking. La mer

131. Xia H, Li S, Shi M (2001) Three. D numerical simulation of wind-driven current and density current in the Beibu Gulf. Acta Oceanologica Sinica

132. Wu D, Wang Y, Lin X et al. (2008) On the mechanism of the cyclonic circulation in the Gulf of Tonkin in the summer. J. Geophys. Res. 113(C9): 1. doi: 10.1029/2007JC004208

133. Wu D, Wang Y, Lin X et al. (2008) On the mechanism of the cyclonic circulation in the Gulf of Tonkin in the summer. J. Geophys. Res. 113(C9): 1. doi: 10.1029/2007JC004208

134. Wattayakorn G, King B, Wolanski E et al. (1998) Seasonal dispersion of petroleum contaminants in the Gulf of Thailand. Continental Shelf Research 18(6): 641–659

135. Yuan Y, Bu X, Liao G et al. (2004) Diagnosticcalculation of the upper—layer circulation in the South China Sea during the winter of 1998

136. Xie S-P (2003) Summer upwelling in the South China Sea and its role in regional climate variations. J. Geophys. Res. 108(C8): 2305. doi: 10.1029/2003JC001867

137. Liu Q (2004) A gap in the Indo-Pacific warm pool over the South China Sea in boreal winter: Seasonal development and interannual variability. J. Geophys. Res. 109(C7): 2205. doi: 10.1029/2003JC002179

138. Chen C, Lai Z, Beardsley RC et al. (2012) Current separation and upwelling over the southeast shelf of Vietnam in the South China Sea. J. Geophys. Res. 117(C3). doi: 10.1029/2011JC007150

139. Hein H (2008) Vietnam Upwelling: Analysis of the upwelling and related processes in the coastal area off South Vietnam. Dissertation, Universität Hamburg

140. Jungclaus JH, Fischer N, Haak H et al. (2013) Characteristics of the ocean simulations in the Max Planck Institute Ocean Model (MPIOM) the ocean component of the MPI-Earth system model. J. Adv. Model. Earth Syst. 5(2): 422–446. doi: 10.1002/jame.20023

141. Marsland SJ, Haak H, Jungclaus JH et al. (2003) The Max-Planck-Institute global ocean/sea ice model with orthogonal curvilinear coordinates. Ocean Modelling 5(2): 91–127

142. Griffies SM, Böning C, Bryan FO et al. (2000) Developments in ocean climate modelling. Ocean Modelling 2(3-4): 123–192. doi: 10.1016/S1463-5003(00)00014-7

143. Wu S (2013) Solving Disputes for Regional Cooperation and Development in the South China Sea: Recent developments and regional cooperation in the South China Sea. Chandos Publishing

144. Wyrtki K (1959-1961) Physical Oceanography of the Southeast Asian waters

145. Ning X, Chai F, Xue H et al. (2004) Physical-biological oceanographic coupling influencing phytoplankton and primary production in the South China Sea. J. Geophys. Res. 109(C10): 917. doi: 10.1029/2004JC002365

146. Tang D, Kawamura H, Lee M-A et al. (2003) Seasonal and spatial distribution of chlorophyll-a concentrations and water conditions in the Gulf of Tonkin, South China Sea. Remote Sensing of Environment 85(4): 475–483. doi: 10.1016/S0034-4257(03)00049-X

147. Chen Y, Tang D (2011) Remote Sensing Analysis of Impact of Typhoon on Environment in the Sea Area South of Hainan Island. Procedia Environmental Sciences 10: 1621–1629. doi: 10.1016/j.proenv.2011.09.256

148. Li F, Lei L, Wang X et al. (2002) Water masses in the South China Sea and water exchange between the Pacific and the South China Sea. Journal of Ocean University of Qingdao 1(1): 19–24

149. Qu T, Girton JB, Whitehead JA (2006) Deepwater overflow through Luzon Strait. J. Geophys. Res. 111(C1): 14345. doi: 10.1029/2005JC003139

150. Wang G, Xie S-P, Qu T et al. (2011) Deep South China Sea circulation. Geophys. Res. Lett. 38(5): n/a-n/a. doi: 10.1029/2010GL046626

151. Geyh MA, Streif H, Kudrass HR (1979) Sea-level changes during the late Pleistocene and Holocene in the Strait of Malacca. Nature 278(5703): 441–443

152. Hanebuth TJJ, Voris HK, Yokoyama Y et al. (2011) Formation and fate of sedimentary depocentres on Southeast Asia's Sunda Shelf over the past sea-level cycle and biogeographic implications. Earth-Science Reviews 104(1-3): 92–110. doi: 10.1016/j.earscirev.2010.09.006

153. Tjia HD (1980) The sunda shelf, southeast Asia. Zeitschrift für Geomorphologie Stuttgart 24(4): 405-227

154. Louys J, Meijaard E (2010) Palaeoecology of Southeast Asian megafauna-bearing sites from the Pleistocene and a review of environmental changes in the region. Journal of Biogeography 11: 155. doi: 10.1111/j.1365-2699.2010.02297.x

155. Hanebuth Tl, Stattegger K, Saito Y (2002) The stratigraphic architecture of the central Sunda Shelf (SE Asia) recorded by shallow-seismic surveying. Geo-Marine Letters 22(2): 86–94. doi: 10.1007/s00367-002-0102-1

156. Hanebuth T, Stattegger K, Grootes PM (2000) Rapid flooding of the Sunda Shelf: a late-glacial sea-level record. Science 288(5468): 1033–1035

157. Wong HK, Lüdmann T, Haft C et al. (2003) Quaternary sedimentation in the Molengraaff paleo-delta, northern Sunda Shelf (southern South China Sea).

158. Frey SR (2013) Agent Orange and America at war in Vietnam and Southeast Asia. Human Ecology Review 20(1): 1–10

159. Zhang X, Sühring R, Serodio D et al. (2016) Novel flame retardants: Estimating the physical-chemical properties and environmental fate of 94 halogenated and organophosphate PBDE replacements. Chemosphere 144: 2401–2407. doi: 10.1016/j.chemosphere.2015.11.017

160. Regnery J, Püttmann W (2010) Occurrence and fate of organophosphorus flame retardants and plasticizers in urban and remote surface waters in Germany. Water Research 44(14): 4097–4104. doi: 10.1016/j.watres.2010.05.024

161. Regnery J, Püttmann W (2010) Seasonal fluctuations of organophosphate concentrations in precipitation and storm water runoff. Chemosphere 78(8): 958–964. doi: 10.1016/j.chemosphere.2009.12.027

162. Hollerbach A (1985) Ausgewählte Anwendungsgebiete der organischen Geochemie. Grundlagen der organischen Geochemie (pp. 151-172). Springer Berlin Heidelberg

163. Nultsch W (2000) Allgemeine Botanik, 11th edn. Georg Thieme Verlag, Stuttgart

164. Müller PJ (1977) C/N ratios in Pacific deep-sea sediments: Effect of inorganic ammonium and organic nitrogen compounds sorbed by clays. Geochimica et Cosmochimica Acta 41(6): 765–776

165. Müller PJ, Suess E, AndréUngerer C (1986) Amino acids and amino sugars of surface particulate and sediment trap material from waters of the Scotia Sea. Deep Sea Research Part A. Oceanographic Research Papers 33(6): 819–838

166. Tissot BP, Welte DH (2013) Petroleum formation and occurrence. Springer Science & Business Media

167. Thompson S, Eglinton G (1978) The fractionation of a recent sediment for organic geochemical analysis. Geochimica et Cosmochimica Acta 42(2): 199–207

168. Schroeder PA, Ingall ED (1994) A method for the determination of nitrogen in clays, with application to the burial diagenesis of shales. Journal of Sedimentary Research 64(3a): 694–697

169. Lagalya G, Ogawab M, Dékányc I (2013) Clay mineral–organic interactions. Developments in clay science(5): 435–505

170. Scheffer F., Schachtschabel P (2010) Lehrbuch der Bodenkunde, 16th edn. Spektrum Akademischer Verlag

171. Gaye B, Nagel B, Dähnke K et al. (2013) Amino acid composition and δ15 N of suspended matter in the Arabian Sea: implications for organic matter sources and degradation. Biogeosciences 10(11): 7689–7702. doi: 10.5194/bg-10-7689-2013

172. Honjo S (1996) Fluxes of particles to the interior of the open ocean. Particle flux in the ocean

173. Evans CD, Monteith DT, Cooper DM (2005) Long-term increases in surface water dissolved organic carbon: observations, possible causes and environmental impacts. Environ Pollut 137(1): 55–71. doi: 10.1016/j.envpol.2004.12.031

174. Müller PJ, Suess E (1979) Productivity, sedimentation rate, and sedimentary organic matter in the oceans—I. Organic carbon preservation. Deep Sea Research Part A. Oceanographic Research Papers 26(12): 1347–1362. doi: 10.1016/0198-0149(79)90003-7

175. Nieuwenhuize J, Maas YEM, Middelburg JJ (1994) Rapid analysis of organic carbon and nitrogen in particulate materials. Marine Chemistry 45(3): 217–224. doi: 10.1016/0304-4203(94)90005-1

176. Verardo DJ, McIntyre A (1994) Production and destruction Control of biogenous sedimentation in the tropical Atlantic 0300,000 years B.P. Paleoceanography 9(1): 63–86

177. Wagner T, Magill C, Herrle JO (2018) Carbon Isotopes. In: White WM (ed) Earth Sciences Series. Encyclopedia of Marine Geosciences. Springer International Publishing AG

178. Hoefs J (2015) Stable Isotope Geochemistry. Springer International Publishing, Cham

179. Galfetti T, Bucher H, Brayard A et al. (2007) Late Early Triassic climate change: Insights from carbonate carbon isotopes, sedimentary evolution and ammonoid paleobiogeography. Palaeogeography, Palaeoclimatology, Palaeoecology 243(3-4): 394–411. doi: 10.1016/j.palaeo.2006.08.014

180. Traugott Ml, Kamenova S, Ruess L et al. (2013) Empirically Characterising Trophic Networks: What Emerging DNA- Based Methods, Stable Isotope and Fatty Acid Analyses Can Offer. In: Ecological Networks in an Agricultural World, vol 49. Elsevier, pp 177–224

181. Fritz P, Fontes JC (eds) (1980) Handbook of Environmental Isotope Geochemistry

182. Schubert CJ, Nielsen B (2000) Effects of decarbonation treatments on d13C values in marine sediments. Marine Chemistry 72: 55–59

183. Zhang Q, Li W (1987) Mass spectrometric determination of the absolute isotopic abundance of carbon in NBS-20. Proc. 2nd Beijing Conf. and Exhib. on Instrum. Analysis (pp. 391-392)

184. Craig H (1953) The geochemistry of the stable carbon isotopes. Geochemica et Cosmochimica Acta 3: 53–92

185. Salomons W, Mook WG (1976) Isotope geochemistry of carbonate dissolution and reprecipitation in soils. Soil Sci 122(1): 15–24

186. Tanoue E, Handa N (1979) Distribution of particulate organic carbon and nitrogen in the Bering Sea and northern North Pacific Ocean. Journal of the Oceanographical Society of Japan 35(1): 47–62. doi: 10.1007/BF02108282

187. Pedersen TF, Calvert SE (1990) Anoxia vs. productivity: what controls the formation of organic-carbon-rich sediments and sedimentary Rocks?(1). Aapg Bulletin 74(4): 454–466

188. Kleber M, Sollins P, Sutton R (2007) A conceptual model of organo-mineral interactions in soils: self-assembly of organic molecular fragments into zonal structures on mineral surfaces. Biogeochemistry 85(1): 9–24. doi: 10.1007/s10533-007-9103-5

189. Blair NE, Aller RC (2012) The fate of terrestrial organic carbon in the marine environment. Ann Rev Mar Sci 4: 401–423. doi: 10.1146/annurev-marine-120709-142717

190. Mayer LM (1994) Relationships between mineral surfaces and organic carbon concentrations in soils and sediments. Chemical Geology 114: 347-363

191. Mayer LM (1994) Surface area control of organic carbon accumulation in continental shelf sediments. Geochimica et Cosmochimica Acta 58(4): 1271–1284

192. Brunauer S, Emmett PH, Teller E (1938) Adsorption of Gases in Multimolecular Layers. J. Am. Chem. Soc. 60(2): 309–319. doi: 10.1021/ja01269a023

193. White WM (ed) (2018) Earth Sciences Series. Encyclopedia of Marine Geosciences. Springer International Publishing AG

194. Libby WF (1961) Radiocarbon Dating: The method is of increasing use to the archeologist, the geologist, the meteorologist, and the oceanogr. Science, New Series 133, No. 3453: 621–629

195. Vries DA de (1958) Simultaneous transfer of heat and moisture in porous media. Eos, Transactions American Geophysical Union 39(5): 909–916

196. Suess HE (1965) Secular variations of the cosmicrayproduced carbon 14 in the atmosphere and their interpretations. Journal of Geophysical Research 70(23): 5937–5952

197. Stuiver M (1961) Variations in radiocarbon concentration and sunspot activity. J. Geophys. Res. 66(1): 273–276. doi: 10.1029/JZ066i001p00273

198. Ramnarine R, Voroney RP, Wagner-Riddle C et al. (2011) Carbonate removal by acid fumigation for measuring the δ 13 C of soil organic carbon. Can. J. Soil. Sci. 91(2): 247–250. doi: 10.4141/cjss10066

199. Komada T, Anderson MR, Dorfmeier CL (2008) Carbonate removal from coastal sediments for the determination of organic carbon and its isotopic signatures, δ13C and Δ14C: comparison of fumigation and direct acidification by hydrochloric acid. Limnology and Oceanography Bulletin 17(3): 86. doi: 10.1002/lob.200817386

200. McIntyre CP, Wacker L, Haghipour N et al. (2017) Online 13 C and 14 C Gas Measurements by EA-IRMS–AMS at ETH Zürich. Radiocarbon 59(3): 893–903

201. Synal H-A, Stocker M, Suter M (2007) MICADAS: A new compact radiocarbon AMS system. Nuclear Instruments and Methods in Physics Research Section B: Beam Interactions with Materials and Atoms 259(1): 7–13. doi: 10.1016/j.nimb.2007.01.138

202. Brodie CR, Leng MJ, Casford JSL et al. (2011) Evidence for bias in C and N concentrations and δ13C composition of terrestrial and aquatic organic materials due to pre-analysis acid preparation methods. Chemical Geology 282(3-4): 67–83. doi: 10.1016/j.chemgeo.2011.01.007

203. Larson TE, Heikoop JM, Perkins G et al. (2008) Pretreatment technique for siderite removal for organic carbon isotope and C:N ratio analysis in geological samples. Rapid Commun Mass Spectrom 22(6): 865–872. doi: 10.1002/rcm.3432

204. Olsson IU (1970) The use of oxalic acid as a standard. Radiocarbon variations and absolute chronology: 17

205. Bianchi TS, Cui X, Blair NE et al. (2018) Centers of organic carbon burial and oxidation at the land-ocean interface. Organic Geochemistry 115: 138–155. doi: 10.1016/j.orggeochem.2017.09.008

206. Trumbore SE, Sierra CA, Hicks Pries CE (2016) Radiocarbon Nomenclature, Theory, Models, and Interpretation: Measuring Age, Determining Cycling Rates, and Tracing Source Pools. In: Schuur EAG, Druffel E, Trumbore SE (eds) Radiocarbon and Climate Change, vol 230. Springer International Publishing, Cham, pp 45–82

207. Volkman JK, Jeffrey SW, Nichols PD et al. (1989) Fatty acid and lipid composition of 10 species of microalgae used in mariculture. Journal of Experimental Marine Biology and Ecology 128(3): 219–240. doi: 10.1016/0022-0981(89)90029-4

208. Rezanka T, Sigler K (2009) Odd-numbered very-long-chain fatty acids from the microbial, animal and plant kingdoms. Prog Lipid Res 48(3-4): 206–238. doi: 10.1016/j.plipres.2009.03.003

209. Niggemann J, Schubert CJ (2006) Fatty acid biogeochemistry of sediments from the Chilean coastal upwelling region: Sources and diagenetic changes. Organic Geochemistry 37(5): 626–647. doi: 10.1016/j.orggeochem.2005.11.004

210. Canuel EA, Martens CS (1996) Reactivity of recently deposited organic matter: Degradation of lipid compounds near the sediment-water interface. Geochimica et Cosmochimica Acta 60(10): 1793–1806

211. Magill CR, Denis, E., H., Freeman, K., H. (2015) Rapid sequential separation of sedimentary lipid biomarkers via selective accelerated solvent extraction. Organic Geochemistry 88: 29–34. doi: 10.1016/j.orggeochem.2015.07.009

212. Poerschmann J, Carlson R (2006) New fractionation scheme for lipid classes based on "in-cell fractionation" using sequential pressurized liquid extraction. J Chromatogr A 1127(1-2): 18–25. doi: 10.1016/j.chroma.2006.07.063

213. Quénéa K, Mathieu J, Derenne S (2012) Soil lipids from accelerated solvent extraction: Influence of temperature and solvent on extract composition. Organic Geochemistry 44: 45–52. doi: 10.1016/j.orggeochem.2011.11.009

214. Denis EH, Toney JL, Tarozo R et al. (2012) Polycyclic aromatic hydrocarbons (PAHs) in lake sediments record historic fire events: Validation using HPLC-fluorescence detection. Organic Geochemistry 45: 7–17. doi: 10.1016/j.orggeochem.2012.01.005

215. Still WC, Kahn M, Mitra A (1978) Rapid chromatographic technique for preparative separations with moderate resolution. J. Org. Chem 43(14): 2923-2925

216. Bastow TP, van Aarssen BGK, Lang D (2007) Rapid small-scale separation of saturate, aromatic and polar components in petroleum. Organic Geochemistry 38(8): 1235–1250. doi: 10.1016/j.orggeochem.2007.03.004

217. Houghton JT, Ding YDJG, Griggs DJ et al. (2001) Climate change 2001: the scientific basis. The Press Syndicate of the University of Cambridge

218. Li D, Xu Y, Li Y et al. (2018) Sedimentary records of human activity and natural environmental evolution in sensitive ecosystems: A case study of a coral nature reserve in Dongshan Bay and a mangrove forest nature reserve in Zhangjiang River estuary, Southeast China. Organic Geochemistry 121: 22–35. doi: 10.1016/j.orggeochem.2018.02.011

219. Meyers PA (2003) Applications of organic geochemistry to paleolimnological reconstructions: a summary of examples from the Laurentian Great Lakes. Organic Geochemistry 34: 261–289

220. Lamb AL, Wilson GP, Leng MJ (2006) A review of coastal palaeoclimate and relative sea-level reconstructions using δ13C and C/N ratios in organic material. Earth-Science Reviews 75(1-4): 29–57. doi: 10.1016/j.earscirev.2005.10.003

221. Wang Y, Liu D, Richard P et al. (2013) A geochemical record of environmental changes in sediments from Sishili Bay, northern Yellow Sea, China: anthropogenic influence on organic matter sources and composition over the last 100 years. Mar Pollut Bull 77(1-2): 227–236. doi: 10.1016/j.marpolbul.2013.10.001

222. Soares ARA, Lapierre J-F, Selvam BP et al. (2019) Controls on Dissolved Organic Carbon Bioreactivity in River Systems. Sci Rep 9(1): 14897. doi: 10.1038/s41598-019-50552-y

223. Aufdenkampe AK, Mayorga E, Raymond PA et al. (2011) Riverine coupling of biogeochemical cycles between land, oceans, and atmosphere. Frontiers in Ecology and the Environment 9(1): 53–60. doi: 10.1890/100014

224. Spencer RGM, Hernes PJ, Dinga B et al. (2016) Origins, seasonality, and fluxes of organic matter in the Congo River. Global Biogeochem. Cycles 30(7): 1105–1121. doi: 10.1002/2016GB005427

225. Clark ID, Fritz P (1997) The environmental isotopes. Environmental Isotopes in Hydrogeology: 2–34

226. Eiche E, Berg M, Hönig SM et al. (2017) Origin and availability of organic matter leading to arsenic mobilisation in aquifers of the Red River Delta, Vietnam. Applied Geochemistry 77: 184–193. doi: 10.1016/j.apgeochem.2016.01.006

227. Naafs BDA, Inglis GN, Blewett J et al. (2019) The potential of biomarker proxies to trace climate, vegetation, and biogeochemical processes in peat: A review. Global and Planetary Change 179: 57–79. doi: 10.1016/j.gloplacha.2019.05.006

228. Volkman JK (2006) Marine Organic Matter: Biomarkers, Isotopes and DNA, 2N. Springer-Verlag, Berlin/Heidelberg

229. Cranwell PA (1974) Monocarboxylic acids in lake sediments: indicators, derived from terrestrial and aquatic biota, of paleoenvironmental trophic levels. Chemical Geology 14(1-2): 1–14

230. Claustre H, Marty J.-C., Cassiani L et al. (1989) Fatty acid dynamics in phytoplankton and microzooplankton communities during a spring bloom in the coastal Ligurian Sea: Ecological implications. Marine Microbial Food Webs 3(2): 51–66

231. Carrie RH, Mitchell L, Black KD (1998) Fatty acids in surface sediment at the Hebridean shelf edge, west of Scotland. Organic Geochemistry 29(5-7): 1583–1593

232. Smedman AE, Gustafsson IB, Berglund LG et al. (1999) Pentadecanoic acid in serum as a marker for intake of milk fat: relations between intake of milk fat and metabolic risk factors. The American journal of clinical nutrition 69(1): 22–29

233. Huang Y, Street-Perrot FA, Perrot A et al. (1999) Glacial–interglacial environmental changes inferred from molecular and compound-specific 13C analyses of sediments from Sacred Lake, Mt. Kenya. Geochemica et Cosmochimica Acta 63(9): 1383–1404,

234. Wang P, Sun X (1994) Last glacial maximum in China: comparison between land and sea. Catena 23(3-4): 341–353

235. Wang XM, Sun X, Wang P et al. (2009) Vegetation on the Sunda Shelf, South China Sea, during the Last Glacial Maximum. Palaeogeography, Palaeoclimatology, Palaeoecology 278(1-4): 88–97. doi: 10.1016/j.palaeo.2009.04.008

236. Hu J, Peng PA, Jia G et al. (2002) Biological markers and their carbon isotopes as an approach to the paleoenvironmental reconstruction of Nansha area, South China Sea, during the last 30 ka. Organic Geochemistry 33(10): 1197–1204

237. Hu J, Peng P, Jia G et al. (2006) Distribution and sources of organic carbon, nitrogen and their isotopes in sediments of the subtropical Pearl River estuary and adjacent shelf, Southern China. Marine Chemistry 98(2-4): 274–285. doi: 10.1016/j.marchem.2005.03.008

238. Fry B, Sherr EB (1989) δ 13 C measurements as indicators of carbon flow in marine and freshwater ecosystems. In: In Stable isotopes in ecological research, pp 196–229

239. Freudenthal T, Wagner T, Wenzhöfer F et al. (2001) Early diagenesis of organic matter from sediments of the eastern subtropical Atlantic: Evidence from stable nitrogen and carbon isotopes. Geochimica et Cosmochimica Acta 65(11): 1795–1808

240. Schubert CJ, Calvert SE (2001) Nitrogen and carbon isotopic composition of marine and terrestrial organic matter in Arctic Ocean sediments: implications for nutrient utilization and organic matter composition. Deep Sea Research Part I: Oceanographic Research Papers 48(3): 789–810

241. Osmond CB, Valaane N, Haslam SM et al. (1981) Comparisons of δ 13 C values in leaves of aquatic macrophytes from different habitats in Britain and Finland; some implications for photosynthetic processes in aquatic plants. Oecologia 50(1): 117–124

242. Keeley JE, Sandquist DR (1992) Carbon: freshwater plants. Plant, Cell & Environment 15(9): 1021–1035

243. Prahl FG, Bennett JT, Carpenter R (1980) The early diagenesis of aliphatic hydrocarbons and organic matter in sedimentary particulates from Dabob Bay, Washington. Geochimica et Cosmochimica Acta 44(12): 1967–1976

244. Tyson RV (1995) Sedimentary organic matter: organic facies and palynofacies

245. Meyers PA (1994) Preservation of elemental and isotopic source identification of sedimentary organic matter. Chemical Geology 114(3-4): 289–302

246. Schidlowski M, Hayes JM, Kaplan IR (1983) Isotopic inferences of ancient biochemistries-Carbon, sulfur, hydrogen, and nitrogen.

247. Haines EB (1976) Stable carbon isotope ratios in the biota, soils and tidal water of a Georgia salt marsh. Estuarine and Coastal Marine Science 4(6): 609–616

248. Chivas AR, García A, van der Kaars S et al. (2001) Sea-level and environmental changes since the last interglacial in the Gulf of Carpentaria, Australia: an overview 83: 19–46

249. Coffin RB, Fry B, Peterson BJ et al. (1989) Carbon isotopic compositions of estuarine bacteria. Limnology and Oceanography 34(7): 1305–1310

250. Nakagawa F, Yoshida N, Sugimoto A et al. (2002) Stable isotope and radiocarbon compositions of methane emitted from tropical rice paddies and swamps in Southern Thailand. Biogeochemistry 61(1): 1–19

251. Yamaguchi H, Montani S, Tsutsumi H et al. (2003) Estimation of particulate organic carbon flux in relation to photosynthetic production in a shallow coastal area in the Seto Inland Sea. Mar Pollut Bull 47(1-6): 18–24. doi: 10.1016/S0025-326X(02)00414-9

252. Bordovskiy OK (1965) Accumulation and transformation of organic substances in marine sediments. Mar. Geol 3: 3–114

253. Weiguo L, Zisheng A, Weijian Z et al. (2003) Carbon isotope and C/N ratios of suspended matter in rivers. Applied Geochemistry 18(8): 1241–1249. doi: 10.1016/S0883-2927(02)00249-4

254. Tue NT, Quy TD, Hamaoka H et al. (2012) Sources and Exchange of Particulate Organic Matter in an Estuarine Mangrove Ecosystem of Xuan Thuy National Park, Vietnam. Estuaries and Coasts 35(4): 1060–1068. doi: 10.1007/s12237-012-9487-x

255. Tue NT, Quy TD, Amano A et al. (2012) Historical Profiles of Trace Element Concentrations in Mangrove Sediments from the Ba Lat Estuary, Red River, Vietnam. Water Air Soil Pollut 223(3): 1315–1330. doi: 10.1007/s11270-011-0947-x

256. Volkman JK, Barrett SM, Blackburn SI et al. (1998) Microalgal biomarkers: A review of recent research developments. Organic Geochemistry 29(5-7): 1163–1179. doi: 10.1016/S0146-6380(98)00062-X

257. Eglinton G, Hamilton RJ (1967) Leaf epicuticular waxes. Science 156(3780): 1322–1335

258. Su J, Pohlmann T (2009) Wind and topography influence on an upwelling system at the eastern Hainan coast. J. Geophys. Res. 114(C6): 165. doi: 10.1029/2008JC005018

259. Tanski G, Lantuit H, Ruttor S et al. (2017) Transformation of terrestrial organic matter along thermokarst-affected permafrost coasts in the Arctic. Sci Total Environ 581-582: 434–447. doi: 10.1016/j.scitotenv.2016.12.152

260. Mudge SM, Ball AS (1964) Sewage. In: Environmental Forensics; Academic Press, pp 35–53

261. Jost R (2000) Milk and Dairy Products. In: Ullmann's Encyclopedia of Industrial Chemistry, 1 - 3. Wiley-VCH Verlag GmbH & Co. KGaA, Weinheim, Germany, p 3228

262. Gagosian RB, Smith S, Lee C et al. (1980) Steroid transformations in Recent marine sediments. Physics and Chemistry of the Earth 12: 407–419

263. Kohnen MEL, Sinninghe Damsté JS, Knock-van Dalen AC et al. (1990) Origin and diagenetic transformation of C25 and C30 highly branched isoprenoid sulphur compounds: Further evidence for the organically bound sulphur during early diagenesis. Geochimica et Cosmochimica Acta 54: 3053–3063

264. Wang L, Pan W, Zhuang W et al. (2018) Analysis of seasonal characteristics of water exchange in Beibu Gulf based on a particle tracking model. Regional Studies in Marine Science 18: 35–43. doi: 10.1016/j.rsma.2017.12.009

265. Kumari R, Mallavarapu GR, Jain VK et al. (2012) Chemical composition of the fatty oils of the seeds of Cleome viscosa accessions. Natural product communications 7(10): 1934578X1200701029

266. Horvat RJ (1978) Identification of Some New Minor Acids from Chicken Skin Lipids. Poultry Sci 57: 827–828

267. Torres AG, Ney JG, Meneses F et al. (2006) Polyunsaturated fatty acids and conjugated linoleic acid isomers in breast milk are associated with plasma non-esterified and erythrocyte membrane fatty acid composition in lactating women. Br J Nutr 95(3): 517–524. doi: 10.1079/BJN20051645

268. Dabire CLB, Niango Ba M, Sanon A (2008) Effects of crushed fresh Cleome viscosa L. (Capparaceae) plants on the cowpea storage pest, Callosobruchus maculatus Fab. (Coleoptera: Bruchidae). International Journal of Pest Management 54(4): 319–326. doi: 10.1080/09670870802266953

269. Hansen RP, Shorland FB, Cooke NJ (1954) The occurrence of n-heptadecanoic acid (margaric acid) in hydrogenated mutton fat. Biochemical Journal 58(4): 513

270. Lim TK (2012) Durio graveolens. In: T. K. L (ed) Edible Medicinal and Non-Medicinal Plants, vol 4. Springer Netherlands, Dordrecht, pp 552–555

271. Su G, Wang T (1994) Basic characteristics of modern sedimentation in the South China Sea.: In: Zhou, D.; Liang, Y.B.; Zheng, C.K. (eds.), Oceanology of China Seas. Kluwer, New York, pp. 407-418

272. Skerratt JH, Nichols PD, Bowman JP et al. (1992) Occurrence and significance of long-chain (ω-1)-hydroxy fatty acids in methane-utilizing bacteria. Organic Geochemistry 18(2): 189–194

273. Klok J, Baas M, Cox HC et al. (1988) The mode of occurrence of lipids in a Namibian Shelf diatomaceous ooze with emphasis on the β-hydroxy fatty acids. Organic Geochemistry 12(1): 75–80

274. Voss M, Bombar D, Loick N et al. (2006) Riverine influence on nitrogen fixation in the upwelling region off Vietnam, South China Sea. Geophys. Res. Lett. 33(7): 1356. doi: 10.1029/2005GL025569

275. Gaye B, Wiesner MG, Lahajnar N (2009) Nitrogen sources in the South China Sea, as discerned from stable nitrogen isotopic ratios in rivers, sinking particles, and sediments. Marine Chemistry 114(3-4): 72–85. doi: 10.1016/j.marchem.2009.04.003

276. Grosse J, Bombar D, Doan HN et al. (2010) The Mekong River plume fuels nitrogen fixation and determines phytoplankton species distribution in the South China Sea during low- and high-discharge season. Limnology and Oceanography 55(4): 1668–1680

277. Zimmerman AR, Canuel EA (2001) Bulk Organic Matter and Lipid Biomarker Composition of Chesapeake Bay Surficial Sediments as Indicators of Environmental Processes. Estuarine, Coastal and Shelf Science 53(3): 319–341. doi: 10.1006/ecss.2001.0815

278. Eglinton G, Hunneman DH, Douraghi-Zadeh K (1968) Gas Chromatographic- Mass Spectrometric Studies of Long Chain Hydroxy Acids-II: The Hydroxy Acids and Fatty Acids of a 5000 Year old Lacustrine sediement. Pergamon Press 1968 24,.: 5929–5941

279. Ludwig W, Probst J-L, Kempe S (1996) Predicting the oceanic input of organic carbon by continental erosion. Global Biogeochemical Cycles 10(1): 23–41

280. Galy V, France-Lanord C, Beyssac O et al. (2007) Efficient organic carbon burial in the Bengal fan sustained by the Himalayan erosional system. Nature 450(7168): 407

281. Schlünz B, Schneider RR (2000) Transport of terrestrial organic carbon to the oceans by rivers: re-estimating flux-and burial rates. International Journal of Earth Sciences 88(4): 599–606

282. Burdige DJ (2005) Burial of terrestrial organic matter in marine sediments: A re-assessment. Global Biogeochem. Cycles 19(4): n/a-n/a. doi: 10.1029/2004GB002368

283. Berner R (1982) Burial of Organic Carbon and Pyrite sulphur in the modern Ocean: Its Geochemical and Environmental significance. American Journal of Science 282: 451–473

284. Hedges JI, Keil RG (1995) Sedimentary organic matter preservation: an assessment and speculative synthesis. Marine Chemistry 49: 137–139

285. Huang TH, Chen CTA, Tseng HC et al. (2017) Riverine carbon fluxes to the South China Sea. J. Geophys. Res. Biogeosci. 122(5): 1239–1259. doi: 10.1002/2016JG003701

286. Vannote RL, Minshall GW, Cummins KW et al. (1980) The River Continuum Concept. Canadian journal of fisheries and aquatic sciences: 130–137

287. Poole GC (2002) Fluvial landscape ecology: addressing uniqueness within the river discontinuum. Freshwater Biology 47(4): 641–660

288. Townsend-Small A, McClain ME, Brandes JA (2005) Contributions of carbon and nitrogen from the Andes Mountains to the Amazon River: Evidence from an elevational gradient of soils, plants, and river material. Limnology and Oceanography 50(2): 672–685

289. Stern MK, Day JW, Teague KG (1991) Nutrient transport in a riverine-influenced, tidal freshwater bayou in Louisiana. Estuaries 14(4): 382–394

290. DeLaune RD, Pezeshki SR, Jugsujinda A (2005) Impact of Mississippi River freshwater reintroduction on Spartina patens marshes: responses to nutrient input and lowering of salinity. Wetlands 25(1): 155–161

291. Rojana-anawat P, Pradit S, Sukramongkol N (2001) Temperature, Salinity, Dissolved Oxygen and Water Masses of Vietnamese Waters. Southeast Asian Fisheries Development Center 18-20: 46–355

292. Alcaraz M, Marrasé C, Peters F et al. (2001) Seawater–atmosphere O2 exchange rates in open-top laboratory microcosms: application for continuous estimates of planktonic primary production and respiration. Journal of Experimental Marine Biology and Ecology 257(1): 1–12

293. Ganzeveld L, Helmig D, Fairall CW et al. (2009) Atmosphere-ocean ozone exchange: A global modeling study of biogeochemical, atmospheric, and waterside turbulence dependencies. Global Biogeochem. Cycles 23(4): n/a-n/a. doi: 10.1029/2008GB003301

294. Caradec S, Grossi V, Gilbert F et al. (2004) Influence of various redox conditions on the degradation of microalgal triacylglycerols and fatty acids in marine sediments. Organic Geochemistry 35(3): 277–287. doi: 10.1016/j.orggeochem.2003.11.006

295. Basile-Doelsch I, Amundson R, Stone WEE et al. (2007) Mineral control of carbon pools in a volcanic soil horizon. Geoderma 137(3-4): 477–489. doi: 10.1016/j.geoderma.2006.10.006

296. Eusterhues K, Rumpel C, Kleber M et al. (2003) Stabilisation of soil organic matter by interactions with minerals as revealed by mineral dissolution and oxidative degradation. Organic Geochemistry 34(12): 1591–1600. doi: 10.1016/j.orggeochem.2003.08.007

297. Aller RC, Blair NE (2006) Carbon remineralization in the Amazon–Guianas tropical mobile mudbelt: A sedimentary incinerator. Continental Shelf Research 26(17-18): 2241–2259. doi: 10.1016/j.csr.2006.07.016

298. Aller RC, Blair NE, Brunskill GJ (2008) Early diagenetic cycling, incineration, and burial of sedimentary organic carbon in the central Gulf of Papua (Papua New Guinea). J. Geophys. Res. 113(F1): 2395. doi: 10.1029/2006JF000689

299. Saidy AR, Smernik RJ, Baldock JA et al. (2013) The sorption of organic carbon onto differing clay minerals in the presence and absence of hydrous iron oxide. Geoderma 209-210: 15–21. doi: 10.1016/j.geoderma.2013.05.026

300. Wang X, Ma H, Li R et al. (2012) Seasonal fluxes and source variation of organic carbon transported by two major Chinese Rivers: The Yellow River and Changjiang (Yangtze) River. Global Biogeochem. Cycles 26(2): n/a-n/a. doi: 10.1029/2011GB004130

301. Yu Z, Wang X, Han G et al. (2018) Organic and inorganic carbon and their stable isotopes in surface sediments of the Yellow River Estuary. Sci Rep 8(1): 10825. doi: 10.1038/s41598-018-29200-4

302. Yu F, Zong Y, Lloyd JM et al. (2010) Bulk organic δ13C and C/N as indicators for sediment sources in the Pearl River delta and estuary, southern China. Estuarine, Coastal and Shelf Science 87(4): 618–630. doi: 10.1016/j.ecss.2010.02.018

303. Ramaswamy V, Gaye B, Shirodkar PV et al. (2008) Distribution and sources of organic carbon, nitrogen and their isotopic signatures in sediments from the Ayeyarwady (Irrawaddy) continental shelf, northern Andaman Sea. Marine Chemistry 111(3-4): 137–150

304. Ray R, Michaud E, Aller RC et al. (2018) The sources and distribution of carbon (DOC, POC, DIC) in a mangrove dominated estuary (French Guiana, South America). Biogeochemistry 138(3): 297–321. doi: 10.1007/s10533-018-0447-9

305. Gingele FX, Deckker P de, Hillenbrand CD (2001) Clay mineral distribution in surface sediments between Indonesia and NW Australia—source and transport by ocean currents. Marine Geology 179(3-4): 135–146

306. Dauwe B, Middelburg JJ, Herman PMJ (2001) Effect of oxygen on the degradability of organic matter in subtidal and intertidal sediments of the North Sea area. Marine Ecology Progress Series 215: 13–22

307. Drake DE, Eganhouse R, McArthur W (2002) Physical and chemical effects of grain aggregates on the Palos Verdes margin, southern California. Continental Shelf Research 22(6-7): 967–986

308. Wefer G (1991) Stofftransport zum Meeresboden: Eine Übersicht. Naturwissenschaften 78(1): 1–6. doi: 10.1007/BF01134033

309. Stein R, Grobe H, Wahsner M (1994) Organic carbon, carbonate, and clay mineral distributions in eastern central Arctic Ocean surface sediments. Marine Geology 119(3-4): 269–285

310. Ding Y, Chen C, Beardsley RC et al. (2013) Observational and model studies of the circulation in the Gulf of Tonkin, South China Sea. J. Geophys. Res. Oceans 118(12): 6495–6510. doi: 10.1002/2013JC009455

311. Kennedy MJ, Pevear DR, Hill RJ (2002) Mineral surface control of organic carbon in black shale. Science 295(5555): 657–660. doi: 10.1126/science.1066611

312. Liu Z, Zhao YL, Li JR et al. (2007) Late Quaternary clay minerals off Middle Vietnam in the western South China Sea: Implications for source analysis and East Asian monsoon evolution. SCI CHINA SER D 50(11): 1674–1684. doi: 10.1007/s11430-007-0115-8

313. Liu Z, Colin C, Li X et al. (2010) Clay mineral distribution in surface sediments of the northeastern South China Sea and surrounding fluvial drainage basins: Source and transport. Marine Geology 277(1-4): 48–60. doi: 10.1016/j.margeo.2010.08.010

314. Liu Zi, Li XJ, Colin C et al. (2010) A high-resolution clay mineralogical record in the northern South China Sea since the Last Glacial Maximum, and its time series provenance analysis. Chin. Sci. Bull. 55(35): 4058–4068. doi: 10.1007/s11434-010-4149-5

315. Palamenghi L, Keil H, Spiess V (2015) Sequence stratigraphic framework of a mixed turbidite-contourite depositional system along the NW slope of the South China Sea. Geo-Mar Lett 35(1): 1–21. doi: 10.1007/s00367-014-0385-z

316. Stattegger K, Kuhnt W, Wong HK et al. (1997) Cruise Report SO-115 SUNDAFLUT: Berichte-Report 86, Institut für Geowissenschaften, Univ. Kiel 211 pp.

317. Katona O, Sipos G, Onaca A et al. (2012) Reconstruction of paleo-hydrology and fluvial architecture at the Orosháza paleo-channel of River Maros, Hungary. Journal of Environmental Geography 5(2)

318. Keil RG, Mayer LM, Quay PD et al. (1997) Loss of organic matter from riverine particles in deltas. Geochimica et Cosmochimica Acta 61(7): 1507–1511

319. Leithold EL, Blair NE, Wegmann KW (2016) Source-to-sink sedimentary systems and global carbon burial: A river runs through it. Earth-Science Reviews 153: 30–42. doi: 10.1016/j.earscirev.2015.10.011

320. Larsen IJ, Montgomery DR, Greenberg HM (2014) The contribution of mountains to global denudation. Geology 42(6): 527–530. doi: 10.1130/G35136.1

321. Hilton RG, Galy A, Hovius N (2008) Riverine particulate organic carbon from an active mountain belt: Importance of landslides. Global Biogeochem. Cycles 22(1): n/a-n/a. doi: 10.1029/2006GB002905

322. Hilton RG, Galy A, Hovius N et al. (2010) The isotopic composition of particulate organic carbon in mountain rivers of Taiwan. Geochimica et Cosmochimica Acta 74(11): 3164–3181. doi: 10.1016/j.gca.2010.03.004

323. Hilton RG, Meunier P, Hovius N et al. (2011) Landslide impact on organic carbon cycling in a temperate montane forest. Earth Surface Processes and Landforms 36(12): 1670–1679

324. Hilton RG, Galy A, Hovius N et al. (2012) Climatic and geomorphic controls on the erosion of terrestrial biomass from subtropical mountain forest. Global Biogeochem. Cycles 26(3): 383. doi: 10.1029/2012GB004314

325. Clark KE, Malhi Y, New M et al. (2013) New views on "old" carbon in the Amazon River: Insight from the source of organic carbon eroded from the Peruvian Andes. Geochemistry, Geophysics, Geosystems 14(5): 1644–1659

326. Tue NT, Nguyen PT, Quan DM et al. (2018) Sedimentary composition and organic carbon sources in mangrove forests along the coast of northeast Vietnam. Regional Studies in Marine Science 17: 87–94. doi: 10.1016/j.rsma.2017.12.001

327. Dedieu K, Rabouille C, Gilbert F et al. (2007) Coupling of carbon, nitrogen and oxygen cycles in sediments from a Mediterranean lagoon: a seasonal perspective. Mar. Ecol. Prog. Ser. 346: 45–59. doi: 10.3354/meps07031

328. Holmer M (1999) The Effect of Oxygen Depletion on Anaerobic Organic Matter Degradation in Marine Sediments. Estuarine, Coastal and Shelf Science 48(3): 383–390

329. Arndt S, Jørgensen BB, LaRowe DE et al. (2013) Quantifying the degradation of organic matter in marine sediments: A review and synthesis. Earth-Science Reviews 123: 53–86. doi: 10.1016/j.earscirev.2013.02.008

330. Weng Y-T, Wang C-C, Chiang C-C et al. (2018) In situ evidence of mineral physical protection and carbon stabilization revealed by nanoscale 3-D tomography. Biogeosciences 15(10): 3133–3142. doi: 10.5194/bg-15-3133-2018

331. Schimanski A, Stattegger K (2005) Deglacial and Holocene evolution of the Vietnam shelf: stratigraphy, sediments and sea-level change. Marine Geology 214(4): 365–387. doi: 10.1016/j.margeo.2004.11.001

332. Galy V, Eglinton TI (2011) Protracted storage of biospheric carbon in the Ganges–Brahmaputra basin. Nature Geosci 4(12): 843–847. doi: 10.1038/ngeo1293

333. Rosenheim BE, Roe KM, Roberts BJ et al. (2013) River discharge influences on particulate organic carbon age structure in the Mississippi/Atchafalaya River System. Global Biogeochem. Cycles 27(1): 154–166. doi: 10.1002/gbc.20018

334. Feng X, Feakins SJ, Liu Z et al. (2016) Source to sink: Evolution of lignin composition in the Madre de Dios River system with connection to the Amazon basin and offshore. J. Geophys. Res. Biogeosci. 121(5): 1316–1338. doi: 10.1002/2016JG003323

335. Kastner TP, Goñi MA (2003) Constancy in the vegetation of the Amazon Basin during the late Pleistocene: Evidence from the organic matter composition of Amazon deep sea fan sediments. Geol 31(4): 291. doi: 10.1130/0091-7613(2003)031<0291:CITVOT>2.0.CO;2

336. Kuehl SA, DeMaster DJ, Nittrouer CA (1986) Nature of sediment accumulation on the Amazon continental shelf. Continental Shelf Research 6(1-2): 209–225

337. Showers WJ, Angle DG (1986) Stable isotopic characterization of organic carbon accumulation on the Amazon continental shelf. Continental Shelf Research 6(1-2): 227–244

338. Sun S, Schefuß E, Mulitza S et al. (2017) Origin and processing of terrestrial organic carbon in the Amazon system: lignin phenols in river, shelf, and fan sediments. Biogeosciences 14(9): 2495–2512. doi: 10.5194/bg-14-2495-2017

339. Williams EK, Rosenheim BE, Allison M et al. (2015) Quantification of refractory organic material in Amazon mudbanks of the French Guiana Coast. Marine Geology 363: 93–101. doi: 10.1016/j.margeo.2015.02.009

340. Bianchi TS, Mitra S, McKee BA (2002) Sources of terrestrially-derived organic carbon in lower Mississippi River and Louisiana shelf sediments: implications for differential sedimentation and transport at the coastal margin. Marine Chemistry 77(2-3): 211–233

341. Goñi MA, Ruttenberg KC, Eglinton TI (1998) A reassessment of the sources and importance of land-derived organic matter in surface sediments from the Gulf of Mexico. Geochimica et Cosmochimica Acta 62(18): 3055–3075

342. Gordon ES, Goñi MA (2003) Sources and distribution of terrigenous organic matter delivered by the Atchafalaya River to sediments in the northern Gulf of Mexico. Geochimica et Cosmochimica Acta 67(13): 2359–2375. doi: 10.1016/S0016-7037(02)01412-6

343. Gordon ES, Goñi MA (2004) Controls on the distribution and accumulation of terrigenous organic matter in sediments from the Mississippi and Atchafalaya river margin. Marine Chemistry 92(1-4): 331–352. doi: 10.1016/j.marchem.2004.06.035

344. Sampere TP, Bianchi TS, Allison MA (2011) Historical changes in terrestrially derived organic carbon inputs to Louisiana continental margin sediments over the past 150 years. J. Geophys. Res. 116(G1): 143. doi: 10.1029/2010JG001420

345. Sampere TP, Bianchi TS, Allison MA et al. (2011) Burial and degradation of organic carbon in Louisiana shelf/slope sediments. Estuarine, Coastal and Shelf Science 95(1): 232–244. doi: 10.1016/j.ecss.2011.09.003

346. Sampere TP, Bianchi TS, Wakeham SG et al. (2008) Sources of organic matter in surface sediments of the Louisiana Continental margin: Effects of major depositional/transport pathways and Hurricane Ivan. Continental Shelf Research 28(17): 2472–2487. doi: 10.1016/j.csr.2008.06.009

347. Wakeham SG, Canuel EA, Lerberg EJ et al. (2009) Partitioning of organic matter in continental margin sediments among density fractions. Marine Chemistry 115(3-4): 211–225. doi: 10.1016/j.marchem.2009.08.005

348. Waterson EJ, Canuel EA (2008) Sources of sedimentary organic matter in the Mississippi River and adjacent Gulf of Mexico as revealed by lipid biomarker and δ13CTOC analyses. Organic Geochemistry 39(4): 422–439. doi: 10.1016/j.orggeochem.2008.01.011

349. Wang J, Yao P, Bianchi TS et al. (2015) The effect of particle density on the sources, distribution, and degradation of sedimentary organic carbon in the Changjiang Estuary and adjacent shelf. Chemical Geology 402: 52–67. doi: 10.1016/j.chemgeo.2015.02.040

350. Wang XC, Li AC (2007) Preservation of black carbon in the shelf sediments of the East China Sea. Chin. Sci. Bull. 52(22): 3155–3161. doi: 10.1007/s11434-007-0452-1

351. Wu Y, Eglinton T, Yang L et al. (2013) Spatial variability in the abundance, composition, and age of organic matter in surficial sediments of the East China Sea. J. Geophys. Res. Biogeosci. 118(4): 1495–1507. doi: 10.1002/2013JG002286

352. Yao P, Yu Z, Bianchi TS et al. (2015) A multiproxy analysis of sedimentary organic carbon in the Changjiang Estuary and adjacent shelf. J. Geophys. Res. Biogeosci. 120(7): 1407–1429. doi: 10.1002/2014JG002831

353. Liu Z, Zhao M, Sun H et al. (2017) "Old" carbon entering the South China Sea from the carbonate-rich Pearl River Basin: Coupled action of carbonate weathering and aquatic photosynthesis. Applied Geochemistry 78: 96–104. doi: 10.1016/j.apgeochem.2016.12.014

354. Tao S, Eglinton TI, Montluçon DB et al. (2016) Diverse origins and pre-depositional histories of organic matter in contemporary Chinese marginal sea sediments. Geochimica et Cosmochimica Acta 191: 70–88. doi: 10.1016/j.gca.2016.07.019

355. Blair NE, Leithold EL, Aller RC (2004) From bedrock to burial: the evolution of particulate organic carbon across coupled watershed-continental margin systems. Marine Chemistry 92(1-4): 141–156. doi: 10.1016/j.marchem.2004.06.023

356. Huy PQ (2012) Overview of Coal Mine Methane in Vietnam, Hanoi

357. DeMaster D, Thomas CJ, Blair NE et al. (2002) Deposition of bomb 14Cin continental slope sediments of the Mid-Atlantic Bight: assessing organic matter sources and burial rates. Deep-Sea Research II 49: 4667–4685

358. Purinton BL, DeMaster DJ, Thomas CJ et al. (2008) 14C as a tracer of labile organic matter in Antarctic benthic food webs. Deep Sea Research Part II: Topical Studies in Oceanography 55(22-23): 2438–2450. doi: 10.1016/j.dsr2.2008.06.004

359. Thompson C (2009) Tracking Organic Matter from Source to Sink in the Waiapu River Watershed, New Zealand: A Geochemical Perspective. Dissertation

360. Komada T, Burdige DJ, Magen C et al. (2016) Recycling of Organic Matter in the Sediments of Santa Monica Basin, California Borderland. Aquat Geochem 22(5-6): 593–618. doi: 10.1007/s10498-016-9308-0

361. Foster IDL, Walling DE (1994) Using reservoir deposits to reconstruct changing sediment yields and sources in the catchment of the Old Mill Reservoir, South Devon, UK, over the past 50 years. Hydrological Sciences Journal 39(4): 347–368. doi: 10.1080/02626669409492755

362. Rowntree K, Foster I (2012) A reconstruction of historical changes in sediment sources, sediment transfer and sediment yield in a small, semi-arid Karoo catchment, semi-arid South Africa. Zeitschrift für Geomorphologie, Supplementary Issues 56(1): 87–100. doi: 10.1127/0372-8854/2012/S-00074

363. Wang H, Dai M, Liu J et al. (2016) Eutrophication-Driven Hypoxia in the East China Sea off the Changjiang Estuary. Environ Sci Technol 50(5): 2255–2263. doi: 10.1021/acs.est.5b06211

364. Ellison AM (2004) Bayesian inference in ecology. Ecol Letters 7(6): 509–520. doi: 10.1111/j.1461-0248.2004.00603.x

365. Fernandes R, Millard AR, Brabec M et al. (2014) Food reconstruction using isotopic transferred signals (FRUITS): a Bayesian model for diet reconstruction. PLoS ONE 9(2): e87436. doi: 10.1371/journal.pone.0087436

366. Masjkur M, Folmer H (2017) Bayesian estimation of linear and nonlinear mixed models of fertilizer dosing with independent normally distributed random components. IOP Conf. Ser.: Earth Environ. Sci. 58: 12006. doi: 10.1088/1755-1315/58/1/012006

367. Lamade E, Setiyo IE, Girard S et al. (2009) Changes in 13C/12C of oil palm leaves to understand carbon use during their passage from heterotrophy to autotrophy. Rapid Commun Mass Spectrom 23(16): 2586–2596. doi: 10.1002/rcm.4169

368. Rosenheim BE, Galy V (2012) Direct measurement of riverine particulate organic carbon age structure. Geophys. Res. Lett. 39(19): n/a-n/a. doi: 10.1029/2012GL052883

369. Phillips DL, Gregg JW (2003) Source partitioning using stable isotopes: coping with too many sources. Oecologia 136(2): 261–269. doi: 10.1007/s00442-003-1218-3

370. Liu Z, Yang H, Liu Q (2001) Regional Dynamics of Seasonal Variability in the South China Sea. J. Phys. Oceanogr. 31(1): 272–284. doi: 10.1175/1520-0485(2001)031<0272:RDOSVI>2.0.CO;2

371. Zhong M, Tang J, Mi L et al. (2017) Occurrence and spatial distribution of organophosphorus flame retardants and plasticizers in the Bohai and Yellow Seas, China. Mar Pollut Bull 121(1-2): 331–338. doi: 10.1016/j.marpolbul.2017.06.034

372. Timmons FL (2005) A History of Weed Control in the United States and Canada. Weed Science 53(6): 748–761

373. Shaner DL (2014) Herbicide Handbook. Weed Science Society of America Tenth Edition. 810E. 10th Street Lawrence

374. Leiber MA, Berk HC (1984) Development and validation of an air monitoring method for 1,3-dichloropropene, trans-1,2,3-trichloropropene, cis-1,2,3-trichloropropene, 1,1,2,3-tetrachloropropene, 2,3,3-trichloro-2-propen-1-ol, and 1,1,2,2,3-pentachloropropane. Analytical chemistry 56(12): 2134–2137

375. Christensen VG (2007) Nutrients, Suspended Sediment, and Pesticides in Water of the Red River of the North Basin, Minnesota and North Dakota, 1990-2004: Scientific Investigations Report 2007–5065. U.S Geological Survey Scientific Investigations Report 2007–5065,: 36p.

376. Monsanto Company (1989 (May)) Toxicology Information Summary for Triallate. Monsanto Co., St. Louis, MO

377. Meister RT (ed) (1991) Farm Chemicals Handbook '91. Meister Publishing Company, Willoughby, OH.

378. US EPA. (2001) Office of Pesticide Programs: US EPA - Pesticides - Fact Sheet for Triallate. National Service Center for Environmental Publications (EPA/NSCEP), PO Box 42419, Cincinnati, OH

379. Cao S, Zeng X, Song H et al. (2012) Levels and distributions of organophosphate flame retardants and plasticizers in sediment from Taihu Lake, China. Environ Toxicol Chem 31(7): 1478–1484. doi: 10.1002/etc.1872

380. Wang Y, Wu X, Zhang Q et al. (2017) Organophosphate esters in sediment cores from coastal Laizhou Bay of the Bohai Sea, China. Sci Total Environ 607-608: 103–108. doi: 10.1016/j.scitotenv.2017.06.259

381. Marklund A, Andersson B, Haglund P (2003) Screening of organophosphorus compounds and their distribution in various indoor environments. Chemosphere 53(9): 1137–1146. doi: 10.1016/S0045-6535(03)00666-0

382. Marklund A, Andersson B, Haglund P (2005) Organophosphorus flame retardants and plasticizers in Swedish sewage treatment plants. Environ Sci Technol 39(19): 7423–7429. doi: 10.1021/es051013l

383. Salamova A, Hermanson MH, Hites RA (2014) Organophosphate and halogenated flame retardants in atmospheric particles from a European Arctic site. Environ Sci Technol 48(11): 6133–6140. doi: 10.1021/es500911d

384. Sühring R, Byer J, Freese M et al. (2014) Brominated flame retardants and Dechloranes in European and American eels from glass to silver life stages. Chemosphere 116: 104–111

385. van den Eede N, Neels H, Jorens PG et al. (2013) Analysis of organophosphate flame retardant diester metabolites in human urine by liquid chromatography electrospray ionisation tandem mass spectrometry. J Chromatogr A 1303: 48–53. doi: 10.1016/j.chroma.2013.06.042

386. Tollbäck J, Isetun S, Colmsjö A et al. (2010) Dynamic non-equilibrium SPME combined with GC, PICI, and ion trap MS for determination of organophosphate esters in air. Anal Bioanal Chem 396(2): 839–844. doi: 10.1007/s00216-009-3221-y

387. Takigami H, Suzuki G, Hirai Y et al. (2009) Flame retardants in indoor dust and air of a hotel in Japan. Environ Int 35(4): 688–693. doi: 10.1016/j.envint.2008.12.007

388. Stapleton HM, Klosterhaus S, Eagle S et al. (2009) Detection of organophosphate flame retardants in furniture foam and U.S. house dust. Environ Sci Technol 43(19): 7490–7495. doi: 10.1021/es9014019

389. Chen X, Bester K (2009) Determination of organic micro-pollutants such as personal care products, plasticizers and flame retardants in sludge. Anal Bioanal Chem 395(6): 1877–1884. doi: 10.1007/s00216-009-3138-5

390. Martínez-Carballo E, González-Barreiro C, Sitka A et al. (2007) Determination of selected organophosphate esters in the aquatic environment of Austria. Sci Total Environ 388(1-3): 290–299. doi: 10.1016/j.scitotenv.2007.08.005

391. Bacaloni A, Cucci F, Guarino C et al. (2008) Occurrence of organophosphorus flame retardant and plasticizers in three volcanic lakes of central Italy. Environ Sci Technol 42(6): 1898–1903. doi: 10.1021/es702549g

392. Bollmann UE, Möller A, Xie Z et al. (2012) Occurrence and fate of organophosphorus flame retardants and plasticizers in coastal and marine surface waters. Water Research 46(2): 531–538. doi: 10.1016/j.watres.2011.11.028

393. Regnery J, Püttmann W, Merz C et al. (2011) Occurrence and distribution of organophosphorus flame retardants and plasticizers in anthropogenically affected groundwater. J Environ Monit 13(2): 347–354. doi: 10.1039/c0em00419g

394. Wang R, Tang J, Xie Z et al. (2015) Occurrence and spatial distribution of organophosphate ester flame retardants and plasticizers in 40 rivers draining into the Bohai Sea, north China. Environ Pollut 198: 172–178. doi: 10.1016/j.envpol.2014.12.037

395. Reemtsma T, Quintana JB, Rodil R et al. (2008) Organophosphorus flame retardants and plasticizers in water and air I. Occurrence and fate. TrAC Trends in Analytical Chemistry 27(9): 727–737. doi: 10.1016/j.trac.2008.07.002

396. García-López M, Rodríguez I, Cela R (2009) Pressurized liquid extraction of organophosphate triesters from sediment samples using aqueous solutions. J Chromatogr A 1216(42): 6986–6993. doi: 10.1016/j.chroma.2009.08.068

397. García-López M, Rodríguez I, Cela R et al. (2009) Determination of organophosphate flame retardants and plasticizers in sediment samples using microwave-assisted extraction and gas chromatography with inductively coupled plasma mass spectrometry. Talanta 79(3): 824–829. doi: 10.1016/j.talanta.2009.05.006

398. Chung H-W, Ding W-H (2009) Determination of organophosphate flame retardants in sediments by microwave-assisted extraction and gas chromatography-mass spectrometry with electron impact and chemical ionization. Anal Bioanal Chem 395(7): 2325–2334. doi: 10.1007/s00216-009-3139-4

399. Ma Y, Xie Z, Lohmann R et al. (2017) Organophosphate Ester Flame Retardants and Plasticizers in Ocean Sediments from the North Pacific to the Arctic Ocean. Environ Sci Technol 51(7): 3809–3815. doi: 10.1021/acs.est.7b00755

400. Mihajlović I, Miloradov MV, Fries E (2011) Application of Twisselmann extraction, SPME, and GC-MS to assess input sources for organophosphate esters into soil. Environ Sci Technol 45(6): 2264–2269. doi: 10.1021/es103870f

401. Shah M, Meija J, Cabovska B et al. (2006) Determination of phosphoric acid triesters in human plasma using solid-phase microextraction and gas chromatography coupled to inductively coupled plasma mass spectrometry. J Chromatogr A 1103(2): 329–336. doi: 10.1016/j.chroma.2005.11.042

402. Schindler BK, Förster K, Angerer J (2009) Determination of human urinary organophosphate flame retardant metabolites by solid-phase extraction and gas chromatography-tandem mass spectrometry. J Chromatogr B Analyt Technol Biomed Life Sci 877(4): 375–381. doi: 10.1016/j.jchromb.2008.12.030

403. Kim J-W, Isobe T, Muto M et al. (2014) Organophosphorus flame retardants (PFRs) in human breast milk from several Asian countries. Chemosphere 116: 91–97. doi: 10.1016/j.chemosphere.2014.02.033

404. Möller A, Sturm R, Xie Z et al. (2012) Organophosphorus flame retardants and plasticizers in airborne particles over the Northern Pacific and Indian Ocean toward the Polar Regions: evidence for global occurrence. Environ Sci Technol 46(6): 3127–3134. doi: 10.1021/es204272v

405. Castro-Jiménez J, González-Gaya B, Pizarro M et al. (2016) Organophosphate Ester Flame Retardants and Plasticizers in the Global Oceanic Atmosphere. Environ Sci Technol 50(23): 12831–12839. doi: 10.1021/acs.est.6b04344

406. Möller A, Xie Z, Caba A et al. (2011) Organophosphorus flame retardants and plasticizers in the atmosphere of the North Sea. Environ Pollut 159(12): 3660–3665. doi: 10.1016/j.envpol.2011.07.022

407. Castro-Jiménez J, Berrojalbiz N, Pizarro M et al. (2014) Organophosphate ester (OPE) flame retardants and plasticizers in the open Mediterranean and Black Seas atmosphere. Environ Sci Technol 48(6): 3203–3209. doi: 10.1021/es405337g

408. Dachs J, Lohmann R, Ockenden WA et al. (2002) Oceanic biogeochemical controls on global dynamics of persistent organic pollutants. Environ Sci Technol 36(20): 4229–4237. doi: 10.1021/es025724k

409. Jaward FM, Farrar NJ, Harner T et al. (2004) Passive air sampling of PCBs, PBDEs, and organochlorine pesticides across Europe. Environ Sci Technol 38(1): 34–41. doi: 10.1021/es034705n

410. Meyer J, Bester K (2004) Organophosphate flame retardants and plasticisers in wastewater treatment plants. J Environ Monit 6(7): 599–605. doi: 10.1039/b403206c

411. van der Veen I, Boer Jd (2012) Phosphorus flame retardants: properties, production, environmental occurrence, toxicity and analysis. Chemosphere 88(10): 1119–1153. doi: 10.1016/j.chemosphere.2012.03.067

412. Dachs J, Eisenreich SJ, Baker, J, E. et al. (1999) Coupling of Phytoplankton Uptake and Air−Water Exchange of Persistent Organic Pollutants. Environ. Sci. Technol. 33(20): 3653–3660. doi: 10.1021/es990168o

413. Cristale J, García Vázquez A, Barata C et al. (2013) Priority and emerging flame retardants in rivers: occurrence in water and sediment, Daphnia magna toxicity and risk assessment. Environ Int 59: 232–243. doi: 10.1016/j.envint.2013.06.011

414. Truong JW, Diamond ML, Helm PA et al. (2017) Isomers of tris(chloropropyl) phosphate (TCPP) in technical mixtures and environmental samples. Anal Bioanal Chem 409(30): 6989–6997. doi: 10.1007/s00216-017-0572-7

415. Truong JW (2016) Organophosphate Esters (OPEs) as Emerging Contaminants in the Environment: Indoor Sources and Transport to Receiving Waters. Doctoral dissertation, University of Toronto

416. Rios LM, Jones PR, Moore C et al. (2010) Quantitation of persistent organic pollutants adsorbed on plastic debris from the Northern Pacific Gyre's "eastern garbage patch". J Environ Monit 12(12): 2226–2236. doi: 10.1039/c0em00239a

417. Antunes JC, Frias JGL, Micaelo AC et al. (2013) Resin pellets from beaches of the Portuguese coast and adsorbed persistent organic pollutants. Estuarine, Coastal and Shelf Science 130: 62–69. doi: 10.1016/j.ecss.2013.06.016

418. Jambeck JR, Geyer R, Wilcox C et al. (2015) Plastic waste inputs from land into the ocean. Science 347(6223): 768–771. doi: 10.1126/science.1260879

419. Grover R (1974) Adsorption and Desorption of Trifluralin, Triallate, and Diallate by Various Adsorbents. Weed sci. 22(4): 405–408. doi: 10.1017/S004317450003753X

420. Eglinton TI, Aluwihare LI, Bauer JE et al. (1996) Gas chromatographic isolation of individual compounds from complex matrices for radiocarbon dating. Analytical chemistry 68(5): 904–912

421. Eglinton TI, Benitez-Nelson BC, Pearson A et al. (1997) Variability in Radiocarbon Ages of Individual Organic Compounds from Marine Sediments. Science 277(5327): 796–799. doi: 10.1126/science.277.5327.796

422. Pearson A, McNichol AP, Schneider RJ et al. (1997) Microscale AMS 14 C measurement at NOSAMs. Radiocarbon 40(1): 61–75

Appendix 1) Results of estuary and marine surface sediments measurements of carbon, nitrogen, organic carbon, $\delta^{13}C_{org}$, mineral surface area and radiocarbon ^{14}C

sample no.	Lat. N DD	Long. E DD	depth [m]	C_{total} [%]	N_{total} [%]	C_{org} [%]	$\delta^{13}C_{org}$	surface area [$m^2\ g^{-1}$]	F_m
SCS-SO-220-19-27	20.29	109.14	19.00	0.94	0.07	0.55	-22.4	18.44	0.78
SCS-SO-220-22-3	20.48	108.75	43.00	1.49	0.13	0.89	-21.5	23.52	0.86
SCS-SO-220-23-3	21.10	108.73	22.00	0.64	0.05	0.34	-22.4	14.50	
SCS-SO-220-24-1	21.11	108.71	22.00	0.98	0.11	0.70	-22.2	18.11	0.87
SCS-SO-220-26-4	21.06	108.34	27.00	1.13	0.09	0.76	-21.8	22.54	0.90
SCS-SO-220-27-1	21.04	108.30	27.00	1.16	0.12	0.80	-21.9	20.57	0.87
SCS-SO-220-28-3	20.83	108.29	43.00	1.20	0.11	0.78	-21.6	22.05	0.87
SCS-SO-220-29-3	20.40	108.38	44.00	0.61	0.04	0.27	-22.3	6.51	0.84
SCS-SO-220-30-28	20.05	108.03	48.00	0.59	0.03	0.16	-23.5	4.05	0.78
SCS-SO-220-31-2	20.01	108.09	27.00	1.11	0.03	0.21	-23.5	11.72	
SCS-SO-220-32-3	19.99	108.12	63.00	1.67	0.07	0.48	-22.1	17.99	
SCS-SO-220-33-3	19.99	108.34	56.00	0.96	0.04	0.23	-22.2	7.50	
SCS-SO-220-34-3	19.46	108.29	57.00	1.53	0.10	0.75	-21.9	21.42	0.83
SCS-SO-220-35-3	19.23	108.15	44.00	1.44	0.09	0.56	-21.3	17.48	
SCS-SO-220-37-3	19.38	107.70	61.00	1.13	0.06	0.35	-21.5	12.23	
SCS-SO-220-38-3	19.42	107.57	61.00	1.38	0.10	0.63	-21.5	11.15	0.85
SCS-SO-220-39-3	19.42	107.36	63.00	1.49	0.09	0.59	-21.4	14.21	
SCS-SO-220-40-2	19.42	107.30	58.00	0.91	0.05	0.28	-21.4	10.62	
SCS-SO-220-42-28	18.74	107.16	60.00	1.77	0.11	0.75	-21.5	17.17	0.84
SCS-SO-220-43-2	18.79	107.17	60.00	1.74	0.12	0.71	-21.3	18.92	0.85
SCS-SO-220-44-3	18.74	107.20	67.00	1.84	0.09	0.74	-21.4	17.38	0.84
SCS-SO-220-45-2	18.73	107.27	66.00	1.73	0.12	0.77	-21.3	18.44	0.84
SCS-SO-220-51-3	18.38	108.06	75.00	1.58	0.09	0.57	-21.4	14.06	0.82
SCS-SO-220-52-1	18.37	108.06	72.00	1.53	0.08	0.52	-21.6	11.61	
SCS-SO-220-53-3	17.90	107.91	89.00	1.92	0.09	0.54	-21.6	7.92	
SCS-SO-220-54-2	17.89	107.90	90.00	1.66	0.06	0.56	-21.7	14.82	
SCS-SO-220-55-3	17.70	108.12	83.00	1.52	0.06	0.34	-21.7	10.75	
SCS-SO-220-57-3	17.64	108.40	105.00	1.84	0.07	0.40	-21.7	12.90	
SCS-SO-220-58-1	17.67	108.42	104.00	2.47	0.04	0.27	-21.9	5.98	0.87
SCS-SO-220-60-2	16.73	109.59	546.00	2.04	0.10	0.84	-21.9	11.39	0.80
SCS-SO-187-3-59-1	12.62	109.53	133.00	1.82	0.11	0.88	-22.6	9.70	0.91
SCS-SO-187-3-60-1	11.08	110.01	1859.00	2.04	0.15	0.95	-21.9		0.83
SCS-SO-187-3-61-1	11.43	111.28	2227.00	3.00	0.15	0.97	-21.3		0.82
SCS-SO-187-3-62-1	11.05	109.47	127.00	6.98	0.02	1.68	-23.2	2.64	0.60
SCS-SO-187-3-63-1	10.92	109.06	109.00	1.08	0.02	0.17	-22.8	3.36	0.83
SCS-SO-187-3-64-3	10.91	109.05	107.00	2.67	0.03	0.53	-22.8	5.46	0.85
SCS-SO-187-3-65-1	10.64	109.04	112.00	1.15	0.03	0.29	-22.8	5.80	0.87
SCS-SO-187-3-66-1	10.26	108.91	87.00	3.44	0.02	0.11	-23.1	2.27	0.74
SCS-SO-187-3-67-1	10.22	108.43	56.00	3.39	0.05	0.36	-21.8	5.82	0.89
SCS-SO-187-3-68-1	10.28	108.42	60.00	3.07	0.09	0.70	-22.0	12.55	0.93
SCS-SO-187-3-69-1	10.38	108.01	43.00	2.20	0.06	0.44	-21.9	9.91	0.89
SCS-SO-187-3-70-1	10.37	108.01	41.50	1.98	0.04	0.33	-21.7	8.72	0.91
SCS-SO-187-3-71-1	10.40	108.01	38.00	2.60	0.05	0.31	-21.5	4.04	0.92
SCS-SO-187-3-72-1	10.26	107.29	26.00	1.36	0.04	0.30	-22.1	3.98	
SCS-SO-187-3-73-1	10.24	107.28	31.00	1.51	0.05	0.37	-21.5	5.26	0.75
SCS-SO-187-3-74-1	10.23	107.28	29.00	1.32	0.04	0.28	-21.6	6.04	0.91
SCS-SO-187-3-75-1	10.11	107.11	21.00	0.85	0.01	0.08	-23.9	3.43	0.80

sample no.	Lat. N DD	Long. E DD	depth [m]	C_{total} [%]	N_{total} [%]	C_{org} [%]	$\delta^{13}C_{org}$	surface area [m^2 g^{-1}]	F_m
SCS-SO-187-3-76-1	9.48	106.82	24.00	0.46	0.02	0.11	-23.0	2.49	0.83
SCS-SO-187-3-77-B1	9.36	106.63	25.00	0.64	0.02	0.10	-23.6	3.37	
SCS-SO-187-3-78-1	8.97	106.70	32.00	0.43	0.01	0.07	-24.3	2.64	0.76
SCS-SO-187-3-79-1	9.14	107.07	33.00	1.51	0.01	0.11	-23.4	3.99	0.86
SCS-SO-187-3-80-1	9.23	107.28	38.00	1.25	b.d	0.08	-22.9	4.81	0.79
SCS-SO-187-3-81-1	9.26	107.33	38.00	2.13	0.01	0.10	-22.7	4.95	0.63
SCS-SO-187-3-82-1	9.52	107.50	39.00	0.66	0.02	0.13	-23.8	2.38	0.86
SCS-SO-187-3-83-1	9.90	107.50	31.00	0.84	0.01	0.10	-23.0	3.41	0.80
SCS-SO-187-3-84-1	9.73	107.29	33.00	0.80	0.01	0.08	-23.3	3.36	0.82
SCS-SO-187-3-85-1	9.80	107.04	27.00	0.75	0.02	0.12	-23.3	3.70	0.84
SCS-SO-187-3-86-1	8.74	106.16	27.00	0.71	0.01	0.09	-21.8	2.73	0.86
SCS-SO-187-3-87-2	9.04	106.08	20.00	9.09	0.792	4.312	-20.3	2.53	1.06
SCS-SO-187-3-91-1	8.44	105.24	31.00	2.61	0.05	0.46	-22.7	10.35	0.87
SCS-SO-187-3-92-1	8.42	105.20	30.00	1.80	0.10	0.69	-22.3	19.98	0.89
SCS-SO-187-3-93-1	8.39	105.11	32.00	2.47	0.10	0.78	-23.8	15.31	0.76
SCS-SO-187-3-94-1	8.37	104.63	24.00	7.11	0.05	3.21	-23.4	9.47	0.75
SCS-SO-187-3-95-1	8.38	104.62	29.00	4.49	0.04	0.49	-24.4	13.98	0.49
SCS-SO-187-3-96-1	8.41	104.57	31.00	1.53	0.10	0.87	-23.5	23.57	0.79
SCS-SO-187-3-97-2	8.41	104.56	30.00	2.22	0.10	0.75	-22.8	23.68	0.85
SCS-SO-187-3-98-1	8.46	104.47	30.00	2.16	0.10	0.79	-23.2	22.91	0.83
SCS-SO-187-3-99-1	8.47	104.46	30.00	1.36	0.12	0.90	-23.2	22.58	0.88
SCS-SO-187-3-100-1	8.52	104.34	28.00	3.00	0.04	0.24	-23.2	23.22	0.82
SCS-SO-187-3-102-1	8.44	104.23	29.00	1.47	0.11	0.81	-23.0	23.53	0.86
SCS-SO-187-3-103-1	8.43	104.21	28.00	3.60	0.08	0.52	-22.7	17.66	0.84
SCS-SO-187-3-104-1	8.38	104.22	26.00	6.42	0.04	0.30	-22.4	9.37	0.82
SCS-SO-187-3-105-1	8.19	104.52	25.00	3.74	0.04	0.29	-22.8	8.49	0.79
SCS-SO-187-3-106-1	8.19	104.56	26.00	2.41	0.07	0.64	-22.6	13.99	0.84
SCS-SO-187-3-107-1	8.16	104.57	27.50	1.89	0.10	0.67	-22.5	17.38	0.84
SCS-SO-187-3-108-1	8.12	104.95	32.00	6.27	0.04	0.22	-21.8	5.02	0.86
SCS-SO-187-3-109-1	8.12	105.24	33.00	4.06	0.03	0.24	-22.0	4.71	0.84
SCS-SO-187-3-110-1	8.12	105.28	32.00	9.73	0.02	0.15	-22.3	4.25	0.76
SCS-SO-187-3-111-1	8.12	105.38	34.00	6.28	0.04	0.26	-22.1	3.79	0.81
SCS-SO-187-3-112-1	8.12	105.39	33.00	6.75	0.04	0.24	-22.3	4.65	0.84
SCS-SO-187-3-113-1	8.12	105.48	32.00	5.65	0.03	0.21	-22.1	4.49	0.83
SCS-SO-187-3-114-1	8.12	105.59	32.00	2.99	0.03	0.19	-22.5	4.34	0.85
SCS-SO-187-3-115-1	8.12	105.60	32.00	2.84	0.05	0.29	-21.8	4.67	0.86
SCS-SO-187-3-116-1	8.12	105.94	33.00	3.35	0.03	0.26	-22.6	8.25	0.83
SCS-SO-187-3-117-1	8.12	105.95	32.00	2.85	0.03	0.17	-22.1	3.45	0.85
SCS-SO-140-01-18373-1	6.73	107.65	73.50	1.99	0.06	0.20	-23.1	4.31	
SCS-SO-140-02-18374-1	6.91	107.67	74.40	1.50	0.04	0.14	-22.9	4.34	
SCS-SO-140-03-18375-1	7.00	107.91	86.20	1.12	0.05	0.21	-23.3	3.77	0.81
SCS-SO-140-04-18376-1	7.09	108.11	89.60	1.05	0.03	0.10	-23.8	3.37	
SCS-SO-140-05-18377-1	7.18	108.34	98.80	0.90	0.03	0.15	-23.9	3.43	0.72
SCS-SO-140-06-18378-1	7.24	108.48	107.90	1.94	0.04	0.15	-23.4	3.48	
SCS-SO-140-07-18379-2	7.34	108.74	119.00	1.18	0.04	0.10	-24.2	2.68	0.68
SCS-SO-140-08-18380-1	7.44	108.99	149.70	0.64	0.04	0.08	-24.9	3.06	0.69

sample no.	Lat. N DD	Long. E DD	depth [m]	C_{total} [%]	N_{total} [%]	C_{org} [%]	$\delta^{13}C_{org}$	surface area [m^2 g^{-1}]	F_m
SCS-SO-140-09-18381-1	7.50	109.13	213.90	2.28	0.07	0.32	-22.2	5.99	
SCS-SO-140-10-18382-1	7.53	109.21	283.90	3.30	0.09	0.47	-21.9	7.61	0.79
SCS-SO-140-11-18383-1	7.64	109.49	710.70	2.82	0.16	0.99	-21.7	7.26	0.85
SCS-SO-140-12-18384-1	7.77	109.81	829.10	3.54	0.16	1.01	-21.5	12.49	0.89
SCS-SO-140-13-18385-2	7.86	110.02	73.60	11.78	0.03	0.17		0.38	
SCS-SO-140-14-18386-1	7.90	110.13	380.40	9.10	0.10	0.47	-21.4	5.14	0.63
SCS-SO-140-15-18387-1	8.10	110.64	381.60	9.17	0.13	0.55	-20.6	3.90	0.89
SCS-SO-140-16-18388-1	9.14	108.62	108.80	0.52	0.04	0.16	-24.2	2.00	0.77
SCS-SO-140-17-18389-1	9.27	108.65	109.20	0.42	0.03	0.08	-23.8	1.69	0.85
SCS-SO-140-18-18390-1	9.34	108.68	101.40	0.79	0.04	0.08	-24.2	2.17	0.81
SCS-SO-140-19-18391-1	9.57	108.83	122.40	1.87	0.10	0.52	-22.0	9.15	0.92
SCS-SO-140-20-18392-1	9.62	108.91	116.10	2.00	0.07	0.29	-22.2	6.41	0.88
SCS-SO-140-21-18393-1	9.76	109.13	155.90	3.47	0.08	0.37	-22.0	6.94	
SCS-SO-140-22-18394-1	9.79	109.18	183.00	2.35	0.09	0.63	-22.0	11.22	0.88
SCS-SO-140-23-18395-1	9.99	109.48	280.10	2.86	0.09	0.47	-22.0	8.89	0.81
SCS-SO-140-24-18396-1	15.43	108.89	60.80	1.28	0.11	0.72	-23.0	16.93	0.87
SCS-SO-140-25-18397-1	12.25	109.33	45.50	1.82	0.13	0.93	-22.3	17.34	0.95
SCS-SO-140-26-18398-1	12.24	109.38	59.30	1.54	0.13	0.98	-22.6	16.87	0.94
SCS-SO-140-27-18399-1	12.23	109.41	92.20	1.26	0.10	0.61	-22.5	15.99	0.89
SCS-SO-140-28-18400-1	12.23	109.43	103.60	1.49	0.12	0.81	-22.4	15.64	0.92
SCS-SO-140-29-18401-1	12.21	109.53	134.20	1.66	0.11	0.69	-22.2	13.23	0.87
SCS-SO-140-30-18402-1	13.12	109.69	224.50	4.58	0.06	0.21	-22.3	4.71	
SCS-SO-140-32-18404-1	13.50	109.56	169.10	4.02	0.06	0.26	-22.3	5.74	
SCS-SO-140-33-18405-1	13.69	109.45	129.30	1.86	0.11	0.62	-22.3	10.53	0.83
SCS-SO-140-34-18406-1	14.00	109.32	50.60	0.63	0.06	0.28	-23.7	2.49	0.87
SCS-SO-140-35-18407-1	14.08	109.42	134.70	1.99	0.09	0.42	-22.3	9.42	
SCS-SO-140-36-18408-1	14.25	109.34	116.50	1.73	0.11	0.66	-22.7	14.79	0.88
SCS-SO-140-37-18409-1	15.69	108.67	40.00	0.85	0.10	0.54	-23.1	14.91	0.92
SCS-SO-140-38-18410-1	15.48	108.87	57.70	1.09	0.13	0.82	-22.8	13.85	0.90
SCS-SO-140-39-18411-2	15.33	108.92	56.80	1.28	0.09	0.48	-23.0	13.70	0.89
SCS-SO-140-40-18412-2	15.22	109.01	58.40	1.33	0.12	0.70	-23.1	6.46	0.88
SCS-SO-140-41-18413-1	15.20	109.00	52.00	1.70	0.07	0.26	-23.0	6.02	
SCS-SO-140-42-18414-2	15.10	108.96	20.70	0.36	0.05	0.16	-24.4	4.36	
SCS-SO-140-43-18415-1	15.08	109.00	34.60	1.44	0.14	1.12	-24.5	15.91	0.97
SCS-SO-140-44-18416-1	15.04	109.15	62.70	3.14	0.04	0.11	-23.1	2.59	
SCS-SO-140-45-18417-2	14.75	109.29	97.90	1.17	0.04	0.17	-22.6	5.31	
SCS-SO-140-46-18418-1	14.40	109.31	100.00	1.71	0.11	0.60	-22.7	10.82	0.89
SCS-SO-140-47-18419-1	14.54	109.24	80.70	2.13	0.08	0.44	-23.0	10.05	0.87
SCS-SO-140-48-18420-1	14.57	109.19	61.50	1.58	0.09	0.48	-23.1	13.20	0.91
SCS-SO-140-49-18421-1	15.75	108.89	82.50	2.11	0.04	0.20	-22.7	3.59	0.80
SCS-SO-140-50-18422-1	15.75	108.89	84.50	1.58	0.07	0.40	-22.4	3.54	0.87
SCS-SO-140-51-18423-1	16.28	108.66	96.50	2.12	0.05	0.20	-22.1	5.51	0.80
SCS-SO-140-52-18424-1	16.48	108.44	91.10	1.91	0.13	0.71	-21.7	16.03	0.86
SCS-SO-140-53-18425-1	16.58	108.47	94.40	2.31	0.10	0.47	-21.7	14.97	0.86
SCS-SO-140-54-18426-1	16.74	108.46	92.90	2.24	0.12	0.59	-21.9	12.82	0.84
SCS-SO-140-55-18427-1	16.48	109.19	114.80	1.31	0.07	0.33	-22.1	9.14	0.78

sample no.	Lat. N DD	Long. E DD	depth [m]	C_{total} [%]	N_{total} [%]	C_{org} [%]	$\delta^{13}C_{org}$	surface area [m^2 g^{-1}]	F_m
SCS-SO-140-56-18428-1	16.39	109.42	196.60	1.58	0.11	0.61	-22.0	11.68	0.83
SCS-SO-140-57-18429-1	16.35	109.54	756.30	2.38	0.17	1.03	-21.7	11.45	0.82
SCS-SO-140-58-18430-1	11.92	110.00	1906.00	2.11	0.14	0.82	-21.9		0.81
SCS-SO-115-01-18248-1	9.25	108.73	103.00	0.18	0.009	0.103	-26.1	1.33	0.56
SCS-SO-115-02-18249-1	9.40	108.92	133.00	3.40		0.25	-23.1	4.83	
SCS-SO-115-03-18250-1	9.40	108.97	148.00	2.63		0.73	-23.0	4.61	0.58
SCS-SO-115-05-18252-1	9.25	109.39	1277.00	2.27	0.14	0.83	-22.2		0.81
SCS-SO-115-06-18253-1	9.40	109.50	1478.00	2.51	0.13	0.86	-21.8		0.82
SCS-SO-115-07-18254-1	9.63	109.04	145.00	3.23		0.74	-23.1	9.80	0.82
SCS-SO-115-08-18255-1	9.70	108.78	102.00	2.58		0.44	-23.8	9.66	0.74
SCS-SO-115-09-18256-1	9.58	108.70	92.00	2.57		2.37	-25.3	3.61	0.60
SCS-SO-115-10-18257-2	9.40	108.59	88.00	1.47		0.25	-24.9	3.12	
SCS-SO-115-11-18258-1	9.25	108.49	88.00	1.13		0.25	-24.8	3.21	
SCS-SO-115-12-18259-2	9.17	108.45	88.00	1.50		0.19	-27.7	3.55	
SCS-SO-115-13-18260-1	9.40	108.34	74.00	1.36		0.32	-24.7	4.51	0.76
SCS-SO-115-14-18261-3	9.25	108.12	68.00	1.57		0.29	-24.4	3.72	
SCS-SO-115-15-18262-1	9.25	107.99	56.00	3.31		0.23	-25.0	3.56	
SCS-SO-115-17-18264-1	9.40	107.81	48.00	5.14	0.03	0.18	-23.2	3.25	0.76
SCS-SO-115-17-18264-1 0 cm	9.40	107.81	48.00	6.21	0.03	0.17	-23.9	3.34	
SCS-SO-115-18-18265-1	9.39	107.75	47.00	6.44		0.26	-24.2	3.93	
SCS-SO-115-19-18266-1	9.38	107.74	47.00	3.84		0.24	-24.3	3.29	
SCS-SO-115-20-18267-1	6.37	111.88	1852.00	3.39	0.06	0.35	-21.8		0.82
SCS-SO-115-21-18268-1	6.65	111.87	1974.00	3.29		1.27	-22.0	22.28	0.78
SCS-SO-115-22-18269-1	4.77	109.44	114.00	3.00		0.45	-23.3	4.81	0.75
SCS-SO-115-22-18269-1 0 cm	4.77	109.44	114.00					5.08	0.79
SCS-SO-115-23-18270-1	4.72	109.48	106.00	2.63		0.55	-23.2	4.36	0.71
SCS-SO-115-24-18271-1	4.64	109.55	116.00	4.16		0.28	-22.5	8.53	
SCS-SO-115-25-18272-1	4.63	109.56	121.00	4.76		0.72	-22.8	7.73	0.74
SCS-SO-115-26-18273-1	4.62	109.57	127.00	4.60		0.63	-22.2	7.65	0.78
SCS-SO-115-27-18274-1	4.61	109.58	117.00	3.98		0.33	-23.1	4.75	
SCS-SO-115-28-18275-1	4.59	109.59	109.00	2.53		0.26	-23.7	3.76	
SCS-SO-115-29-18276-1	4.75	109.75	120.00	3.35		0.42	-23.5	5.32	
SCS-SO-115-30-18277-1	4.94	109.94	134.00	3.68		0.68	-22.8	8.30	0.74
SCS-SO-115-31-18278-1	5.02	110.02	137.00	3.62		0.63	-23.0	7.42	0.73
SCS-SO-115-32-18279-1	5.04	110.04	139.00	5.95		2.40	-22.8	6.47	0.70
SCS-SO-115-33-18280-1	5.10	110.10	144.00	3.78		0.66	-22.7	6.64	0.71
SCS-SO-115-34-18281-1	5.13	110.13	145.00	3.64		0.53	-22.5	7.18	0.75
SCS-SO-115-35-18282-1	5.25	110.24	152.00	3.50	0.06	0.35	-22.3	6.53	0.71
SCS-SO-115-36-18283-1	5.42	110.42	166.00	3.05		0.47	-23.0	7.34	0.65
SCS-SO-115-37-18284-1	5.54	110.54	226.00	2.56		0.42	-23.5	5.77	
SCS-SO-115-47-18294-3	6.13	111.30	846.00	4.34		1.13	-21.8	8.10	0.89
SCS-SO-115-48-18295-1	4.93	109.30	117.00	3.85		0.44	-22.6	10.23	
SCS-SO-115-49-18296-1	5.00	109.24	118.00	4.01		0.59	-22.7	8.04	0.79
SCS-SO-115-50-18297-1	4.74	109.03	112.00	3.68		0.57	-22.4	7.76	0.80
SCS-SO-115-51-18298-1	4.52	108.83	103.00	4.71	0.06	0.38	-21.9	5.91	0.73
SCS-SO-115-52-18299-2	4.53	108.83	102.00	5.17	0.05	0.35	-22.1	6.20	0.76

sample no.	Lat. N DD	Long. E DD	depth [m]	C_{total} [%]	N_{total} [%]	C_{org} [%]	$\delta^{13}C_{org}$	surface area [$m^2\ g^{-1}$]	F_m
VA-10	10.200	111.100	3244.00			0.78	-21.5		0.76
VA-11	10.200	110.000	1401.00			1	-21.5		0.76
VA-12	9.400	110.800	2791.00			0.93	-21.4		0.78
Con River St. 1	13.854	109.140		0.22	0.021	0.15	-25.5		0.71
Hathan River St. 1a	13.700	109.220		0.75	0.045	0.76	-26.4		
Hathan River St. 1b	13.784	109.220		0.89	0.075	0.89	-26.5		0.84
Hathan River St. 2	13.784	109.223		0.26	0.020	0.26	-24.0		0.87
Lai Giang River St.2a	14.472	109.091		0.12	0.010	0.12	-26.9		
Lai Giang Riverband St. 2b	14.47	109.09		0.11	0.009	0.11	-27.2		
Lai Giang Riverband St. 1b	14.41	109.01		3.23	0.245	3.21	-26.7		1.02
Lai Giang River St. 1a	14.41	109.01		0.22	0.014	0.22	-25.2		0.77
MK-01	6.20	102.20		0.94	0.074	0.94	-28.5		0.96
MK-08	3.51	103.39		1.65	0.135	1.72	-28.4		1.00
MK-10	3.51	103.44		1.23	0.102	1.24	-28.1		1.00
MK-11	4.23	103.43		1.28	0.101	1.29	-28.2		0.95
MK-14	5.34	103.12		2.04	0.161	2.06	-28.6		
MK-15	2.24	111.81		1.12	0.118	1.14	-27.7		
MK-17	2.33	111.83		0.85	0.072	0.85	-29.0		
MR-02	10.56	106.41		1.46	0.122	1.46	-27.0		0.85
MR-03	10.33	106.38		1.20	0.130	1.20	-26.0		0.89
MR-04	10.24	106.37		1.30	0.149	1.31	-25.8		0.90
MR-06-1	10.20	106.71		0.80	0.064	0.81	-25.6		0.92
MR-10-2	10.41	105.62		0.62	0.083	0.62	-24.9		0.88
MR-13	10.42	105.41		1.58	0.173	1.45	-27.0		0.92
MR-14	10.34	105.48		0.98	0.161	0.98	-25.8		
MR-15	10.10	105.72		0.81	0.118	0.82	-25.6		
MR-16	9.74	106.07		1.05	0.117	1.06	-26.6		
MR-17	10.25	106.03		0.67	0.062	0.68	-26.2		0.86
SU-02	0.61	101.59		2.79	0.120	2.73	-29.0		0.91
SU-05	-0.37	102.53		0.94	0.080	0.91	-26.1		0.70
SU-09	-1.58	103.57		1.17	0.113	1.14	-28.0		0.88
SU-11	-2.38	103.94		2.18	0.164	2.03	-27.4		1.06
SU-13	-3.02	104.72		1.55	0.118	1.56	-27.7		0.85
Thu Bon River St. 1	15.85	108.28		0.12	0.006	0.12	-25.2		0.65
Thu Bon River St. 2	15.85	108.28		0.12	0.009	0.12	-25.8		0.66
Thu Bon River St. 3	15.87	108.39		0.06	0.003	0.06	-26.6		0.74
Thu Bon River St. 4	15.87	108.39		0.07	0.004	0.07	-26.0		0.72
Tra Khuc River St. 1a	15.13	108.80		0.08	0.004	0.08	-26.5		0.99
Tra Khuc River St. 1b	14.41	109.01		3.60	0.323	3.61	-25.6		1.08
Tra Khuc River St. 2	15.13	108.88		0.06	0.003	0.06	-26.3		0.70
WK-04	0.39	109.96		2.62	0.062	2.65	-29.0		
WK-07	0.32	108.97		2.01	0.142	1.95	-27.5		0.89
WK-08	-0.27	109.36		2.79	0.174	2.80	-29.1		
VN-07110302 SED	10.68	107.78		1.99	0.18	2.04	-26.0		1.10
VN-09110301 SED	11.22	108.50		0.11	0.04	0.11	-26.3		
VN-10110301 SED	11.24	108.73		2.94	0.19	2.55	-27.2		

sample no.	Lat. N DD	Long. E DD	depth [m]	C_{total} [%]	N_{total} [%]	C_{org} [%]	$\delta^{13}C_{org}$	surface area [m^2 g^{-1}]	F_m
VN-12110301 SED	12.49	109.13		1.04	0.09	1.01	-25.7		0.98
VN-14110301 SED	12.25	109.20		2.40	0.18	2.37	-27.4		
VN-15110306 SED	11.60	108.94		0.84	0.08	0.88	-24.6		1.06
Red River 7W SED	20.07	106.47		1.17	0.13	0.88	-23.8		0.85
Song Ba St. 1 SED	13.09	109.09		2.79	0.20	2.80	-25.4		
Song Ba St. 2 SED	13.06	109.32		1.96	0.19	2.00	-23.9		1.04
Song Ba St. 3a SED	13.05	109.05		1.95	1.15	2.01	-24.0		
Song Ba St. 3b SED	13.05	109.05		0.06	0.004	0.07	-26.8		0.79
Cuu Long Grab St.11 SED	9.69	106.69		1.08	0.114	1.07	-25.5		0.93
Cuu Long Grab St.20 SED	9.56	106.56		1.02	0.081	1.03	-26.4		0.99
Cuu Long Grab St. 4 SED	10.27	106.27		1.02	0.048	0.82	-26.5		0.86
RS-30	20.44	106.22		1.29	0.090	0.87	-24.9		0.85
RS-32	20.37	106.34		1.02	0.083	0.67	-23.8		0.78
RS-33-1	20.46	106.35		1.06	0.084	0.67	-24.1		0.82
RS-34	20.79	106.52		0.94	0.068	0.61	-24.8		0.74
RS-35	20.91	106.62		0.43	0.042	0.34	-25.3		0.56
VN-38-1	16.12	108.12		3.29	0.286	3.09	-28.4		1.06
VN-44	16.83	107.10		1.11	0.137	1.12	-25.9		1.01
VN-46	17.34	106.70		1.19	0.100	1.12	-25.1		1.05
VN-49	17.77	106.33		0.36	0.037	0.28	-26.0		1.01
VN-53	18.46	105.77		1.36	0.146	1.37	-24.9		0.92
VN-55	18.59	105.69		0.46	0.056	0.40	-26.0		
VN-59	19.84	105.79		0.74	0.064	0.71	-25.6		0.86
VN-63	20.26	105.98		12.08	0.260	9.69	-24.5		0.03
HN-02	19.90	109.68		0.43	0.021	0.24	-25.3		0.06
HN-04	19.23	108.90		0.41	0.035	0.14	-25.1		0.86
HN-06	18.52	110.02		0.08	0.009	0.08	-27.6		0.79
HN-07	19.15	110.55		0.41	0.015	0.18	-27.2		0.85
GX-01	21.68	109.16		0.45	0.028	0.45	-27.0		0.83
GX-05	21.95	108.62		0.27	0.024	0.27	-26.3		0.68
TH-01	13.54	100.25		2.52	0.241	2.36	-25.0		0.91
TH-02	13.38	99.98		2.34	0.171	1.96	-25.6		0.86
TH-04	13.07	99.95		1.20	0.088	1.21	-27.0		0.62
TH-05	13.70	99.85		0.57	0.036	0.46	-24.7		0.84
TH-07	13.95	99.64		1.46	0.098	1.32	-26.8		0.84
TH-08-2	13.80	100.19		3.78	0.314	3.31	-27.6		0.98
TH-09	13.92	100.49		0.83	0.063	0.84	-26.4		0.86
TH-11	14.29	100.56		1.40	0.101	1.34	-26.1		0.77
TH-13	14.94	100.37		1.06	0.098	1.07	-26.0		0.95
TH-15	14.56	100.72		1.37	0.117	1.23	-26.0		0.91
TH-18	13.99	101.69		0.34	0.031	0.35	-26.1		0.93
TH-20	13.73	101.21		1.44	0.150	1.46	-25.0		1.00
TH-21	13.49	101.00		1.63	0.147	1.63	-24.7		0.97

sample no.	Lat. N DD	Long. E DD	depth [m]	C_{total} [%]	N_{total} [%]	C_{org} [%]	$\delta^{13}C_{org}$	surface area [$m^2 g^{-1}$]	F_m	fatty acid methyl ester [µg/g]
VN-12110301 SED	12.49	109.13		1.04	0.09	1.01	-25.7		0.98	1139.62
VN-14110301 SED	12.25	109.20		2.40	0.18	2.37	-27.4			19105.38
VN-15110306 SED	11.60	108.94		0.84	0.08	0.88	-24.6		1.06	4715.54
Red River 7W SED	20.07	106.47		1.17	0.13	0.88	-23.8		0.85	977.20
Song Ba St. 1 SED	13.09	109.09		2.79	0.20	2.80	-25.4			172.78
Song Ba St. 2 SED	13.06	109.32		1.96	0.19	2.00	-23.9		1.04	11291.50
Song Ba St. 3a SED	13.05	109.05		1.95	1.15	2.01	-24.0			5923.33
Song Ba St. 3b SED	13.05	109.05		0.06	0.004	0.07	-26.8		0.79	1278.34
Cuu Long Grab St.11 SED	9.69	106.69		1.08	0.114	1.07	-25.5		0.93	3679.85
Cuu Long Grab St.20 SED	9.56	106.56		1.02	0.081	1.03	-26.4		0.99	2864.10
Cuu Long Grab St. 4 SED	10.27	106.27		1.02	0.048	0.82	-26.5		0.86	594.36
RS-30	20.44	106.22		1.29	0.090	0.87	-24.9		0.85	3096.00
RS-32	20.37	106.34		1.02	0.083	0.67	-23.8		0.78	1513.86
RS-33-1	20.46	106.35		1.06	0.084	0.67	-24.1		0.82	980.80
RS-34	20.79	106.52		0.94	0.068	0.61	-24.8		0.74	866.73
RS-35	20.91	106.62		0.43	0.042	0.34	-25.3		0.56	970.89
VN-38-1	16.12	108.12		3.29	0.286	3.09	-28.4		1.06	16940.86
VN-44	16.83	107.10		1.11	0.137	1.12	-25.9		1.01	1809.38
VN-46	17.34	106.70		1.19	0.100	1.12	-25.1		1.05	3344.72
VN-49	17.77	106.33		0.36	0.037	0.28	-26.0		1.01	1843.62
VN-53	18.46	105.77		1.36	0.146	1.37	-24.9		0.92	7941.95
VN-55	18.59	105.69		0.46	0.056	0.40	-26.0			422.43
VN-59	19.84	105.79		0.74	0.064	0.71	-25.6		0.86	2829.17
VN-63	20.26	105.98		12.08	0.260	9.69	-24.5		0.03	2948.87
HN-02	19.90	109.68		0.43	0.021	0.24	-25.3		0.06	1574.61
HN-04	19.23	108.90		0.41	0.035	0.14	-25.1		0.86	197.05
HN-06	18.52	110.02		0.08	0.009	0.08	-27.6		0.79	709.09
HN-07	19.15	110.55		0.41	0.015	0.18	-27.2		0.85	1070.33
GX-01	21.68	109.16		0.45	0.028	0.45	-27.0		0.83	1103.53
GX-05	21.95	108.62		0.27	0.024	0.27	-26.3		0.68	2586.16
TH-01	13.54	100.25		2.52	0.241	2.36	-25.0		0.91	9047.30
TH-02	13.38	99.98		2.34	0.171	1.96	-25.6		0.86	522.61
TH-04	13.07	99.95		1.20	0.088	1.21	-27.0		0.62	841.67
TH-05	13.70	99.85		0.57	0.036	0.46	-24.7		0.84	317.79
TH-07	13.95	99.64		1.46	0.098	1.32	-26.8		0.84	755.14
TH-08-2	13.80	100.19		3.78	0.314	3.31	-27.6		0.98	17678.45
TH-09	13.92	100.49		0.83	0.063	0.84	-26.4		0.86	744.83
TH-11	14.29	100.56		1.40	0.101	1.34	-26.1		0.77	330.99
TH-13	14.94	100.37		1.06	0.098	1.07	-26.0		0.95	190.92
TH-15	14.56	100.72		1.37	0.117	1.23	-26.0		0.91	902.14
TH-18	13.99	101.69		0.34	0.031	0.35	-26.1		0.93	384.41
TH-20	13.73	101.21		1.44	0.150	1.46	-25.0		1.00	12037.09
TH-21	13.49	101.00		1.63	0.147	1.63	-24.7		0.97	1229.71

Appendix 2) Results of biomarker analysis of fatty acids (n-$C_{10:0}$ –n-$C_{24:0}$, measurements for n-$C_{19:0}$ is missing)

sample no.	Lat. N DD	Long. E DD	depth [m]	weight [g]	*n*-$C_{10:0}$	*n*-$C_{11:0}$	*n*-$C_{12:0}$	*n*-$C_{13:0}$	*n*-$C_{14:0}$	*n*-$C_{15:0}$	*n*-$C_{16:0}$	*n*-$C_{17:0}$	*n*-$C_{18:0}$	*n*-$C_{20:0}$	*n*-$C_{21:0}$	*n*-$C_{22:0}$	*n*-$C_{23:0}$	*n*-$C_{24:0}$
SO-220-19-27	20.29	109.14	19.00	5.84	6.25	0.00	8.11	6.90	11.98	11.05	42.87	9.52	31.29	10.62	9.46	13.91	11.64	16.17
SO-220-22-3	20.48	108.75	43.00	3.58	0.00	0.00	0.00	0.00	0.00	0.00	8.37	0.00	8.33	0.00	0.00	0.00	0.00	3.55
SO-220-23-3	21.10	108.73	22	5.14	0.00	0.00	0.00	0.00	10.73	11.21	44.49	12.23	38.96	14.23	11.64	16.60	13.21	15.85
SO-220-24-1	21.11	108.71	22.00	2.70	46.72	0.00	7.16	5.75	30.06	25.64	153.44	16.60	116.10	9.44	12.55	6.66	5.06	3.83
SO-220-26-4	21.06	108.34	27.00	9.17	1.53	0.00	1.39	1.15	5.54	4.19	43.44	3.16	19.93	3.97	1.87	3.75	1.33	4.72
SO-220-27-1	21.04	108.30	27.00	4.50	3.57	0.00	0.00	0.00	6.00	7.68	50.64	10.07	35.18	12.22	9.53	12.80	10.89	11.40
SO-220-28-3	20.83	108.29	43.00	1.19	11.96	0.00	0.00	0.00	23.51	24.10	190.96	29.84	122.89	26.15	19.79	28.60	24.25	24.48
SO-220-29-3	20.40	108.38	44.00	4.28	0.00	9.60	9.24	9.61	26.68	33.58	296.33	39.68	179.46	36.90	32.97	60.13	43.60	49.41
SO-220-30-28	20.05	108.03	48.00	9.11	3.96	4.27	7.28	5.37	15.62	12.02	82.50	11.23	57.99	11.65	9.18	13.89	10.64	10.26
SO-220-31-2	20.01	108.09	27.00	6.80	5.59	5.37	7.64	6.15	17.73	21.54	266.56	31.12	111.86	23.47	19.28	61.16	32.30	47.48
SO-220-32-3	19.99	108.12	63.00	5.77	6.31	0.00	7.97	6.93	13.16	11.20	52.83	9.99	34.35	10.30	8.67	12.32	9.92	11.90
SO-220-33-3	19.99	108.34	56.00	7.80	0.00	0.00	4.74	0.00	6.32	5.40	14.59	4.73	12.88	5.30	4.50	5.32	4.63	6.43
SO-220-34-3	19.46	108.29	57.00	4.43	3.27	0.00	0.00	0.00	3.71	3.12	20.31	3.13	16.07	3.93	3.06	4.04	2.86	5.23
SO-220-35-3	19.23	108.15	44.00	3.43	0.00	0.00	10.68	0.00	12.26	11.41	45.57	11.09	48.07	12.16	10.20	17.13	10.25	12.66
SO-220-37-3	19.38	107.70	61.00	6.83	5.46	0.00	6.92	5.46	8.92	6.32	23.72	5.65	18.20	6.22	5.27	7.29	5.51	8.00
SO-220-38-2	19.42	107.57	61.00	4.67	2.70	0.00	0.00	0.00	2.81	0.00	16.95	2.83	19.81	3.06	0.00	3.03	0.00	3.08
SO-220-39-3	19.42	107.36	63.00	4.57	7.86	0.00	0.00	0.00	11.40	8.99	33.16	8.40	31.27	9.37	7.88	13.15	7.88	10.28
SO-220-40-2	19.42	107.30	58.00	5.21	0.00	0.00	6.86	0.00	8.16	7.73	24.65	7.38	22.71	8.17	7.16	14.19	7.05	9.68
SO-220-42-28	18.74	107.16	60.00	6.88	2.03	0.00	0.00	0.00	1.84	0.00	7.93	0.00	4.03	2.17	0.00	2.86	2.02	3.93
SO-220-43-2	18.79	107.17	60.00	3.75	3.35	0.00	0.00	0.00	0.00	0.00	18.75	3.38	21.25	3.65	0.00	4.81	0.00	3.67
SO-220-44-3	18.74	107.20	67.00	5.60	0.00	0.00	0.00	0.00	2.76	2.30	13.41	2.33	9.35	2.61	0.00	2.71	0.00	3.25
SO-220-45-2	18.73	107.27	66.00	8.02	0.00	0.00	0.00	0.00	3.55	2.37	49.35	2.45	19.52	3.98	2.42	4.87	2.79	5.88
SO-220-51-3	18.38	108.06	75.00	5.44	7.05	0.00	8.97	7.05	22.09	12.66	71.36	8.36	67.88	10.94	8.48	10.85	7.83	15.43
SO-220-52-1	18.37	108.06	72.00	6.03	6.54	5.90	9.85	6.61	23.17	11.40	74.39	8.21	75.11	11.30	8.60	12.51	8.94	20.93
SO-220-53-3	17.90	107.91	89.00	5.63	8.51	0.00	7.13	0.00	13.95	9.11	62.82	7.56	72.85	8.31	0.00	6.93	0.00	7.29
SO-220-54-2	17.89	107.90	90.00	2.82	0.00	0.00	13.03	0.00	31.44	19.03	263.11	19.83	329.13	25.25	14.26	19.94	15.78	26.57
SO-220-55-3	17.70	108.12	83.00	5.09	6.98	0.00	7.25	6.72	13.77	8.73	29.24	7.20	32.76	7.74	6.94	7.20	6.80	8.47
SO-220-57-3	17.64	108.40	105.00	5.28	7.11	0.00	0.00	0.00	12.88	8.64	34.59	7.73	38.35	9.06	7.43	9.31	7.79	12.65
SO-220-58-1	17.67	108.42	104.00	5.89	6.85	0.00	0.00	0.00	10.93	7.02	15.53	5.89	12.60	6.00	0.00	6.14	0.00	6.93
SO-220-60-2	16.73	109.59	546.00	3.75	4.93	0.00	0.00	0.00	2.72	0.00	19.97	4.54	57.76	0.00	3.12	4.34	3.06	5.68
SO-187-3-59-1	12.62	109.53	133.00	7.34	0.00	0.00	7.85	1.63	63.40	10.53	182.36	3.68	105.38	6.31	3.14	7.98	5.61	13.81
SO-187-3-60-1	11.08	110.01	1859.00	5.57	7.56	7.58	36.20	10.42	138.94	34.88	110.57	9.59	58.20	12.20	9.49	17.38	12.10	32.27
SO-187-3-61-1	11.43	111.28	2227.00	5.66	9.93	7.69	23.15	9.27	58.67	50.09	361.87	11.57	239.82	15.54	10.62	17.86	13.96	30.27
SO-187-3-62-1	11.05	109.47	127.00	7.79	2.04	0.00	0.00	0.00	19.48	1.86	69.56	2.24	55.32	2.47	0.00	2.32	1.70	2.18
SO-187-3-63-1	10.92	109.06	109.00	7.90	0.00	0.00	7.46	0.00	101.77	1.67	48.15	1.97	25.64	2.14	0.00	1.85	1.85	2.64
SO-187-3-64-3	10.91	109.05	107.00	6.40	5.69	0.00	5.04	1.80	115.35	3.40	82.92	3.86	42.29	7.90	1.90	5.99	3.76	0.00
SO-187-3-65-1	10.64	109.04	112.00	6.99	0.00	0.00	3.83	1.88	110.43	5.48	155.87	7.04	82.22	7.17	4.63	8.41	10.07	13.83
SO-187-3-66-1	10.26	108.91	87.00	7.16	5.36	0.00	17.04	5.09	16.21	6.81	35.27	5.76	33.83	5.67	0.00	5.74	5.16	6.55
SO-187-3-67-1	10.22	108.43	56.00	7.35	2.13	0.00	7.58	3.12	93.30	4.25	168.58	3.33	77.55	5.06	2.02	4.07	3.83	7.41
SO-187-3-68-1	10.28	108.42	60.00	6.74	0.00	0.00	2.00	0.00	0.00	2.09	63.98	2.00	38.68	2.54	1.52	2.41	1.75	3.86
SO-187-3-69-1	10.38	108.01	43.00	8.07	7.60	4.77	15.81	5.25	73.14	16.26	76.81	6.34	42.84	7.55	5.17	7.96	6.46	11.10
SO-187-3-70-1	10.37	108.01	41.50	6.39	5.67	5.55	22.66	6.30	54.50	19.41	143.80	7.86	93.84	8.21	6.81	9.09	7.20	14.35
SO-187-3-71-1	10.40	108.01	38.00	7.43	0.00	4.85	6.22	0.00	9.66	6.02	21.08	5.02	17.26	5.50	7.51	5.86	5.08	7.86
SO-187-3-72-1	10.26	107.29	26.00	5.93	6.10	0.00	12.88	6.24	13.49	8.30	80.80	7.03	51.94	7.70	7.27	8.58	7.12	13.21
SO-187-3-73-1	10.24	107.28	31.00	6.02	0.00	0.00	12.46	0.00	90.61	2.41	74.12	2.55	52.45	4.50	2.34	5.65	3.22	11.30
SO-187-3-74-1	10.23	107.28	29.00	8.13	5.11	6.74	12.08	5.34	54.05	10.82	151.13	7.89	114.29	11.91	8.83	11.79	8.04	20.67
SO-187-3-75-1	10.11	107.11	21.00	7.38	4.85	0.00	10.20	4.94	63.16	9.06	96.77	5.23	58.43	5.53	4.71	5.38	4.73	6.45

sample no.	Lat. N DD	Long. E DD	depth [m]	weight [g]	*n*-$C_{10:0}$	*n*-$C_{11:0}$	*n*-$C_{12:0}$	*n*-$C_{13:0}$	*n*-$C_{14:0}$	*n*-$C_{15:0}$	*n*-$C_{16:0}$	*n*-$C_{17:0}$	*n*-$C_{18:0}$	*n*-$C_{20:0}$	*n*-$C_{21:0}$	*n*-$C_{22:0}$	*n*-$C_{23:0}$	*n*-$C_{24:0}$
SO-187-3-76-1	9.48	106.82	24.00	7.22	15.47	6.87	9.70	6.03	82.25	11.65	75.94	6.75	52.74	9.31	7.55	10.18	10.39	15.57
SO-187-3-77B-1	9.36	106.63	25.00	6.37	6.14	0.00	12.49	5.76	81.42	13.27	182.65	6.33	120.41	7.92	5.63	7.35	5.83	8.64
SO-187-3-78-1	8.97	106.70	32.00	6.10	0.00	0.00	4.55	0.00	26.70	1.73	121.54	2.43	102.68	2.57	0.00	1.67	0.00	1.90
SO-187-3-79-1	9.14	107.07	33.00	7.71	8.10	4.60	13.31	4.82	51.50	10.01	104.16	5.40	76.70	6.04	4.56	6.46	4.73	7.13
SO-187-3-80-1	9.23	107.28	38.00	16.60	2.10	0.00	5.76	2.16	7.26	2.63	15.91	2.23	11.53	2.23	0.00	2.23	0.00	2.47
SO-187-3-81-1	9.26	107.33	38.00	8.03	0.00	0.00	13.19	0.00	20.73	6.27	71.61	0.00	35.18	4.67	0.00	4.97	0.00	5.42
SO-187-3-82-1	9.52	107.50	39.00	7.17	0.00	0.00	0.00	0.00	2.80	0.00	21.05	0.00	15.06	0.00	0.00	0.00	0.00	0.00
SO-187-3-83-1	9.90	107.50	31.00	9.27	4.16	0.00	8.96	3.91	12.76	5.41	30.84	4.01	19.33	4.34	0.00	4.15	0.00	5.21
SO-187-3-84-1	9.73	107.29	33.00	6.53	0.00	0.00	0.00	0.00	4.26	0.00	46.81	2.00	31.88	1.92	0.00	2.23	0.00	0.00
SO-187-3-85-1	9.80	107.04	27.00	6.32	2.74	0.00	3.76	0.00	22.87	2.45	67.69	2.67	44.28	3.09	0.00	0.00	0.00	2.29
SO-187-3-86-1	8.74	106.16	27.00	6.60	2.35	0.00	2.54	0.00	23.94	2.28	67.43	2.49	55.21	2.73	0.00	2.14	0.00	2.59
SO-187-3-87-1	9.04	106.08	20.00	1.05	151.75	754.40	407.80	185.88	418.31	178.25	3353.13	247.67	3244.43	257.66	458.14	263.31	189.53	421.07
SO-187-3-91-1	8.44	105.24	31.00	5.89	2.28	0.00	0.00	0.00	22.98	0.00	37.52	2.19	29.81	2.42	0.00	4.39	0.00	2.42
SO-187-3-92-1	8.42	105.20	30.00	5.26	5.56	0.00	16.04	2.98	73.40	8.94	343.22	6.85	251.89	11.21	4.04	9.29	5.54	11.95
SO-187-3-93-1	8.39	105.11	32.00	5.68	7.26	0.00	2.78	0.00	6.01	2.53	45.02	2.34	31.13	2.97	0.00	3.09	2.40	4.17
SO-187-3-94-1	8.37	104.63	24.00	6.55	6.45	0.00	4.02	0.00	7.94	3.08	51.36	2.83	38.95	4.21	14.54	5.49	3.74	8.87
SO-187-3-95-1	8.38	104.62	29.00	6.89	2.11	0.00	0.00	0.00	3.77	1.84	21.53	1.83	17.75	2.15	0.00	2.06	1.92	2.56
SO-187-3-96-1	8.41	104.57	31.00	6.88	0.00	0.00	20.60	1.66	22.24	4.88	80.28	4.34	50.86	6.16	3.19	11.33	6.01	21.47
SO-187-3-97-2	8.41	104.56	30.00	7.45	1.39	1.45	14.61	2.32	16.36	5.83	101.56	4.16	69.90	6.54	3.29	8.88	4.73	14.37
SO-187-3-98-1	8.46	104.47	30.00	7.26	1.80	0.00	1.72	0.00	3.69	1.91	14.78	1.80	9.81	2.06	1.74	2.44	1.94	2.90
SO-187-3-99-1	8.47	104.46	30.00	5.94	2.38	0.00	4.78	2.06	8.74	8.99	115.83	5.70	49.83	7.89	5.65	12.14	7.87	17.86
SO-187-3-100-1	8.52	104.34	28.00	8.13	1.42	0.00	2.23	0.00	9.36	2.85	77.89	2.42	61.34	4.14	2.40	5.45	3.47	7.69
SO-187-3-102-1	8.44	104.23	29.00	7.45	2.83	0.00	0.00	0.00	10.05	3.98	58.70	3.79	26.22	4.57	2.69	4.84	2.66	5.38
SO-187-3-103-1	8.43	104.21	28.00	6.75	28.40	0.00	7.53	1.58	9.58	3.59	68.55	3.23	34.24	6.16	3.56	8.90	4.31	7.86
SO-187-3-104-1	8.38	104.22	26.00	7.50	0.00	0.00	1.39	0.00	1.94	0.00	26.17	0.00	20.86	1.47	0.00	1.73	1.47	3.02
SO-187-3-105-1	8.19	104.52	25.00	7.39	186.33	7.89	10.63	5.26	10.67	6.48	17.99	5.61	13.62	6.35	6.26	9.68	6.86	13.22
SO-187-3-106-1	8.19	104.56	26.00	7.27	6.71	0.00	7.77	6.10	12.41	8.07	17.15	8.71	21.82	8.31	13.40	7.89	8.43	9.96
SO-187-3-107-1	8.16	104.57	27.50	7.04	6.44	5.92	10.70	5.57	10.30	7.06	31.03	6.40	19.98	7.10	6.96	10.63	8.51	20.07
SO-187-3-108-1	8.12	104.95	32.00	7.28	0.00	0.00	9.18	5.06	10.08	6.43	32.92	5.73	26.66	5.83	6.52	6.42	6.59	9.72
SO-187-3-109-1	8.12	105.24	33.00	7.29	7.08	0.00	13.76	0.00	9.71	0.00	32.91	0.00	26.76	0.00	0.00	6.24	0.00	9.49
SO-187-3-110-1	8.12	105.28	32.00	6.20	0.00	0.00	9.59	0.00	8.97	8.60	68.08	8.65	54.10	6.43	9.52	6.54	6.76	8.94
SO-187-3-111-1	8.12	105.38	34.00	8.55	5.07	4.19	7.08	4.80	9.00	5.79	27.39	4.57	24.70	4.88	6.41	13.03	5.33	8.14
SO-187-3-112-1	8.12	105.39	33.00	7.32	0.00	0.00	4.76	0.00	0.00	0.00	4.73	0.00	4.95	0.00	0.00	0.00	0.00	0.00
SO-187-3-113-1	8.12	105.48	32.00	7.18	7.02	6.55	17.66	5.39	13.31	6.79	48.32	6.52	44.60	7.39	9.38	8.64	8.82	13.41
SO-187-3-114-1	8.12	105.59	32.00	8.72	4.30	0.00	4.54	0.00	8.92	7.22	17.33	4.50	11.53	5.43	5.20	7.12	6.25	13.35
SO-187-3-115-1	8.12	105.60	32.00	7.05	5.41	0.00	12.39	5.35	16.99	9.26	39.09	6.34	32.50	7.25	6.94	9.87	8.94	14.81
SO-187-3-116-1	8.12	105.94	33.00	7.67	5.58	4.79	15.86	5.33	13.61	8.46	97.50	5.71	63.55	6.49	6.95	7.03	6.25	10.33
SO-187-3-117-1	8.12	105.95	32.00	7.05	27.59	5.22	8.98	5.42	8.53	8.60	18.58	6.21	15.37	6.34	5.34	7.07	5.69	8.52
SO-140-01-18373-1	6.73	107.65	73.50	6.88	5.81	6.90	37.30	8.21	95.23	14.42	437.14	10.96	253.84	11.78	7.49	9.49	7.43	12.72
SO-140-02-18374-1	6.91	107.67	74.40	6.77	0.00	1.65	13.67	4.86	71.51	10.73	89.27	6.82	34.47	5.90	2.46	6.16	2.73	9.47
SO-140-03-18375-1	7.00	107.91	86.20	5.72	1.89	0.00	9.52	0.00	17.29	4.59	180.76	9.93	261.67	7.23	107.76	5.54	3.53	4.81
SO-140-04-18376-1	7.09	108.11	89.60	6.20	2.75	0.00	0.00	0.00	2.55	0.00	55.39	0.00	43.68	2.20	2.17	0.00	0.00	2.18
SO-140-05-18377-1	7.18	108.34	98.80	7.99	4.98	4.48	11.92	4.65	37.76	9.95	181.69	7.83	109.54	6.46	4.63	5.53	4.70	6.89
SO-140-06-18378-1	7.24	108.48	107.90	6.90	0.00	0.00	10.00	1.92	20.39	120.38	348.32	5.15	156.55	4.92	2.13	2.78	2.19	4.64
SO-140-07-18379-2	7.34	108.74	119.00	7.15	0.00	0.00	2.08	0.00	75.71	42.11	285.71	4.32	186.11	4.26	2.65	2.25	1.76	4.21
SO-140-08-18380-1	7.44	108.99	149.70	8.48	0.00	0.00	1.81	0.00	12.03	2.09	207.39	9.04	138.10	2.88	2.15	2.41	3.21	2.91

sample no.	Lat. N DD	Long. E DD	depth [m]	weight [g]	*n*-$C_{10:0}$	*n*-$C_{11:0}$	*n*-$C_{12:0}$	*n*-$C_{13:0}$	*n*-$C_{14:0}$	*n*-$C_{15:0}$	*n*-$C_{16:0}$	*n*-$C_{17:0}$	*n*-$C_{18:0}$	*n*-$C_{20:0}$	*n*-$C_{21:0}$	*n*-$C_{22:0}$	*n*-$C_{23:0}$	*n*-$C_{24:0}$
SO-140-09-18381-1	7.50	109.13	213.90	3.61	10.75	11.41	73.74	18.93	78.91	139.14	585.81	18.53	183.28	19.43	9.61	16.08	7.67	27.96
SO-140-10-18382-1	7.53	109.21	283.90	2.83	0.00	4.30	29.61	11.69	89.31	50.67	198.73	9.77	63.34	10.15	4.60	9.75	5.36	13.37
SO-140-11-18383-1	7.64	109.49	710.70	2.61	14.03	0.00	14.07	10.97	232.26	21.58	618.41	15.90	328.70	17.21	8.59	17.62	13.64	26.62
SO-140-12-18384-1	7.77	109.81	829.10	1.54	0.00	0.00	13.79	10.65	481.36	30.62	938.27	19.86	512.38	26.16	13.27	28.94	18.58	47.39
SO-140-13-18385-2	7.86	110.02	73.60	6.51	0.00	0.00	5.55	0.00	7.26	7.16	84.07	0.00	44.50	5.43	0.00	0.00	0.00	5.55
SO-140-14-18386-1	7.90	110.13	380.40	6.77	5.80	5.33	23.58	6.20	83.20	22.41	398.91	8.10	228.01	5.06	7.33	8.74	7.32	11.66
SO-140-15-18387-1	8.10	110.64	381.60	6.91	5.42	0.00	8.01	5.26	123.25	19.09	241.62	6.68	120.68	5.26	8.76	9.09	8.07	12.88
SO-140-16-18388-1	9.14	108.62	108.80	7.18	6.11	5.34	10.97	5.47	67.47	12.66	210.76	6.38	101.07	6.30	6.09	5.03	5.72	5.34
SO-140-17-18389-1	9.27	108.65	109.20	8.10	4.70	5.97	13.64	4.65	63.48	10.86	240.74	4.97	135.51	5.41	0.00	5.50	4.31	5.27
SO-140-18-18390-1	9.34	108.68	101.40	6.74	8.03	0.00	7.26	5.53	153.81	11.27	93.49	5.67	45.94	6.50	0.00	5.25	0.00	5.63
SO-140-19-18391-1	9.57	108.83	122.40	5.75	6.51	6.24	15.43	8.92	38.50	11.16	167.59	10.36	97.73	9.43	8.57	10.15	9.12	15.19
SO-140-20-18392-1	9.62	108.91	116.10	6.63	2.43	0.00	47.74	2.06	86.17	10.83	336.75	5.36	188.44	6.88	2.38	4.34	2.65	7.88
SO-140-21-18393-1	9.76	109.13	155.90	6.90	0.00	0.00	2.65	0.00	61.95	2.12	185.45	2.48	95.67	3.20	0.00	2.44	2.64	4.69
SO-140-22-18394-1	9.79	109.18	183.00	1.99	0.00	0.00	22.21	17.22	283.68	34.23	668.70	23.58	178.49	20.04	8.76	24.37	16.76	52.72
SO-140-23-18395-1	9.99	109.48	280.10	6.51	0.00	0.00	15.17	0.00	228.27	8.45	393.50	13.82	166.46	12.12	0.00	9.91	9.44	12.01
SO-140-24-18396-1	15.43	108.89	60.80	3.97	2.97	3.31	30.17	21.82	103.60	61.11	450.89	47.28	121.10	19.82	8.08	17.82	6.78	16.04
SO-140-25-18397-1	12.25	109.33	45.50	2.66	0.00	3.91	17.64	6.82	25.73	13.83	87.48	8.77	34.69	9.98	5.27	12.69	6.89	25.69
SO-140-26-18398-1	12.24	109.38	59.30	6.93	0.00	0.00	6.58	2.24	126.83	5.56	295.90	4.52	151.97	9.39	4.01	17.38	6.59	20.94
SO-140-27-18399-1	12.23	109.43	103.60	4.21	63.76	33.51	87.01	36.02	104.30	63.26	197.88	14.41	60.53	24.46	13.87	26.22	20.26	29.66
SO-140-28-18400-1	12.21	109.53	134.20	6.36	0.00	0.00	2.63	1.58	54.19	17.93	117.59	3.16	41.37	6.85	3.20	6.55	4.95	11.25
SO-140-29-18401-1	13.12	109.69	224.50	8.17	1.45	0.00	1.31	0.00	2.16	1.44	22.74	11.17	8.65	0.00	9.90	3.84	3.44	1.50
SO-140-30-18402-1	13.50	109.56	169.10	1.70	25.13	0.00	21.17	20.73	93.54	32.76	113.19	21.00	82.72	23.49	0.00	21.81	0.00	22.13
SO-140-32-18404-1	13.69	109.45	129.30	6.92	5.97	5.20	33.05	6.15	70.01	17.76	342.65	8.49	191.65	9.49	6.51	9.41	7.02	16.37
SO-140-33-18405-1	14.00	109.32	50.60	6.34	0.00	1.80	8.30	8.55	80.78	11.09	179.41	10.20	51.83	9.22	3.95	9.60	4.87	18.15
SO-140-34-18406-1	14.08	109.42	134.70	7.90	0.00	0.00	0.00	0.00	16.45	0.00	42.87	1.47	23.81	1.73	0.00	1.38	1.43	2.17
SO-140-35-18407-1	14.25	109.34	116.50	6.83	5.44	0.00	17.05	5.75	61.09	16.73	83.96	7.43	29.27	10.74	6.70	6.83	7.93	11.87
SO-140-36-18408-1	15.69	108.67	40.00	7.40	1.94	3.09	11.15	6.49	32.22	13.16	194.12	9.90	60.85	9.91	3.79	11.06	5.22	24.60
SO-140-37-18409-1	15.48	108.87	57.70	6.49	28.22	3.90	20.19	5.96	73.55	43.83	228.52	11.69	64.91	11.48	27.23	15.31	5.76	22.39
SO-140-38-18410-1	15.33	108.92	56.80	6.13	4.58	4.96	34.04	8.24	59.16	66.97	283.24	29.35	81.22	14.36	25.06	12.68	6.30	21.03
SO-140-39-18411-2	15.22	109.01	58.40	5.46	0.00	0.00	0.00	0.00	3.35	0.00	11.90	0.00	4.36	0.00	0.00	2.39	0.00	3.36
SO-140-40-18412-2	15.20	109.00	52.00	5.33	2.59	0.00	11.98	4.92	125.60	11.44	194.11	9.43	71.47	8.39	2.99	8.22	5.26	14.01
SO-140-41-18413-1	15.10	108.96	20.70	7.73	7.45	0.00	4.66	0.00	37.96	7.59	15.65	4.49	9.92	5.34	0.00	4.59	0.00	4.60
SO-140-42-18414-2	15.08	109.00	34.60	7.29	8.96	0.00	5.04	0.00	20.31	5.64	18.15	0.00	8.50	0.00	4.75	0.00	0.00	0.00
SO-140-43-18415-1	15.04	109.15	62.70	6.47	4.90	0.00	2.73	2.06	66.22	8.17	91.94	3.15	32.86	5.58	3.05	8.03	7.20	17.48
SO-140-44-18416-1	14.75	109.29	97.90	7.11	8.38	0.00	5.37	0.00	44.09	7.52	27.97	0.00	12.67	5.43	5.09	0.00	0.00	5.70
SO-140-46-18418-1	14.40	109.31	100.00	6.28	102.53	1.73	5.99	1.89	103.11	3.28	94.19	2.99	38.13	4.47	2.17	4.30	3.10	8.09
SO-140-47-18419-1	14.54	109.24	80.70	6.52	0.00	0.00	5.57	0.00	134.20	3.29	220.17	3.10	90.62	5.14	2.10	4.02	2.96	5.49
SO-140-48-18420-1	14.57	109.19	61.50	6.48	3.90	0.00	2.28	0.00	82.27	2.68	62.73	2.54	22.03	4.30	2.68	3.64	4.50	7.86
SO-140-49-18421-1	15.75	108.89	82.50	7.47	9.47	4.66	6.11	5.06	140.19	8.42	62.01	5.09	27.61	7.91	4.91	5.83	5.60	8.45
SO-140-50-18422-1	15.75	108.89	84.50	7.97	10.60	0.00	5.30	0.00	82.16	8.86	31.86	0.00	15.11	0.00	0.00	5.45	0.00	7.80
SO-140-51-18423-1	16.28	108.66	96.50	6.37	0.00	0.00	7.07	0.00	167.42	15.05	156.59	7.33	66.52	8.08	7.79	17.65	7.84	14.63
SO-140-52-18424-1	16.48	108.44	91.10	6.68	106.87	6.09	13.26	6.49	90.24	15.41	211.06	8.31	92.83	9.79	8.33	12.69	11.24	28.56
SO-140-53-18425-1	16.58	108.47	94.40	4.43	8.49	8.99	56.23	8.24	128.75	13.80	355.23	11.85	233.12	18.11	11.67	11.72	9.68	11.52
SO-140-54-18426-1	16.74	108.46	92.90	7.64	2.58	0.00	2.00	1.77	107.73	3.76	64.99	4.25	38.44	4.88	2.53	4.15	2.59	5.19
SO-140-55-18427-1	16.48	109.19	114.80	6.67	57.97	5.57	9.12	6.01	61.13	14.45	85.17	6.43	34.97	8.82	6.38	6.67	7.96	9.01
SO-140-56-18428-1	16.39	109.42	196.60	6.65	0.00	5.84	43.03	0.00	63.28	20.87	158.42	7.22	97.87	8.88	5.72	8.32	9.49	12.53

sample no.	Lat. N DD	Long. E DD	depth [m]	weight [g]	*n*-$C_{10:0}$	*n*-$C_{11:0}$	*n*-$C_{12:0}$	*n*-$C_{13:0}$	*n*-$C_{14:0}$	*n*-$C_{15:0}$	*n*-$C_{16:0}$	*n*-$C_{17:0}$	*n*-$C_{18:0}$	*n*-$C_{20:0}$	*n*-$C_{21:0}$	*n*-$C_{22:0}$	*n*-$C_{23:0}$	*n*-$C_{24:0}$
SO-140-57-18429-1	16.35	109.54	756.30	7.20	59.43	4.27	16.52	10.42	101.90	17.26	241.22	15.59	108.55	20.30	11.40	31.85	16.11	50.26
SO-140-58-18430-1	11.92	110.00	1906.00	5.78	47.99	8.71	26.02	10.57	123.19	41.30	148.17	10.40	61.27	18.42	13.39	29.18	14.38	41.49
SO-115-01-18248-1	9.25	108.73	103.00	9.77	3.77	0.00	3.69	0.00	7.15	4.95	29.39	4.13	24.66	3.70	0.00	0.00	0.00	3.72
SO-115-02-18249-1	9.40	108.92	133.00	7.12	4.97	0.00	24.99	4.82	4.77	10.21	289.12	6.33	207.99	6.70	4.81	5.79	5.95	6.20
SO-115-03-18250-1	9.40	108.97	148.00	6.41	2.09	0.00	0.00	0.00	4.81	0.00	55.64	0.00	41.88	2.22	0.00	2.10	2.07	3.08
SO-115-05-18252-1	9.25	109.39	1277.00	6.27	6.79	8.11	26.27	10.23	167.60	40.04	196.64	15.86	104.73	35.62	19.71	34.01	18.87	42.92
SO-115-06-18253-1	9.40	109.50	1478.00	6.47	12.68	16.50	37.42	20.75	178.10	41.93	143.73	18.75	61.36	23.23	14.56	22.26	14.41	26.93
SO-115-07-18254-1	9.63	109.04	145.00	6.50	9.92	0.00	3.48	0.00	127.78	2.58	122.88	2.63	78.90	3.71	20.82	2.90	2.24	6.78
SO-115-08-18255-1	9.70	108.78	102.00	6.76	0.00	0.00	8.65	0.00	84.87	4.40	75.79	2.71	59.29	3.96	1.65	2.19	3.83	2.97
SO-115-09-18256-1	9.58	108.70	92.00	7.06	0.00	0.00	0.00	0.00	25.64	0.00	20.24	0.00	20.76	1.80	0.00	1.78	0.00	0.00
SO-115-10-18257-2	9.40	108.59	88.00	6.85	0.00	0.00	11.97	0.00	15.79	7.12	51.26	5.73	43.09	5.37	0.00	5.23	0.00	5.44
SO-115-11-18258-1	9.25	108.49	88.00	6.29	5.81	0.00	8.58	6.01	160.73	10.84	48.73	5.86	39.34	8.39	0.00	5.90	0.00	6.41
SO-115-12-18259-2	9.17	108.45	88.00	7.33	5.17	0.00	7.19	5.04	79.73	12.06	75.02	5.23	35.76	0.00	5.24	8.70	7.06	22.83
SO-115-14-18261-3	9.25	108.12	68.00	6.69	5.52	5.34	27.88	5.51	145.14	12.74	91.33	5.76	77.66	6.86	5.30	7.18	5.38	6.65
SO-115-15-18262-1	9.25	107.99	56.00	6.77	5.19	0.00	6.27	5.23	47.69	10.79	48.43	5.70	43.03	6.67	0.00	5.69	0.00	5.93
SO-115-17-18264-1 0cm	9.40	107.81	48.00	6.45	6.03	0.00	7.88	0.00	12.66	0.00	12.48	0.00	8.10	0.00	0.00	0.00	0.00	0.00
SO-115-17-18264-1	9.40	107.81	48.00	6.89	5.98	0.00	13.27	5.34	46.81	9.00	126.91	5.45	76.96	7.07	0.00	6.15	5.42	7.95
SO-115-18-18265-1	9.39	107.75	47.00	5.55	0.00	0.00	0.00	0.00	89.55	7.76	46.35	0.00	30.42	0.00	0.00	0.00	0.00	8.26
SO-115-19-18266-1	9.38	107.74	47.00	8.92	0.00	0.00	0.00	0.00	0.00	0.00	4.29	0.00	4.52	0.00	0.00	0.00	0.00	0.00
SO-115-20-18267-1	6.37	111.88	1852.00	5.88	6.67	6.07	14.14	8.03	78.98	33.61	127.94	12.58	90.43	19.09	18.52	22.22	19.22	44.92
SO-115-21-18268-1	6.65	111.87	1974.00	5.94	2.03	0.00	3.11	2.93	92.18	18.14	497.27	24.30	285.06	25.05	18.80	47.88	35.34	74.09
SO-115-22-18269-1	4.77	109.44	114.00	5.51	3.41	0.00	0.00	0.00	67.89	4.49	167.03	3.87	90.40	5.18	3.46	4.46	3.20	5.68
SO-115-22-18269-1 0cm	4.77	109.44	114.00	5.51	8.86	0.00	47.61	6.90	86.36	15.11	173.79	8.37	136.71	12.65	7.32	7.60	6.50	7.33
SO-115-23-18270-1	4.72	109.48	106.00	6.46	0.00	0.00	2.47	0.00	124.59	3.10	82.58	3.07	54.62	1.69	1.64	1.66	1.93	2.22
SO-115-24-18271-1	4.64	109.55	116.00	6.63	0.00	0.00	0.00	0.00	120.41	3.02	108.92	2.80	74.01	4.03	1.71	2.90	2.28	3.49
SO-115-25-18272-1	4.63	109.56	121.00	5.77	5.41	0.00	10.12	0.00	70.36	3.42	250.70	3.38	175.29	5.37	11.85	3.07	2.79	5.06
SO-115-26-18273-1	4.62	109.57	127.00	5.52	6.59	0.00	14.54	6.79	130.49	14.77	306.06	7.96	145.44	9.44	7.63	9.37	8.02	11.91
SO-115-27-18274-1	4.61	109.58	117.00	5.97	6.61	0.00	6.17	0.00	11.25	6.51	66.04	5.96	62.26	6.46	0.00	6.26	6.00	6.69
SO-115-28-18275-1	4.59	109.59	109.00	5.68	7.66	6.28	11.73	6.42	193.85	9.84	52.18	7.51	29.18	11.13	0.00	6.74	6.22	6.87
SO-115-29-18276-1	4.75	109.75	120.00	6.75	0.00	0.00	29.59	5.40	120.06	13.37	148.22	6.75	85.69	8.31	0.00	6.20	5.53	6.64
SO-115-30-18277-1	4.94	109.94	134.00	5.40	0.00	0.00	5.89	0.00	149.51	2.93	86.00	2.45	60.06	4.42	2.30	3.05	2.86	5.32
SO-115-31-18278-1	5.02	110.02	137.00	7.47	0.00	0.00	11.05	0.00	56.70	4.04	240.38	4.06	159.82	4.34	5.11	3.12	5.58	3.53
SO-115-32-18279-1	5.04	110.04	139.00	5.64	0.00	0.00	9.98	0.00	85.68	3.40	468.00	3.63	375.25	5.54	0.00	2.47	2.27	3.27
SO-115-33-18280-1	5.10	110.10	144.00	5.58	2.55	0.00	12.75	0.00	167.21	3.97	520.77	6.03	379.45	6.90	3.07	4.15	3.21	5.49
SO-115-334-18281-1	5.13	110.13	145.00	6.47	0.00	0.00	0.00	0.00	123.62	2.42	235.26	3.00	175.51	4.33	0.00	2.82	2.99	4.70
SO-115-36-18283-1	5.42	110.42	166.00	6.30	1.77	0.00	2.85	0.00	100.96	3.25	76.11	2.01	48.96	0.00	1.89	2.22	2.68	3.77
SO-115-36-18283-1	5.25	110.24	152.00	6.77	6.93	0.00	10.23	5.24	127.31	9.02	47.75	5.66	31.61	0.00	0.00	5.42	0.00	6.09
SO-115-37-18284-1	5.54	110.54	226.00	6.08	0.00	0.00	15.89	0.00	72.22	9.32	288.28	6.67	175.60	8.46	0.00	7.24	6.36	9.12
SO-115-47-18294-3	6.13	111.30	846.00	7.10	0.00	0.00	0.00	0.00	2.21	1.91	9.58	0.00	5.34	1.47	0.00	2.25	1.93	4.94
SO-115-48-18295-1	4.93	109.30	117.00	7.06	5.00	4.91	13.75	5.23	81.09	10.35	113.69	5.78	71.48	6.55	5.39	6.47	5.46	7.55
SO-115-49-18296-1	5.00	109.24	118.00	6.66	0.00	0.00	7.04	0.00	123.26	3.92	111.27	3.45	66.16	4.92	2.05	3.44	3.08	5.07
SO-115-50-18297-1	4.74	109.03	112.00	6.84	0.00	0.00	5.28	0.00	100.29	3.49	105.66	3.09	60.89	3.72	3.60	2.62	1.82	3.71
SO-115-51-18298-1	4.52	108.83	103.00	7.94	6.69	4.58	33.12	4.98	59.57	9.17	369.84	5.91	199.10	9.04	6.31	5.73	6.02	7.58
SO-115-52-18299-2	4.53	108.83	102.00	5.03	6.90	7.20	7.43	0.00	14.65	8.59	46.74	7.31	31.13	7.82	6.94	7.81	8.15	9.12
SO-115-53-18300-1	4.36	108.65	94.00	5.97	0.00	0.00	5.42	0.00	125.63	3.11	123.58	2.45	86.86	4.58	0.00	2.85	2.64	3.58
SO-115-54-18301-1	4.36	108.65	92.00	7.14	6.07	5.13	21.95	5.38	68.78	8.60	161.40	5.94	99.80	7.54	5.72	6.00	5.79	7.39

sample no.	Lat. N DD	Long. E DD	depth [m]	weight [g]	*n*-$C_{10:0}$	*n*-$C_{11:0}$	*n*-$C_{12:0}$	*n*-$C_{13:0}$	*n*-$C_{14:0}$	*n*-$C_{15:0}$	*n*-$C_{16:0}$	*n*-$C_{17:0}$	*n*-$C_{18:0}$	*n*-$C_{20:0}$	*n*-$C_{21:0}$	*n*-$C_{22:0}$	*n*-$C_{23:0}$	*n*-$C_{24:0}$
SO-115-55-18302-1	4.16	108.58	83.00	5.95	10.77	5.97	28.68	6.39	116.45	9.01	181.87	6.95	103.05	11.18	6.06	7.01	8.07	8.62
SO-115-56-18303-1	4.44	108.93	107.00	6.64	2.44	0.00	49.04	2.07	76.05	11.70	622.78	6.47	447.74	11.60	3.21	5.40	6.95	7.86
SO-115-57-18304-1	4.36	109.00	104.00	5.83	0.00	0.00	46.67	2.63	173.50	6.44	162.19	4.90	99.98	7.77	3.23	7.27	6.07	9.50
SO-115-59-18306-1	3.59	108.44	88.00	5.59	6.70	6.16	19.39	7.74	76.37	12.71	134.04	8.62	80.37	13.31	10.04	11.73	10.35	11.06
SO-115-59-18306-2	3.59	108.44	88.00	6.20	0.00	0.00	0.00	0.00	3.45	2.36	87.33	2.16	65.09	3.15	0.00	2.73	2.48	3.18
SO-115-60-18307-1	3.63	108.53	100.00	7.21	0.00	0.00	9.07	1.47	63.22	4.02	89.45	2.41	46.28	5.75	1.94	3.84	3.87	4.82
SO-115-61-18308-1	3.30	108.79	80.00	6.30	5.82	0.00	8.89	5.67	125.53	15.79	162.24	7.78	126.60	0.00	5.91	7.00	6.07	7.71
SO-115-62-18309-1	3.47	108.69	84.00	6.55	0.00	0.00	5.45	5.98	89.54	6.78	20.52	5.48	13.82	7.03	0.00	5.34	0.00	5.67
SO-115-63-18310-1	3.54	108.54	101.00	4.92	7.86	7.50	13.88	0.00	14.34	8.45	97.75	0.00	56.12	7.99	8.22	7.86	7.93	8.95
SO-115-64-18311-1	3.69	108.45	60.00	7.39	4.77	0.00	28.38	4.99	17.02	7.34	463.39	7.00	347.42	9.17	5.72	7.66	6.36	12.22
SO-115-65-18312-1	3.71	108.71	101.00	5.56	6.38	6.40	19.80	6.38	144.12	10.37	197.98	6.99	130.32	10.43	6.32	7.73	6.91	9.15
SO-115-66-18313-1	3.87	108.87	99.00	6.25	0.00	0.00	0.00	0.00	0.00	0.00	14.14	0.00	11.26	0.00	0.00	0.00	0.00	0.00
SO-115-67-18314-1	3.99	108.99	100.00	6.29	5.67	0.00	0.00	0.00	0.00	0.00	7.67	0.00	7.21	0.00	0.00	0.00	0.00	0.00
SO-115-68-18315-3	2.03	107.03	69.00	5.64	6.23	6.26	11.76	6.46	46.75	7.44	19.95	0.00	14.87	7.10	0.00	6.41	0.00	0.00
SO-115-70-18317-1	2.61	107.38	96.00	5.62	0.00	0.00	7.94	0.00	81.78	10.69	92.15	9.45	63.21	11.59	7.00	8.69	7.55	9.30
SO-115-71-18318-1	2.61	107.38	86.00	7.34	6.91	5.06	15.06	6.01	63.75	7.68	346.15	6.09	239.61	12.60	10.97	18.04	10.16	25.81
SO-115-73-18320-1	2.61	107.37	76.00	6.32	6.66	0.00	9.58	5.64	85.76	7.94	74.11	7.79	62.93	8.72	6.51	8.33	7.75	10.99
SO-115-74-18321-1	2.31	107.42	109.00	4.48	0.00	0.00	40.02	7.90	106.12	11.39	100.30	9.53	66.79	10.87	8.37	10.63	8.09	12.63
SO-115-75-18322-1	2.31	107.63	70.00	6.87	0.00	0.00	5.76	5.18	78.35	8.18	60.67	6.41	47.77	8.79	7.96	7.41	6.14	9.15
SO-115-76-18323-1	2.78	107.89	92.00	5.91	5.89	5.83	22.62	6.30	61.17	10.06	71.38	7.42	44.07	9.86	8.35	6.91	6.27	7.19
A7	18.00	109.50	66.00	4.22	0.00	12.88	69.25	16.31	1079.13	98.98	1730.33	36.77	919.98	92.79	27.14	80.76	28.86	140.92
B254	18.00	109.30	55.00	5.31	17.34	15.15	144.22	14.88	802.57	81.67	1430.73	42.33	686.20	101.34	32.50	84.13	28.95	136.58
B309	18.20	110.10	91.00	6.61	8.00	0.00	24.68	0.00	566.49	19.85	641.00	15.02	461.05	31.26	0.00	24.02	14.69	29.29
B358	18.50	110.60	97.00	6.23	0.00	0.00	52.09	12.07	452.93	66.80	1698.12	38.03	737.52	71.93	17.69	80.53	17.52	115.92
B380	18.00	109.80	81.00	4.66	19.23	11.49	102.35	12.38	657.92	82.24	1726.39	29.62	851.14	121.37	30.50	72.29	17.90	111.64
C110	18.70	110.90	127.00	6.11	14.12	12.10	32.40	9.84	183.62	50.20	926.11	30.62	557.18	64.33	21.83	86.88	29.43	127.48
C112	18.90	110.90	96.00	5.93	13.93	12.10	28.85	0.00	612.86	27.88	813.57	17.36	495.94	44.39	18.46	39.01	21.27	65.42
C59	18.50	108.40	40.00	4.98	105.09	19.65	1483.06	17.37	2918.54	70.33	1622.07	33.92	828.93	110.26	18.82	237.28	85.64	146.67
C68	18.00	108.80	57.00	5.96	0.00	0.00	18.61	0.00	543.09	18.12	644.10	12.65	430.04	36.62	0.00	29.80	17.03	44.65
C71	18.00	109.00	44.00	5.38	0.00	0.00	0.00	0.00	17.78	0.00	157.58	0.00	117.81	0.00	0.00	0.00	0.00	13.07
C81	18.00	110.40	136.00	5.28	0.00	0.00	50.73	12.29	409.94	70.63	1842.49	43.90	1089.92	104.97	48.97	116.87	42.53	311.01
C84	18.30	110.40	97.00	4.76	0.00	0.00	30.30	0.00	385.03	22.72	718.98	19.69	417.49	41.12	0.00	38.74	14.71	48.91
VA-01	14.50	111.90	1618.00	4.09	60.10	25.17	70.56	21.44	291.34	118.44	1589.02	62.23	796.54	92.02	31.02	157.99	136.53	258.53
VA-02	14.80	110.80	1204.00	4.33	0.00	0.00	40.92	14.51	243.39	81.13	1254.58	55.67	718.06	74.47	23.31	146.08	47.34	247.20
VA-03	14.00	111.10	2760.00	4.60	16.86	0.00	23.32	0.00	240.27	57.54	896.49	37.04	545.99	64.63	29.79	128.64	30.42	197.07
VA-04	13.10	111.40	2615.00	4.45	39.12	34.72	80.33	28.24	520.43	155.57	2278.05	83.80	1178.61	160.66	45.60	274.80	175.94	495.43
VA-05	12.60	110.60	2555.00	3.55	0.00	0.00	30.02	0.00	182.43	65.16	1208.84	37.58	772.86	67.40	25.32	136.05	53.51	227.37
VA-06	12.30	111.10	2095.00	4.10	22.10	12.55	39.79	12.37	176.35	61.19	1210.66	35.54	836.88	70.57	24.22	136.55	35.36	212.79
VA-07	11.80	111.70	3334.00	4.08	23.27	20.07	49.05	16.16	260.05	73.05	1487.86	43.54	1033.14	75.89	24.52	132.24	46.74	188.24
VA-08	11.00	111.40	3235.00	4.73	0.00	0.00	24.06	0.00	322.60	49.36	997.89	37.25	627.89	63.62	21.76	105.64	34.18	146.12
VA-09	11.00	110.60	1970.00	4.09	0.00	13.34	51.88	21.15	387.40	131.23	1664.47	72.79	681.10	117.88	44.33	285.89	97.22	465.23
VA-10	10.20	111.10	3244.00	4.39	24.40	0.00	35.20	11.26	277.61	65.70	1055.09	43.64	646.29	76.97	26.75	153.94	60.07	237.95
VA-11	10.20	110.00	1401.00	4.47	0.00	0.00	35.26	16.36	296.85	105.78	1385.38	59.00	685.89	108.09	53.23	241.76	80.20	402.86
VA-12	9.40	110.80	2791.00	4.17	0.00	0.00	28.51	0.00	170.26	53.03	854.83	35.47	544.72	58.25	17.73	102.25	62.25	139.30
BN-12	21.95	108.62		2.83	0.00	0.00	19.60	0.00	1016.31	43.48	589.25	18.17	366.45	96.95	18.89	105.15	95.88	216.02
Con River St. 1	21.68	109.16		3.95	0.00	0.00	11.95	0.00	633.53	19.77	196.15	11.49	142.34	21.84	0.00	26.90	0.00	39.55

sample no.	Lat. N DD	Long. E DD	depth [m]	weight [g]	*n*-$C_{10:0}$	*n*-$C_{11:0}$	*n*-$C_{12:0}$	*n*-$C_{13:0}$	*n*-$C_{14:0}$	*n*-$C_{15:0}$	*n*-$C_{16:0}$	*n*-$C_{17:0}$	*n*-$C_{18:0}$	*n*-$C_{20:0}$	*n*-$C_{21:0}$	*n*-$C_{22:0}$	*n*-$C_{23:0}$	*n*-$C_{24:0}$
Cuu Long Grab 11	20.91	106.62		6.90	0.00	0.00	0.00	0.00	534.30	13.84	229.61	11.66	75.07	24.78	0.00	26.48	0.00	55.15
Cuu Long Grab 4	20.79	106.52		9.59	0.00	0.00	15.61	0.00	158.39	21.23	270.38	15.52	124.48	48.93	10.74	59.76	23.83	117.85
Cuu Long Grab St. 20	20.46	106.35		4.33	0.00	0.00	13.25	0.00	483.19	18.39	201.97	11.53	132.41	31.49	0.00	32.74	0.00	55.83
GX-01	20.44	106.22		4.48	0.00	0.00	69.91	0.00	1713.54	32.42	581.98	0.00	286.43	78.69	0.00	93.56	49.65	189.82
GX-05	20.37	106.34		2.89	0.00	0.00	24.82	0.00	609.57	28.56	394.55	14.96	274.92	49.45	0.00	48.86	0.00	68.18
Hathanh River 1a	20.26	105.98		6.33	0.00	0.00	35.40	0.00	766.81	19.78	780.76	0.00	1058.04	63.30	0.00	61.35	64.14	99.28
Hathanh River St. 1b	20.07	106.47		2.25	62.88	28.39	66.06	31.63	152.25	55.49	254.24	27.33	164.68	29.38	17.03	24.48	21.48	41.89
Hathanh River St. 2	19.90	109.68		12.12	0.00	0.00	0.00	0.00	838.64	0.00	364.78	0.00	217.83	44.09	0.00	36.51	20.55	52.21
HN-02	19.84	105.79		2.68	0.00	0.00	24.78	0.00	1256.22	44.10	738.53	20.28	381.17	81.12	0.00	82.73	31.87	168.37
HN-04	19.23	108.90		9.52	0.00	0.00	0.00	0.00	10.06	0.00	92.85	0.00	69.80	7.68	0.00	8.22	0.00	8.44
HN-06	19.15	110.55		4.45	0.00	0.00	0.00	0.00	695.88	0.00	192.00	0.00	150.18	15.99	0.00	0.00	0.00	16.28
HN-07	18.59	105.69		3.67	0.00	0.00	0.00	0.00	19.47	11.28	149.07	0.00	116.31	23.29	0.00	32.21	17.65	53.15
Lai Giang River St. 2a	18.52	110.02		6.81	0.00	0.00	0.00	0.00	504.22	0.00	131.26	0.00	60.42	13.19	0.00	0.00	0.00	0.00
Lai Giang Riverband St. 1b	18.46	105.77		7.12	45.43	23.23	225.46	27.05	1776.34	185.92	1966.43	174.82	832.84	335.42	105.10	602.51	399.59	1241.81
Lai Giang Riverband St. 2b	17.77	106.33		4.44	0.00	0.00	21.84	0.00	903.10	24.62	444.29	16.08	246.78	46.68	0.00	46.28	26.61	67.34
MK-01	17.34	106.70		2.65	0.00	0.00	61.51	0.00	403.49	53.52	669.92	39.64	328.40	204.00	54.27	447.37	250.29	832.32
MK-10	16.83	107.10		2.29	26.75	0.00	32.18	13.55	300.95	35.80	540.59	22.23	357.20	85.17	16.44	129.67	56.05	192.79
MK-11	16.12	108.12		2.27	178.27	159.11	462.13	48.27	1308.80	365.94	4249.97	350.30	1744.35	1035.50	922.70	2270.42	1201.67	2643.42
MK-14	15.87	108.39		2.44	14.72	6.71	24.99	10.56	103.61	49.98	239.86	17.30	66.56	11.89	7.04	8.46	12.58	10.68
MK-15	15.87	108.39		2.42	16.17	6.49	9.04	6.64	6.30	10.31	42.01	6.91	41.17	8.88	6.99	6.34	0.00	7.80
MK-17	15.85	108.28		2.18	677.92	150.96	712.22	196.53	1197.26	555.95	99.20	166.20	823.24	183.65	19.97	48.04	66.13	27.70
MR-02	15.13	108.88		1.39	14.35	8.98	48.99	16.82	110.97	54.34	293.94	23.07	144.41	19.39	7.41	9.56	13.18	9.38
MR-03	15.13	108.88		2.16	148.07	23.33	141.51	26.84	457.68	56.63	666.26	26.84	281.30	37.59	2.37	14.33	20.57	16.08
MR-04	15.13	108.80		2.21	20.83	8.04	21.29	8.68	53.99	18.63	73.91	8.06	50.11	6.79	0.00	5.62	12.76	5.21
MR-06-1	14.47	109.09		2.03	30.87	12.70	63.78	17.11	135.29	35.46	234.24	17.22	114.09	19.86	6.52	10.45	62.20	10.74
MR-10-2	14.47	109.09		1.75	1189.85	364.75	1554.84	442.01	3505.53	1820.28	0.00	1397.29	0.00	3258.18	1108.64	6213.33	2523.80	0.00
MR-13	14.41	109.01		1.56	12.28	8.21	38.91	14.62	109.05	35.85	212.63	21.34	146.07	20.66	7.09	11.55	9.66	11.72
MR-14	14.41	109.01		2.02	122.57	71.06	477.28	146.69	1229.73	489.01	12508.68	354.04	3252.35	1392.09	327.96	2404.05	1290.37	3874.39
MR-15	13.85	109.14		2.70	0.00	0.00	25.55	0.00	65.20	21.12	380.52	0.00	374.79	44.33	0.00	49.03	19.03	45.38
MR-16	13.78	109.22		1.50	95.80	13.76	70.79	16.63	336.78	203.45	1878.64	74.86	671.47	107.89	11.54	81.86	91.49	104.60
MR-17	13.78	109.22		2.53	1917.27	194.02	1091.43	407.74	3296.90	2222.85	15844.12	870.30	5497.54	1011.49	113.12	723.31	331.67	1269.04
Red River 7W 0.05	13.70	109.22		3.01	33.33	19.93	118.81	44.68	698.80	358.50	3640.45	209.78	1065.10	180.68	56.71	242.89	116.74	352.89
RS-30	13.09	109.33		3.05	0.00	0.00	0.00	0.00	37.92	0.00	99.90	0.00	34.96	0.00	0.00	0.00	0.00	0.00
RS-32	13.09	109.33		3.68	212.11	136.13	397.63	121.83	910.25	349.28	4280.06	261.95	2450.10	355.20	137.61	517.03	335.46	826.87
RS-33-1	13.06	109.32		4.65	82.19	31.78	150.90	37.06	884.97	106.07	2562.91	72.66	962.77	194.57	38.52	277.50	159.11	362.33
RS-34	13.05	109.30		8.64	0.00	6.09	46.59	12.61	221.11	19.55	424.48	16.78	481.87	21.91	0.00	10.79	0.00	16.56
RS-35-1	12.49	109.13		4.24	16.21	15.90	44.61	22.18	122.48	49.50	345.50	26.05	161.87	48.12	26.05	69.78	47.14	144.25
Song Ba St. 1	12.25	109.20		1.72	263.74	126.85	510.34	100.56	4612.66	319.95	5038.76	267.37	2518.44	562.01	177.62	1350.75	630.91	2625.41
Song Ba St. 2	11.60	108.94		1.47	103.10	40.21	96.81	0.00	1831.18	71.24	1199.81	36.02	583.54	132.02	0.00	175.62	113.16	332.84
Song Ba St. 3a	11.24	108.73		4.95	453.27	225.47	700.19	222.50	1720.85	947.77	11911.92	464.48	3389.30	1232.61	337.23	2427.99	1227.33	3054.36
Song Ba St. 3b	11.22	108.50		9.64	28.69	0.00	200.99	0.00	1866.90	56.67	1470.03	34.95	705.36	66.24	0.00	52.62	0.00	30.90
SU-02	10.68	107.78		2.04	105.93	55.44	165.89	80.09	1637.77	381.34	3874.98	126.79	817.93	256.67	74.17	676.67	323.98	1110.41
SU-05	10.56	106.41		2.50	0.00	0.00	143.77	42.23	1457.86	318.68	4012.65	280.14	2192.35	566.23	257.17	1510.48	1070.97	3549.42
SU-09	10.42	105.41		2.82	0.00	0.00	199.43	37.63	4982.68	141.31	3390.47	111.59	1950.14	287.26	36.97	353.30	224.52	752.18
SU-11	10.41	105.62		2.11	0.00	0.00	71.81	91.23	2581.42	43.55	1297.48	65.92	725.85	104.19	0.00	108.31	42.37	365.57
SU-13	10.34	105.48		3.58	17.33	0.00	17.68	18.42	158.40	38.83	138.80	22.61	92.48	23.69	16.88	23.58	22.62	26.93

sample no.	Lat. N DD	Long. E DD	depth [m]	weight [g]	*n*-$C_{10:0}$	*n*-$C_{11:0}$	*n*-$C_{12:0}$	*n*-$C_{13:0}$	*n*-$C_{14:0}$	*n*-$C_{15:0}$	*n*-$C_{16:0}$	*n*-$C_{17:0}$	*n*-$C_{18:0}$	*n*-$C_{20:0}$	*n*-$C_{21:0}$	*n*-$C_{22:0}$	*n*-$C_{23:0}$	*n*-$C_{24:0}$
Thu Bon River St. 1	10.33	106.38		13.51	0.00	0.00	25.68	17.94	146.71	26.22	54.67	16.45	39.15	18.81	16.74	21.57	21.72	30.13
Thu Bon River St. 2	10.27	106.94		7.39	35.46	12.09	59.06	23.59	685.71	152.46	911.01	65.41	348.94	81.52	23.59	131.81	92.34	241.10
Thu Bon River St. 3	10.25	106.03		6.31	14.38	0.00	0.00	0.00	108.85	22.82	112.60	15.46	87.14	20.70	15.00	21.87	18.18	29.72
Thu Bon River St. 4	10.24	106.37		5.66	0.00	0.00	168.33	67.58	4024.09	285.49	2804.91	285.82	1541.42	313.71	111.23	586.43	369.83	1203.07
Tra Khuc River St. 1a	10.20	106.71		6.78	26.77	0.00	96.08	0.00	2918.93	63.21	1478.74	38.56	714.53	90.01	0.00	105.37	63.57	225.41
Tra Khuc River St. 1b	10.10	105.72		1.58	13.59	0.00	14.27	0.00	176.50	21.16	122.97	15.11	85.10	24.34	13.84	22.38	18.71	29.92
Tra Khuc River St. 2	9.74	106.07		22.32	34.77	0.00	38.64	0.00	1192.79	74.42	1263.87	152.75	697.19	124.71	49.28	243.65	350.99	395.48
VN-07110302 SED	9.69	106.74		3.06	85.55	37.10	133.17	41.83	744.50	156.61	1198.16	87.76	426.43	127.70	46.87	194.55	95.64	303.98
VN-09110301 SED	9.56	106.60		1.97	25.97	14.73	32.54	32.82	68.13	34.94	152.94	23.34	74.12	21.14	11.59	25.13	26.79	50.19
VN-10110301 SED	6.20	102.20		2.20	18.86	19.14	74.15	44.32	2100.26	116.30	2067.69	83.18	859.63	225.22	59.64	598.26	295.29	1168.62
VN-12110301 SED	5.34	103.12		2.80	20.78	0.00	76.37	0.00	1236.51	83.20	2004.88	69.23	746.35	231.23	57.05	544.23	248.17	1092.05
VN-14110301 SED	4.60	113.95		0.80	15.17	14.09	23.02	17.19	117.42	28.42	293.65	23.86	128.56	32.20	23.24	55.01	33.16	90.02
VN-15110306 SED	4.23	103.43		1.73	19.02	16.53	43.49	18.60	121.85	26.93	180.11	21.65	95.89	28.66	20.23	56.67	38.61	96.70
VN-38-1	3.51	103.44		3.71	19.45	16.07	26.81	17.46	96.33	28.64	209.73	21.07	94.08	29.02	17.66	51.76	33.93	86.38
VN-44	2.33	111.83		4.01	18.58	17.82	25.21	17.96	133.50	32.34	251.50	20.86	129.01	44.92	23.01	79.75	55.62	148.73
VN-46	2.24	111.81		4.81	15.70	14.72	18.92	0.00	206.40	28.19	122.72	15.35	67.64	26.37	14.91	25.80	18.76	38.96
VN-49	0.61	101.59		3.65	28.26	23.96	54.03	24.90	281.45	73.48	510.89	34.17	265.36	84.45	51.98	201.75	134.38	576.46
VN-53	0.39	109.96		2.97	11.48	11.55	15.75	10.96	78.03	19.88	148.83	13.10	74.68	23.60	13.07	48.84	25.30	87.72
VN-55	0.32	108.97		5.66	18.44	15.12	23.90	16.08	187.53	25.35	167.84	21.44	83.16	24.28	18.28	34.42	25.18	71.55
VN-59	-0.27	109.36		3.20	25.82	23.11	41.51	21.06	195.57	50.50	332.42	25.37	131.51	56.78	38.23	200.20	113.55	393.24
VN-63	-0.37	102.53		2.60	14.72	16.69	20.57	16.04	136.38	29.88	309.38	22.17	160.66	26.91	16.92	32.51	26.14	60.01
WK-04	-1.58	103.57		3.47	16.50	13.32	16.51	12.98	87.05	26.65	156.77	15.84	84.40	23.49	19.64	47.45	33.82	92.22
WK-07	-2.38	103.94		2.36	24.59	22.38	38.53	21.21	134.32	37.93	321.45	54.46	171.71	46.56	33.66	68.48	54.58	106.15
WK-08	-3.02	104.72		2.11	11.60	11.51	24.01	11.64	65.15	21.30	159.70	19.99	95.36	30.03	20.65	61.39	45.44	111.30
TH-01	13.54	100.25		1.09	0.00	0.00	135.02	51.85	1075.21	341.96	3398.75	172.95	1596.88	345.95	83.12	538.91	224.85	1081.87
TH-02	13.38	99.98		2.59	26.37	14.50	28.34	16.22	46.92	29.15	118.96	18.53	48.72	24.36	18.71	39.89	25.27	66.68
TH-04	13.07	99.95		2.26	16.21	15.75	17.68	15.99	168.28	26.03	264.41	20.25	105.30	25.86	18.25	42.22	36.46	68.99
TH-05	13.70	99.85		4.04	11.52	9.41	10.13	0.00	74.20	12.46	78.02	10.35	51.49	13.03	8.90	12.32	11.16	14.81
TH-07	13.95	99.64		2.26	16.60	0.00	17.34	0.00	230.93	21.59	154.83	18.49	95.39	33.62	18.04	46.75	34.78	66.79
TH-08-2	13.80	100.19		1.24	101.14	64.88	363.17	174.25	2763.59	421.08	5611.46	328.08	2370.54	738.68	248.53	1401.95	689.55	2401.54
TH-09	13.92	100.49		2.15	19.63	16.43	18.74	16.37	228.31	24.52	158.18	19.42	105.40	27.33	18.43	27.90	26.90	37.29
TH-11	14.29	100.56		3.94	9.87	0.00	11.29	9.48	58.62	13.63	79.76	10.70	46.86	15.05	10.67	19.20	15.11	30.75
TH-13	14.94	100.37		3.90	9.79	0.00	9.35	0.00	15.48	11.18	26.35	8.93	17.48	11.17	13.11	21.25	18.96	27.86
TH-15	14.56	100.72		2.39	16.64	17.94	24.80	17.13	194.81	29.72	225.32	22.41	122.60	35.17	21.62	53.15	37.72	83.11
TH-18	13.99	101.69		3.62	10.18	9.72	10.43	9.39	126.47	20.65	61.48	10.62	43.90	15.29	11.11	18.09	15.13	21.94
TH-20	13.73	101.21		1.23	57.15	57.74	229.92	130.86	2944.09	241.71	4431.78	176.26	1875.64	369.08	88.99	495.85	168.00	770.04
TH-21	13.49	101.00		2.13	18.74	18.68	27.04	22.85	172.54	54.64	302.13	44.04	155.14	74.69	56.94	96.96	65.38	119.93

Appendix 3) Measurements of triallate tris (2-chloroethyl) phosphate (TCPP1) and tris (2-chloroethyl) phosphate (TCPP2) normalised against sample (SO-187-3-98-1) multiplied by a factor of ten for a better readability

sample no.	Lat. N DD	Long. E DD	depth [m]	Triallate *m/z* 86 conc. Norm.	TCPP1 *m/z* 277 conc.norm.	TCPP2 *m/z* 277 conc.norm.	TCPP1/TCPP2
SCS-SO-220-19-27	20.29	109.14	19.00	0.03	0.06	0.01	8.76
SCS-SO-220-22-3	20.48	108.75	43.00	0.01	0.26	0.03	8.72
SCS-SO-220-23-3	21.10	108.73	22.00	0.01	0.03	0.00	8.49
SCS-SO-220-24-1	21.11	108.71	22.00	0.01	0.26	0.03	8.92
SCS-SO-220-26-4	21.06	108.34	27.00	0.08	1.09	0.13	8.09
SCS-SO-220-27-1	21.04	108.30	27.00	0.07	1.05	0.08	12.39
SCS-SO-220-28-3	20.83	108.29	43.00	0.01	0.18	0.01	12.86
SCS-SO-220-29-3	20.40	108.38	44.00	0.01	0.49	0.05	10.51
SCS-SO-220-30-28	20.05	108.03	48.00	0.05	0.41	0.04	9.97
SCS-SO-220-31-2	20.01	108.09	27.00	0.08	0.41	0.04	10.62
SCS-SO-220-32-3	19.99	108.12	63.00	0.00	0.00	0.00	13.86
SCS-SO-220-33-3	19.99	108.34	56.00	0.10	0.21	0.03	8.53
SCS-SO-220-34-3	19.46	108.29	57.00	0.00	0.01	0.00	5.67
SCS-SO-220-35-3	19.23	108.15	44.00	0.00	0.04	0.01	7.26
SCS-SO-220-37-3	19.38	107.70	61.00	0.03	0.08	0.01	7.15
SCS-SO-220-38-3	19.42	107.57	61.00	0.02	0.32	0.03	9.76
SCS-SO-220-39-3	19.42	107.36	63.00	0.00	0.04	0.01	7.63
SCS-SO-220-40-2	19.42	107.30	58.00	0.00	0.00	0.00	12.09
SCS-SO-220-42-28	18.74	107.16	60.00	0.03	0.70	0.07	9.70
SCS-SO-220-43-2	18.79	107.17	60.00	0.00	0.22	0.02	9.86
SCS-SO-220-44-3	18.74	107.20	67.00	0.07	0.81	0.07	11.03
SCS-SO-220-45-2	18.73	107.27	66.00	0.07	1.73	0.22	8.02
SCS-SO-220-51-3	18.38	108.06	75.00	0.03	0.24	0.03	8.31
SCS-SO-220-52-1	18.37	108.06	72.00	0.11	0.50	0.07	7.66
SCS-SO-220-53-3	17.90	107.91	89.00	0.01	0.10	0.01	8.70
SCS-SO-220-54-2	17.89	107.90	90.00	0.02	0.16	0.02	8.02
SCS-SO-220-55-3	17.70	108.12	83.00	0.00	0.08	0.01	7.30
SCS-SO-220-57-3	17.64	108.40	105.00	0.01	0.20	0.03	8.02
SCS-SO-220-58-1	17.67	108.42	104.00	0.00	0.19	0.02	8.17
SCS-SO-220-60-2	16.73	109.59	546.00	0.00	0.35	0.04	8.39
SCS-SO-187-3-59-1	12.62	109.53	133.00	0.26	9.35	1.68	5.55
SCS-SO-187-3-60-1	11.08	110.01	1859.00	0.04	0.46	0.05	8.78
SCS-SO-187-3-61-1	11.43	111.28	2227.00	0.17	1.22	0.16	7.49
SCS-SO-187-3-62-1	11.05	109.47	127.00	0.03	14.33	1.12	12.81
SCS-SO-187-3-63-1	10.92	109.06	109.00	0.01	8.89	1.56	5.71
SCS-SO-187-3-64-3	10.91	109.05	107.00	0.01	1.30	0.16	8.26
SCS-SO-187-3-65-1	10.64	109.04	112.00	0.09	14.40	2.38	6.06
SCS-SO-187-3-66-1	10.26	108.91	87.00	0.00	0.10	0.01	7.63
SCS-SO-187-3-67-1	10.22	108.43	56.00	1.73	14.00	2.36	5.93
SCS-SO-187-3-68-1	10.28	108.42	60.00	0.01	5.53	0.83	6.65
SCS-SO-187-3-69-1	10.38	108.01	43.00	0.05	2.05	0.23	9.00
SCS-SO-187-3-70-1	10.37	108.01	41.50	0.00	0.81	0.09	8.70
SCS-SO-187-3-71-1	10.40	108.01	38.00	0.01	0.31	0.04	8.35
SCS-SO-187-3-72-1	10.26	107.29	26.00	0.01	0.26	0.03	7.47
SCS-SO-187-3-73-1	10.24	107.28	31.00	0.09	7.73	1.31	5.89
SCS-SO-187-3-74-1	10.23	107.28	29.00	0.08	0.65	0.07	8.75
SCS-SO-187-3-75-1	10.11	107.11	21.00	0.06	0.88	0.10	8.58

sample no.	Lat. N DD	Long. E DD	depth [m]	Triallate *m/z* 86 conc. Norm.	TCPP1 *m/z* 277 conc.norm.	TCPP2 *m/z* 277 conc.norm.	TCPP1/TCPP2
SCS-SO-187-3-76-1	9.48	106.82	24.00	0.01	0.26	0.03	7.80
SCS-SO-187-3-77-B1	9.36	106.63	25.00	0.02	0.93	0.11	8.36
SCS-SO-187-3-78-1	8.97	106.70	32.00	0.05	2.08	0.25	8.27
SCS-SO-187-3-79-1	9.14	107.07	33.00	0.00	0.29	0.04	7.16
SCS-SO-187-3-80-1	9.23	107.28	38.00	0.01	0.27	0.03	7.79
SCS-SO-187-3-81-1	9.26	107.33	38.00	0.01	0.48	0.06	8.77
SCS-SO-187-3-82-1	9.52	107.50	39.00	0.03	4.23	0.37	11.45
SCS-SO-187-3-83-1	9.90	107.50	31.00	0.01	0.40	0.05	8.56
SCS-SO-187-3-84-1	9.73	107.29	33.00	0.07	7.62	0.55	13.83
SCS-SO-187-3-85-1	9.80	107.04	27.00	0.09	13.65	1.01	13.49
SCS-SO-187-3-86-1	8.74	106.16	27.00	0.08	8.63	0.59	14.63
SCS-SO-187-3-87-2	9.04	106.08	20.00	0.04	0.22	0.03	6.74
SCS-SO-187-3-91-1	8.44	105.24	31.00	0.06	3.49	0.29	12.03
SCS-SO-187-3-92-1	8.42	105.20	30.00	0.27	12.67	0.92	13.73
SCS-SO-187-3-93-1	8.39	105.11	32.00	0.09	5.16	0.38	13.77
SCS-SO-187-3-94-1	8.37	104.63	24.00	6.87	6.10	0.45	13.53
SCS-SO-187-3-95-1	8.38	104.62	29.00	3.01	7.91	0.61	13.03
SCS-SO-187-3-96-1	8.41	104.57	31.00	8.45	3.94	0.71	5.59
SCS-SO-187-3-97-2	8.41	104.56	30.00	3.40	2.92	0.42	6.98
SCS-SO-187-3-98-1	8.46	104.47	30.00	10.00	5.40	0.42	12.74
SCS-SO-187-3-99-1	8.47	104.46	30.00	2.65	2.72	0.41	6.57
SCS-SO-187-3-100-1	8.52	104.34	28.00	3.19	2.48	0.36	6.96
SCS-SO-187-3-102-1	8.44	104.23	29.00	0.04	1.41	0.18	8.04
SCS-SO-187-3-103-1	8.43	104.21	28.00	0.00	3.44	0.50	6.85
SCS-SO-187-3-104-1	8.38	104.22	26.00	0.01	0.09	0.01	7.70
SCS-SO-187-3-105-1	8.19	104.52	25.00	0.01	0.24	0.03	7.95
SCS-SO-187-3-106-1	8.19	104.56	26.00	0.07	1.34	0.12	11.31
SCS-SO-187-3-107-1	8.16	104.57	27.50	0.01	0.17	0.02	8.19
SCS-SO-187-3-108-1	8.12	104.95	32.00	0.00	0.32	0.04	8.72
SCS-SO-187-3-109-1	8.12	105.24	33.00	0.00	0.16	0.02	8.35
SCS-SO-187-3-110-1	8.12	105.28	32.00	0.00	0.20	0.02	8.19
SCS-SO-187-3-111-1	8.12	105.38	34.00	0.01	0.30	0.04	8.21
SCS-SO-187-3-112-1	8.12	105.39	33.00	0.00	0.24	0.03	8.50
SCS-SO-187-3-113-1	8.12	105.48	32.00	0.01	0.26	0.03	9.24
SCS-SO-187-3-114-1	8.12	105.59	32.00	3.80	1.60	0.21	7.44
SCS-SO-187-3-115-1	8.12	105.60	32.00	4.65	0.77	0.10	7.64
SCS-SO-187-3-116-1	8.12	105.94	33.00	0.58	0.78	0.10	7.63
SCS-SO-187-3-117-1	8.12	105.95	32.00	1.77	1.25	0.17	7.29
SCS-SO-140-01-18373-1	6.73	107.65	73.50	0.00	0.08	0.01	7.03
SCS-SO-140-02-18374-1	6.91	107.67	74.40	3.08	1.91	0.33	5.70
SCS-SO-140-03-18375-1	7.00	107.91	86.20	1.15	0.49	0.05	8.89
SCS-SO-140-04-18376-1	7.09	108.11	89.60	0.03	1.93	0.20	9.87
SCS-SO-140-05-18377-1	7.18	108.34	98.80	0.52	0.26	0.04	7.33
SCS-SO-140-06-18378-1	7.24	108.48	107.90	0.79	0.50	28.20	0.02
SCS-SO-140-07-18379-2	7.34	108.74	119.00	1.08	20.22	3.81	5.31
SCS-SO-140-08-18380-1	7.44	108.99	149.70	0.00	3.23	0.48	6.68

sample no.	Lat. N DD	Long. E DD	depth [m]	Triallate *m/z* 86 conc. Norm.	TCPP1 *m/z* 277 conc.norm.	TCPP2 *m/z* 277 conc.norm.	TCPP1/TCPP2
SCS-SO-140-09-18381-1	7.50	109.13	213.90	2.38	4.83	9.99	0.48
SCS-SO-140-10-18382-1	7.53	109.21	283.90	1.48	0.19	14.21	0.01
SCS-SO-140-11-18383-1	7.64	109.49	710.70	0.75	2.06	0.27	7.77
SCS-SO-140-12-18384-1	7.77	109.81	829.10	0.83	3.27	0.50	6.56
SCS-SO-140-13-18385-2	7.86	110.02	73.60	0.00	0.36	0.05	6.91
SCS-SO-140-14-18386-1	7.90	110.13	380.40	0.00	0.10	0.01	9.67
SCS-SO-140-15-18387-1	8.10	110.64	381.60	0.00	0.64	0.09	7.25
SCS-SO-140-16-18388-1	9.14	108.62	108.80	1.79	2.98	0.36	8.24
SCS-SO-140-17-18389-1	9.27	108.65	109.20	0.00	0.32	0.04	7.93
SCS-SO-140-18-18390-1	9.34	108.68	101.40	0.00	0.29	0.04	7.27
SCS-SO-140-19-18391-1	9.57	108.83	122.40	0.03	0.15	0.02	7.49
SCS-SO-140-20-18392-1	9.62	108.91	116.10	2.08	7.77	1.24	6.26
SCS-SO-140-21-18393-1	9.76	109.13	155.90	1.55	3.91	0.67	5.80
SCS-SO-140-22-18394-1	9.79	109.18	183.00	1.00	1.66	0.27	6.26
SCS-SO-140-23-18395-1	9.99	109.48	280.10	2.07	6.94	1.15	6.01
SCS-SO-140-24-18396-1	15.43	108.89	60.80	0.08	0.75	0.11	6.72
SCS-SO-140-25-18397-1	12.25	109.33	45.50	0.07	0.94	0.11	8.16
SCS-SO-140-26-18398-1	12.24	109.38	59.30	1.20	6.90	1.18	5.84
SCS-SO-140-27-18399-1	12.23	109.41	92.20	1.75	1.24	0.18	6.78
SCS-SO-140-28-18400-1	12.23	109.43	103.60	1.74	7.21	1.20	5.99
SCS-SO-140-29-18401-1	12.21	109.53	134.20	0.13	1.50	0.21	7.07
SCS-SO-140-30-18402-1	13.12	109.69	224.50	0.00	0.03	0.00	7.65
SCS-SO-140-32-18404-1	13.50	109.56	169.10	0.00	0.28	0.04	7.48
SCS-SO-140-33-18405-1	13.69	109.45	129.30	0.01	0.01	0.00	9.47
SCS-SO-140-34-18406-1	14.00	109.32	50.60	2.80	5.31	0.79	6.74
SCS-SO-140-35-18407-1	14.08	109.42	134.70	2.69	6.99	0.91	7.69
SCS-SO-140-36-18408-1	14.25	109.34	116.50	4.44	7.48	1.46	5.11
SCS-SO-140-37-18409-1	15.69	108.67	40.00	2.91	8.29	1.39	5.97
SCS-SO-140-38-18410-1	15.48	108.87	57.70	2.71	11.89	0.75	15.75
SCS-SO-140-39-18411-2	15.33	108.92	56.80	0.03	0.60	0.06	9.45
SCS-SO-140-40-18412-2	15.22	109.01	58.40	2.12	3.65	0.57	6.42
SCS-SO-140-41-18413-1	15.20	109.00	52.00	0.00	0.21	0.03	8.01
SCS-SO-140-42-18414-2	15.10	108.96	20.70	0.00	0.43	0.06	7.24
SCS-SO-140-43-18415-1	15.08	109.00	34.60	5.22	27.26	2.17	12.55
SCS-SO-140-44-18416-1	15.04	109.15	62.70	0.00	0.20	0.02	8.22
SCS-SO-140-46-18418-1	14.40	109.31	100.00	2.96	8.18	1.48	5.52
SCS-SO-140-47-18419-1	14.54	109.24	80.70	2.56	13.49	2.49	5.41
SCS-SO-140-48-18420-1	14.57	109.19	61.50	5.46	17.03	1.27	13.46
SCS-SO-140-49-18421-1	15.75	108.89	82.50	0.79	0.57	0.07	8.55
SCS-SO-140-50-18422-1	15.75	108.89	84.50	0.00	0.26	0.03	7.41
SCS-SO-140-51-18423-1	16.28	108.66	96.50	0.01	0.15	0.01	9.88
SCS-SO-140-52-18424-1	16.48	108.44	91.10	0.00	0.23	0.04	6.14
SCS-SO-140-53-18425-1	16.58	108.47	94.40	0.02	0.56	0.07	8.51
SCS-SO-140-54-18426-1	16.74	108.46	92.90	0.02	9.09	0.67	13.47
SCS-SO-140-55-18427-1	16.48	109.19	114.80	0.27	10.23	0.73	13.95
SCS-SO-140-56-18428-1	16.39	109.42	196.60	0.00	0.18	0.02	9.58

sample no.	Lat. N DD	Long. E DD	depth [m]	Triallate *m/z* 86 conc. Norm.	TCPP1 *m/z* 277 conc.norm.	TCPP2 *m/z* 277 conc.norm.	TCPP1/TCPP2
SCS-SO-140-57-18429-1	16.35	109.54	756.30	0.16	1.63	0.20	8.00
SCS-SO-140-58-18430-1	11.92	110.00	1906.00	0.20	11.49	1.44	8.00
SCS-SO-115-01-18248-1	9.25	108.73	103.00	0.01	0.01	0.00	11.78
SCS-SO-115-02-18249-1	9.40	108.92	133.00	0.00	0.04	0.00	9.54
SCS-SO-115-03-18250-1	9.40	108.97	148.00	0.01	0.50	0.05	9.40
SCS-SO-115-05-18252-1	9.25	109.39	1277.00	0.10	0.22	0.03	7.73
SCS-SO-115-06-18253-1	9.40	109.50	1478.00	3.05	8.98	1.11	8.07
SCS-SO-115-07-18254-1	9.63	109.04	145.00	2.69	7.39	1.30	5.69
SCS-SO-115-08-18255-1	9.70	108.78	102.00	1.55	3.27	0.50	6.50
SCS-SO-115-09-18256-1	9.58	108.70	92.00	3.58	14.75	0.84	17.46
SCS-SO-115-10-18257-2	9.40	108.59	88.00	2.08	0.49	0.06	8.12
SCS-SO-115-11-18258-1	9.25	108.49	88.00	0.00	0.11	0.01	9.46
SCS-SO-115-12-18259-2	9.17	108.45	88.00	0.00	0.05	0.01	8.70
SCS-SO-115-14-18261-3	9.25	108.12	68.00	0.00	0.06	0.01	9.54
SCS-SO-115-15-18262-1	9.25	107.99	56.00	0.00	0.06	0.01	9.23
SCS-SO-115-17-18264-1	9.40	107.81	48.00	0.41	0.18	0.02	7.59
SCS-SO-115-17-18264-1 0 cm	9.40	107.81	48.00	0.01	0.12	0.02	8.09
SCS-SO-115-18-18265-1	9.39	107.75	47.00	0.00	0.00	n.a.	n.a.
SCS-SO-115-19-18266-1	9.38	107.74	47.00	0.00	0.63	0.07	9.24
SCS-SO-115-20-18267-1	6.37	111.88	1852.00	0.01	0.03	0.00	7.46
SCS-SO-115-21-18268-1	6.65	111.87	1974.00	0.14	0.53	0.06	9.15
SCS-SO-115-22-18269-1	4.77	109.44	114.00	0.01	0.12	0.02	7.55
SCS-SO-115-22-18269-1 0 cm	4.77	109.44	114.00	8.74	61.63	5.54	11.12
SCS-SO-115-23-18270-1	4.72	109.48	106.00	1.74	4.68	0.80	5.84
SCS-SO-115-24-18271-1	4.64	109.55	116.00	0.03	2.65	0.39	6.86
SCS-SO-115-25-18272-1	4.63	109.56	121.00	5.24	2.04	0.15	13.38
SCS-SO-115-26-18273-1	4.62	109.57	127.00	0.00	0.07	0.01	8.01
SCS-SO-115-27-18274-1	4.61	109.58	117.00	0.00	0.00	0.00	10.44
SCS-SO-115-28-18275-1	4.59	109.59	109.00	0.00	0.09	0.01	7.41
SCS-SO-115-29-18276-1	4.75	109.75	120.00	0.00	0.02	0.00	9.78
SCS-SO-115-30-18277-1	4.94	109.94	134.00	3.05	4.82	0.82	5.88
SCS-SO-115-31-18278-1	5.02	110.02	137.00	0.57	0.78	0.10	8.03
SCS-SO-115-32-18279-1	5.04	110.04	139.00	0.68	2.82	0.42	6.78
SCS-SO-115-33-18280-1	5.10	110.10	144.00	1.37	2.27	0.34	6.77
SCS-SO-115-34-18281-1	5.13	110.13	145.00	1.19	3.00	0.49	6.16
SCS-SO-115-35-18282-1	5.25	110.24	152.00	0.00	0.01	0.00	11.00
SCS-SO-115-36-18283-1	5.42	110.42	166.00	1.26	3.18	0.53	5.96
SCS-SO-115-37-18284-1	5.54	110.54	226.00	1.89	0.88	0.11	8.10
SCS-SO-115-47-18294-3	6.13	111.30	846.00	1.01	0.80	0.08	9.47
SCS-SO-115-48-18295-1	4.93	109.30	117.00	0.00	0.15	0.02	8.80
SCS-SO-115-49-18296-1	5.00	109.24	118.00	0.73	5.93	0.93	6.38
SCS-SO-115-50-18297-1	4.74	109.03	112.00	2.53	13.68	2.88	4.74
SCS-SO-115-51-18298-1	4.52	108.83	103.00	3.11	2.13	0.28	7.71
SCS-SO-115-52-18299-2	4.53	108.83	102.00	0.01	0.09	0.01	7.67
SCS-SO-115-53-18300-1	4.36	108.65	94.00	1.86	3.71	0.63	5.85
SCS-SO-115-54-18301-1	4.36	108.65	92.00	3.61	1.77	0.23	7.81

sample no.	Lat. N DD	Long. E DD	depth [m]	Triallate *m/z* 86 conc. Norm.	TCPP1 *m/z* 277 conc.norm.	TCPP2 *m/z* 277 conc.norm.	TCPP1/TCPP2
SCS-SO-115-55-18302-1	4.16	108.58	83.00	2.08	0.76	0.10	7.78
SCS-SO-115-56-18303-1	4.44	108.93	107.00	0.03	0.01	0.00	9.17
SCS-SO-115-57-18304-1	4.36	109.00	104.00	4.25	3.64	0.58	6.32
SCS-SO-115-59-18306-1	3.59	108.44	88.00	1.85	0.91	0.12	7.72
SCS-SO-115-59-18306-2	3.59	108.44	88.00	0.36	0.78	0.09	8.75
SCS-SO-115-60-18307-1	3.63	108.53	100.00	2.51	5.32	0.86	6.21
SCS-SO-115-61-18308-1	3.30	108.79	80.00	0.00	0.00	0.00	1.01
SCS-SO-115-62-18309-1	3.47	108.69	84.00	0.96	0.45	0.05	8.36
SCS-SO-115-63-18310-1	3.54	108.54	101.00	0.00	0.09	0.01	7.59
SCS-SO-115-64-18311-1	3.69	108.45	60.00	0.00	0.00	0.00	15.05
SCS-SO-115-65-18312-1	3.71	108.71	101.00	0.00	0.03	0.00	7.72
SCS-SO-115-66-18313-1	3.87	108.87	99.00	0.27	1.02	0.13	7.68
SCS-SO-115-67-18314-1	3.99	108.99	100.00	0.00	0.00	n.a.	n.a.
SCS-SO-115-68-18315-3	2.03	107.03	69.00	0.00	0.02	0.00	7.90
SCS-SO-115-70-18317-1	2.61	107.38	96.00	0.00	0.04	0.00	8.46
SCS-SO-115-71-18318-1	2.61	107.38	86.00	4.56	6.43	1.12	5.73
SCS-SO-115-73-18320-1	2.61	107.37	76.00	0.00	0.05	0.01	7.61
SCS-SO-115-74-18321-1	2.31	107.42	109.00	0.00	0.00	8.00	n.a.
SCS-SO-115-75-18322-1	2.31	107.63	70.00	0.84	0.59	0.08	7.80
SCS-SO-115-76-18323-1	2.78	107.89	92.00	2.95	1.44	0.19	7.55
B254	18.00	109.30	55.00	0.01	0.93	0.11	8.15
B309	18.20	110.10	91.00	0.00	0.01	0.00	11.50
C71	18.00	109.00	44.00	0.00	0.34	0.03	10.30
VA-01	14.50	111.90	1618.00	0.06	2.01	0.31	6.51
VA-02	14.80	110.80	1204.00	0.02	0.26	0.03	9.73
VA-06	12.30	111.10	2095.00	0.00	0.10	0.01	8.78
VA-11	10.20	110.00	1401.00	0.00	0.68	0.08	8.77
RS-34	20.79	106.52		0.00	0.44	0.05	9.46
BN-12	4.60	113.95		0.14	0.16	0.02	7.27
Con River St. 1	13.85	109.14		0.00	0.15	0.02	8.25
Cuu Long Grab St.11 SED	9.69	106.69		0.15	1.22	0.16	7.45
Cuu Long Grab St.20 SED	9.56	106.562		0.20	0.14	0.02	7.57
Hathan River St. 1a	13.70	109.22		0.00	0.01	0.00	8.02
Hathan River St. 1b	13.78	109.22		0.05	0.02	0.26	0.07
Hathan River St. 2	13.78	109.22		0.01	0.72	0.09	7.72
HN-02	19.90	109.68		0.00	0.38	0.04	10.58
HN-04	19.23	108.90		0.02	4.82	0.70	6.92
HN-06	18.52	110.02		0.02	3.21	0.53	6.07
HN-07	19.15	110.55		0.00	0.00	0.00	16.18
Lai Giang River St. 1a	14.41	109.01		3.31	1.19	0.16	7.38
Lai Giang River St.2a	14.47	109.09		3.24	2.03	0.29	7.04
Lai Giang Riverband St. 2b	14.47	109.09		0.00	0.00	0.00	9.30
MK-01	6.20	102.20		0.76	0.67	0.09	7.84
MK-10	3.51	103.44		1.27	0.33	0.04	8.19
MK-11	4.23	103.43		0.90	0.33	0.05	7.43
MK-14	5.34	103.12		0.00	0.01	0.00	8.14

sample no.	Lat. N DD	Long. E DD	depth [m]	Triallate *m/z* 86 conc. Norm.	TCPP1 *m/z* 277 conc.norm.	TCPP2 *m/z* 277 conc.norm.	TCPP1/TCPP2
MK-15	2.24	111.81		0.55	0.36	0.04	8.08
MK-17	2.33	111.83		0.17	0.19	0.02	8.30
MR-02	10.56	106.41		0.01	0.88	0.15	5.96
MR-03	10.33	106.38		0.84	0.38	0.05	8.30
MR-04	10.24	106.37		0.00	0.07	0.01	9.47
MR-06-1	10.20	106.71		0.01	0.83	0.09	9.06
MR-13	10.42	105.41		0.00	0.00	n.a.	n.a.
MR-14	10.34	105.48		0.48	0.16	0.02	7.64
MR-15	10.10	105.72		0.64	0.41	0.05	7.95
MR-17	10.25	106.03		0.46	0.39	0.05	7.85
Red River 7W SED	20.07	106.47		2.25	0.70	0.10	7.25
Song Ba St. 3a SED	13.05	109.05		0.03	0.51	0.07	7.82
SU-02	0.61	101.59		1.10	0.54	0.07	7.23
SU-05	-0.37	102.53		1.01	0.58	0.08	7.65
SU-09	-1.58	103.57		0.43	0.47	0.05	8.98
SU-11	-2.38	103.94		0.17	0.14	0.02	7.32
SU-13	-3.02	104.72		1.17	1.00	0.14	7.30
Thu Bon River St. 2	15.85	108.28		3.57	1.29	0.19	6.86
Thu Bon River St. 3	15.87	108.39		3.36	1.08	0.14	7.87
Thu Bon River St. 4	15.87	108.39		0.00	0.12	0.01	8.63
Tra Khuc River St. 1a	15.13	108.80		1.43	1.05	0.15	7.13
Tra Khuc River St. 2	15.13	108.88		0.48	3.75	0.51	7.37
VN-09110301 SED	11.22	108.50		0.02	3.46	0.56	6.13
VN-10110301 SED	11.24	108.73		0.02	0.65	0.08	8.56
VN-12110301 SED	12.49	109.13		1.21	1.23	0.17	7.10
VN-63	19.84	105.79		0.01	1.18	0.12	9.80
WK-04	0.39	109.96		1.38	0.75	0.10	7.54
WK-07	0.32	108.97		2.36	0.50	0.06	7.74
WK-08	-0.27	109.36		0.00	0.00	0.00	23.46
TH-02	13.38	99.98		0.22	0.05	0.01	8.89
TH-04	13.07	99.95		0.58	0.22	0.03	8.55
TH-05	13.70	99.85		0.22	0.11	0.01	8.55
TH-07	13.95	99.64		0.36	0.21	0.03	8.19
TH-09	13.92	100.49		0.14	0.07	0.01	8.11
TH-11	14.29	100.56		0.60	0.38	0.04	8.60
TH-13	14.94	100.37		0.24	0.03	0.00	9.18
TH-15	14.56	100.72		0.36	0.49	0.06	8.32
TH-18	13.99	101.69		0.34	0.19	0.02	8.57
TH-21	13.49	101.00		0.42	0.18	0.02	8.19

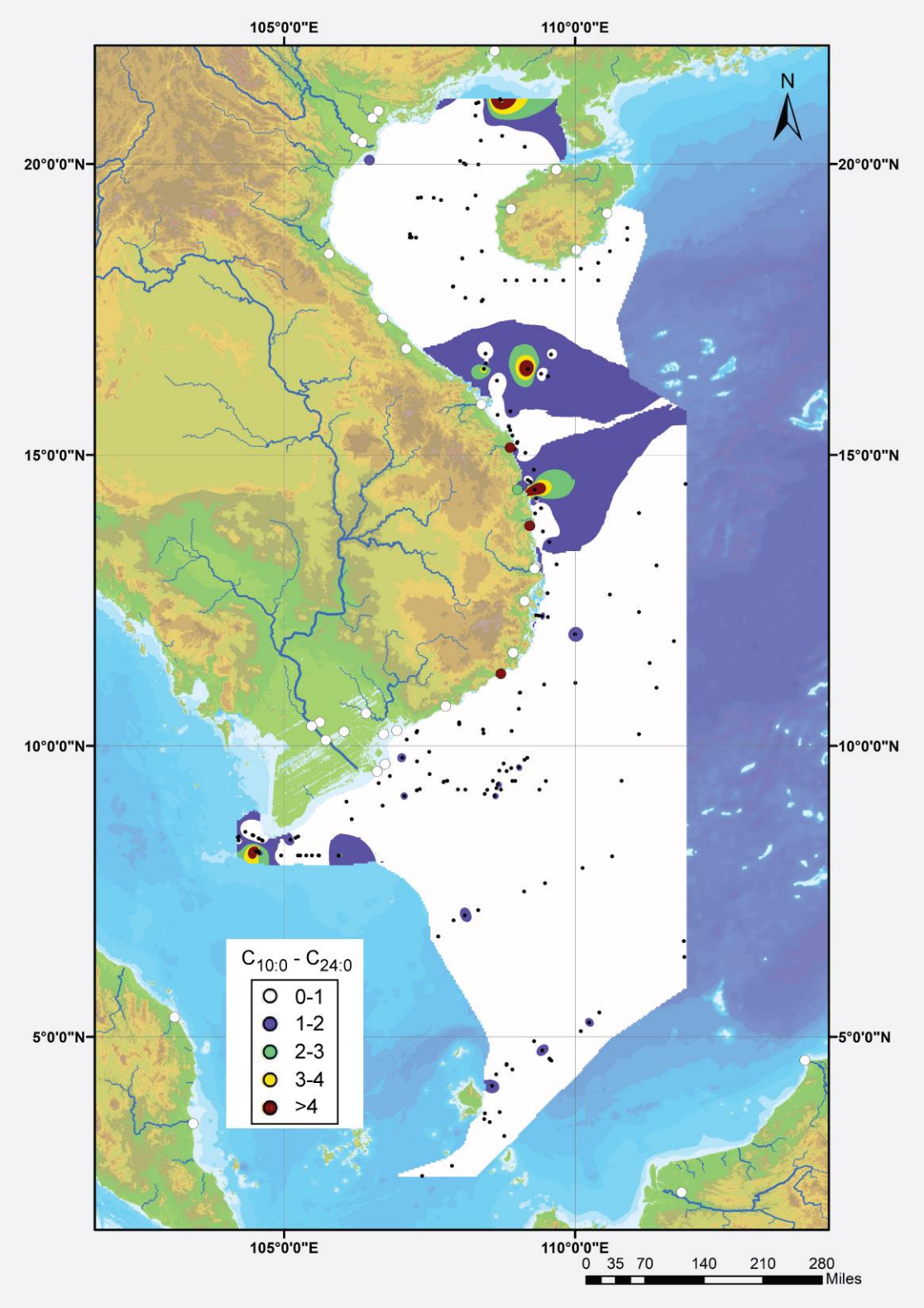

Appendix 4) Inverse distance weighted interpolation of the *n*-$C_{10:0}$/*n*-$C_{24:0}$ fatty acid methyl ester ratio. Values between 0-1 are characteristic for terrestrial dominance, values greater one are considered to be marine dominated.